Fullerene bisadduct for organic photovoltaics

Bouwer, Ricardo Klaas Maarten

Fullerene bisadducts for organic photovoltaics

Ricardo K. M. Bouwer

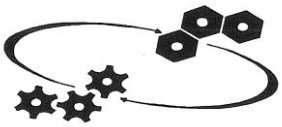

University of Groningen
Zernike Institute
for Advanced Materials

The work in this thesis was performed in the research group Chemistry of (Bio)Molecular Materials and Devices, Molecular Electronics, Stratingh Institute for Chemistry and Zernike Institute for Advanced Materials, University of Groningen, The Netherlands. This research is financially supported by the Dutch Polymer Institute (DPI), project #524.

Zernike Institute PhD thesis series 2012-04
ISSN 1570-1530
ISBN: 978-90-367-5304-3 (printed version)
ISBN: 978-90-367-5303-6 (electronic version)

This research forms part of the research programme of the Dutch Polymer Institute (DPI), Technology Area Functional Polymer Systems, DPI project #524

RIJKSUNIVERSITEIT GRONINGEN

Fullerene bisadducts for organic photovoltaics

Proefschrift

ter verkrijging van het doctoraat in de
Wiskunde en Natuurwetenschappen
aan de Rijksuniversiteit Groningen
op gezag van de
Rector Magnificus, dr. E. Sterken,
in het openbaar te verdedigen op
vrijdag 20 januari 2012
om 12.45 uur

door

Ricardo Klaas Maarten Bouwer

geboren op 16 november 1981
te Velsen

Promotor:	Prof. dr. J. C. Hummelen
Beoordelingscommissie:	Prof. dr. S. Harder Prof. dr. K. Meerholz Prof. dr. J. F. Nierengarten

Table of contents

Chapter 1 Introduction 1

1.1 Energy consumption 2

1.2 Solar cells 2

1.2.1 Inorganic solar cells 2

1.2.2 Organic solar cells 4

1.2.2.1 Brief history of the organic solar cell 5

1.2.3 Working principles of organic solar cells 7

1.2.4 Morphology of the active layer 10

1.2.5 Solar cell parameters with emphasis on organic photovoltaics 12

1.3 Materials 14

1.3.1 Donor material, the conjugated polymer 14

1.3.2 The acceptor of choice, fullerenes 16

1.3.2.1 Background 16

1.3.2.2 Fullerenes for photovoltaic applications 18

1.3.2.3 Improving the fullerene acceptor for use in bulk heterojunction architectures 18

1.3.3 State of the art acceptor materials 20

1.4 Outine of this thesis 23

1.5 References 25

Chapter 2 Bisadduct analogues of PCBM and their use in bulk heterojunction solar cells 31

2.1 Introduction 32

2.1.1 Higher fullerene adducts as n-type materials 32

2.2 Fullerene bisadducts 33

2.2.1 Reactivity and formation of adducts 33

2.2.2 Bisadduct isomers 34
2.2.3 Regioselectivity of bisadditons 35
2.2.4 Relative orientation of C_s symmetric addends 36
2.2.5 Chirality 37
2.2.6 Methanofullerene or homofulleroid 38
2.3 Reactivity of the parent monoadduct 39
2.3.1 Bond length distortion 39
2.3.2 Frontier orbitals 43
2.4 Experimental results 45
2.4.1 Synthesis of bis-PCBM 45
2.4.2 Isomerization of bis-PCBM 46
2.4.3 Separating bis-PCBM into single isomers 49
2.4.3.1 Fractionation by Soxhlet extraction 49
2.4.3.2 Fractionation by column chromatography 49
2.4.3.3 Subfractions of bis-PCBM by preparative HPLC 49
2.4.4 Cyclic voltammetry on bis-PCBM subfractions 50
2.4.5 Isolation of single isomers of bis-PCBM 51
2.4.5.1 Single isomers obtained through recycle preparative HPLC 51
2.5 Single isomers of bis-PCBM 52
2.5.1 HPLC and UV-Vis 52
2.5.2 NMR 54
2.5.3 Cyclic voltammetry 57
2.5.4 Solar cell devices 58
2.6 Conclusions 59
2.7 Outlook 59
2.8 Experimental 60
2.8.1 Device fabrication 60
2.8.2 Materials 60
2.8.3 Synthesis 61
2.9 References 65

Chapter 3 Tethered synthesis of bis-PCBM 69
3.1 Introduction 70
3.2 Synthetic methods to reduce the number of isomers of fullerene higher adducts 72
3.2.1 Directed synthesis 72
3.2.2 Tether-directed synthesis 74
3.2.3 Reducing the number of possible isomers of bis-PCBM through the use of tethered addends 75
3.3 Synthesis and characterization 76
3.3.1 Synthesis of the tethered addends and bis-PCBM subfractions 76
3.3.2 HPLC analysis 78
3.3.3 NMR 81
3.3.4 Molecular modeling 81
3.3.5 Cyclic voltammetry 83
3.4 Device testing 84
3.4.1 P3HT devices 84
3.4.2 PF10TBT devices 88
3.5 Conclusions 89
3.6 Outlook 90
3.7 Experimental 91
3.7.1 Device fabrication 91
3.7.2 Materials 91
3.7.3 Synthesis 92
3.7.4 Molecular modeling 104
3.8 References 106

Chapter 4 PCXMs: PCBM-like analogues with varying alkanoic acid moieties 109
4.1 Introduction 110

4.1.1 PCBM 110
4.2 Modifying the PCBM substituent 112
4.2.1 The ester moiety 112
4.2.2 The phenyl group 115
4.2.3 The bridgehead 117
4.2.4 The carbon chain length 117
4.3 Experimental results 120
4.3.1 Synthesis 120
4.3.2 PCXM monoadducts 121
4.3.2.1 UV-Vis 121
4.3.2.2 HPLC analysis 122
4.3.2.3 Cyclic voltammetry measurements 122
4.3.2.4 Molecular modeling 123
4.3.3 PCXM bisadducts 123
4.3.3.1 HPLC analysis 123
4.3.3.2 Cyclic voltammetry measurements 125
4.4 Device testing 125
4.4.1 PCXM monoadducts 126
4.4.2 PCXM bisadducts 127
4.5 Conclusions 128
4.6 Outlook 128
4.7 Experimental 129
4.7.1 Device fabrication 129
4.7.2 Materials 129
4.7.3 Synthesis 130
4.8 References 141

Chapter 5 PCBM analogues for blends with fluorene-based small bandgap polymers 145
5.1 Introduction 146
5.1.1 Small bandgap polymers 146

5.2 Optimizing the morphology of the active layer 147
5.2.1 Morphology 147
5.2.2 Additives 148
5.2.3 Compatibilizers 149
5.2.4 Compatible fullerenes 150
5.2.5 Locking the morphology 150
5.3 Fluorene-bearing small bandgap polymers 151
5.4 Experimental results 152
5.4.1 Synthesis of F_nCBM 152
5.4.2 Friedel Crafts acylation of fluorene 153
5.4.3 Cyclic voltammetry 154
5.5 Device testing 155
5.5.1 Monoadducts 155
5.5.2 Bisadducts 156
5.5.3 F_6CBM as compatibilizer in PF10TBT devices 158
5.5.4 $\Delta\Delta V_{oc}$ 159
5.6 Conclusions 160
5.7 Outlook 160
5.8 Experimental 161
5.8.1 Device fabrication 161
5.8.2 Materials 161
5.8.3 Synthesis 162
5.9 References 174

Chapter 6 Charge separation and recombination in small bandgap oligomer-fullerene triads 179
6.1 Introduction 180
6.1.1 Small bandgap polymers 180
6.1.2 Electronic transitions 181
6.1.3 Photoinduced absorption 182

6.2 Experimental results 183
6.2.1 Synthesis 183
6.2.1.1 Thienopyrazine-thiophene-fullerene triads 183
6.2.1.2 Diketopyrrolopyrrole-thiophene-fullerene triads 184
6.2.2 Photoinduced absorption 185
6.2.2.1 Thienopyrazine-thiophene-fullerene triads 186
6.2.2.2 Diketopyrrolopyrrole-thiophene-fullerene triads 186
6.3 Conclusions 187
6.4 Outlook 188
6.5 Experimental 189
6.5.1 General procedures 189
6.5.2 Synthesis 191
6.6 References 197

Summary 201
Samenvatting 205
Dankwoord (Acknowledgements) 210

Chapter 1

Introduction

Abstract. This chapter gives a short introduction on solar cells with emphasis on organic photovoltaics, focusing on devices comprising polymer:fullerene mixtures as photoactive layer. The important parameters in device fabrication, characterization as well as state of the art materials comprising the photoactive layer in these cells are described. An outline for this thesis is given at the end of this chapter.

1.1 Energy consumption

The ever increasing energy demand of the world is still mostly stilled by non-renewable energy sources, resulting in an increased emission of greenhouse gasses and a growing shortage of fossil energy resources. The emission of these gasses, with CO_2 as largest contributor, is altering the energy balance of the climate system with unforeseen consequences for the planet.[1,2] The increasing shortage of oil and its increasing price will also lead to severe economic consequences. It is therefore of the utmost importance to change energy production towards renewable energy sources.

One source of renewable energy that is abundantly available is solar radiation. The Earth receives 174 petawatts of solar energy at the upper atmosphere of which around 30% is directly reflected back into space. The total solar energy absorbed by the atmosphere, oceans and land masses is almost 4 million exajoules per year. In 2002, this was more energy in one hour than the world used in one year. The amount of solar energy reaching the surface of the planet is so vast that it surpasses that of all non-renewable resources of coal, oil, natural gas, and mined uranium that can ever be obtained in less than one year. This solar energy can be converted to thermal energy used for hot water, heating, or the production of electrical energy. Electrical energy can also be obtained directly from solar radiation through photovoltaics.[3] This thesis will only deal with photovoltaics in which light is directly converted to electrical energy through solar cells.

1.2 Solar cells

1.2.1 Inorganic solar cells

Since the development of the first crystalline silicon solar cell by Chapin, Fuller and Pearson in 1954, the majority of solar cells nowadays are based on silicon. Monocrystalline silicon solar cells reach efficiencies of up to 25% (14-17% in production).[3] However, much energy is required for their production which makes these solar cells expensive.

To produce a monocrystalline silicon cell, absolutely pure silicon is necessary. Monocrystalline rods are extracted from molten silicon and then sawed into thin plates, resulting in relative high losses of material. The production of polycrystalline cells is more cost-efficient. In this process, liquid silicon is poured into blocks that are subsequently sawed into plates. During solidification of the material, different crystal domains of various sizes are formed, at whose borders defects emerge. As a result of these crystal defects, the solar cell is less efficient reaching lab efficiencies of around 20% (13-15% in production). If silicon is deposited on glass or another substrate material, the resuling cell is called an amorphous silicon cell. The production costs are even lower due to the low amounts of material needed. However, the efficiency of amorphous cells is much lower than that of the other two cell types, lab effiencies reaching 13% (5-7% in production). Because of this, they are primarily used in low power equipment (e.g. watches and pocket calculators).

Alternatives are thin film solar cells which require even less material and can be produced by more efficient processes. Thin film solar cells from inorganic materials like cadmium telluride (CdTe) or copper indium gallium selenide (CIGS) can reach efficiencies up to 16.7 and 19.4% respectively, but most of these materials are toxic or rather rare.[3] The low amounts needed, less than 2% of the equivalent semiconductor content found in crystalline silicon PV modules, and the short production time of less than 2.5 hours allow the price to be low (below 1$ per Wp in 2008), even lower costs are predicted for coming years through an increase in their production.

The leading manufacturer in the field is First Solar using cadmium telluride (CdTe) as the semiconductor material. Annual manufacturing capacity was in excess of 1 gigawatt in 2009. Capacity in excess of 1.4 GW was announced for the end of 2010. Lifetimes of their modules is in excess of 25 years. However even these thin film solar cells are still rather heavy due to the use of glass as protective layer; 1.2 m x 0.6 m x 6.8 mm modules weigh 12.0 kg.

1.2.2 Organic solar cells

A promising class of thin film solar cells is based on organic materials, the so-called organic solar cells. This relatively new field can be divided into three subclasses; small molecule, dye-sensitized, and polymer-based organic solar cells.

Small molecule solar cells are fabricated by thermal evaporation of the active material. Control of the deposition processes gives easy access to different device architectures.[4] However, the vacuum based deposition technique needed for the production of this class of solar cells may prevent low cost, high throughput fabrication techniques and large area applications.

The dye-sensitized solar cell (or Grätzel cell, **Figure 1.1**) was first introduced by O'Reagan and Grätzel in 1991 and consists of a donor material (the dye, often ruthenium based) attached to a mesoporous TiO_2 network which also acts as the acceptor material.[5] An electrolyte (usually I^-/I_3^-) regenerates the dye and is responsible for the hole transport to the appropriate electrode.

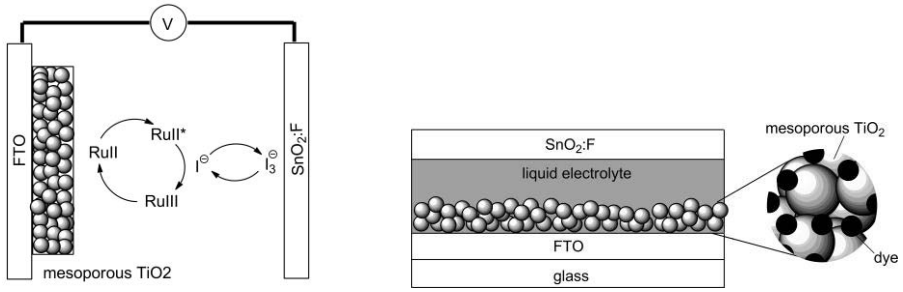

Figure 1.1: *Left: the working principle of a Grätzel cell; upon absorption of light the ruthenium(II) dye is excited and undergoes charge transfer to the TiO_2 resulting in a ruthenium(III) complex. This is regenerated by the I_3^-/I^- electrolyte couple by transferring the hole to the counter electrode. Right: a schematic representation of a Grätzel cell.*

Efficiencies up to 11.2% have been obtained using this type of solar cell. A major advantage of dye-sensitized solar cells over both other organic counter parts is that no exciton diffusion is required. Charge separation takes place immediately after excitation of the dye due to direct contact with the TiO_2 acceptor. The use of a liquid electrolyte to regenerate the dye hereafter is one of the main disadvantages of this class due to inherent stability problems associated with encapsulation of a liquid. Replacing the liquid electrolyte with a solid is the current topic of interest in this class of organic solar cells.[6]

The main advantage of polymer solar cells (from now on named organic solar cell throughout this thesis) over their inorganic and other organic counterparts is that the organic materials comprising the active layer can be solution processed allowing for low cost deposition techniques such as spin coating, doctor blading, inkjet printing, and ultimately enabling roll-to-roll production, making their production fast, cheap, and accessible for large area applications.[7] Furthermore, these cells are light-weight and flexible. The high absorption coefficient of organic materials allows organic solar cells to absorb most of the light in thin layers reducing materials usage significantly. However, compared to the traditional inorganic solar cells a big disadvantage up to now is their rather low efficiency and limited lifetime. Effort to overcome these disadvantages is undertaken by a growing number of research groups and companies which resulted in the first products entering the market in 2010.[8-10]

1.2.2.1 Brief history of the organic solar cell

In 1986, Tang and coworkers reported the first proper working solar cell made from organic materials. They combined a perylenetetracarboxylic acid diimide derivative (PV, **(1.1)**) and copper phthalocyanine (CuPc, **(1.2)**) in a bilayer device, sandwiched between two electrodes. This now so-called Tang-cell reached efficiencies of about 1%.[11] A milestone for organic photovoltaics was the observation of photoinduced

electron transfer from a conjugated polymer to C_{60} **(1.3)**.[12,13] Bilayer devices comprising these materials showed PCEs below 1%.[14]

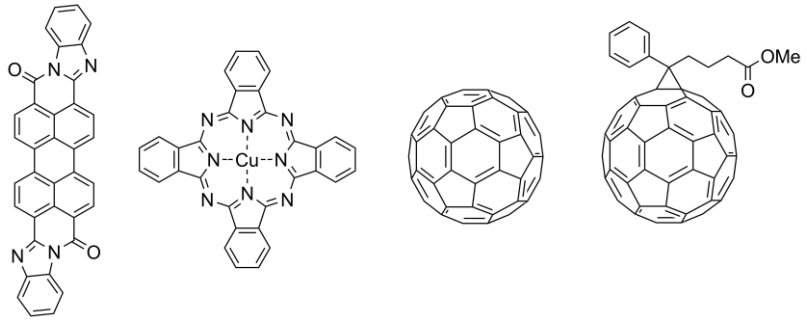

(**1.1**) (**1.2**) (**1.3**) (**1.4**)

Figure 1.2: *Perylenetetracarboxylic acid diimide derivative* ***(1.1)****, copper phthalocyanine* ***(1.2)****,* C_{60} ***(1.3)*** *and [60]PCBM* ***(1.4)****.*

A major limitation of the bilayer architecture is the limited interface between both materials whereby only excited states created in vicinity of the interface can be converted into free charges. When C_{60} was replaced by the more soluble fullerene derivative phenyl-C_{61}-butyric acid methyl ester (PCBM, **(1.4)**) a different device architecture, where both materials are mixed together in one active layer, was possible (**Figure 1.3**). This so-called bulk heterojunction architecture increases the interface area and improves the dissociation of excitons.[15] Ideally, all absorbed photons will be in the vicinity of an interface and can contribute to the generated photocurrent.

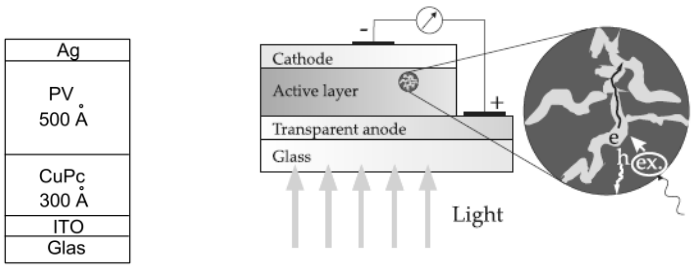

***Figure 1.3**: A schematic representation of the heterojunction Tang cell combining a perylenetetracarboxylic acid diimide derivative (PV) and copper phthalocyanine (CuPc) (left) and of a bulk heterojunction solar cell with an intimately mixed, bicontinuous, active layer (right).*

1.2.3 Working principles of organic solar cells

Compared to traditional solar cells made from inorganic semiconductors the most striking difference with organic solar cells lays in the generation of free charges. Inorganic semiconductor solar cells readily generate free charges upon light absorption.[16] Solar cells based on organic semiconductors on the other hand, produce a neutral mobile excited state (exciton) after absorption of light. Due to the low dielectric constant of the molecular materials, free charges are only generated by electron transfer to a material with a higher electron affinity. In organic solar cells a donor-acceptor system is generally employed in which the active layer consists of two materials: the donor or p-type material and the acceptor or n-type material (**Figure 1.4**).[17]

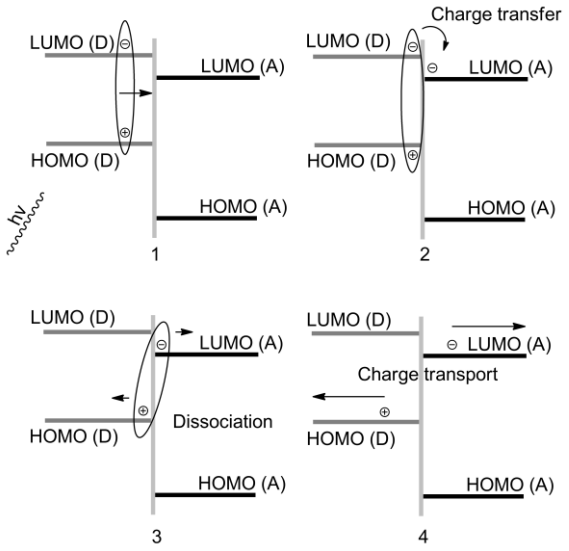

Figure 1.4: *The classical representation of the processes in the active layer of an organic solar cell; Light is absorbed by the active layer and an exciton is generated which diffuses to the interface (1). Charge transfer takes place at the interface of donor and acceptor (2). The charges are now on the different materials, but are still tightly bound and need to dissociate (3). The free charges are transported to the appropriate electrodes (4).*
However hole transfer from the excited acceptor is nowadays also recognized as an important process in organic solar cells, resulting in a mechanism that is a mirror image of that represented here.

When incident light is absorbed in the active layer an electron is excited from the HOMO into the LUMO (this can be in both the donor and the acceptor) and an excited state or so-called exciton is created. This exciton has to diffuse towards a donor-acceptor interface. This diffusion is limited to a length of 5 to 14 nm due to its limited lifetime and diffusion rate otherwise the excited state recombines.[18,19] When the exciton reaches the interface charge transfer can occur (this can be electron transfer from the excited donor material as well as hole transfer from the excited acceptor, **Figure 1.5**).

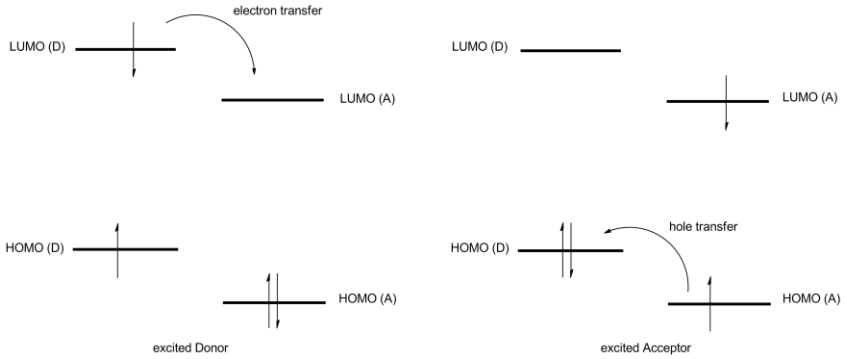

Figure 1.5: *When light is absorbed by the donor, electron transfer takes place from the LUMO of the donor to the LUMO of the acceptor. When, on the other hand, light is absorbed by the acceptor, hole transfer from the HOMO of the acceptor to the HOMO of the donor can take place.*

The driving force for this charge transfer is the difference in ionization potential and electron affinity of both materials. Photoinduced charge transfer takes place within the femtosecond range. Since competing processes like photoluminescence (~ns) and recombination (~µs) take place on much longer timescale, the charge separation is a highly efficient process.[20-22] As a result, the photoinduced charge transfer is accompanied by a strong quenching of the luminescence of the conjugated polymer.[12,13]

When the charges have been successfully separated, a bicontinuous interpenetrating network of donor and acceptor material is required to transport the free charges to the respective electrodes to provide an external current. With every new material combination the parameters for an optimal film formation have to be established.

When the charges are transported within the different phases towards the electrodes, the probability for recombination is reduced considerably, ensuring longer lifetimes of the free charges. Mobilities in conjugated polymers are around 10^{-4} cm^2/Vs, thus these longer lifetimes are also required for extracting all charges from the active layer.

However during all of the above mentioned processes energy can be lost in various stages, some of which have been mentioned shortly. First of all, not all photons are absorbed by the active layer, not only due to the bandgap of the materials, but also due to the limited thickness of the active layer. Secondly, excitons created too far from the donor-acceptor interface will decay. Even after electron transfer, geminate recombination of the initial electron hole pair (i.e. the CT state) can occur as well as bimolecular recombination of the free charges during transport to the electrodes. Nevertheless, devices with internal quantum efficiencies reaching 100% have been developed.[23]

This mechanism is also applicable to an all polymer system in which both donor and acceptor are polymers.[24,25] However, the main problem in these systems is the electron mobility, which generally is low compared to other acceptor materials. Even when good electron mobility is reached problems occur due to low dielectric constants and strong intermixing of the polymers resulting in difficulties with the separation of electron-hole pairs at the interfaces.[26-28] A method to overcome these problems with mobility and separation of charges would be to use traditional acceptor materials with improved absorption properties. The replacement of [60]PCBM with the better absorbing [70]PCBM in combination with small bandgap materials is a good example of the influence of improved light absorption by the acceptor.[29-31]

1.2.4 Morphology of the active layer

The morphology of the active layer in bulk heterojunction solar cells is of paramount importance, it determines to a large extent the efficiency of the device. Since charges can only be separated at the interface of donor and acceptor, it is important to optimize this interface area. For every new donor-acceptor combination it is a challenge to achieve an optimal morphology.

The nanophase segregated morphology initially formed in polymer fullerene blends is a kinetically trapped, non-equilibrium state that is formed during spin-casting and subsequent evaporation of the solvent at temperatures below that of the glass transition (Tg) of the polymers. In an efficient device the donor and the acceptor material will have formed a bicontinuous interpenetrating network of domains which size does not exceed the exciton diffusion length in the respective material.[18,19] If the domains are too big, the interfacial area is reduced and the exciton diffusion length is exceeded resulting in (partly luminescent) decay of photogenerated excitons. When the domains are not connected and do not form pathways to the respective electrodes, the created charge carriers are lost. However the immiscibility of both donor and acceptor and their tendency to crystallize can drive larger scale phase segregation and can cause discontinuity of the bicontinuous network. The morphology of the active layer can be manipulated during film formation or by post process treatment of the film. This can be through the choice of solvent, donor-acceptor ratio, concentration, slow drying of the active layer, the use of additives, or thermal annealing.

A striking example of solvent effects on the morphology of the active layer is the difference between spincoating PCBM:MDM-PPV solar cells from toluene or from chlorobenzene. Spincoating from chlorobenzene resulted in a decrease in domain size, e.a. an increase in interface area between the donor and acceptor, compared to that found for spincoating from toluene resulting in a threefold increase in efficiency.[32] Thermally annealing the active layer after spincoating can cause the donor polymer to partially crystallize, which can lead to increased hole mobility in the polymer phase as well as increasing its absorption properties (red shift).[33,34] Recently, new methods to optimize and stabilize the morphology of the active layer have been developed which will be discussed in more detail in Chapter 5 which consist of the addition of small amounts of volatile additives[35-38] and compatibilizers[39-42] or through locking the morphology[19,43-45] through the use of materials which are solution processable but

become insoluble after a thermal treatment thus providing better stability for the active layer.

1.2.5 Solar cell parameters with emphases on organic photovoltaics

The performance of a solar cell can be determined by measuring current-voltage (*J*-*V*) characteristics in the dark and under illumination. A proper working device shows a diode character when measured under a varied bias voltage. The parameters to calculate the power conversion efficiency can be measured when the solar cell is illuminated under conditions resembling the Sun's irradiation (1000 W/m^2). These conditions are defined as AM 1.5 which is the solar spectrum on a clear sunny day with the incoming light at an angle of 42° with the Earth's surface.[46]

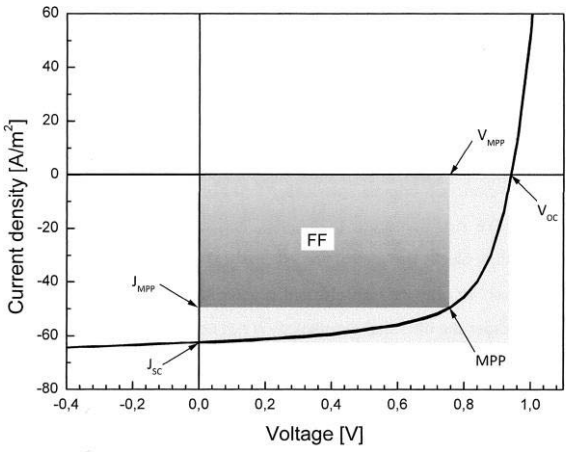

Figure 1.6: *Current-Voltage characteristic of a solar cell under illumination.*

Several parameters can be directly derived from the *J*-*V* characteristic of a solar cell (**Figure 1.6**): The short circuit current density (J_{sc}), defined as the current at zero voltage, the open circuit voltage (V_{oc}), which is the voltage when no current flows, and the maximum power point (MPP), which is the point where the product of current and voltage is maximal. An important value to determine the quality of a solar cell is its fill factor (FF), which is the ratio of the actual maximal obtained power (J_{MPP} x V_{MPP})

divided by the power given by the product of J_{sc} and V_{oc}. The fill factor depends on series and parallel resistance of the device which is *inter alia* influenced by layer thickness, balance of charge transport and quality of the electrode interfaces.[47,48] Present highly efficient organic solar cells reach fill factors of around 0.70.

$$FF = \frac{J_{MPP} * V_{MPP}}{J_{SC} + V_{OC}} \qquad (1)$$

The main characteristic of the performance of a solar cell is the power conversion efficiency η which can be calculated as follows, where P_{IN} is the incident light power density.

$$\eta = \frac{P_{MPP}}{P_{IN}} \qquad (2)$$

The short circuit current density (J_{sc}) depends on the number of absorbed photons which are converted to electrical current. It is therefore correlated to the incident light intensity, absorption properties, and generation, transportation, and collection of charges.[49] The open circuit voltage (V_{oc}) on the other hand is correlated to the difference between the highest occupied molecular orbital (HOMO) of the donor material and the lowest unoccupied molecular orbital (LUMO) of the acceptor material.[50] However, the actual value is lowered by recombination processes at the donor/acceptor interface and at the electrode interfaces. The exact origin of these recombinational losses is still under investigation.[51-53]

Additional tools to determine the quality of a solar cell are its quantum efficiencies, which define the efficiency of photon to electron conversion at a certain wavelength. One distinguishes between the external quantum efficiency (EQE) and the internal quantum efficiency (IQE). The external quantum efficiency is defined by the ratio of collected electrons to the incident photons, whereas the internal quantum efficiency defines the ratio of the conversion of absorbed photons to electrons.

It has been predicted by calculations that efficiencies of ~11% for single junction organic solar cells and ~15% for organic tandem solar cells are possible if materials with the right electrical and optical properties are used and an optimal morphology is formed.[54,55] However assumptions have been made with respect to both donor and acceptor which with the development of new materials can turn out to be outdated. A good example is the absorption of the acceptor which in the calculation was assumed to be negligible. As already addressed above, absorption of the acceptor can be important especially in small bandgap materials. Therefore even higher efficiencies are expected to be within range for organic photovoltaics.

1.3 Materials

1.3.1 Donor material, the conjugated polymer

Research on the semiconducting properties of conjugated organic polymers started in 1977 with the discovery of conductivity in a chemically doped conjugated polymer.[56,57] These conjugated materials consist of alternating single and double carbon-carbon bonds. The mutual overlap between the p_z orbitals of the carbon atoms results in delocalization of the π-electrons in extended molecular orbitals along the backbone. These delocalized π-electrons are the origin of the intrinsic semiconductor behavior of conjugated polymers. As mentioned above the charge generation as well as transport in organic semiconductors is different from traditional inorganic physics where the concepts of free charges and band conduction is used. In organic semiconductors holes and electrons move through the materials from one localized state to another, a process called hopping.[58] Compared to inorganic materials this hopping process results in a relatively low charge carrier mobility. The strength of these organic materials lies in applications where ease of processing is combined with moderate transport performance requirements.

The first generation of bulk heterojunction organic solar cells was mainly based on mixtures of poly[2-methoxy,5-(2'-ethyl-hexyloxy)-*p*-phenylene vinylene] (MEH-PPV) or

poly[2-methoxy,5-(3',7'-dimethyloctyloxy)-*p*-phenylene vinylene] (MDMO-PPV, **(1.5)**) as donor and PCBM as acceptor material. The highest reported efficiencies reached 3%, but the polymers were limited by a non-optimal light absorption and showed rather low mobilities.[59,60] The PPVs were followed by polythiophenes, in particular regioregular poly-3-hexyl-thiophene (rr-P3HT, **(1.6)**), which still remains the work horse material and benchmark in the field at present. After extensive research on methods to optimize the processing conditions of the active layer efficiencies of up to 5% were reached.[61,62]

In the past years, a variety of conjugated copolymers have been synthesized and tested as donor material in bulk heterojunction organic solar cells.[63] These polymers consist of electron rich and electron poor units, like *e.g.* fluorenes, thiophenes, carbazoles or benzothiazoles (**(1.7)** and **(1.8)**). By combining these building blocks the optical and electronical properties of the resulting polymer can be controlled. However, to prepare highly efficient organic solar cells with these polymers remains challenging; in many cases the obtained morphology is not optimal.[64-66] Nevertheless, several of these materials helped to further improve the efficiency of organic solar cells.[67,68] Recently, record efficiencies of 7.4% were reported for solar cells made from PTB7 (**1.9**).[69] The highest certified efficiencies claimed up to date were set by Solarmer in December 2009 at 7.9% (NREL 0.1 cm^2), Heliatec and Iapp in April 2010 at 7.7% (Fraunhofer Institute for Solar Energy Systems ISE in Freiburg, 1.1 cm^2) with the current world record by Konarka in December 2010 at 8.3% (NREL 1.0 cm^2).

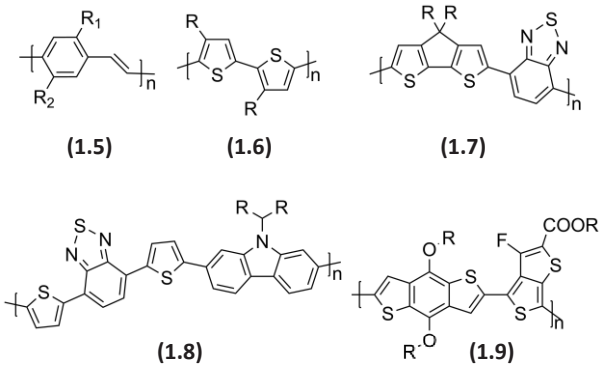

Figure 1.7: *Structures of polymers used in organic solar cells: PPV's* ***(1.5)****, rr-P3HT* ***(1.6)****, PCPDTBT* ***(1.7)****, PCDTBT* ***(1.8)*** *and PTB7* ***(1.9)****.*

1.3.2 The acceptor of choice, fullerenes

As already mentioned shortly the discovery of ultrafast (subpicosecond) electron transfer from excited conjugated polymers to C_{60} marks one of the milestones in the development of organic solar cells.[12,13] However, the limited solubility of pristine C_{60} limited the device architecture to bilayer cells until it was replaced by the more soluble fullerene derivative PCBM enabling solution processing leading to the introduction of the bulk heterojunction architecture.[14,15] This improved the power conversion efficiency (PCE) and was one of the groundbreaking steps in the development of organic solar cells.

1.3.2.1 Background

Fullerenes are carbon allotropes like diamond and graphite, however unlike these other forms fullerenes comprise the only soluble allotrope of carbon. They are spherically shaped and consist of pentagons and hexagons. The pentagons are required to provide the curvature typical for these molecules. Each fullerene consists of 12 pentagons of which each is surrounded by hexagons. This construction obeys the Eulers theorem, which states that for the closure of each spherical network of n hexagons, 12 pentagons are required with the exception of n = 1.[70,71] By definition, fullerenes obey the isolated pentagon rule (IPR). This means that every pentagon is

surrounded by hexagons only. The smallest stable structure made entirely of carbon atoms which obeys the IPR is C_{60}, called Buckminsterfullerene, named after architect Richard Buckminster Fuller who was known for his geodesic domes which underlie similar building principles as C_{60} **(1.3)**.[72] He also was the namesake for the whole class of fullerenes which proceeds with the higher fullerenes C_{70} **(1.10)**, C_{74}, C_{76}, C_{78}, C_{80}, C_{82}, C_{84} **(1.11)**, and so on.[73,74]

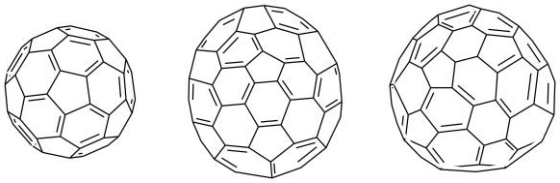

(**1.3**) (**1.10**) (**1.11**)

Figure 1.8: *C_{60}* ***(1.3)****, C_{70}* ***(1.10)*** *and one of the 24 isomers of C_{84}* ***(1.11)****.*

Since the discovery of C_{60} in 1985, fullerenes have become a subject of intense research.[75] Due to their unique chemical and physical properties a new research field developed, searching for applications *inter alia* in the field of medicine and electronics. For their role in the discovery of the fullerenes Robert F. Curl, Harold W. Kroto, and Richard E. Smalley were awarded the Nobel prize in Chemistry in 1996.[76] The trigger for fullerene research was in 1990, when Krätschmer and Huffman found a method to prepare C_{60} in large quantities by vaporizing two graphite rods in a helium atmosphere and extracting the resulting carbon condensate with organic solvents.[77,78]

Fullerenes, especially C_{60}, are known for their intrinsic properties. They are strong electron acceptors and capable of accepting up to 6 electrons.[79] Due to their low reorganization energy fullerenes are excellent electron conductors,[80,81] this combined with their solubility in organic solvents and easy functionalisation makes fullerenes interesting for applications in photovoltaics and non-linear optics like xerography or holographic imaging.[82-84]

1.3.2.2 Fullerenes for photovoltaic applications

Over the years many different polymers were developed and used as donor material in organic solar cells, but as acceptor material PCBM is still widely used. Although many attempts were made to replace PCBM by other fullerene derivatives, it still remains the n-type material of choice in organic solar cells. It shows similar crystal-packing as C_{60}, which results in a higher electron mobility, compared to other fullerene derivatives.[85] However, [60]PCBM **(1.4)** is more and more replaced by [70]PCBM **(1.12)** which has similar electronic properties but a significantly higher absorption coefficient especially at shorter wave lengths. This improved absorption can complement the light absorption of small bandgap polymers which have improved absorption towards longer wavelength, but lack absorption in the blue-green part of the solar spectrum.[29-31]

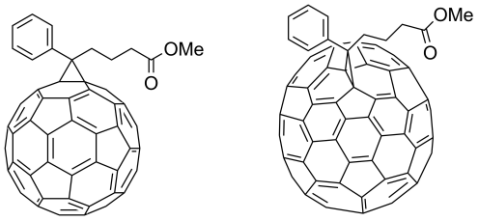

(**1.4**) (**1.12**)

Figure 1.9: *[60]PCBM **(1.4)** and one major isomer of the isomeric mixture called [70]PCBM **(1.12)**.*

1.3.2.3 Improving the fullerene acceptor for use in bulk heterojunction architectures

Improving the device performance compared to benchmark devices comprising P3HT:PCBM either consists of raising the efficiency through improved current or voltage obtained from a cell or by extending the lifetime of the cell. Methods to increase the lifetime of devices mostly consist of improving their resistance to both air and water, or by increasing the thermal stability of the active layer morphology. The latter will be briefly discussed in Chapter 5.

Because current is hard to influence through structural manipulation and depends strongly on processing conditions, the most straight forward method to improve the performance of the solar cell is through its open circuit voltage. The most direct method to influence the V_{oc} of donor-acceptor based OPV devices is to alter the offset between the LUMO of the donor and the LUMO of the acceptor. The open circuit voltage is ultimately limited by the difference between the HOMO of the donor and the LUMO of the acceptor. The offset between the LUMO of the donor and LUMO of the acceptor enables electron transfer and the offset between the HOMOs drives the hole transfer, but these offsets also result in a loss in V_{oc}. For P3HT:PCBM cells this LUMO-LUMO offset is much larger than the 0.3-0.5 eV necessary for electron transfer to occur resulting in an open circuit voltage of only 0.6 V, much smaller than the 2 eV bandgap of P3HT. It is the reduction of this LUMO-LUMO offset where a large increase in device efficiency can be gained, especially with P3HT:PCBM.

Three strategies can be employed to reduce the LUMO-LUMO offset (**Figure 1.10**).

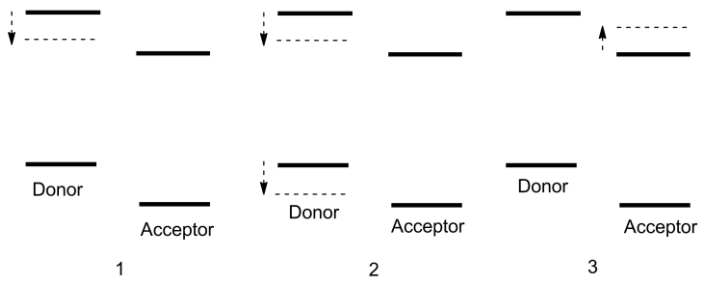

Figure 1.10: *Three possible methods for lowering the LUMO-LUMO offset between donor and acceptor; 1. Lowering the LUMO of the donor, 2. Lowering both the LUMO and the HOMO of the donor, 3. Raising the LUMO of the acceptor.*

Firstly, the LUMO of the donor can be lowered (**Figure 1.10, 1**).This does not increase V_{oc}, but potentially increases the short circuit current. By decreasing the bandgap the absorption of the donor material is extended towards longer

wavelengths resulting in an increase in the amount of absorbed photons and hence current.

Alternatively, both LUMO and HOMO level of the donor can be lowered as a whole (**Figure 1.10, 2**). This does not alter the bandgap itself and the device gains in efficiency due to a higher V_{oc}. An additional advantage is the expected air stability once the HOMO of the polymer is lower than 5.4 eV.[86]

The LUMO-LUMO offset can also be reduced by raising only the LUMO of the acceptor (**Figure 1.10, 3**). By reducing the acceptor strength the LUMO level is raised, resulting in a higher open circuit voltage. The attachment of electron donating groups or the saturation of multiple double bonds on the fullerene cage raises the LUMO energy of the resulting fullerene moiety, thereby increasing V_{oc} without negatively impacting the bandgap of the donor (and hence the ability of the OPV device to absorb light).[87] Previous work from our group has shown that introducing electron donating groups on the phenyl ring of PCBM yields a small increase in the V_{oc} of OPVs with P3HT as donor.[88] Recently, higher adducts of fullerenes were used to further increase the V_{oc} of P3HT-based OPVs by approximately 100 meV per saturated double bond (i.e., 1,2-adduct).[89,90]

1.3.3 State of the art acceptor materials

Even though many acceptors other than PCBM have been developed, among them conjugated polymers, perylenes, carbon nanotubes, inorganic semiconducting nanoparticles, and various other fullerene derivatives, non have been able to outperform PCBM. Replacing [60]PCBM with [70]PCBM has proven to be a significant efficiency improvement for various small bandgap donors due to the enhanced absorption properties of C_{70} compared to C_{60}. The biggest gain in efficiency on the acceptor side is expected to come from tuning the LUMO level of the fullerenes relative to that of the donor in order to minimize energy losses.

Synthetically modifying the fullerene LUMO level to a significant extent has proven to be challenging. Until recently, only relatively small shifts of up to ~50 mV were reported for PCBM derivatives with electron donating groups attached to the phenyl ring. An alternative method to decrease the LUMO-LUMO offset between donor and acceptor was introduced by the group of Drees who, instead of introducing addends which would result in an decrease of acceptor strength, used trimetallic nitride endohedral fullerenes, $M_3N@C_{80}$ with M = La or Lu, as a starting point, parent fullerenes possessing already a higher LUMO level than either C_{60} or C_{70}.[91] Methanofullerene derivatives were synthesized, as endohedral analogues to PCBM **(1.13)**, comprising a hexyl ester instead of a methyl ester. Devices based on P3HT:$Lu_3N@C_{80}$ showed a V_{oc} of 890 mV, the highest reported open circuit voltage for a P3HT/fullerene solar cell. This increase in open circuit resulted in efficiencies of 4-4.5% with short circuit current and fill factor similar to P3HT:PCBM. Nevertheless, as long as these endohedral fullerenes are not commercially available against reasonable prices, this class of acceptors is only of academic relevance.

The major breakthrough came from this group when it was successfully demonstrated that fullerene bisadducts, e.g. bis-PCBM **(1.14),** give a ~100 mV higher lying LUMO compared to their parent monoadducts. Even though these higher adducts consist of complex mixture of both regio and stereo isomers they brought a significant efficiency increase for P3HT based devices, due to the corresponding increase in an open circuit voltage.

Higher multiadducts, such as tris-PCBM and analogs thereof were shown to improve the V_{oc} by an additional ~100 mV, but these trisadduct mixtures were poor conductors and trapping of electrons in the active layer has so far prevented an overall increase in device efficiency.[92]

Following the introduction of higher adducts of PCBM and analogs thereof other examples of higher fullerene adducts have recently appeared in literature. Starting with the introduction of [60]ICBA **(1.15)** and [70]ICBA, bisadducts of indene with C_{60} and C_{70} respectively, by the group of Li resulted in efficiencies of 6.5% (after device optimalization) and 5.6% respectively in combination with P3HT, outperforming even the best known acceptors to date.[45,93]

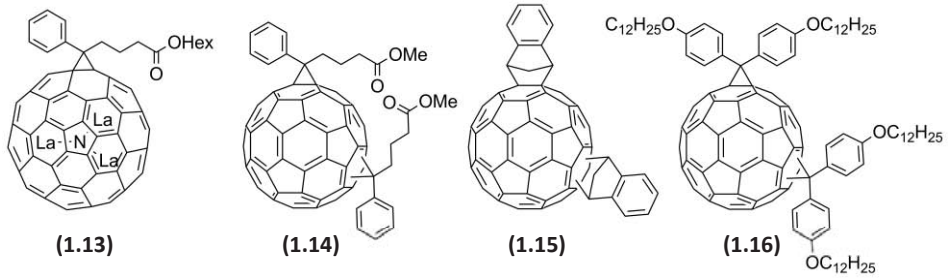

(1.13) **(1.14)** **(1.15)** **(1.16)**

Figure 1.1: *State of the art fullerene acceptors. $La_3N@C_{80}$PCBH **(1.13)**, bis-PCBM **(1.14)**, ICBA **(1.15)** and bis-DPM12 **(1.16)**.*

Recently the bisadducts analog of DPM12 **(1.16)** developed by the group of Martin was introduced. This bisadduct of DPM12 has its first reduction potential 100 mV higher than its parent monoadduct.[94] Scale up of higher adducts, compared to that of endohedral fullerenes, is not expected to become a major issue, however until now efficiency improvement has only successfully been demonstrated with devices based on P3HT.

The latest acceptors in this line are the mono- and bisadduct of diindene and C_{60}, bis-diindene (**(1.17)** and **(1.18)**), however the performance, efficiencies of 2.21% were reported for the monoadduct and 0.67% for the bisadduct in combination with P3HT, is inferior to those of previous reported indene adducts.[95] A major issue with bisadducts is the fact that many isomers can, and mostly will, be formed. This thesis addresses this issue in depth.

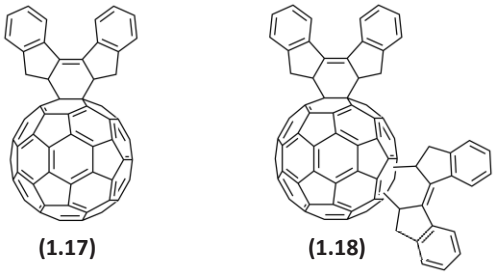

(1.17) **(1.18)**

Figure 1.12: The mono- **(1.17)** and bisadduct **(1.18)** of diindene.

1.4 Outline of this thesis

Fullerenes play an important role in the field of organic photovoltaics with new derivatives being introduced regularly. However there is still little understanding on the structural influence of these derivatives on device performance. This especially is the case with higher adducts of C_{60} which exist as complex mixtures of both regio- and stereoisomers. The aim of this thesis therefore is to develop a broader understanding of the formation of fullerene bisadducts with an emphasis on bis-PCBM and analogues thereof, their isomer distribution, single isomer characteristics and their performance in organic photovoltaic devices. A central theme in this thesis is the chemical modification of fullerenes to influence their LUMO level while maintaining the overall performance. A second theme is the control of the morphology of the active layer when bisadducts are used.

The formation and distributing of isomers of bis-PCBM as well as their influence on device performance is the main theme of Chapter 2. Both modeling as well as attempts to separate, characterize, and identify single isomers of bis-PCBM are described. Preliminary device results of the first individual isomer of bis-PCBM as acceptor material in bulk heterojunction solar cells are given.

Chapter 3 describes our efforts to synthetically reduce the number of isomers of bis-PCBM through the use of tethered addends and the effect of these subpopulations of

bis-PCBM as acceptor material on device performance compared to the full isomeric mixture.

Chapter 4 deals with the synthesis, characterization, and use in bulk heterojunction solar cells of PCBM analogs with different length alkyl spacers between the cyclopropane ring and the ester moiety. Mono- as well as bisadducts were synthesized, characterized and tested in solar cell devices.

Chapter 5 describes the synthesis, characterization and application in bulk heterojunction solar cells of fluorene containing PCBM analogues. These materials are candidates both as a substitute for PCBM and as additive to improve the morphology of the active layer in bulk heterojunction solar cells comprising PF10TBT as the donor.

Chapter 6 describes the synthesis and characterization of two series of molecular dyads made of small bandgap oligomers, consisting of thienopyrazines-thiophene and DPP-thiophene, and C_{60} end-caps at both ends. Photoinduced electron transfer between the oligomer and the fullerene was investigated through the use of femtosecond photoinduced absorption.

1.5 References

1 Parry ML, *Cambridge Univ Press, Cambridge, UK, and New York*, 2007

2 S. Solomon, G. K. Plattner, R. Knutti and P. Friedlingstein, *Proc. Natl. Acad. Sci. U. S. A.* 2009, **106**, 1704

3 M. A. Green, K. Emery, Y. Hishikawa and W. Warta, *Prog. Photovoltaics,* 2009, **17**, 320

4 J. Xue, B. P. Rand, S. Uchida and S. R. Forrest, *Adv. Mater*., 2005, **17**, 66

5 B. O'reagan and M. Grätzel, *Nature*, 1991, **353**, 737

6 U. Bach, D. Lupo, P. Comte, J. E. Moser, F. Weissörtel, J. Salbeck, H. Spreitzer and M. Grätzel, *Nature*, 1998, **395**, 583

7 C. J. Brabec and J. D. Durrant, *MRS Bull*., 2008, **33**, 607

8 H. Hoppe and N. S. Sariciftci: *Polymer Solar Cells,* S. R. Marder, K.-S. Lee (eds.): *Photoresponsive Polymers II.* Springer, Berlin/Heidelberg, 2008, **214**, 1

9 B. C. Thompson and J. M. J. Frechet, *Angew. Chem. Int. Ed*., 2008, **47**, 58

10 G. Dennler, M. C. Scharber and C. J. Brabec, *Adv. Mater.,* 2009, **21**, 1323

11 C. W. Tang, *Appl. Phys. Lett.,* 1986, **48**, 183

12 N. S. Sariciftci, L. Smilowitz, A. J. Heeger and F. Wudl, *Science,* 1992, **258**, 1474

13 B. Kraabel, C. H. Lee, D. Mcbranch, D. Moses, N. S. Sariciftci and A. J. Heeger, *Chem. Phys. Lett.*, 1993, **213**, 389

14 N. S. Sariciftci, D. Braun, C. Zhang, V. I. Srdanov, A. J. Heeger, G. Stucky and F. Wudl, *Appl. Phys. Lett.*, 1993, **62**, 585

15 G. Yu, J. Gao, J. C. Hummelen, F. Wudl and A. J. Heeger, *Science,* 1995, **270**, 1789

16 P. Würfel, *Physics of solar cells : from principles to new concepts*, Wiley-VCH, Weinheim, 2005

17 P. Würfel, *Chimia,* 2007, **61**, 770.

18 J. J. M. Halls, K. Pichler, R. H. Friend, S. C. Moratti and A. B. Holmes, *Appl. Phys. Lett.,* 1996, **68**, 3120

19 D. E. Markov, E. Amsterdam, P. W. M. Blom, A. B. Sieval and J. C. Hummelen, *J. Phys. Chem. A,* 2005, **109**, 5266

20 I. Montanari, A. F. Nogueira, J. Nelson, J. R. Durrant, C. Winder, M. A. Loi, N. S, Sariciftci and C. J. Brabec, *Appl. Phys. Lett*., 2001, **81**, 3001

21 A. F. Nogueira, I. Montari, J. Nelson, J. R. Durrant, C. Winder, N. S. Saraciftci and C. J. Brabec, *J. Phys. Chem. B*, 2003, **107**, 1567

22 J. Nelson, *Phys. Rev. B*, 2003, **67**, 155209

23 S. H. Park, A. Roy, S. Beaupré, S. Cho, N. Coates, J. S. Moon, D. Moses, M. Leclerc, K. Lee and A. J. Heeger *Nature Photonics,* 2009, **3**, 297

24 J. J. M. Halls, C. A. Walsh, N. C. Greenham, E. A. Marseglia, R. H. Friend, S. C. Moratti and A. B. Holmes, *Nature*, 1995, **376**, 498

25 C. R. McNeill, A. Abrusci, J. Zaumseil, R. Wilson, M. J. McKiernan, J. H. Burroughes, J. J. M. Halls, N. C. Greenham and R. H. Friend, *Appl. Phys. Lett*., 2007, **90**, 193506

26 A. J. Breeze, Z. Schsinger, S. A. Carter, H. Teilan and H. H. Hörhold, *Sol. En. Mater. Sol. Cells*, 2004, **83**, 63

27 P. A. C. Quist, T. J. Savenije, M. M. Koetse, S. C. Veenstra, J. M. Kroon and L. D. A. Siebbeles, *Adv. Funct. Mater*., 2005, **15**, 469

28 M. M. Mandoc, W. Veurman, L. J. A. Koster, B. de Boer and P.W. M. Blom, *Adv. Funct. Mater*., 2007, **17**, 2167

29 S. Yoo, W. J. Potscavage, B. Domercq, J. Kim, J. Holt and B. Kippelen, *Appl. Phys. Lett.,* 2006, ***89***, 233516

30 Y. Yao, C. J. Shi, G. Li, V. Shrotriya, Q. B. Pei and Y. Yang, *Appl. Phys. Lett.,* 2006, **89**,153507

31 M. M. Wienk, J. M. Kroon, W. J. H. Verhees, J. Knol, J. C. Hummelen, P. A. van Hal and R. A. J. Janssen, *Angew. Chem. Int. Ed*., 2003, **42**, 3371

32 S. E. Shaheen, C. J. Brabec, N. S. Sariciftci, F. Padinger, T. Fromhertz and J. C. Hummelen, *Appl. Phys. Lett.*, 2001, **78**, 841

33 F. Padinger, R. S. Rittberger and N. S. Sariciftci, *Adv. Funct. Mater*., 2003, **13**, 85

34 G. Li, V. Shrotriya, J. Huang, Y. Yao, T. Moriarty, K. Emery and Y. Yang, *Nat. Mater*., 2005, **4**, 864

35 J. K. Lee, W. L. Ma, C. J. Brabec, J. Yuen, J. S. Moon, J. Y. Kim, K. Lee, G. C. Bazan and A. J. Heeger, *J. Am. Chem. Soc*., 2008, **130**, 3619

36 B. Park, Y. H. Huh and M. Kim, *J. Mater. Chem*., 2010, **20**, 10862

37 Y. I. Lee, M. Kim, Y. H. Huh, J. S. Lim, S. C. Yoon and B. Park*, Sol. Energy. Mater. Sol Cells.*, 2010, **94**, 1152

38 C. S. Kim, L. L. Tinker, B. F. DiSalle, E. D. Gomez, S. Lee, S. Bernhard and Y. Loo, *Adv. Mater*., 2009, **21**, 3110

39 J. B. Kim, K. Allen, S. J. Oh, S. Lee, M. F. Toney, Y. S. Kim, C. R. Kagan, C. Nuckolls and Y. Loo, *Chem. Mater*., 2010, **22**, 5762

40 J. U. Lee, J. W. Jung, T. Emrick, T. P. Russel and W. H. Jo, *J. Mater. Chem*. 2010, **20**, 3287

41 C. Yang, J. K. Lee, A. J. Heeger and F. Wudl, *J. Mater. Chem*., 2009, **19**, 5416

42 K. Sivula, Z. T. Ball, N. Watanabe and J. M. J. Fréchet, *Adv. Mater*., 2006, **18**. 206

43 Y. Cheng, C. Hsieh, Y. He, C. Hsu and Y. Li, *J. Am. Chem. Soc*., 2010, **132**, 17381

44 V. A. Kostyanovsky, D. K. Susarova, A. S. Peregudov and P. A. Troshin, *Thin Solid Films*, 2010, **519**, 4119

45 B. Gholamkhass and S. Holdcroft, *Chem. Mater*., 2010, **22**, 5371

46 J. M. Kroon, M. M. Wienk, W. J. H. Verhees and J. C. Hummelen, *Thin Solid Films*, 2002, **403**, 223

47 V. D. Mihailetchi, J. Wildeman and P. W. M. Blom, *Phys. Rev. Lett.,* 2005, **94** , 126602

48 M. S. Kim, B. G. Kim and J. Kim, *ACS Appl. Mater. Interfaces,* 2009, **1**, 1264

49 P. W. M. Blom, V. D. Mihailetchi, L. J. A. Koster and D. E. Markov, *Adv. Mater*., 2007, **19**, 1551

50 L. J. A. Koster, V. D. Mihailetchi, R. Ramaker and P. W. M. Blom, *Appl. Phys. Lett*., 2005, **86**, 123509

51 V. D. Mihailetchi, L. J. A. Koster, J. C. Hummelen and P. W. M. Blom, *Phys. Rev. Lett.*, 2004, **93**, 216601

52 L. J. A. Koster, E. C. P. Smits, V. D. Mihailetchi and P. W. M. Blom, *Phys. Rev. B*, 2005, **72**, 085205

53 D. Veldman, O. Ipek, S. C. J. Meskers, J. Sweelssen, M. M. Koetse, S. C. Veenstra, J. M. Kroon, S. S. van Bavel, J. Loos and R. A. J. Janssen, *J. Am. Chem. Soc*., 2008, **130**, 7721

54 G. Dennler, M. C. Scharber, T. Ameri, P. Denk, K. Forberich, C. Waldauf and C. J. Brabec, *Adv. Mater.,* 2008, **20**, 579

55 M. C. Scharber, D. Wuhlbacher, M. Koppe, P. Denk, C. Waldauf, A. J. Heeger and C. L. Brabec, *Adv. Mater.,* 2006, **18**, 789

56 C. K. Chiang, C. R. Fisher, Y. W. Park, A. J. Heeger, H. Shirakawa, E. J. Louis, S. C. Gau and A. G. MacDiarmid, *Phys. Rev. Lett*., 1977, **39**, 1098

57 H. Shirakawa, E. J. Louis, A. G. MacDiarmid, C. K. Chiang and A. J. Heeger, *J. Chem. Soc. Chem. Commun*., 1977, 578

58 D. Hertel and H. Bassler, *ChemPhysChem*., 2008, **9**, 666

59 C. J. Brabec, S. E. Shaheen, C. Winder, N. S. Sariciftci and P. Denk, *Appl. Phys. Lett.,* 2002, **80**, 1288

60 V. D. Mihailetchi, L. J. A. Koster, P. W. M. Blom, C. Melzer, B. de Boer, J. K. J. van Duren and R. A. J. Janssen, *Adv. Funct. Mater.,* 2005, **15**, 795

61 W. L. Ma, C. Y. Yang, X. Gong, K. Lee and A. J. Heeger, *Adv. Funct. Mater.,* 2005, **15**, 1617

62 M. D. Irwin, B. Buchholz, A. W. Hains, R. P. H. Chang and T. J. Marks, *Proc. Natl. Acad. Sci. U. S. A.,* 2008, **105**, 2783

63 R. Kroon, M. Lenes, J. C. Hummelen, P. W. M. Blom and B. De Boer, *Polym. Rev.,* 2008, **48**, 531

64 L. M. Campos, A. Tontcheva, S. Gunes, G. Sonmez, H. Neugebauer, N. S. Sariciftci and F. Wudl, *Chem. Mater.,* 2005, **17**, 4031

65 M. Lenes, M. Morana, C. J. Brabec and P. W. M. Blom, *Adv. Funct. Mater.,* 2009, **19**, 1106

66 F. L. Zhang, E. Perzon, X. J. Wang, W. Mammo, M. R. Andersson and O. Inganäs, *Adv. Funct. Mater.,* 2005, **15**, 745

67 J. Peet, J. Y. Kim, N. E. Coates, W. L. Ma, D. Moses, A. J. Heeger and G. C. Bazan, *Nat. Mater.,* 2007, **6**, 497

68 S. H. Park, A. Roy, S. Beaupre, S. Cho, N. Coates, J. S. Moon, D. Moses, M. Leclerc, K. Lee and A. J. Heeger, *Nat. Photonics,* 2009, **3**, 297

69 Y. Liang, Z. Xu, J. Xia, S.-T. Tsai, Y. Wu, G. Li, C. Ray and L. Yu, *Adv. Mater.,* 2010, **22**, E135

70 T. G. Schmalz, W. A. Seitz, D. J. Klein and G. E. Hite, *Chem. Phys. Lett.,* 1986, **130**, 203

71 H. W. Kroto, *Nature,* 1987, **329**, 529

72 H. W. Kroto, A. W. Allaf and S. P. Balm, *Chem. Rev.,* 1991, **91**, 1213

73 B. L. Zhang, C. Z. Wang and K. M. Ho, *Chem. Phys. Lett.,* 1992, **193**, 225

74 F. Diederich, R. Ettl, Y. Rubin, R. L. Whetten, R. Beck, M. Alvarez, S. Anz, D. Sensharma, F. Wudl, K. C. Khemani and A. Koch, *Science,* 1991, **252**, 548

75 H. W. Kroto, J. R. Heath, S. C. Obrien, R. F. Curl and R. E. Smalley, *Nature,* 1985, **318**, 162

76 http://nobelprize.org/nobel_prizes/chemistry/laureates/1996/press.html

77 W. Krätschmer, K. Fostiropoulos and D. R. Huffman, *Chem. Phys. Lett.,* 1990, **170**, 167

78 W. Krätschmer, L. D. Lamb, K. Fostiropoulos and D. R. Huffman, *Nature,* 1990, **347**, 354.

79 Q. S. Xie, E. Perezcordero and L. Echegoyen, *J. Am. Chem. Soc.,* 1992, **114**, 3978

80 H. Imahori and Y. Sakata, *Eur. J. Org. Chem.,* 1999, 2445

81 D. M. Guldi, *Chem. Commun.,* 2000, 321

82 H. S. Nalwa, *Adv. Mater.,* 1993, **5**, 341

83 S. Köber, F. Gallego-Gomez, M. Salvador, F.B. Kooistra, J.C. Hummelen, K. Aleman, S. Mansurova and K. Meerholz, *J. Mater. Chem.,* 2010*,* **20** , 6170

84 S. Köber, J. Prauzner, M. Salvador, F.B. Kooistra, J.C. Hummelen, K. Meerholz, *Adv. Mater.,* 2010 , **22**, 1383

85 M. T. Rispens, A. Meetsma, R. Rittberger, C. J. Brabec, N. S. Sariciftci and J. C. Hummelen, *Chem. Commun.,* 2003, 2116

86 J. Locklin, M. M. Ling, A. Sung, M. E. Roberts and Z. Bao, *Adv. Mater*., 2006, **18**, 2989

87 C. J. Brabec, A. Cravino, D. Meissner, N. S. Sariciftci, T. Fromherz, M. T. Rispens, L. Sanchez and J. C. Hummelen, *Adv. Funct. Mater*., 2001, **11**, 374

88 F. B. Kooistra, J. Knol, F. Kastenberg, L. M. Popescu, W. J. H. Verhees, J. M. Kroon and J. C. Hummelen, *Org. Lett*., 2007, **9**, 551.

89 M. Lenes, G. A. H. Wetzelaer, F. B. Kooistra, S. C. Veenstra, J. C. Hummelen and P. W. M. Blom, *Adv. Mater*, 2008, **20**, 2116.

90 Y. He, H. Chen, J. Hou and Y. Li, *J. Am. Chem. Soc*., 2010, **132**, 1377

91 R. B. Ross, C. M. Cardona, D. M. Guldi, S. G. Sankaranarayanan, M. O. Reese, N. Kopidakis, J. Peet, B. Walker, G. C. Bazan, E. Van Keuren, B. C. Holloway and M. Drees, *Nat. Mater.*, 2009, **8**, 208

92 M. Lenes, S. W. Shelton, A. B. Sieval, D. F. Kronholm, J. C. Hummelen and P. W. M. Blom, *Adv. Funct. Mater.*, 2009, **19**, 3002

93 Y. He, G. Zhou, B. Peng and Y. Li, *Adv. Funct. Mater*. 2010, **20**, 3383

94 N. Martin, J. L. Delgado and S. Filippone, *Meet. Abstr. - Electrochem. Soc.*, 2009, **901,** 1119

95 Y. He, H. Chen, G. Zhao, J. Hou and Y. Li, *Solar Energy Mater. Solar Cells*, 2011, **95**, 899

Chapter 2

Bisadduct analogues of PCBM and their use in bulk heterojunction solar cells

Abstract. This chapter describes the synthesis of bis-PCBM, the reactivity of its monoadduct parent PCBM, and explores the isomeric nature of this [60]fullerene bisadduct. An understanding of the isomeric composition is sought through molecular modeling of the individual bisadducts and the reactivity of PCBM. Attempts to isolate single isomers through a combination of column chromatography and preparative HPLC were undertaken. The resulting isomers (or isomer subfractions) were analyzed with NMR and their electronic properties were examined with cyclic voltammetry. Preliminary results in bulk heterojunction solar cells are presented at the end.

Part of the work described in this chapter is a cooperation with Dr J. Dennis from Queen Mary University London. Device fabrication and testing was perfomed by W. Zou and G. A. H. Wetzelaer.

2.1 Introduction

2.1.1 Higher fullerene adducts as n-type materials

Higher adducts of C_{60} (that is, adducts with two or more addends added to the fullerene cage) are attracting increased attention as acceptor material in organic bulk heterojunction solar cells. Bis-PCBM **(2.1)** was introduced in 2008,[1,2] followed by bis-ThCBM[3] and tris-PCBM,[3] and recently ICBA **(2.2),**[4-6] its dimeric addend diindene,[7] and the bisadduct analog of DPM12.[8-11] A PCE of 4.5% was reached with bis-PCBM combined with rr-P3HT in bulk heterojunction solar cells.[1]

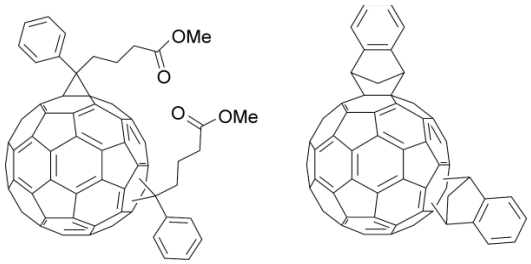

(2.1) **(2.2)**

Figure 2.1: *Bis-PCBM and ICBA, two of the best performing fullerene bisadducts in organic photovoltaics.*

Even higher efficiencies for a ICBA:P3HT cell (6.48%) have been claimed after optimalization of the active layer.[12] The main improvement compared to monoadducts is the increased open circuit voltage that is obtained with bisadducts due to their higher LUMO energy compared to their monoadduct analogues, thus decreasing the LUMO-LUMO offset between donor and acceptor, a major loss factor in organic solar cells especially those comprising P3HT as donor material. The V_{oc} is enhanced by roughly 100 mV per saturated double bond in the case of doubly cyclopropanated adducts as, for example bis-PCBM and by as much as ~140 mV in the case of ICBA.[1,4,8] However there are some major drawbacks to these higher adducts as n-type materials that are inherent to their nature.

2.2 Fullerene bisadducts

2.2.1 Reactivity and formation of adducts

Reactions of fullerenes are driven by the release of strain energy from the bent (pyramidalized) "sp^2" bonds. C_{60} has two types of bonds; the longer [5,6]-bonds (1.45 Å) which are shared between hexagons and pentagons and the shorter, more strained, [6,6]-bonds (1.38 Å) which are located between adjacent hexagons and exhibit more pronounced double bond character and, as a consequence, are susceptible to a broad variety of addition reactions such as cycloadditions leading to the most efficient release of strain energy.[13]

PCBM and its bisadduct analogue bis-PCBM, both methanofullerenes, are formed in the same reaction through 1,3-dipolar diazoalkane addition (**Figure 2.2**).[14] The reactive diazoalkane compound is generated *in situ* through deprotonation and heating of the appropriate tosylhydrazone in the presence of C_{60}. Addition occurs to a [6,6]-double bond of the fullerene framework resulting in a 5-membered dinitrogen containing ring: a diazoline.

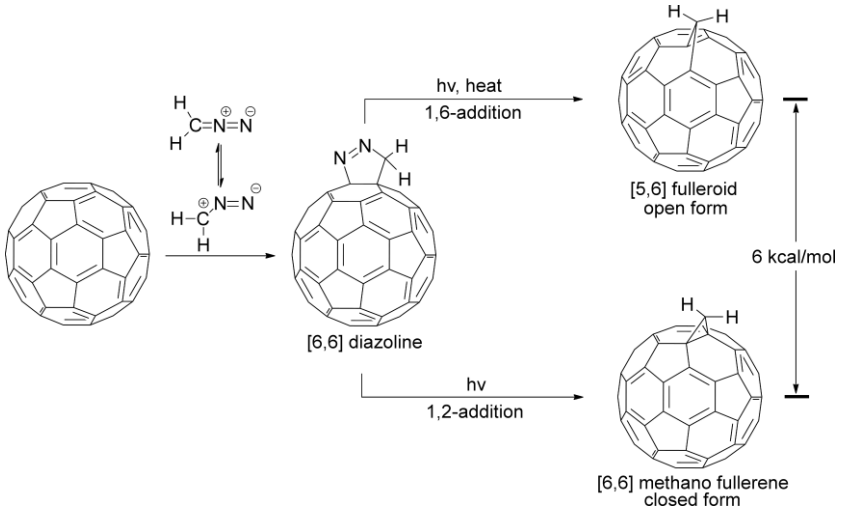

Figure 2.2: *Mechanism of the 1,3-dipolar cycloaddition of diazoalkanes to C_{60}.*

This fullerodiazoline intermediate readily eliminates N_2 to yield a [5,6] open fulleroid. The open form isomerizes catalyzed by light, heat, acid, or by electrochemical reduction to the thermodynamically more stable [6,6] closed form. This isomerization step is a di-π-methane (Zimmermann) rearrangement.[15,16] The addition reaction does not solely form monoadducts, but also higher adducts are formed as in later stages of the reaction the concentration of monoadduct increases and addition to monoadduct competes with addition to pristine C_{60} and a statistical mixture forms. In principle, separation of the addition products can be achieved by column chromatography.

2.2.2 Bisadduct isomers

As mentioned in Chapter 1, bis-PCBM as all higher adducts of C_{60} obtained through subsequent additions, consists of a mixture of isomers. The inherent regioselectivity of this second addition to the fullerene framework is only moderate, leading to the formation of mixtures of often difficult to separate regioisomers.[17] C_{60} has I_h symmetry making all 30 [6,6]-double bonds available for addition equivalent ensuring that the monoadduct is isomerically pure (this is not the case with C_{70} and higher fullerenes). After a first addition to either one of the [6,6]-double bonds of the fullerene core, the remaining 29 [6,6]-double bonds that are still available have lost their equivalence. Due to the high symmetry of C_{60} a second addition to one of the remaining 29 [6,6]-double bonds results in only eight different regioisomers, which can be officially and unambiguously named by IUPAC nomenclature[18] or by indicating their relative addition pattern as proposed by Hirsch *et al.*[19] If two symmetric but structurally different addends are used the formation of a ninth isomer is possible upon double cyclopropanation depending on the orientation of the equatorial site with respect to the first addend. Attack can take place at either of two different equatorial sites*, e'* or *e"*. For identical addends attack at either of both *e* sites leads to the same product and only eight regioisomers are possible.

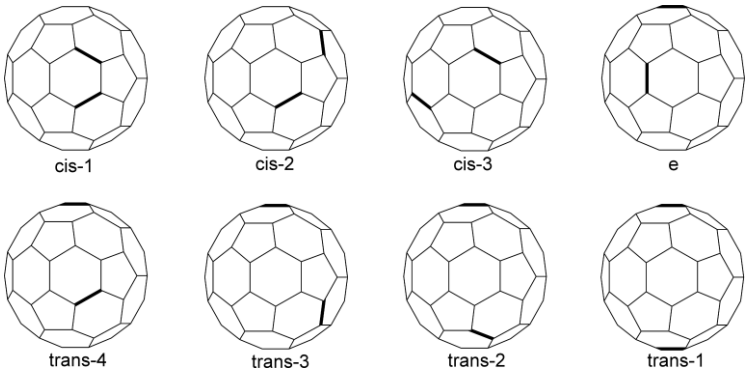

Figure 2.3: *Regioisomers of bisadducts of C_{60}. Bold bonds indicate the attachment points of the addends.*

In principle one can distinguish three different groups of bisadduct addition patterns based on their symmetry: C_2 (*cis-3*, *trans-2* and *trans-3*), C_s (*cis-1* and *cis-2*, *trans-4* and *e*) and D_{2h} (*trans-1*).

However this maximum of nine different isomers is only true when both addends are structurally the same and C_{2v} symmetric. For bis-PCBM having two structurally identical but non-symmetric addends, i.e. the bridging carbon atom of the cyclopropanyl has two different sidegroups, this is unfortunately not the case. Multiple stereoisomers can be formed at each addition position, based on the relative orientation of the addends.

2.2.3 Regioselectivity of bisadditions

Tremendous effort has been undertaken by different research groups in analyzing and understanding the different bisadduct mixtures of C_{60} obtained from double cyclopropanation.[20-29] It was found that the formation of bisadducts of [60]methanofullerenes does not proceed statistically, but with a preference for attack at the *e* and *trans-3* bonds for sterically demanding addends and at *e*, *trans-3* and *cis-1* bonds for sterically less demanding addends. Attack at the *e"* position is slightly preferred over that at *e'*. For even higher additions the regioselectivity, especially that

of *e* additions, becomes successively more pronounced; this explains, for example, the high regioselectivity towards T_h-symmetric hexakisadducts. However the bisadducts used in these studies consist mostly of small, rigid and most importantly symmetric addends, limiting the possible isomers that can be formed to the regioisomers only.

For reactions under kinetic control, nucleophilic cycloadditions to [6,6]-double bonds, such as cyclopropanation used to from PCBM fall into this category, there is little difference in isomer distribution for the various bisadduct regioisomers. Reversible additions to the fullerene cage can potentially lead to the thermodynamically most stable isomer as the only reaction product, however this is mostly the case for even higher adducts, as for example, with the synthesis of octahedral hexaadducts of T_h symmetry.

2.2.4 Relative orientation of C_s symmetric addends

For a bisadduct having two identical but non-symmetric addends, like bis-PCBM (and also ICBA), the number of possible bisadduct isomers further increases when the relative orientation of the addends is considered. For non-symmetric addends the first addition leads to a division of the fullerene cage into two different sides. For PCBM, for example, the second addend can either add to the phenyl side or to the ester side of the monoadduct. This would double the number of isomers that are possible. However because the second addend is also non-symmetric each addition can occur in two different orientations of the second addend resulting in up to four possibilities for *cis-1*, *cis-2*, *cis-3*, *trans-4*, *trans-3* and *trans-2*; the phenyl groups can either point towards each other (which we will denote as **endo-endo**), away from each other (**exo-exo**), or one phenyl points towards the ester moiety (**endo-exo** or **exo-endo**). For the *e* isomers there are only two orientations possible. The second addend can add with either the phenyl group or the ester group pointing towards the first addend. The *trans-1* isomer has, because of its symmetry only two possible orientations: the phenyl can point in the same direction or one phenyl can point towards an ester group. This increases the

number of possible isomers to 22.

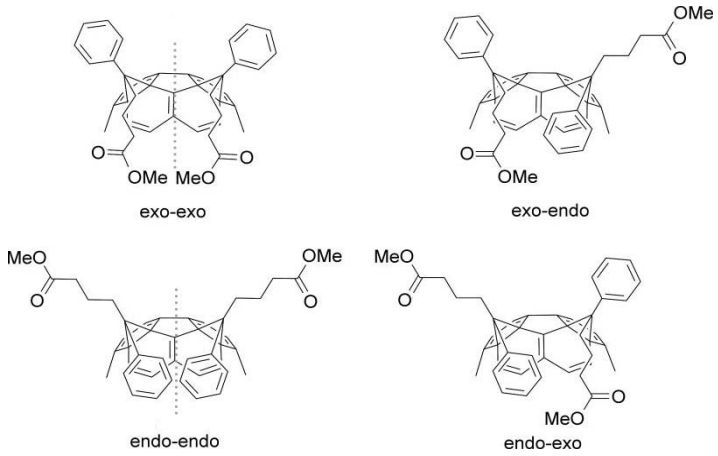

Figure 2.4: *The four possible orientations of the two addends of bis-PCBM with respect to each other.*

2.2.5 Chirality

The number of bisadduct isomers can increase even further when chirality is also considered. When two stereoisomers of an adduct form diastereoisomers, they will show up as two distinctly different isomers with different physical properties and detection and isolation is possible on a achiral stationary phase.[30] The C_2 symmetric *cis-3*, *trans-3* and *trans-2* addition patterns are inherently chiral, that is, addition of any two addends (identical or different, symmetric or not, chiral or achiral) will lead to a chiral molecule. For bis-PCBM this means that for these regioisomers those with both phenyl groups pointing towards each other and those with the phenyls pointing away from each other are chiral. This results in the formation of enantiomers, however, because we use achiral stationary phases in chromatographic analysis this does not increase the observed number of isomers. The other possible isomer is not C_2 symmetric due to the orientation of the addends and therefore two different isomers are formed. This increases the number of isomers by three, one for each non-

symmetric *cis-3*, *trans-3* and *trans-2*. Thus leading to a total of 25 regio- and stereoisomers, of which several are chiral.

The *cis-1*, *cis-2* and *trans-4* addition patterns include a mirror plane and become chiral only when two different addends are used. These addition patterns are therefore termed noninherently chiral. Even though bis-PCBM has two identical addends due to their C_s symmetry two of the four stereoisomers (**endo-exo** and **exo-endo**) can still be chiral, the other isomers (**endo-endo** and **exo-exo**) still have a mirror plane. However these will result in enantiomers only and will not influence the number of observed isomers, in our case.

The remaining *trans-1* pattern is always achiral unless the addends include asymmetric carbon centers. For the *e* addition patterns the bridging carbon atoms become stereogenic centers, resulting in enantiomers, when two identical, but non-symmetric addends, i.e. carrying two different substituents at the bridging carbon atoms, are added, but the addition pattern itself remains achiral.

2.2.6 Methanofullerene or homofulleroid

Up till now we have assumed that all bis-PCBM isomers are [6,6] closed methanofullerenes, similar to their parent fullerene monoadduct. The most direct confirmation of this would be obtained from the bond lengths in the crystal structure of all individual isomers. This would require the isolation of all isomers and their subsequent crystallization. However, also ^{13}C NMR can give a good indication on the nature of the addends without the need for full separation and crystallization. The closed [6,6]methanofullerene has two sp^3 carbon atoms at the bridgehead positions, in the open [6,6]homofullerene these carbon atoms are sp^2 hybridized. This difference is easily distinguished in ^{13}C NMR: the sp^3 carbon atoms at the bridgehead positions resonate between 70-90 ppm, whereas the sp^2 carbon atoms are found in the region of 130-150 ppm together with all other carbon atoms of the fullerene sphere.[31]

Experiment, supported by calculations, shows that for PCBM the closed [6,6]methanofullerene is the lowest energy isomer compared to both open [5,6] and open [6,6]homofullerene isomeric structures by about 6 kcal.[15,32] Does this also hold for the higher adducts? The [6,6]homofullerenes should lead to a less strained structure at least compared to the cyclopropanyl ring that is otherwise formed. However due to the second functionalization the overall strain should be even lower than that for the monoadducts, the need for extra strain release would therefore be expected to be even lower. It is therefore not surprising that many of the bridgehead carbon atoms appear in the region of 70-90 ppm. However due to the large number of sp^2 cage carbon atoms in the full isomer mixture it cannot be excluded through ^{13}C NMR alone that there are no [5,6] open isomers present. To be absolutely sure, ^{13}C NMR spectra (or crystal structures) of all individual isomers must be collected to identify their bridgehead carbons. Because this is not yet possible, we must make due with a combination of high resolution ^{13}C NMR on the full isomeric mixture combined with molecular modeling indicating strongly that all isomers of bis-PCBM exist as closed [6,6]methanofullerenes. The less strained [6,6]homofullerenes do not appear to be formed according to molecular modeling in which all regio- and stereoisomers have both bridgehead carbons within the distance of a C-C single bond length.

2.3 Reactivity of parent monoadducts

2.3.1 Bond length distortion

Hirsch and coworkers have tried to relate the isomer distribution to the bond lengths and thus the distortion of the carbon framework from the high symmetry sphere shape of monoadducts, hoping they could predict the isomer distribution for subsequent additions.[20] By comparing the bond lengths between the crystal structures of monoadducts $C_{61}(anisyl)_2$ and $C_{61}(COOEt)_2$ they showed that the distortion of the fullerene cage was independent of the first addend.

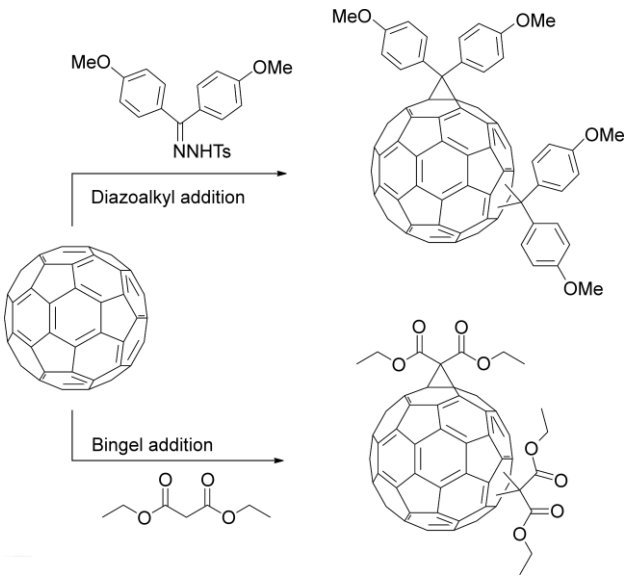

Figure 2.5: *Two of the bisadducts investigated by the group of Hirsch.*

In both cases the same distortion of the fullerene cage was observed, namely, a significant shortening of the *cis-1* bonds and, to a somewhat lesser extent of the *e"* bonds resulting in a compression of the carbon framework along the horizontal axis.

They found the same trend for the calculated (AM1) structures.[20] The *cis-1* bonds are shortened and to a lesser extent the *e"* bonds as well. The *cis-2* and *cis-3* bonds are found to be somewhat elongated, but the *trans* double bonds on the opposing hemisphere are almost not disturbed. They found that these trends were rather insensitive to the nature of the addend.

They also calculated that similarly to the bond length distortions, the polarization (AM1 Mulliken charges) of the carbon framework in the monoadducts under investigation was somewhat larger in the neighborhood of the first addend, but essentially zero in the opposing hemisphere. However due to the high degree of

freedom possessed by the ester groups, we could not perform these calculations for bis-PCBM.

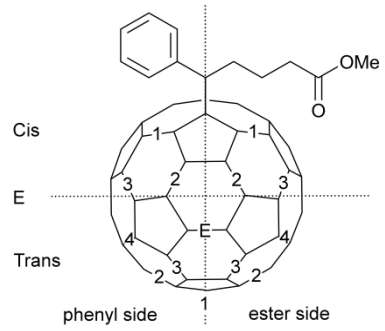

Figure 2.6: *The various double bonds on the PCBM carbon cage.*

Similar comparison between the bond lengths of the different double bonds of PCBM is somewhat more complex. After the first addition the C_s symmetric addend divides the fullerene into two halves; a phenyl side and a ester side (**Figure 2.6**). These halves are further divided in the normal way; *cis* for the same hemisphere, *trans* for opposing hemispheres and *e* for the equator. There are two different *e* sites, one that is on the horizontal axis of which both bonds are the same and one that is parallel with the vertical axis of which one bond is on the ester side and one on the phenyl side.

Two crystal structures are known for PCBM: one of crystals obtained from chlorobenzene and one of crystals obtained from dichlorobenzene.[33] The bond lengths of the C-C double bonds obtained from these crystal as well as those obtained from molecular modeling are compared to those of pristine C_{60}. The differences in bond lengths are given in **Table 2.1**.

	Crystal ODCB		Crystal CB		PM3		AM1	
	ester	phenyl	ester	phenyl	ester	phenyl	ester	phenyl
Cis-1	-0.015	-0.013	-0.012	-0.012	-0.009	-0.009	-0.009	-0.009
Cis-2	0.001	-0.001	0.001	-0.001	0.002	0.002	0.002	0.002
Cis-3	0.007	-0.002	0.001	-0.001	0.002	0.002	0.001	0.001
e vert	0.003	0.006	0.002	0.004	-0.001	-0.001	0.000	0.000
e hor	-0.003	-0.003	-0.003	-0.003	-0.001	-0.001	-0.001	-0.001
Trans-4	-0.006	-0.001	-0.004	-0.002	0.000	0.000	0.000	0.000
Trans-3	0.002	0.003	0.001	0.001	0.000	0.000	0.000	0.000
Trans-2	0.000	-0.005	-0.004	-0.002	0.000	0.000	0.000	0.000
Trans-1	-0.006	-0.006	-0.001	-0.001	0.000	0.000	0.000	0.000

Table 2.1: *Differences in C-C double bond length determined from crystals structures and molecular modeling of PCBM compared to those of pristine C_{60}. Highlighted are the bonds that are shortened compared to pristine C_{60}.*

In all cases the *cis-1* double bond is shortened the most. Next most shortened is the $e_{(hor)}$ bond, hence the *cis-1* position should be the most reactive bond in perspective of the release of strain energy. This is the case for addends that are less sterically demanding than in bis-PCBM. In that case the *cis-1* isomer is the major product. However for more sterically demanding addends, as is the case for bis-PCBM, the *cis-1* addition pattern cannot be formed, leaving the $e_{(hor)}$ as the most reactive bond. AM1 calculations show shortening of only *cis-1* and $e_{(hor)}$, PM3 calculations also shows shortening of these bonds, but also of $e_{(vert)}$. Both crystal structures show similar shortening of the bonds compared to pristine C_{60}, but differ from calculations as such that in both crystal structures the *trans* double bonds are also shortened dramatically, especially in the ODCB case. In the crystal structures there is a difference between the ester side and the phenyl side of the cage. The *cis* double bonds are shortened on the phenyl side (for the ODCB also the *trans-2*) and elongated at the ester side. However these are only moderate differences. They would suggest that the phenyl side is more reactive, perhaps due to π-π overlap between the phenyl ring and the fullerene cage.

However these differences do not appear in the calculated bond lengths which could mean that these are caused by interactions with neighboring PCBM molecules. These calculations are done on single molecules in vacuum. Nevertheless this could still be true under reaction conditions where interactions with neighboring solvent molecules play an important role. It can be concluded that based on the release of strain-energy the phenyl side should be more reactive than the ester side, the *cis-1* would be the major product if it were allowed, followed by the $e_{(hor)}$ isomers. The *trans-3* double bonds (found by Hirsch *et al.* to be one of the major isomers when *cis-1* is not possible) show elongation instead of shortening. The other *trans* bonds show more shortening on the ester side in the crystals structures but not in the calculations. Based on the shortening of bonds seen in the crystal structures the major isomers upon double cyclopropanation would be *trans-4*, *trans-1*, *e* , and *trans-2,* resulting in the largest release of strain.

2.3.2 Frontier orbitals

The frontier orbitals of a fullerene monoadduct are expected to influence the product distribution of further additions. The LUMO coefficients are mainly relevant for nucleophilic additions (e.g. Bingel reactions) and of 1,3-dipolar cycloadditions (e.g. addition of diazo compounds), the HOMO coefficients are more relevant for nitrene or carbene additions.

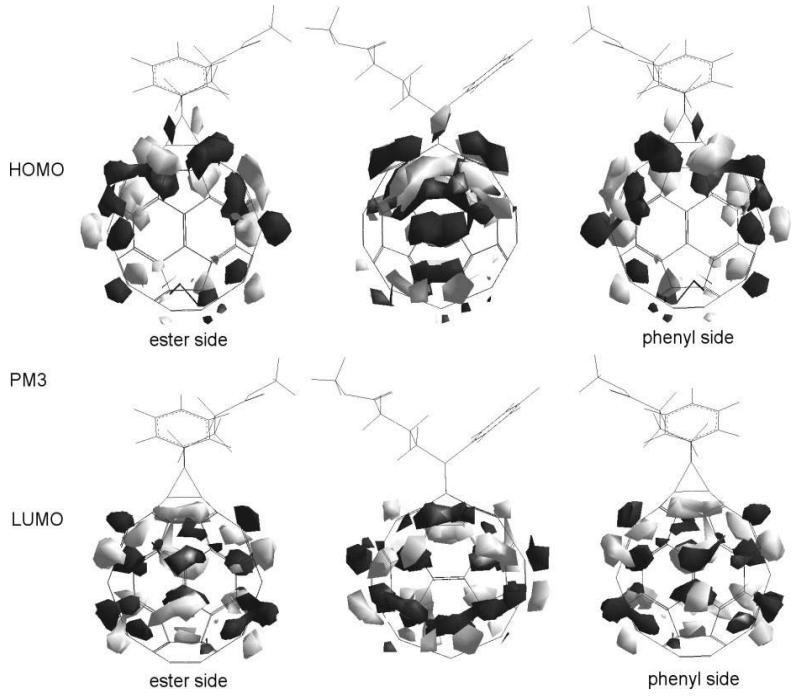

Figure 2.7: *PM3 calculated frontier molecular orbitals of PCBM. Black is positive, grey is negative coefficient.*

For PCBM the calculated HOMO coefficients are most enhanced on the hemisphere around the first addend (**Figure 2.7**). The *trans* double bonds show only small coefficients. The $e_{(vert)}$ double bonds shows almost no HOMO coefficient. The $e_{(hor)}$ shows about the same as the *cis* double bonds. The LUMO coefficients are spread evenly on both hemispheres. Only the $e_{(hor)}$ and the *trans-1* and to somewhat lesser extent the *trans-2* have smaller LUMO coefficients. According to distribution of the LUMO coefficients there should be little or no preference for specific addition patterns with nucleophilic additions on PCBM.

Semiempirical calculations (PM3) were used to model the isomeric distribution of bis-PCBM. It was found that all isomers are within <10 kcal per mole, except the *cis-1*

isomer which is too high in energy due to the steric requirements of the addends. Therefore there is no real preference for specific isomers. Due to the high temperature needed for the formation of the diazoalkyl intermediate a statistical mixture of all 25 isomers is expected. When all isomers would have equal possibilities to be formed there would be around 4% per isomer with slight deviation. However there is only one site for a *trans-1* attack, and two sites for both *e* regioisomers, while all other regioisomers can be formed each on four sites.

2.4 Experimental results

2.4.1 Synthesis of bis-PCBM

Bis-PCBM was synthesized under the same conditions from PCBM or directly from C_{60} without changes in isomer distribution, in agreement with the results obtained by Hirsch and coworkers for Bingel additions and diazoalkane additions.[20] However, changes in reaction conditions (temperature, reaction time and equivalents tosylhydrazone) did influence the outcome of the reaction both in yield of bisadduct fraction and its respective isomer distribution.

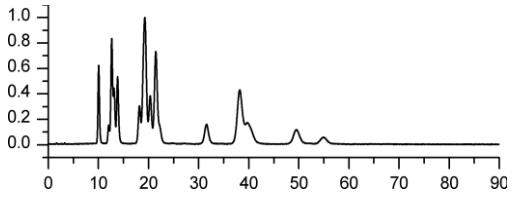

peak	%	peak	%	peak	%
1	3.7	**6**	4.8	**11**	3.9
2	1.3	**7**	22.7	**12**	11.8
3	9.0	**8**	6.4	**13**	4.6
4	5.0	**9**	14.5	**14**	2.4
5	6.4	**10**	2.7	**15**	0.8

Figure 2.8: *Top: HPLC chromatogram of bis-PCBM. Bottom: table showing the relative abundance of the partly resolved peaks numbered from left to right.*

Even though it is not possible to directly correlate the isomer distribution to the relative abundance of the peaks in the HPLC chromatogram of bis-PCBM (assuming molar extinction coefficient to be the same for all isomers) due to overlapping one peak could represent multiple isomers. However if we assume each peak is representing only one isomer and only 15 of the predicted 25 isomers are formed we see some preference for certain isomers. However if we assume that these high abundances are caused by overlapping of multiple smaller peaks no real preference is seen. This would be in agreement with the work of Hirsch et al. who found by comparing the spectroscopic data and the yields of the regioisomers of five series of different bisadducts that they are formed in similar relative yields independent on the orientation of the addends (except *cis-1* adducts, which are formed depending on the steric demands on the addends).[33]

Structural assignment of single isomers of bis-PCBM should be possible based on ^{1}H and ^{13}C NMR from which their symmetry can be deduced and to certain extent from the comparison of their polarity based on the order of elution. However the high degree of freedom in the ester side chains could lead to large differences in polarity in the different structural conformers, which can make the comparison between the different isomer based on polarity difficult. The inherent chirality of certain isomers can also provide extra insight in the assignment of the isomers, especially in the case when adducts with C_2 or C_3 symmetry are compared, e.a. *cis-3*, *trans-2*, and *trans-3*.

2.4.2 Isomerization of bis-PCBM

Addition of diazoalkyl compounds to C_{60} often generates the [5,6] open fulleroid as the kinetic product while the thermodynamic product is the [6,6] closed methanofullerene. The [5,6] open isomers rearrange to [6,6]methanofullerenes thermally, photochemically, or electrochemically. This involves first an electrocyclization to the closed [5,6] fullerene followed by a 1,5-shift to generate the closed [6,6] product. Semiempirical PM3 calculations support such a mechanism.

Should rearrangement be reversible between closed [6,6]methanofullerene and open [5,6]homofullerene then isomerization can lead to the thermodynamically lowest energy isomers of bis-PCBM. However no isomerization was observed from closed [6,6]methanofullerene to open [5,6]homofullerene for monoadducts.[15] The difference in energy between [5,6] open and [6,6] closed is calculated with PM3 molecular modeling to be around 6 kcal. In the bisadduct analog bis-PCBM this difference is slightly larger.

However there are examples in which isomerization between [6,6] and [5,6], as well as isomerization of bisadducts from one isomer to another does occur. Theoretical calculations indicate that for some $M_3N@C_{80}$ endohedral fullerene adducts the [5,6] and [6,6] regioisomers are close in energy.[34] The difference in relative stability is primarily influenced by the size of the encapsulated trimetallic nitrogen. For example when M = Y there is only 1.9 kcal/mol difference between both regioisomers as for M = Sc the [5,6] regioisomer is calculated to be 12 kcal/mol more stable. Rotation of the trimetallic nitrogen is shown to be more easy in [5,6] than [6,6] regioisomer, thus stabilizing the [5,6] isomer as lowest energy isomer. Increasing the size of the metal stabilizes the [6,6] regioisomer with respect to the [5,6] regioisomer and isomerization becomes possible.

Electrochemical isomerization of Bingel bisadducts was shown by the group of Hirsch.[35] It was already known that exhaustive controlled potential electrolysis (CPE) of some Bingel adducts leads to the removal of the cyclopropane rings from the carbon sphere to yield predominantly C_{60}. However when the CPE is not exhaustive migration of the cyclopropane rings on the C_{60} surface is observed. The following mechanism was proposed: introduction of two electrons leads to breaking of one of the carbon bonds of a cyclopropane ring, giving rise to a singly bound stabilized malonate anion which then “walks” around the carbon sphere which presumably delocalizes the second electron until the thermodynamic

equilibrium of the dianionic species is reached.

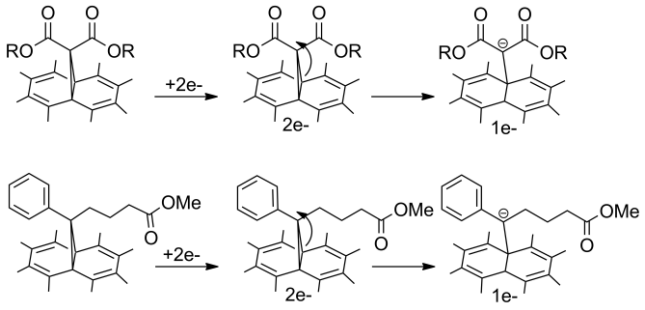

Figure 2.9: *The stabilized anionic maleonate in the case of a bis-Bingel adduct (top) and the non-stabilized form for bis-PCBM (bottom).*

This intramolecular mechanism was supported by the fact that no trisadducts were ever observed. Practically identical relative product distributions for the isolated mixtures of bisadducts were observed, regardless of the starting bisadduct isomer. Strikingly, the product mixtures obtained by electrolysis did not contain any of the *cis* isomers. We do not expect this mechanism to lead to isomerization of the bis-PCBM isomeric mixture, because stabilization of the anionic species is lacking in the case of bis-PCBM (**Figure 2.9**).

Inspired by these results thermal isomerization of the full bis-PCBM isomeric mixture was attempted in refluxing toluene, ODCB, and chloronaphthalene. In both toluene and ODCB the isomeric mixture remained the same even after several days of refluxing, in chloronaphthalene decomposition took place likely due to the high temperature. Because light, oxygen and water were not rigorously excluded their possible contribution to the decomposition pathway cannot be excluded. Isomerization under the influence of light was attempted with similar results: illumination with a 150 W Na-lamp did not result in isomerization, illumination with a 256 nm Mercury lamp resulted in decomposition. Analysis of the decomposition products through LC-MS analysis did not allow for structural identification.

2.4.3 Separating bis-PCBM into single isomers

2.4.3.1 Fractionation by Soxhlet extraction

The large difference in retention time found with analytical HPLC on normal phase silica indicated the possibility of partitioning the isomeric mixture of bis-PCBM based on differences in polarity and solubility. Separation was attempted through subsequent Soxhlet extractions with pentane, methanol, and ODCB. Even though a clear difference in solubility of bis-PCBM was observed between the different solvents, all fractions comprised the same isomeric makeup and no enrichment in particular isomers could be observed.

2.4.3.2 Fractionation by column chromatography

Chromatography on a silica column using toluene as eluent made separation between the isomers possible. However, full separation of isomers or isomeric subfractions could not be obtained, not even after successive columns. Therefore this method proved only useful as prefractionation and higher resolution was needed to separate the isomeric subfractions further to individual isomers.

2.4.3.3 Subfractions of bis-PCBM by preparative HPLC

Preparative HPLC was used to further purify the different prefractionated isomeric subfractions obtained from standard chromatography. It proved possible to reproducibly obtain pure fractions consisting of several isomers which are baseline separated, but not to obtain single isomers from these separated subfractions, with the exception of the first peak (**Figure 2.10**).

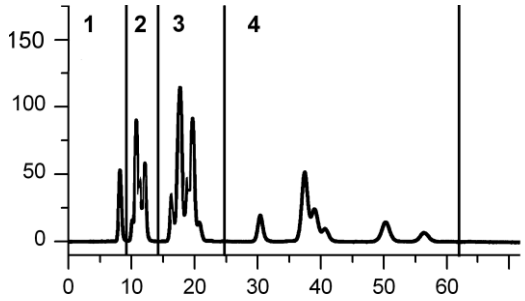

Figure 2.10: *HPLC chromatogram showing the four baseline separated subfractions 1-4.*

Overlapping of the peaks proved to be an insurmountable problem. Only a little amount of pure compound can be obtained per run (peak shaving). However small fluctuations in retention time caused by differences in temperature and column pressure during a sequence lead to contamination of the already collected fractions making collection of usable amounts of higher than 95% purity virtually impossible.

As mentioned above the first peak in the HPLC chromatogram of the full isomeric mixture of bis-PCBM is fully resolved (**Figure 2.10, 1**) and allowed us to isolate the first single isomer of bis-PCBM.

2.4.4 Cyclic voltammetry on bis-PCBM subfractions

Cyclic voltammetry was performed to investigate the influence of the isomeric makeup on the electronic properties of these baseline resolved subfractions and the single isomer obtained from preparative HPLC. The results are given in **Table 2.1**.

Fraction	$E1_{1/2\ red}$	$E2_{1/2red}$	$\Delta E1_{1/2red}^{*}$	$\Delta E2_{1/2red}^{*}$
1	-1.147	-1.547	0.048	0.045
2	-1.167	-1.573	0.027	0.019
3	-1.183	-1.586	0.012	0.006
4	-1.194	-1.592	--	--

Table 2.1: *Cyclic voltammetry data of the bis-PCBM subfractions 1-4. Reduction potentials were measured in 4:1 ODCB/acetonitrile and are relative to ferrocene (that is, $E_{1/2\ ox}$ of ferrocene was placed at 0V). $^{*}\Delta E$ is the energy difference compared to the most negative $E_{1/2\ red}$ within the series.*

It can be seen from the CV data that there is indeed a difference in first reduction potentials between these subfractions with different polarities, even though the differences are smaller than predicted by computational studies.[36] Increasing polarity seems to lead to more negative average first reduction potentials, which is somewhat counterintuitive and will be discussed in more detail further on in this chapter.

2.4.5. Isolation of single isomers of bis-PCBM

Even though full separation into single isomers has proven to be too tedious and increasingly difficult for any practical use in commercial organic solar cells, it is still worthwhile from an academic point of view to further investigate the individual isomers comprising the bis-PCBM mixture. Instead of obtaining the best possible isomer for use in organic bulk heterojunctions it might prove more easy to remove the isomer or isomers that perform less well from the full isomeric mixture, thus improving the performance of this promising material.

2.4.5.1 Single Isomers obtained through recycle preparative-HPLC

In preparative HPLC, column length is one of the keys factors to improve the separation of materials. However, there is a limitation on the possible length of

the column due to pressure problems: increasing the length of the column also requires an increase in pressure over the column. To solve this, a so-called recycling technique can be applied. After passing through the column a first time, recycling technique enables the same sample, which is now partially separated, to pass through the same column again. This cycle can be repeated until baseline resolved separation is achieved. A requirement for this method is that the compounds which are to be separated do not diffuse too much on the column during separation.

In cooperation with Dr. John Dennis from Queen Mary University London full separation of the bis-PCBM mixture into individual isomers starting from prefractionated subfractions obtained from a combination of column chromatography and preparative HPLC is underway.

2.5 Single isomers of bis-PCBM

As mentioned above, the first single isomer of bis-PCBM was obtained through conventional preparative HPLC in reasonable yield. Two more single isomers were obtained through the use of recycling preparative HPLC, however in much smaller amounts. The obtained isomers were further characterized through HPLC, NMR, and UV-Vis. Their electronic properties were investigated through cyclic voltammetry.

2.5.1 HPLC and UV-Vis

The bis-PCBM single isomers were analyzed with analytical HPLC and named in order of polarity, i.e. retention time on analytical silica column (**Figure 2.11**).

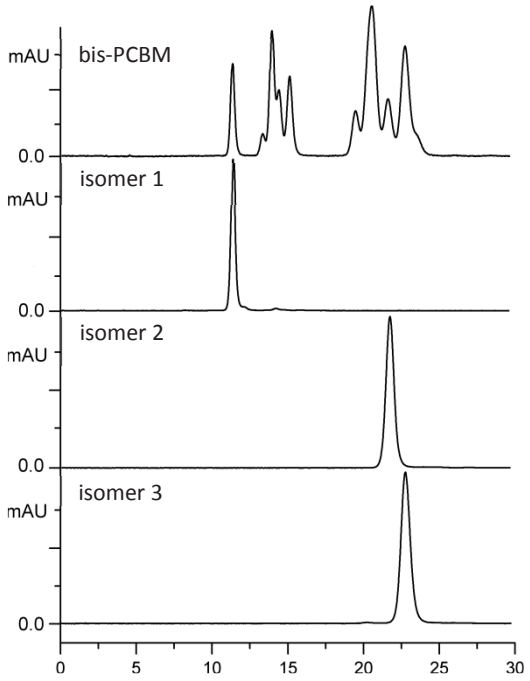

Figure 2.11: *HPLC chromatograms of the first 30 min of bis-PCBM (top) and the single isomers 1-3.*

Their UV-Vis spectra were recorded and are shown in **Figure 2.12**.

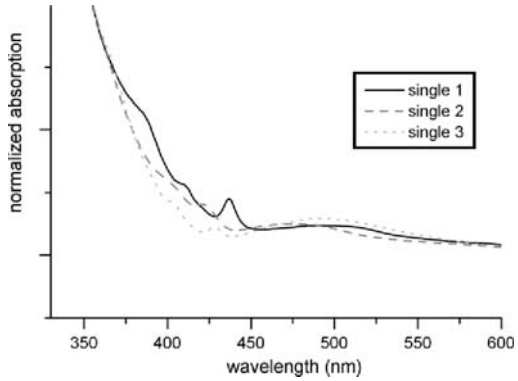

Figure 2.12: *UV-Vis data of bis-PCBM single isomers 1-3.*

Distinct differences in absorption are seen within this series of bis-PCBM single isomers. Especially between 400 and 450 nm there are large differences in absorption. Both isomer **1** and isomer **3** show a small peak in this area which is absent in isomer **2**. Isomer **3** has the weakest absorption compared to the other two isomers in this area, but a slightly higher absorption at 450-600 nm. Isomer **2** lies between the other isomers in the region around 400nm, but shows the lowest absorption of the three at 450-600 nm region. Isomer **1**, the isomer with the shortest retention time has the highest absorption of the three single isomers around 400 nm but only slightly higher absorption than isomer **2** at the 450-600 nm region. These differences are already visible in the color of the samples, ranging from orange-yellow to brown-red.

2.5.2 NMR

High resolution ^{13}C NMR was used to characterize these three single isomers further and to determine their symmetry (**Figure 2.13**).

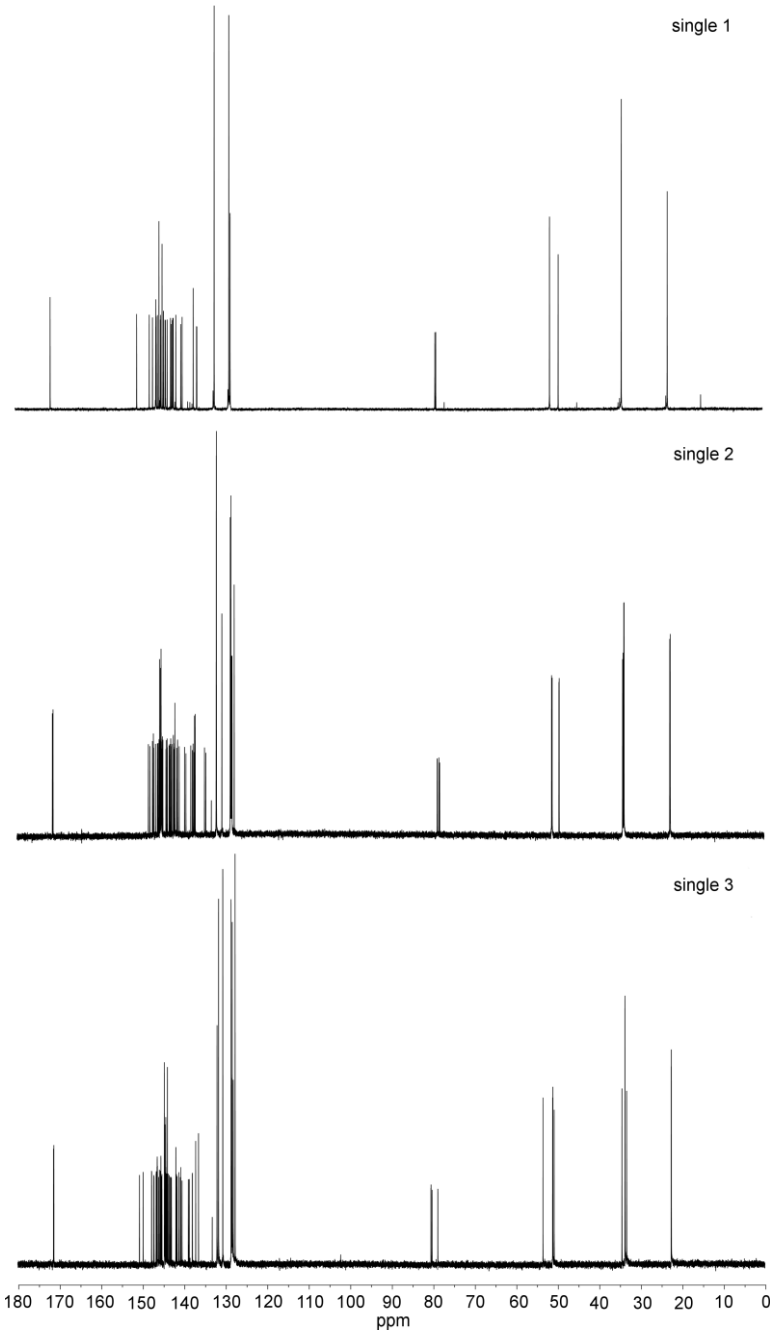

Figure 2.13: *^{13}C NMR spectra of the bis-PCBM single isomers 1-3.*

Isomer **1** shows only one peak in the carbonyl region while the other two isomers show two peaks in this region leading to the conclusion that isomer **1** is symmetric where both others are non-symmetric isomers. This is confirmed at the bridgehead region. All three isomers show bridgehead carbon atoms in the 70-90 ppm region indicating closed [6,6] structures. Isomer **1** only shows two peaks as would be expected for a symmetric substitution pattern, isomers **2** and **3** both show four peaks, confirming the non-symmetric nature of these isomers. Their non-symmetric nature is further supported by the number of sp^2 carbon atoms; isomer **2** shows 52 peaks and isomer **3** 50 peaks where isomer **1** only shows 26 peaks for the sp^2 cage carbon atoms.

Symmetric			Non-symmetric
mirror plane C_s	mirror plane C_{2v}	axis of rotation C_2	C_1
cis 1 exo-exo	*trans 1 exo-exo*	*Cis 3 exo-endo*	*cis 1 exo-endo*
cis 1 endo-endo	*trans 1 endo-exo*	*trans 3 exo-endo*	*cis 2 exo-endo*
cis 2 endo-endo		*trans 2 exo-endo*	*cis 3 endo-endo*
cis 2 exo-exo			*cis 3 exo-exo*
trans 4 endo-endo			*e'*
trans 4 exo-exo			*e"*
			trans 4 endo-exo
			trans 3 endo-endo
			trans 3 exo-exo
			trans 2 exo-exo
			trans 2 endo-endo

Table 2.3: The different isomers of bis-PCBM grouped by their symmetry groups.

Based on the number of peaks observed in the ^{13}C NMR spectra and their polarity as found in the order of elution from the silica HPLC column, isomer **1** should be the least polar isomer and should possess a symmetric substitution pattern.

Isomers **2** and **3** should both possess a non-symmetric substitution pattern as both isomers possess more than 28 observable sp^2 cage carbon atoms. Their retention times are similar and the peaks corresponding to these isomers appear in the middle of the HPLC chromatogram making assignment based on either their polarity or symmetry rather difficult.

For isomer **1** assignment on polarity and symmetry is more straightforward. Isomer **1** should have the smallest permanent dipole moment and either have a mirror plane or an axis of rotation, but not both. Based on polarity the isomers with both addends on the same hemisphere can be disregarded, leaving four different *trans* isomers as potential candidates. From these isomers we would assume the isomer with both addends furthest apart to be the least polar isomer: *trans-2 exo-endo*

2.5.3 Cyclic voltammetry

Cyclic voltammetry was performed on the single isomers of bis-PCBM to investigate their electrical properties. The results are given in **Table 2.4**.

isomer	$E1_{½\ red}$	$E2_{½\ red}$	$\Delta E1_{½\ red}$*	$\Delta E2_{½\ red}$*
1	-1.1465	-1.547	0.071	0.061
2	-1.196	-1.601	0.0215	0.007
3	-1.2175	-1.608	--	--

Table 2.4: *Cyclic Voltammetry results of the bis-PCBM single isomers 1-3. Reduction potentials were measured in 4:1 ODCB/acetonitrile and are relative to ferrocene (that is, $E_{1/2\ ox}$ of ferrocene was placed at 0V).* *$^{*}\Delta E$ is the energy difference compared to the most negative $E_{1/2\ red}$ within the series.*

As can be clearly seen from the CV of the single isomers, there is a distinct difference between the first reduction waves of the isomers. Especially those with different polarities show reduction potentials that are quite different from each

other. Between isomer **1**, the isomer with the shortest retention time and isomer **3** having the longest retention time there is a difference of 71 mV. These results are similar to those found for the isomeric subfractions where the same, somewhat counterintuitive, trend is seen. However the reduction potentials of the single isomers obtained from subfraction 3 are higher than the average value (-1.183 V) obtained for that subfraction. It appears that the specific isomeric makeup of a subfraction has a substantial influence on the electronic properties of that specific subfraction.

2.5.4 Solar cell devices

Due to the limited amount of material available solar cell devices were only made comprising isomer **1** in combination with P3HT. Devices were made with two different hole blocking layers: structure a; ITO/PEDOT:PSS/P3HT:fullerene/LiF/Al and structure b; ITO/PEDOT:PSS/P3HT:fullerene/Sm/Al. The results are given in **Table 2.5**.

Structure (a)

	J_{sc} (A/m^2)	V_{oc} (V)	FF (%)	Efficiency (%)
Bis-PCBM	69	0.72	69	3.3
Single isomer 1	64	0.71	66	3.0

Structure (b)

	J_{sc} (A/m^2)	V_{oc} (V)	FF (%)	Efficiency (%)
Bis-PCBM	63	0.71	69	3.1
Single isomer 1	62	0.71	68	3.0

Table 2.5: *Preliminary solar cell result of bis-PCBM single isomer 1.*

Unfortunately this first single isomer of bis-PCBM did not perform superior to conventional bis-PCBM resulting in similar device characteristics as for the full isomeric mixture in these preliminary tests. A slightly lower V_{oc} compared to bis-PCBM was found in first set of cells. This was already expected from cyclic

voltammetry where the first reduction wave of this single isomer is less negative than that found for the full isomeric mixture. Based on these results it is expected that cells comprising isomer **3** will show an improvement in V_{oc} due to its more negative first reduction potential. Transport characteristics are also expected to differ between the different isomers, due to the different spatial orientations of the addends on the fullerene sphere.

2.6 Conclusions

As for all addition reactions to [6,6] double bonds of [60]methanofullerene monoadducts the formation of bis-PCBM does not proceed statistically. However, thermodynamic arguments alone are not sufficient to explain the regioselectivity, since these calculated differences in stability are small. The experimental and calculated geometries of the monoadduct as well as its frontier orbitals did not result in a satisfactorily explanations with relation to the isomer distribution formed.

To further investigate the content of the isomeric mixture an attempt to isolate individual isomers was undertaken. Three single isomers were obtained through a combination of column chromatography, preparative HPLC, and recycle preparative HPLC. These isomers were further analyzed with NMR and their electronic properties were probed with CV. A distinct difference in reduction potential as well as light absorption was found between these single isomers. Devices comprising isomer **1** did not perform superior to those comprising conventional bis-PCBM.

2.7 Outlook

More material is needed for further investigation of the individual properties and unambiguous identification of these single isomers through crystal structure analyses. In cooperation with John Dennis from Queen Mary University London more material is being isolated. By choosing the isomer, or isomers, with the best electronic and optical properties the best possible solar cell for this material can

be made. Even though this would be interesting from an academic point of view, it would be to tedious for commercial application in solar cell manufacturing. However removal of the isomers that contribute in a negative way either electronically or optically can prove easier by purification or through synthetic methods such as tethering described in Chapter 3. Understanding of the structural relationship with device characteristics is an important issue for further design and development of new acceptor materials.

2.8 Experimental

2.8.1 Device fabrication

P3HT and the fullerene derivatives were dissolved in a 1:1.2 weight ratio in chloroform and stirred overnight. The photoactive layers were spin-cast under nitrogen atmosphere on clean glass substrates pre-patterned with indium tin oxide and a 60 nm thick film of poly(3,4-ethylenedioxythiophene)/poly(styrenesulphonic acid) (VP AI4083, H.C. Starck). The as-cast layers were annealed subsequently at 135 °C for 15 minutes. The devices were finished by thermal evaporation of a LiF(1 nm)/Al(100 nm) cathode. Electrical measurements were conducted in an N_2 controlled atmosphere in the dark and under illumination of a Steuernagel SolarConstant 1200 metal halide lamp, which was set to 1 sun intensity using a silicon reference cell and correcting for spectral mismatch.

2.8.2 Materials

All reagents and solvents were used as received or purified using standard procedures. [60]Fullerene (99.5 %) was purchased from Bucky USA and used without further purification. Flash chromatography was performed using silica gel (Kieselgel Merck Type 9385 (230-400 mesh)). ^{1}H NMR and ^{13}C NMR were performed on a Varian Unity Plus (500MHz), at 298 K using TMS as an internal standard. HPLC analyses were performed on a Hewlett Packard HP LCChemstation 3D (HP 1100 Series) using an analytical Cosmosil Buckyprep. column (4.6 x 250 mm) or a Alltima HP silica column (3

x 100 mm). Preparative HPLC was performed on a Hewlett Packard HP LCChemstation 3D (HP 1100 Series) using a preparative Ecosphere silica column (10 x 250 mm).

2.8.3 Synthesis

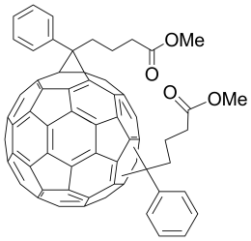

Bis-PCBM. 5.0 g tosylhydrazone (2.2 eq) was dissolved in 75 mL dry pyridine in a flame dried 500 ml three neck flash equipped with nitrogen insert. To this mixture 360 mg sodium methoxide was added. The resulting solution was stirred for 20 minutes. A solution of 2.2 g C_{60} in 300 mL ODCB was prepared. The C_{60} solution was degassed three times and added to the pyridine solution. The resulting mixture was degassed a second time (three vacuum/N_2 purges) and the solution was heated to 85 ^{o}C at which illumination with a 150 W Sodium lamp was started. The reaction mixture was stirred overnight at 85 ^{o}C under illumination. The solvent was concentrated *in vacuo* and purified by column chromatography (SiO_2, toluene). The bis-PCBM fraction was collected, precipitated with methanol, washed twice with methanol, ones with pentane and dried overnight in a vacuum oven at 40 ^{o}C. The pure product was obtained as a mixture of isomers as 1.5 g red powder (1.4 mmol, 45%). ^{1}H NMR (500 MHz, CS_2 with D_2O insert) δ 8.25-7.25 (broad signals 10H), 3.81-3.56 (broad singlets, 6H), and 3.25-1.30 (broad signals, 12H); ^{13}C NMR (126 MHz, CS_2 with D_2O insert) δ 171.93, 171.79, 171.75, 171.74, 171.72, 171.67, 171.64, 171.62, 171.58, 171.57, 171.50, 151.95, 151.70, 151.59, 151.55, 150.77, 150.75, 150.72, 150.61, 150.39, 149.89, 149.86, 149.80, 149.78, 149.51, 149.47, 149.19, 149.16, 149.14, 149.02, 148.93, 148.87, 148.80, 148.75, 148.60, 148.57, 148.39, 148.32, 148.30, 148.27, 148.06, 148.00, 147.96, 147.91, 147.85, 147.84, 147.81, 147.71, 147.65, 147.54, 147.49, 147.48, 147.41, 147.38, 147.35, 147.31, 147.27, 147.22, 147.18, 147.14, 147.11, 147.09, 147.06, 147.04, 147.00, 146.96, 146.95, 146.90, 146.88, 146.85, 146.82, 146.77, 146.75, 146.70, 146.66, 146.65, 146.61, 146.57, 146.54, 146.51, 146.49, 146.48, 146.46, 146.44, 146.42, 146.38, 146.33, 146.28, 146.26, 146.23, 146.17, 146.14, 146.07, 146.05, 146.04, 146.01, 145.97, 145.93,

145.88, 145.85, 145.82, 145.78, 145.73, 145.70, 145.66, 145.65, 145.60, 145.57, 145.52, 145.49, 145.45, 145.40, 145.37, 145.33, 145.31, 145.30, 145.27, 145.25, 145.21, 145.18, 145.16, 145.14, 145.08, 145.05, 145.01, 144.99, 144.96, 144.92, 144.88, 144.83, 144.82, 144.78, 144.75, 144.73, 144.70, 144.67, 144.64, 144.61, 144.57, 144.54, 144.52, 144.42, 144.36, 144.33, 144.30, 144.28, 144.26, 144.24, 144.20, 144.15, 144.09, 144.05, 144.03, 143.99, 143.96, 143.93, 143.89, 143.84, 143.82, 143.78, 143.74, 143.70, 143.67, 143.63, 143.60, 143.57, 143.50, 143.48, 143.45, 143.43, 143.40, 143.38, 143.31, 143.28, 143.26, 143.19, 143.15, 143.11, 143.10, 143.08, 143.04, 142.97, 142.93, 142.91, 142.88, 142.85, 142.81, 142.75, 142.74, 142.72, 142.66, 142.64, 142.61, 142.60, 142.57, 142.54, 142.51, 142.47, 142.39, 142.38, 142.35, 142.30, 142.28, 142.22, 142.20, 142.17, 142.10, 142.08, 142.05, 142.01, 141.99, 141.98, 141.93, 141.90, 141.80, 141.75, 141.72, 141.68, 141.64, 141.59, 141.54, 141.47, 141.45, 141.40, 141.32, 141.28, 141.27, 141.22, 141.20, 141.17, 141.12, 141.07, 141.02, 140.98, 140.94, 140.85, 140.78, 140.74, 140.71, 140.62, 140.56, 140.48, 140.42, 140.39, 140.34, 140.32, 140.30, 140.06, 140.04, 139.74, 139.63, 139.49, 139.25, 139.18, 139.15, 139.12, 138.93, 138.89, 138.68, 138.43, 138.33, 138.17, 138.13, 138.09, 137.97, 137.94, 137.86, 137.77, 137.69, 137.64, 137.61, 137.59, 137.57, 137.43, 137.38, 137.36, 137.30, 137.23, 137.22, 137.21, 137.14, 137.11, 137.08, 137.04, 137.02, 136.99, 136.93, 136.86, 136.85, 136.82, 136.77, 136.75, 136.72, 136.67, 136.65, 136.63, 136.44, 136.42, 136.38, 136.26, 136.21, 136.19, 136.15, 136.09, 135.92, 135.89, 135.80, 135.77, 135.56, 135.54, 135.47, 135.45, 135.10, 135.08, 134.81, 134.48, 134.22, 133.54, 133.07, 133.04, 132.48, 132.34, 132.32, 132.28, 132.20, 132.14, 132.10, 132.06, 132.03, 131.99, 131.93, 131.82, 131.80, 131.62, 131.49, 131.34, 131.25, 130.65, 130.58, 129.19, 129.01, 128.77, 128.62, 128.60, 128.55, 128.53, 128.46, 128.41, 128.36, 128.33, 128.29, 128.24, 128.21, 128.15, 128.12, 127.77, 127.68, 127.38, 125.59, 125.10, 80.66, 80.62, 80.56, 80.52, 80.33, 80.28, 80.16, 80.15, 79.91, 79.90, 79.85, 79.81, 79.32, 79.25, 79.14, 78.94, 78.91, 78.84, 78.81, 78.78, 78.74, 78.70, 78.55, 78.43, 78.38, 78.31, 78.22, 78.18, 78.07, 77.94, 77.82, 76.96, 76.79, 76.69,

76.48, 76.34, 75.31, 75.28, 74.57, 74.47, 53.80, 53.57, 51.30, 51.26, 51.24, 51.20, 51.18, 51.13, 51.10, 51.09, 51.04, 50.98, 50.86, 50.83, 50.79, 49.52, 49.49, 49.41, 49.31, 49.24, 49.23, 49.15, 49.12, 49.02, 48.93, 48.86, 47.75, 47.52, 47.41, 47.38, 47.16, 47.10, 44.77, 34.43, 34.34, 34.29, 34.15, 34.06, 34.01, 33.98, 33.95, 33.87, 33.84, 33.80, 33.76, 33.73, 33.59, 33.49, 33.42, 33.37, 33.29, 33.25, 33.21, 33.10, 32.76, 32.67, 32.50, 32.23, 29.73, 22.99, 22.88, 22.87, 22.79, 22.73, 22.70, 22.65, 22.61, 22.57, 22.53, 22.41, 22.36, 22.28, 21.98, 21.86, 21.76, and 21.69.

Single isomer 1. Obtained from preparative HPLC from the full isomeric mixture. ^{1}H NMR (500 MHz, CS_2 with D_2O insert) δ 7.96 (m, 4H), 7.58 (m, 4H), 7.51 (m, 2H), 3.79 (s, 6H), 3.19 (m, 4H), 2.69 (m, 4H), and 2.38 m, 4H).
^{13}C NMR (126 MHz, CS_2 with D_2O insert) δ 171.58, 150.72, 147.69, 146.92, 146.13, 146.11, 146.02, 145.73, 145.35, 145.02, 144.94, 144.61, 144.30, 144.27, 143.89, 143.80, 143.38, 142.58, 142.42, 142.14, 142.03, 141.92, 141.29, 140.10, 139.76, 137.10, 136.30, 136.22, 132.05, 128.52, 128.21, 78.88, 78.67, 51.25, 49.17, 33.96, 33.95, and 22.90.

Single isomer 2. Obtained from preparative recycle HPLC from fraction 3. ^{1}H NMR (500 MHz, CS_2 with D_2O insert) δ 7.93(m , 4H) 7.61 (m, 1H), 7.42 (m, 4H) , 3.76 (s, 3H) 3.63 (s, 3H), 2.91 (m, 2H), 2.72 (m, 2H), 2.58 (m, 2H), 2.43 (m, 2H), 2.24 (m, 2H), and 2.13 (m, 2H); ^{13}C NMR (126 MHz, CS_2 with D_2O insert) δ 171.47, 171.31, 148.33, 147.99, 147.36, 147.15, 147.14, 147.05, 146.63, 146.17, 145.99, 145.78, 145.76, 145.63, 145.55, 145.48, 145.40, 145.37, 145.29, 145.26, 145.22, 145.16, 145.08, 144.96, 144.84, 144.11, 144.04, 143.82, 143.77, 143.35, 143.18, 142.96, 142.94, 142.74, 142.69, 142.32, 142.31, 142.24, 142.09, 142.01, 141.96, 141.52, 141.33, 141.31, 140.91, 139.63, 139.28, 138.11, 137.73, 137.58, 137.34, 137.22, 137.05, 134.82, 134.52, 133.18, 131.99, 131.96, 130.63, 128.61, 128.46, 128.28, 128.19, 127.66, 78.75, 78.72, 78.35, 78.17, 51.19, 51.05, 49.42, 49.35, 34.08, 33.95, 33.79, 33.72, 22.71, and 22.61.

Single isomer 3. Obtained from preparative recycle HPLC from fraction 3. ^{1}H NMR (500 MHz, CS_2 with D_2O insert) δ 7.79(m, 4H), 7.59 (m, 1H), 7.51 (m, 4H), 7.34 (m, 1H), 3.73 (s, 3H), 3.68 (s, 3H), 2.85 (m, 2H), 2.77 (m, 2H), 2.65 (m, 2H), 2.51 (m, 2H), 2.43 (m, 2H), and 2.10 (m, 2H); ^{13}C NMR (126 MHz, CS_2 with D_2O insert) δ 171.41, 171.33, 150.70, 149.82, 147.80, 147.77, 147.24, 147.20, 146.69, 146.66, 146.49, 146.46, 146.44, 146.42, 146.38, 146.07, 145.98, 145.92, 145.68, 145.54, 145.53, 145.37, 145.29, 144.69, 144.66, 144.60, 144.57, 144.38, 144.35, 144.30, 144.17, 144.14, 143.96, 143.80, 143.54, 143.30, 143.10, 143.00, 141.93, 141.83, 141.78, 141.60, 141.19, 140.86, 140.75, 140.73, 140.44, 138.92, 138.70, 137.98, 137.95, 137.16, 136.47, 133.18, 132.01, 131.64, 130.63, 128.62, 128.41, 128.36, 128.10, 127.66, 80.48, 80.45, 80.20, 78.82, 53.48, 51.16, 51.08, 50.78, 34.46, 33.73, 33.71, 33.32, 22.59, and 22.55.

2.9 References

1 M. Lenes, G. A. H. Wetzelaer, F. B. Kooistra, S. C. Veenstra, J. C. Hummelen and P. W. M. Blom, *Adv. Mater.,* 2008, **20**, 2116

2 M. H. Yun, G. Kim, C. Yang and J. Y. Kim, *J. Mater. Chem*., 2010, **20**, 7710

3 M. Lenes, S. W. Shelton, A. B. Sieval, D. F. Kronholm, J. C. Hummelen and P. W. M. Blom, *Adv. Fuct. Mater.*, 2009, **19**, 3002

4 Y. He, H. Chen, J. Hou and Y. Li, *J. Am. Chem. Soc*., 2010, **132**, 1377

5 Y. Cheng, C. Hsieh, Y. He, C. Hsu and Y. Li*, J. Am. Chem. Soc*., 2010, **132**, 17381

6 Y. He, G. Zhou, B. Peng and Y. Li, *Adv. Funct. Mater*. 2010, **20**, 3383

7 Y. He, H. Chen, G. Zhao, J. Hou and Y. Li, *Solar Energy Mater. Solar Cells*, 2011, **95**, 899

8 N. Martin, J. L. Delgado and S. Filippone, *Meet. Abstr. - Electrochem. Soc.*, 2009, **901,** 1119

9 I. Riedel, N. Martin, F. Giacalone, J. L. Segura, D. Chirvase, J. Parisi and V. Dyakonov, *Thin Solid Films*, 2004, **451-452**, 43

10 I. Riedel, E. von Hauff, J. Parisi, N. Martin, F. Giacalone and V. Dyakonov, *Adv. Funct. Mater*., 2005, **15**, 1979

11 A. Sánchez-Díaz, M. Izquierdo, S. Filippone, N. Martin and E. Palomares, *Adv. Funct. Mater.*, 2010, **20**, 2695

12 G. Zhao, Y. He and Y. Li, *Adv. Mater*., 2010, **22**, 4355

13 A. Hirsch and M. Brettreich, *Fullerenes Chemistry and Reactions*, 2005, Wiley-VCH Verlag GmbH & Co. KGaA, Weinheim, Ch. 1, pp. 29-30

14 J. C. Hummelen, B. W. Knight, F. Lepeq, F. Wudl, J. Yao and C. L. Wilkins, *J. Org. Chem*., 1995, **60**, 532

15 R. A. J. Janssen, J. C. Hummelen and F. Wudl, *J. Am. Chem. Soc*., 1995, **117**, 544

16 H. E. Zimmermann and G. Wu, *Can. J. Chem.*, 1983, **61**, 866

17 A. Hirsch and M. Brettreich, *Fullerenes Chemistry and Reactions*, 2005, Wiley-VCH Verlag GmbH & Co. KGaA, Weinheim, Ch. 10, pp. 289-344

18 W. H. Powell, F. Cozzi, G. P. Moss, C. Thilgen, R. J.-R. Hwu and A. Yerin, *Pure Appl. Chem*., 2002, **74**, 629

19 A. Hirsch, I. Lamparth and H. R. Karfunkel, *Angew. Chem. Int. Ed. Engl.*, 1994, **33**, 437

20 F. Dojo, A. Herzog, I. Lamparth, F. Hampel and A. Hirsch, *Chem. Eur. J.*, 1996, **2**, 1537

21 Y. Nakamura, M. Taki, S. Tobita, H. Shizuka, H. Yokoi, K. Ishiguro, Y. Sawaki and J. Nishimura, *J. Chem. Soc., Perkin Trans. 2*, 1999, 127

22 Y. Nakamura, N. Takano, T. Nishimura, E. Yashima, M. Sato, T. Kudo and J. Nishimura, *Org. Lett*., 2001, **3**, 1193

23 H. Ito, Y. Ishida and K. Saigo, *Tetrahedron Letters*, 2005, **46**, 8757

24 G. Schick, A. Hirsch, H. Mauser and T. Clark, *Chem. Eur. J.* , 1996, **2**, 935

25 F. Diederich and R. Kissinger, *Acc. Chem. Res*., 1999, **32**, 537

26 A. Hirsch, *The Chemical Record*, 2005, **5**, 196

27 Z. Zhou and S. R. Wilson, *Current Organic Chemistry*, 2005, **9**, 789

28 C. Thilgen and F. Diederich, *C. R. Chimie*, 2006, **9**, 868

29 V. V. Zverev, V. I. Kovalenko, I. P. Romanova and O. G. Sinyashin, *Int. J. Quant. Chem.*, 2007, **107**, 2442

30 A. Hirsch and M. Brettreich, *Fullerenes Chemistry and Reactions*, 2005, Wiley-VCH Verlag GmbH & Co. KGaA, Weinheim, Ch. 10.2.2, pp. 302-306

31 M. Prato, V. Luchinni, M. Maggini, E. Simpf, G. Scorrano, M. Eiermann, T. Suzuki and F. Wudl, *J. Am. Chem. Soc*., 1993**, 115**, 8479

32 Z. Li and P. B. Shevlin, *J. Am. Chem. Soc.*, 1997, **119**, 1149

33 M. T. Rispens, A. Meetsma, R. Rittberger, C. j. Brabec, N. S. Sariciftci and J. C. Hummelen, *Chem. Commun*., 2003, 2116

34 A. R. Rodríguez-Fortea, J. M. Campanera, C. M. Cardona, L. Echegoyen and J. M. Poblet, *Angew. Chem*., 2006, **118**, 8356

35 R. Kessinger, M. Gomez-Lopez, C. Boudon, J. Gisselbrecht, M. Gross, L. Echegoyen and F. Diederich, *J. Am. Chem. Soc.*, 1998, **120**, 8545

36 J. M. Frost, M. A. Faist and J. Nelson, *Adv. Mater.*, 2010, **22**, 4881

Chapter 3

Tethered synthesis of bis-PCBM

Abstract. This chapter describes the reduction of the number of possible isomers that are formed upon double cyclopropanation of C_{60} by the use of bidentate tosylhydrazones in which the reactive groups are linked by an alkyl diol tether. Three isomeric subpopulations of bisadduct analogues of [6,6]-phenyl-C61-butyric acid methyl ester (bis-PCBM) isomers were synthesized via this so-called tether-directed control. Photovoltaic devices were made based on P3HT and PF10TBT as the donor materials comprising the different subpopulations of bis-PCBM isomers as acceptor material.

This chapter is part of a cooperation with G. A. H. Wetzelaer and P. W. M. Blom. Part of this chapter has been published: *Chemistry, A European Journal*, 2010, **16**, 11250-11253. "The Use of Tethered Addends to Decrease the Number of Isomers of Bisadduct Analogues of PCBM" and "Influence of the Isomeric Composition of the Acceptor on the Performance of Organic Bulk heterojunction P3HT:bis-PCBM Solar Cells" submitted for publication. Device fabrication and testing was performed by G. A. H. Wetzelaer.

3.1 Introduction

This chapter compares the performances of three different isomeric subpopulations of bis-PCBM isomers in organic solar cells obtained via tether-directed synthesis using alkyl spacers of increasing length. To the best of our knowledge this study is the first example of a comparison between different isomers or isomer sub-populations of fullerene bisadducts (fullerenes with four sp3-hybridized cage carbon atoms) in organic bulk heterojunction solar cells.

As already explored in detail in the previous chapter, each of the eight possible regioisomers of bis-PCBM exists as a mixture of up to four stereoisomers depending on the symmetry of the regioisomer. The *cis-1* isomer, however, is in most cases sterically prohibited by the bulk of the addends.[1,2] This results for bisadducts with structurally the same C_s symmetric addends like bis-PCBM in at least 22 different isomers. The properties of fullerene bis- and higher adducts depend strongly on their substitution pattern because geometry plays a crucial role in their organization in the solid state, thereby influencing the properties of the bulk material.[3-5]

Power conversion efficiencies of up to 4.5% have been reported for bulk heterojunction solar cells comprising a bis-PCBM acceptor and poly(3-hexylthiophene) (P3HT).[6] Due to the significantly higher energies (~100 mV) of the lowest occupied molecular orbitals (LUMO) of the bis-PCBM isomer mixture compared to the monoadduct, PCBM, these devices exhibit higher open-circuit voltages (V_{oc}). The short-circuit current (J_{sc}), however, is generally lower, though it approaches the value obtained for PCBM-based cells in P3HT systems in which the morphology has been optimized by solvent annealing.[6-8] A possible explanation for this decrease in J_{sc} lies in the isomeric nature of bis-PCBM; It is expected that the fact that this is a mixture of isomers influences the properties of the bulk and especially the ability to crystallize, which is important in the formation of a

bicontinuous interpenetrating network of fullerene and polymer. In addition, this low crystallinity might lower the charge transport characteristics compared to a single isomer. For P3HT-based devices it is likely that the polymer predominantly determines the morphology of the active layer. This explains why bis-PCBM shows better performance compared to the monoadduct PCBM as an acceptor material in bulk heterojunctions with P3HT but that this effect is harder to obtain with other, less-crystalline polymers.

The ability of a fullerene derivative to crystallize has been suggested to influence V_{oc}.[9] Moreover, different isomers have different electronegativities, leading to (shallow) trapping.[7,8] It has been calculated for some of the isomers that there is a difference of 180 mV between the highest and lowest isomers and +82 mV to –98 mV from the average.[10] Even though only one orientation per isomer was used in the calculations and the chosen distribution of isomers of bis-PCBM was not optimal, these calculations still provide useful insight in the distribution of energy levels of the different isomers.

The large-scale production of mixtures of isomers of bis-PCBM is likely to suffer from problems in batch-to-batch reproducibility; different isomer ratio/distribution can occur in the chemical synthesis due to slight differences in reaction time, temperature, and concentration or ratio of the reactants, and isolating single isomers from conventional bis-PCBM is time consuming and costly. Even fractionation in subpopulations can lead to variations in isomer distributions within a given subfraction.

For the formation of isomerically pure bisadducts two methods are widely used in fullerene chemistry; directed synthesis and tether-directed synthesis.[5,11-16]

3.2 Synthetic methods to reduce the number of isomers of fullerene higher adducts

3.2.1 Directed synthesis

In directed synthesis the key to isomerically pure adducts is the reversible binding (dynamic covalent bond formation) of Diels-Alder addends, in particular anthracene derivatives, to the fullerene core.[17-19] A large excess of the anthracene derivative results in an equilibrium between the various adducts with those with all *e*-relationships as major product. As described in Chapter 2, reversible addition can lead to the thermodynamically lowest energy isomer, which in most cases is the hexakisadduct with all addends in *e*-relationship.[20,21] The anthracene addends are then replaced by the desired addends (**Figure 3.1**). Yields as high as 50% can be reached for the all *e*-hexakisadduct with this method.[21] However this method will only be useful for the formation of specific higher adducts with all *e*-relationships.

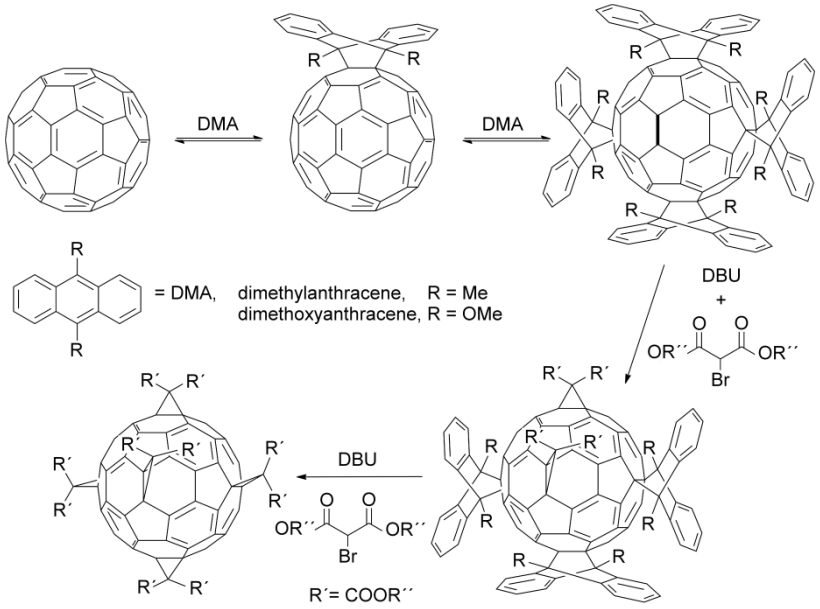

Figure 3.1: *Formation of all e-hexakisadduct through directed synthesis with reversible anthracene derivative additions*

A second method that employs reversible additions which can also be placed under directed reactions is the blocking of sites (also called topochemical control) on the fullerene core by reversible bound addends e.g. Diels-Alder addends[22-24] or possibly even by supramolecular interactions with e.g. crown ethers[25] or calix arenes.[26] The key step is the difference in reaction conditions that are needed for the forward and backward reaction. Instead of forming a template where the reversibly bound addends will be replaced by the desired ones, here the reversibly bound addends form a template in which only specific double bonds remain for addition of the desired addends after which the reversibly bound addends are removed (**Figure 3.2**). These addends are often added through photochemical reaction and removed thermally. However due to the reaction conditions[27] (high temperature) needed for the synthesis of bis-PCBM blocking methods with for example reversibly bound Diels-Alder adducts or supramolecular addends is often not possible.

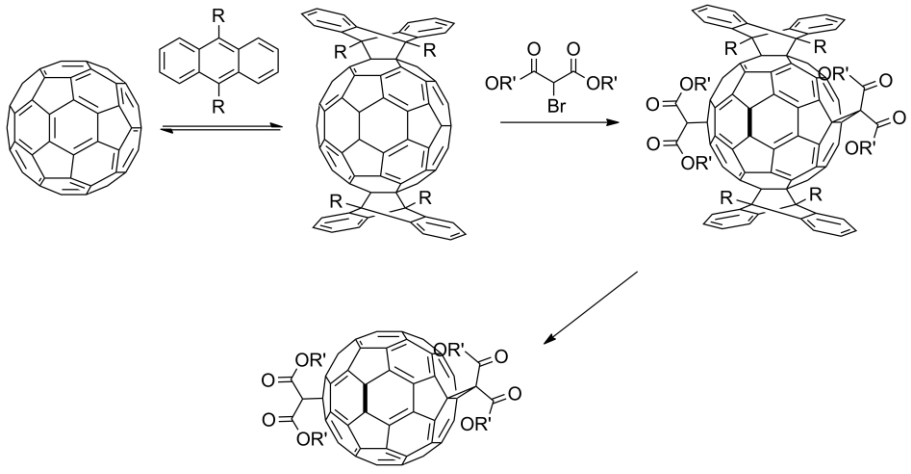

Figure 3.2: *Blocking of reactive sites on the fullerene core by reversible additions, for example employing Diels-Alder reactions for blocking, followed by the removal of these addends after functionalization of the desired adduct is complete.*

3.2.2 Tether-directed synthesis

A different method to obtain isomerically pure higher adducts is through the use of tether-directed synthesis in which both addends are linked together with spacers to an anchoring group.[28] By linking the addends together through a spacer before reacting them with C_{60}, the formation of certain addition patterns is favored.[28] The first attachment acts as an anchor point, imposing a restriction on the reach of the attachment to specific [6,6]-double bonds, depending on the length of the tether. Ideally this should result in high yield and regioselectivity toward one functionalization pattern, preferably employing spacers that are cheap and can be easily synthesized.

Diederich and coworkers first applied tether-directed synthesis in fullerene chemistry in 1994 for the synthesis of different regioisomers and substitution patterns in Bingel additions (addition to a fullerene cage by nucleophilic attack) of malonates to C_{60} (**Figure 3.3**).[29]

Figure 3.3: *Anchor type tethered-directed synthesis.*

By improving the tethers all bisadduct patterns of C_{60} except *cis-1* have been made mainly through Bingel additions in high selectivity. The so called anchor-tether-reactive group conjugates mentioned above (**Figure 3.3**) were designed by PM3 semiempirical calculations with the desired adduct to be the lowest energy isomer.[29,30] Under very dilute conditions these systems afforded the predicted adducts with high regioselectivity. However in this example the anchoring group and the spacers are still present in the end products and in most cases the removal of the directing auxiliaries employed in the synthesis is required to obtain the desired adducts. In later tether-directed functionalisations a practical simplification of the method consisted of

removal of the anchor group transferring its function to each addend already attached to the fullerene to acts as an anchor for the remaining reactive groups.[5,11-16] Conformational preferences of the spacer and steric constraints are the main driving forces for this method. Tethers employing spacers based on the Tröger base[31,32] (two nearly orthogonal aromatic rings) **(3.1)**, xylenens[33-36] **(3.2)**, macrocycles[37,38] **(3.3)**, alkyl of various length[39] and many others[40-43] **(3.4)** have been developed over the years, giving access to various addition patterns for numerous addends.

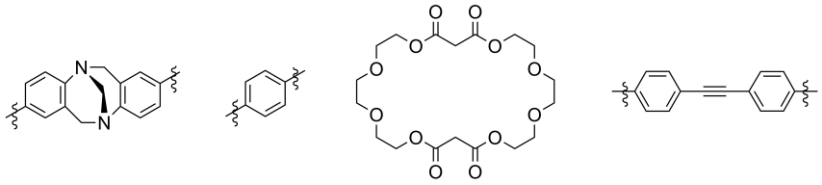

(3.1) **(3.2)** **(3.3)** **(3.4)**

Figure 3.4: *Examples of various tethers used in tether-directed functionalisation of C_{60}.*

3.2.3 Reducing the number of possible isomers of bis-PCBM through the use of tethered addends

To apply this methodology for obtaining isomerically pure bis-PCBM the tether must be chosen in such a way that, after it performed its task during synthesis, it can be easily removed, yielding a bis-PCBM subfraction and allowing comparison with the full isomeric mixture. This limits us to tethers that link the ester groups together, leaving the diazoalkane precursor groups relatively far apart. This is in contrast to the short distance obtained by, for example, linking the phenyl groups together or other tethered systems that have been reported to yield high regioselectivity of the desired addition pattern.[5,8,11-16] Moreover, these other tether systems were specifically designed to target specific addition patterns for chemistry reasons only, not in order to improve a molecular semiconductor. Here, we settle for obtaining subpopulations of isomers because we do not know *a priori* which isomer(s) are the best performing ones. Furthermore, the high temperature needed to form the diazo compound that is

a necessary intermediate in the synthesis of (bis-)PCBM, lowers the stereospecificity of the reaction.[27,44]

A practical reason for accepting subpopulations is that, since large-scale fabrication of organic solar cells would require large quantities of material, highly-diluted reaction conditions that are normally applied in standard tether-directed syntheses to obtain maximized yield of one or two isomers only would be an enormous drawback. For now, we will also accept that concentrated reaction conditions increase the fraction of undesired intermolecular reactions, leading to monoadduct-type impurities and lowering the overall percentage of bisadduct formation.

Interestingly, tether-directed synthesis of bisadducts gives access to isomers that are much less formed in the standard synthetic procedure.[5,11-16]

3.3 Synthesis and characterization

3.3.1 Synthesis of the tethered addends and bis-PCBM subfractions

Esterification of acids and transesterification thereof are well described reactions and many reaction conditions are known.[45,46] The use of transesterification reactions is abundant in tether-directed synthesis of fullerene adducts.

We used three different tethers: ethylene- (C2, **(3.5)**), n-propylene- (C3, **(3.6)**) and n-butylene- (C4, **(3.7)**) moieties.

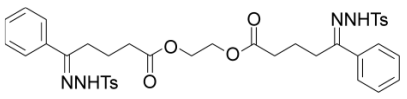

(3.5)

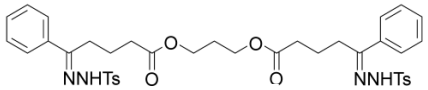

(3.6)

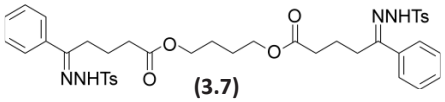

(3.7)

Figure 3.5: *Tethered addends used in the functionalisation of C_{60} to reduce the number of possible isomers that can be formed in the synthesis of bis-PCBM.*

In addition to decreasing the number of possible regioisomers than can form, tethering also reduces the number of possible stereoisomers by restricting the orientation of the ester moiety; only the regioisomers that are close together can have the ester groups pointing in opposite direction due to the short tether. **Scheme 3.1** shows the synthesis of the tethered bis-(4-benzoylbutyric acid tosylhydrazones) and their addition to the fullerene moiety.

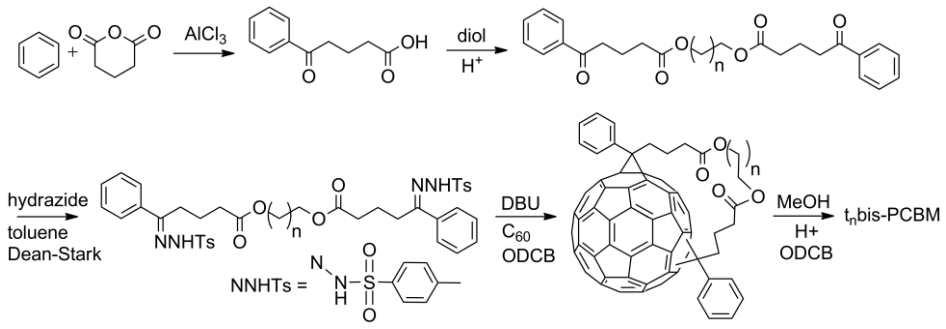

Scheme 3.1: *The synthesis of the tethered tosylhydrazones and their addition to C_{60}. n=1: C2, n=2: C3 and n=3: C4.*

The starting compound 4-benzoyl butyric acid was synthesized, because commercially available material always contains a few percent of methyl-substituted phenyl moiety and upon tethering these impurities double and become significant. 4-Benzoyl butyric acid was reacted in a Dean-Stark apparatus with the appropriate diol in the presence of a catalytic amount of concentrated sulfuric acid. The treatment of the resulting esters with tosylhydrazide in toluene using a Dean-Stark apparatus afforded the bis-tosylhydrazones in good yield. C_{60} and bis-tosylhydrazone were then dissolved in *ortho*-dichlorobenzene. The subsequent addition of t-BuOK induced the transformation of the tosylhydrazone moieties into highly reactive diazo groups, which reacted *in situ* with C_{60} to give the tethered adducts mixtures. The crude product was purified by column chromatography (SiO_2,toluene). The tethered bisadducts were readily transesterified to their corresponding tbis-PCBM subfractions by MeOH in ODCB in the presence of a catalytic amount of concentrated sulfuric acid. While overall yields of bisadducts are not as high as with the conventional synthesis, because of the formation of cross-linked side-products from intermolecular reactions and the partial hydrolysis of the tethered ester by trace amounts of hydroxide in the t-BuOK, resulting in the insoluble acid (carboxylate) analog of PCBM, the isomers obtained are much less represented in the standard full isomer mixture, rendering the isolated yield of the isomers comprising the tethered subpopulations higher than from conventional synthesis (~16% compared to ~11% without using the tether). Employing DBU instead of t-BuOK as the base increased the yield even further to ~25% by eliminating the ester hydrolysis side reaction.

3.3.2 HPLC analysis

Figure 3.6 shows the isomer subpopulations obtained from the three tethered syntheses, analyzed with high performance liquid column chromatography (HPLC). Changes in polarity caused by the different alkyl spacers prohibit a direct comparison of the isomer composition of the three mixtures. However, to a certain extent

(overlapping cannot be excluded), the number of peaks corresponds to the number of isomers represented in the respective subpopulation.

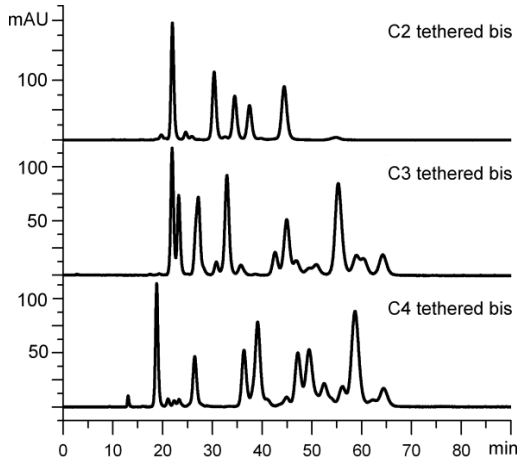

Figure 3.6: *HPLC traces of purified tethered bisadduct samples showing the differences in regioselectivity using tethers with ethylene (top), n-propylene (center), and n-butylene (bottom) moieties.*

The C2-tethered isomer subpopulation (**Figure 3.6** top) shows the highest regioselectivity with only five resolved peaks between 20 and 45 minutes of retention.The C3-tethered subpopulation (**Figure 3.6** middle) also shows five peaks between 20 and 45 minutes, but there is also an additional major peak at 55.3 minutes and there are many minor peaks. The chromatogram of the C4-tethered subpopulation (**Figure 3.6** bottom) shows an expected further increase in number of peaks; 7 major peaks and 9 minor ones.

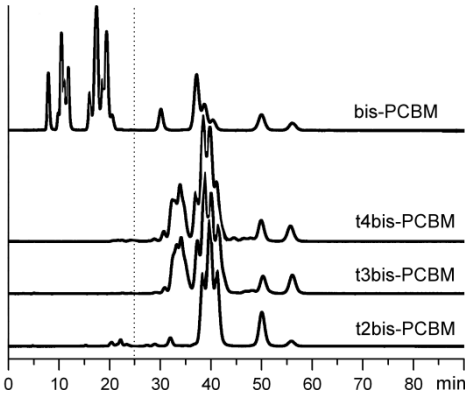

Figure 3.7: *HPLC chromatograms of bis-PCBM and the tbis-PCBM subpopulations.*

Upon transesterification of the C2-, C3-, and C4-tethered bisadduct mixtures to the corresponding bis methyl esters (i.e., bis-PCBMs), all *structural* differences between the three different isomer mixtures are removed. We have thus obtained three bis-PCBM samples with different isomer composition and the peaks belonging to the same isomers in the different subpopulations are now comparable in retention time. **Figure 3.7** shows the HPLC chromatograms of the bis-PCBM subpopulations $t_2$bis-PCBM, $t_3$bis-PCBM and $t_4$bis-PCBM, as well as the full isomeric bis-PCBM. The most striking difference between the HPLC chromatograms of the bisadduct subpopulations formed through tethered synthesis and that of conventional bis-PCBM is the absence of peaks with retention times shorter than 25 minutes. A clear difference between $t_2$bis-PCBM on the one side and $t_3$bis-PCBM and $t_4$bis-PCBM on the other appears. For $t_2$bis-PCBM there are only four major peaks visible in the chromatogram: 38.4 min, 39.8 min, 41.2 min and 50.1 min. These are also visible in the full isomer mixture of bis-PCBM, as well as in both other subpopulations. However, the isomers that represent the peaks at 33 minutes are only present in small quantities in both conventional bis-PCBM and $t_2$bis-PCBM, whereas they become major constituents in $t_3$bis- and $t_4$bis-PCBM.

3.3.3 NMR

High resolution ^{13}C NMR spectra of the tethered bisadduct subpopulations and the tbis-PCBM subpopulations support the HPLC result, clearly indicating an increase in the number of isomers formed with increasing tether length.

3.3.4 Molecular modeling

To gain more insight in the different subpopulations, and the isomers they comprise, we used semi-empirical (PM3) molecular modeling to compare the relative energies of the products with different tether length.

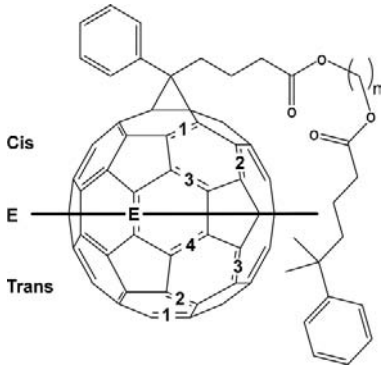

C2	C3	C4
Cis 2a	Cis 2a	Cis 2a
Cis 2b	Cis 2b	Cis 2b
Cis 2c	Cis 2c	Cis 2c
Cis 3b	Cis 3b	Cis3a
Cis 3c	Cis 3c	Cis 3b
Ec	Ec	Cis 3c
Trans 4c	Trans 4b	Eb
	Trans 4c	Ec
	Trans 3a	Trans 4b
	Trans 3b	Trans 4c
		Trans 3a
		Trans 3b
		Trans 2c

Figure 3.9: *Graphical representation of the bisadducts (left), the table showing isomers within 10 kcal/mol of the lowest energy isomer within each series, calculated from* the point-energies *of the PM3-optimized geometries of the tethered bisadducts (right); bold indicating the lowest energy isomer for each tether.*

Figure 3.9 shows the isomers that are within 10 kcal/mol (which is considered easily accessible under the reaction conditions) of the lowest-energy isomer within a series. Isomers with both anchor points on the same hemisphere of the fullerene cage are referred to as *cis*, those with the second attachment point on the equator of the fullerene core as *e* and those bridging both hemispheres as *trans*. The orientation of the addends with respect to each other is designated as *a* when both phenyl groups are pointing towards each other (endo-endo), as *b* when the esters are pointing towards each other (exo-exo), and as *c* when one ester is pointing towards a phenyl group (endo-exo). In agreement with the HPLC data, we observed an increase in the total number of isomers for longer tethers. The major isomers of the C2 subpopulation are predicted to be present in both other subpopulations as major isomers, however with increasing tether length the energy difference between the different isomers also becomes smaller. This is because isomers with anchor positions further apart are more easily accessible with long tethers, but the isomers with anchor points in relatively close proximity will suffer more from steric crowding due to the increasing volume of the tether, resulting in smaller energy differences between the different addition patterns.

Molecular modeling predicts all three *cis-2*, two of the *cis-3* isomers, and one of the two *e* isomers to be the major reaction products. In double cyclopropanations of C_{60}, the *trans-3* and *e* bisadducts are considered to be the major isomers when steric hinder prevents the formation of the *cis-1* isomers.[1] The *cis* isomers are also expected to be the most polar. This is in agreement with the results obtained from HPLC analysis. With increasing tether length the possibility to form *trans* isomers increases, this is consistent with the appearance of the extra peaks with shorter retention time for both the $t_3$bis- and $t_4$bis-PCBM.

3.3.5 Cyclic voltammetry

We measured cyclic voltammograms for the three tethered bisadducts C2, C3, and C4, as well as the bis-PCBM subpopulations $t_2$bis-PCBM, $t_3$bis-PCBM, $t_4$bis-PCBM, and conventional bis-PCBM (**Figure 3.10**).

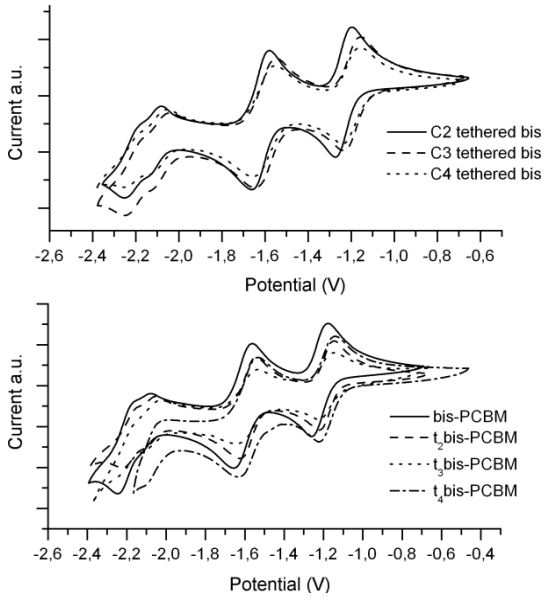

Figure 3.10: *Cyclic voltammograms of the tethered adducts, the transesterified tbis-PCBM subpopulations, and of bis-PCBM obtained through conventional synthesis. Reduction potentials were measured in 4:1 ODCB/acetonitrile and are relative to ferrocene (that is, $E_{1/2\ ox}$ of ferrocene was placed at 0V).*

Comparing the tethered isomer mixtures, the C2 mixture has a slightly more negative first reduction potential than both C3 and C4 mixtures, which exhibit similar potentials ($E_{1/2\ red}$ = -1.24 V for C2 tethered bisadduct vs. $E_{1/2\ red}$ = -1.20 V for C3- and C4-tethered bisadduct). The tbis-PCBM subpopulations show no significant variation in reduction potential ($E_{1/2\ red}$ = -1.18 V, -1.19 V, and -1.18 V for $t_2$bis-, $t_3$bis-, and $t_4$bis-PCBM, respectively). The widths of the first reduction wave of the full isomer mixture and those of both $t_3$bis- and $t_4$bis-PCBM subpopulations are larger than that of the $t_2$bis-

PCBM subpopulation (120 mV compared 90 mV for $t_2$bis-PCBM, based on the width of the onsets, i.e. base-width). This is in accord with the fact that there are less isomers present in the $t_2$bis-PCBM subpopulation. In addition, the first reduction of the full isomer mixture is at a more negative potential than that of the three subpopulations ($E_{1/2\ red}$ = -1.22 V compared to $E_{1/2\ red}$ = -1.18 V / -1.19 V). Apparently the first reduction wave in the full isomer mixture is dominated by isomers that are not (or less) present in the subpopulations formed through tethering with these three alkyl spacers.

3.4 Device testing

3.4.1 P3HT Devices

In order to investigate the effect of the tethered bisadducts and their transesterified tbis-PCBM subpopulations on photovoltaic performance, bulk heterojunction solar cells were fabricated using regioregular P3HT as the electron donor material. P3HT and the fullerene derivatives were dissolved in a 1:1.2 weight ratio in chloroform and stirred overnight. The photoactive layers were spin-cast under nitrogen atmosphere on clean glass substrates pre-patterned with indium tin oxide and a 60 nm thick film of poly(3,4-ethylenedioxythiophene)/poly(styrene sulfonic acid) (VP AI4083, H.C. Starck). The as-cast layers were annealed subsequently at 135 °C for 15 minutes. The devices were finished by thermal evaporation of a LiF(1 nm)/Al(100 nm) cathode. Electrical measurements were conducted in an N_2 controlled atmosphere in the dark and under illumination of a Steuernagel SolarConstant 1200 metal halide lamp, which was set to 1 Sun intensity using a silicon reference cell and correcting for spectral mismatch.

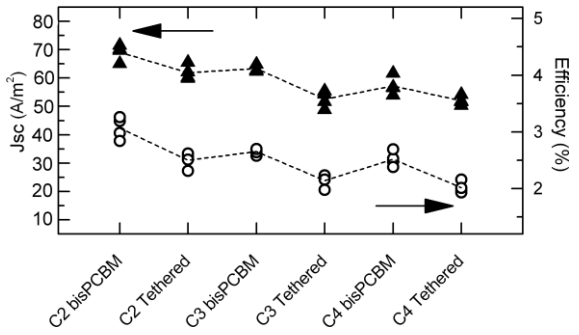

Figure 3.11: *Device performance depicted in efficiency (circles, right axis) and short circuit current (triangle, left axis) of the tethered adducts and their transesterified tbis-PCBM counterparts.*

As can be seen from **Figure 3.11**, the power conversion efficiency decreases for increasing alkyl spacer length. This trend is preserved upon removal of the spacer by transesterification to the corresponding tbis-PCBM subpopulation, however, yielding higher efficiencies. The efficiency decrease with increasing spacer length was found to be governed by a decrease in J_{sc}, showing a similar trend. To assess the origin of this decrease in J_{sc}, various processes causing a reduced photocurrent generation have to be investigated. Since the thickness of the photoactive layer was the same for all devices (230 nm), a variation in light absorption is unlikely. Another potential cause of a low J_{sc} is a less balanced or weak hole and electron transport in the donor and acceptor phase, respectively.

The hole mobility extracted from hole-only devices of the polymer:fullerene blends was observed to be independent of the fullerene derivatives used, yielding a value of 5 × 10^{-8} m^2 V^{-1} s^{-1}, consistent with previous measurements on P3HT:PCBM cells.[47] In addition, the dark *J–V* characteristics of the solar cells, dominated by electron transport in the acceptor phase, were similar for all made with the three tethered derivative samples and slightly lower in current (factor 1.5) than devices made with

their corresponding tbis-PCBM subpopulations, which also showed no mutual variation.

Hence, the transport properties in the blend cannot account for the observed influence on J_{sc} In previous reports, a voltage-dependent photocurrent was observed, caused by a too tightly intermixed blend, leading to incomplete charge dissociation from the geminate ion pair (charge transfer exciton) at short-circuit conditions.[6,7,48,49] At high reverse electric fields, the dissociation is enhanced, finally resulting in saturation of the photo-generated current. However, in our case, the saturated photocurrents follow the same trend as J_{sc} for the different fullerene derivatives, indicating that the amount of charge transfer excitons generated decreases for increasing alkyl spacer lengths. This suggests that less photo-generated excitons undergo charge transfer to the acceptor, which, considering the small exciton diffusion length, could be indicative of a too large phase separation.

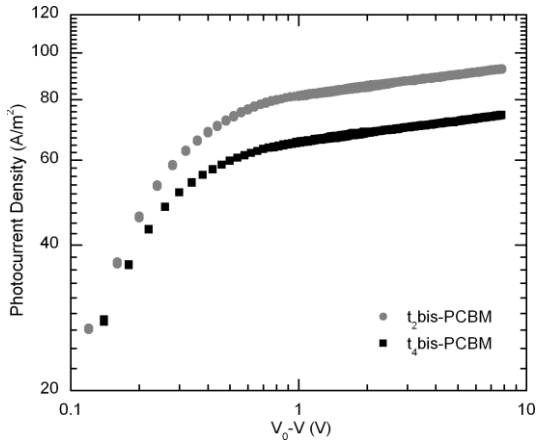

Figure 3.12: *Experimental photocurrent density as a function of the effective applied voltage (V_0-V) for $t_2$bis-PCBM and $t_4$bis-PCBM, where the photocurrent is the difference between the current in dark and under illumination. The compensation voltage V_0 is the voltage where the photocurrent equals zero.*

Another issue that should be addressed is the difference in polarity of the tbis-PCBM subpopulations compared to that of the full isomer mixture. A large contribution of the polar *cis*-isomers is expected to cause an increase in the average relative permittivity of the blend, which may cause an enhanced dissociation of charge transfer excitons. Lenes *et al.* observed an increased charge dissociation in a polymer:fullerene blend system by using a polymer with enhanced permittivity.[50] However, in our measurements the observed J_{sc} trend for different acceptors is caused by a difference in *saturated* photocurrent, rather than a change in voltage dependence of the photocurrent, as observed by Lenes *et al.* (**Figure 3.12**). Therefore, the difference in fullerene polarity is not expected to be the main cause of the reduction in J_{sc} upon using larger alkyl tethers.

In addition to the observed J_{sc} dependence, variations in V_{oc} and fill factors were also observed, where the latter depends mainly on the presence or absence of the spacer. This can be attributed to the aforementioned decrease in the electron transport for the tethered fullerene derivatives, increasing the layer resistance and thereby inducing a decrease in fill factor. The V_{oc} exhibits an almost opposite dependence, indicating that it is also determined, in addition to minor changes in the reduction potential, by a variation in electron transport.

In order to investigate how the performance of the $t_2$bis-PCBM subpopulation compared to that of the full isomer mixture, P3HT-based solar cells were fabricated simultaneously, using the exact same conditions for both fullerene derivatives. The *J*–*V* characteristics of the 300 nm thick devices in dark and under illumination are depicted in **Figure 3.13**.

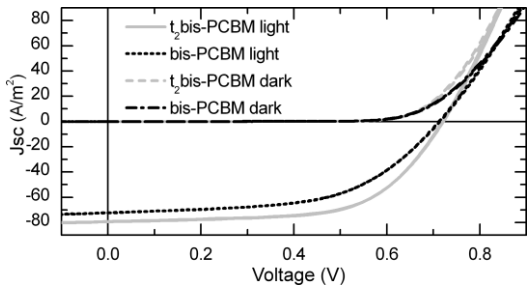

Figure 3.13: *Device performance of the $t_2$bis-PCBM subpopulation directly compared to the performance of a bis-PCBM device.*

A clear improvement was observed when using $t_2$bis-PCBM, yielding a PCE of 3.5% compared to 2.9% obtained for conventional bis-PCBM. This improvement can be attributed to an enhanced microstructure upon using suitable isomer subpopulation. The results obtained here are in line with previous research,[6-8,51] pointing out the large polymer domain sizes in thermally annealed P3HT:bis-PCBM films, compared to their PCBM based analogues. It is therefore expected that an increase in J_{sc} can also be obtained for P3HT:$t_2$bis-PCBM when using the beneficial solvent annealing approach, for which a PCE of 4.5% was obtained using the full isomer mixture.[6-8]

3.4.2 PF10TBT Devices

The bis-PCBM subfraction obtained from the ethylene tethered bisadduct, $t_2$bis-PCBM, as well as conventional bis-PCBM were also tested in organic photovoltaic devices comprising PF10TBT as donor. The prelimary results are given in **Table 3.1**.

Acceptor	J_{sc} (A/m^2)	V_{oc} (V)	FF	MPP (mW/cm^2)
Bis-PCBM	25.18	1.127	0.45	1.27
t_2Bis-PCBM	29.57	1.114	0.46	1.51

Table 3.1: *Preliminary results of the $t_2$bis-PCBM isomeric subfraction compared to conventional bis-PCBM as acceptor material in devices comprising PF10TBT as the donor.*

Also here the reduction of the number of bisadduct isomers has a beneficial effect on the morphology and performance of the active layer as compared to conventional bis-PCBM. The isomeric subfraction obtained from tethering slightly outperforms the conventional bis-PCBM mixture through an increase in short circuit current density. Even though the open circuit voltage is somewhat lower than for conventional bis-PCBM the cell comprising $t_2$bis-PCBM has a higher overall efficiency (MPP 1.51 mW/cm^2 for $t_2$bis-PCBM compared to 1.27 mW/cm^2 for bis-PCBM).

3.5 Conclusions

Three subpopulations of bis-PCBM isomers were synthesized via tether-directed synthesis using different alkyl spacers of increasing length. Molecular modeling (PM3) shows the formation of the more polar *cis-2*, *cis-3* and *e* isomers to be favored, which is in good agreement with HPLC results. Bis-PCBM isomers with both addends on the same hemisphere have a relatively large part of the electronic surface of the fullerene unblocked by their aliphatic tails, similar to their monoadduct analogues, and π-π interactions are relatively undisturbed in all directions which could lead to improved mobilities and be the origin of the higher performance of the $t_2$bis-PCBM subpopulation. A clear improvement in PCE was found (3.5% compared to 2.9% for conventional bis-PCBM), to be caused mainly by an increase in both J_{sc} (72.4 compared to 79.6 A/m^2) and fill factor (0.55 compared to 0.62). Also in combination with PF10TBT the reduction of the number of bisadduct isomers has a beneficial effect on the morphology and performance of the active layer as compared to conventional bis-PCBM. The isomeric subfraction obtained from tethering slightly outperforms the conventional bis-PCBM mixture through an increase in short circuit current density. Even though the open circuit voltage is somewhat lower than for conventional bis-PCBM the cell comprising $t_2$bis-PCBM has a higher overall efficiency. This is promising with regard to other bis-PCBM/polymer combinations in which current density is still the limiting factor on the performance in bulk heterojunctions. Based on these results

the reduction of the number of bisadduct isomers can have a beneficial effect on the morphology and performance in other combinations of polymer and bisadduct. Improving the performance even further will require more rigid tethers that offer more control over the accessibility of double bonds to further reduce the number of isomers of bis-PCBM that are formed, ultimately to single isomers. Morphology studies of blends of single isomers can then give even more insight into which addition patterns would lead to the best performing morphologies. Analysis of the cyclic voltammograms shows the existence of isomers with even more negative reduction potentials, suggesting that further improvements in V_{oc} are possible. This extra increase in LUMO level should manifest itself as an increased V_{oc} which, depending on the balance between highest LUMO and best performing addition pattern, can then lead to further improvements in higher adduct fullerene/polymer bulk heterojunction solar cells. Future work will focus the development of methods to access and isolate these isomers.

3.6 Outlook

Coordinating tethers like porphyrins or more rigid systems based on Tröger base, are a next step for obtaining the further apart lying *trans*-isomers as well as reducing the number of isomers that can be formed even further.[5,11-16] However due to the relative large distance between the functional groups and the spacer compared to other tether system intermolecular bridging between different fullerene moieties would still be a potentially major side reaction.

Placing the ester moieties closer to the cyclopropylring would make tethering more effective by reducing the distance between the reactive groups. Attaching the phenyl rings together would also reduce the freedom of the tethered system. The very best option would be in linking both the esters and the phenyls together in macrocyclic ring systems, simular to those developed by Hirsch based on equalizing the strain in both alkyl chains.[37,38] This would give a high degree in

freedom towards various addition patterns by simply changing the alkyl chain and their relative length while retaining conformational strain needed for high selectivity.

3.7 Experimental

3.7.1 Device fabrication

P3HT and the fullerene derivatives were dissolved in a 1:1.2 weight ratio in chloroform and the solution was stirred overnight. The photoactive layers were spin-cast under nitrogen atmosphere on clean glass substrates pre-patterned with indium tin oxide and a 60 nm thick film of poly(3,4-ethylenedioxythiophene)/poly(styrenesulfonic acid) (VP AI4083, H.C. Starck). The as-cast layers were annealed subsequently at 135 °C for 15 minutes. The devices were finished by thermal evaporation of a LiF(1 nm)/Al(100 nm) cathode. Electrical measurements were conducted in an N_2 controlled atmosphere in dark and under illumination of a Steuernagel SolarConstant 1200 metal halide lamp, which was set to 1 Sun intensity using a silicon reference cell and correcting for spectral mismatch.

3.7.2 Materials

All reagents and solvents were used as received or purified using standard procedures. [60]-Fullerene (99.5 %) was purchased from Bucky USA and used without further purification. Flash chromatography was performed using silica gel (Kieselgel Merck Type 9385 (230-400 mesh)). ^{1}H NMR and ^{13}C NMR spectra were recorded on a Varian Unity Plus (500MHz), on a Varian AMX-400 (400 MHz), or on a Varian VXR-200 (200 MHz) instrument as indicated, at 298 K using TMS as an internal standard, *J* values are given in Hertz. HPLC analyses were performed on a Hewlett Packard HP LCChemstation 3D (HP 1100 Series) using an analytical Cosmosil Buckyprep column (4.6 x 250 mm) or a Econosphere silica column (3 x 100 mm).

3.7.3 Synthesis

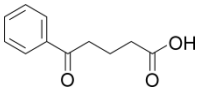

4-benzoyl butyric acid. A 5 L flask equipped with mechanical stirrer and placed in an ice water bath was charged with 500 mL toluene-free benzene and 512 g $AlCl_3$. A solution of 192 g glutaric anhydride (1.68 mol) in 300 mL 1,2-dichloroethane was made, filtered, and loaded in a dropping funnel. The glutaric anhydride solution was added over period of 2.5 hours to the benzene solution under vigorous stirring. The reaction mixture changed from colorless to yellow, to red, to almost black. The mixture was stirred overnight allowing it to slowly warm up to room temperature. The resulting slurry was poured on ice and extracted with ethyl acetate. The organic fraction was collected and evaporated to dryness *in vacuo* to remove the remaining benzene and 1,2-dichloroethane. The crude product was redissolved in ethyl acetate and washed with water. The organic layer was collected and extracted with a KOH/water solution. The aqueous layer was the acidified with HCl and the product was extracted with ethyl acetate. The organic layer was washed two more times with water, followed by brine and dried over Na_2SO_4. The solvent was removed *in vacuo* yielding 260 g crude product. Recrystalisation from hot toluene yielded the pure acid as white crystals (205 g, 63%). ^{1}H NMR (400 MHz, $CDCl_3$) δ 7.67 – 7.53 (m, 2H), 7.41 – 7.18 (m, 1H), 7.18 – 7.03 (m, 2H), 2.71 (td, *J* = 7.3, 2.3, 2H), 2.04 (td, *J* = 7.2, 2.2, 2H), and 1.91 – 1.46 (m, 2H); ^{13}C NMR (101 MHz, $CDCl_3$) δ 199.48, 175.05, 136.74, 133.03, 128.58, 127.90, 37.50, 33.16, and 19.34; mp 127.4°C, lit.: 126-128°C.

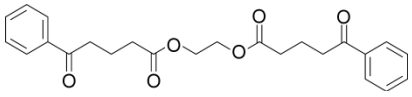

C2 bis(keto ester). A flame dried 250 mL three-neck flask, equipped with stirring bar and Dean Stark setup, was charged with 10.0 g 4-benzoylbutyric acid (52.0 mmol), 1.4 mL ethylene glycol (0.5 eq.), and 100 ml toluene. A few drops of concentrated sulfuric acid were added. The resulting suspension was heated to reflux temperature and stirred overnight. Upon heating a clear solution was formed. The solution was cooled to room temperature and the solvent was removed *in vacuo*. Pure product was obtained after

column chromatography (SiO_2, petroleum ether 40-60/ethyl acetate 2:1), followed by recrystalisation from diethyl ether. The pure product was obtained as 9.0 g white solid (22 mmol, 88%). ^{1}H NMR (400 MHz, $CDCl_3$) δ 8.01 – 7.92 (m, 4H), 7.55 (ddd, *J* = 6.7, 2.5, 1.3, 2H), 7.49 – 7.39 (m, 4H), 4.30 (d, *J* = 1.0, 4H), 3.05 (t, *J* = 7.1, 4H), 2.45 (t, *J* = 7.2, 4H), and 2.07 (p, *J* = 7.1, 4H); ^{13}C NMR (101 MHz, $CDCl_3$) δ 199.48, 173.21, 136.99, 133.31, 128.82, 128.21, 62.34, 37.55, 33.35, and 19.43.

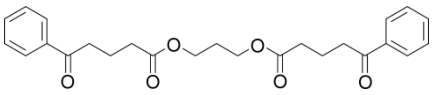

C3 bis(keto ester). 10.0 g 4-benzoylbutyric acid (52 mmol) was dissolved in 100 mL dry toluene along with 1.8 mL 1,3-propanediol (0.5 equiv.) and three drops of concentrated sulfuric acid in a Dean-Stark setup. The resulting mixture was heated to reflux temperature under N_2 atmosphere and stirred at this temperature overnight. The resulting yellow solution was cooled to room temperature and solvent was removed *in vacuo*. The residue was dissolved in ethyl acetate, the solution was washed 10% Na_2CO_3 (2 x 50 mL) to remove starting compounds and side products. The organic layer was washed water (2 x 50 mL) and then with brine (50 mL), dried over Na_2SO_4 and stripped of solvent *in vacuo*, yielding a yellow oil. The oil was absorbed on SiO_2 and purified using column chromatography (SiO_2, heptane/ethyl acetate 1:1). After crystallization from diethyl ether, 8.3 g of pure product was obtained as white crystals (20 mmol, 78%). ^{1}H NMR (400 MHz, $CDCl_3$) δ 7.93-7.89 (m; 4H), 7.53 – 7.47 (m; 2H), 7.43-7.37 (m; 4H), 4.12 (t, *J* = 6.3; 4H), 3.00 (t, *J* = 7.1; 4H), 2.44 (t, *J* = 7.2; 4H), 2.02 (p, *J* = 7.1; 4H), and 1.92 (p, *J* = 6.2; 2H); ^{13}C NMR (101 MHz, $CDCl_3$) δ 199.40, 173.23, 136.90, 133.18, 128.70, 128.51, 128.11, 77.55, 77.23, 76.91, 61.08, 37.50, 33.36, 28.09, 19.40, and 19.27.

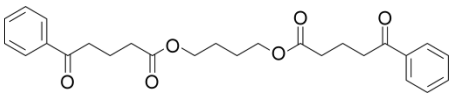

C4 bis(keto ester) 10.0 g benzoylbutyric acid (52 mmol) was dissolved in 100 mL dry toluene in a Dean-Stark setup along with 2.3 mL 1,4-butanediol (0.5 equiv) and three drop of concentrated sulfuric acid.

The solution was heated to reflux temperature and stirred during 48 hours. The resulting yellow solution was cooled to room temperature and solvent was removed *in vacuo*. The residue was dissolved in ethyl acetate and the solution was washed 10% Na_2CO_3 (2 x 50 mL) to remove starting compounds and side products. The organic layer was washed with water (2 x 50 mL) and then with brine (50 mL), dried on Na_2SO_4, and stripped of solvent *in vacuo* yielding a yellow oil. The oil was absorbed on SiO_2 and further purified through column chromatography (SiO_2, heptane/ethyl acetate 1:1). Crystallization from dry diethyl ether yielded 7.1 g of the pure keto ester as white powder (16 mmol, 62%). ^{1}H NMR (400 MHz, $CDCl_3$) δ 7.95 – 7.91 (m; 4H), 7.56 – 7.50 (m; 3H), 7.46 – 7.39 (m; 5H), 4.07 (m; 4H), 3.08-2.99 (m; 4H), 2.47 (t, *J* = 7.1; 2H), 2.41 (t, *J* = 7.2; 4H), 2.13 – 2.03 (m; 4H), and 1.66 (m; 4H); ^{13}C NMR (101 MHz, $CDCl_3$) δ 199.58, 199.48, 178.74, 173.45, 136.96, 136.93, 133.29, 133.27, 128.77, 128.19, 77.55, 77.23, 76.91, 64.06, 37.61, 37.49, 33.50, 33.17, 25.47, 19.53, and 19.20.

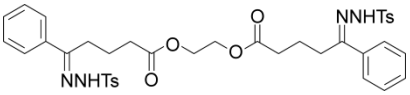

C2 bis(tosyl hydrazine). A flame dried 250 mL three-neck flask, equipped with stirring bar and Dean Stark apparatus, was loaded with 7.0 g C2 bis(keto ester) (17.1 mmol), and 7.0 g tosylhydrazide (2.2 eq.) in 100 mL toluene. The resulting mixture was heated to reflux temperature and stirred overnight. Upon heating a clear solution was formed. The solution was cooled to room temperature. White solids precipitated from the solution upon cooling. The solids were filtered off and placed in a vacuum oven overnight for drying (11.2 g, 88%). ^{1}H NMR (400 MHz, $CDCL_3$) δ 9.27 (s, 2H), 7.89 (d, J = 8.1, 4H), 7.70 – 7.63 (m, 4H), 7.39 – 7.29 (m, 6H), 7.27 – 7.22 (m, 4H), 4.30 (d, J = 1.0, 4H), 2.71 – 2.59 (m, 4H), 2.46 – 2.30 (m, 10H), 2.15 – 2.00 (m, 2H), and 1.81 – 1.61 (m, 2H); ^{13}C NMR (101 MHz, $CDCl_3$) δ 174.37, 154.18, 144.06, 136.37, 136.07, 129.76, 128.67, 128.18, 126.46, 63.14, 32.66, 26.11, 21.83, and 21.10.

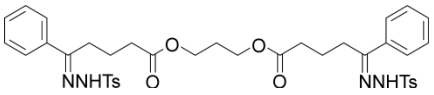

C3 bis(tosylhydrazone). 8.8 g C3 bis(keto ester) (20.7 mmol) was dissolved in 100 mL toluene under N_2 atmosphere in a Dean-Stark setup. 7.7 g tosylhydrazide (41.4 mmol, 2 equiv.) was added and the reaction mixture was stirred overnight at reflux temperature. The resulting yellow solution was cooled to room temperature and placed in an ice/water bath overnight while stirring. The solids were filtered off, washed with diethyl ether, and dried in a vacuum oven. The pure product was obtained as 14.9 g white powder (19.6 mmol, 95%). ^{1}H NMR (400 MHz, $CDCl_3$) δ 9.24 (s; 2H), 7.90 (d, *J* = 8.3; 4H), 7.70 – 7.59 (m; 4H), 7.38 – 7.31 (m; 6H), 7.30 – 7.22 (m; 4H), 4.33 (t, *J* = 6.1; 4H), 2.71 – 2.59 (m; 4H), 2.46 – 2.30 (m; 10H), 2.15 – 2.00 (m; 2H), and 1.81 – 1.61 (m; 4H); ^{13}C NMR (101 MHz, $CDCl_3$) δ 174.60, 154.17, 143.92, 136.31, 136.08, 129.67, 129.62, 128.57, 128.07, 126.39, 61.61, 32.51, 27.94, 26.06, 21.72, and 21.12.

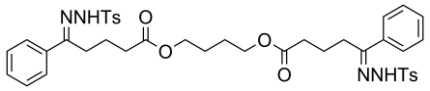

C4 bis(tosylhydrazone). 4.5 g C4 bis(keto ester) (10.2 mmol) was dissolved in 100 mL toluene under N_2 atmosphere in a Dean-Stark setup. 3.8 g tosylhydrazide (20.4 mmol, 2 equiv.) was added and the reaction mixture was stirred overnight at reflux temperature. The solution turned from colorless to orange overnight. It was cooled to room temperature and placed in an ice/water bath overnight. The solids that were formed were filtered off, washed three times with cold diethyl ether and dried in a vacuum oven. The pure product was obtained as 6.5 g white powder (8.4 mmol, 82%). ^{1}H NMR (400 MHz, $CDCl_3$) δ 9.25 (s; 2H), 7.93-9.87 (m; 4H), 7.66 – 7.62 (m; 4H), 7.35–7.30 (m; 6H), 7.30 – 7.25 (m; 4H), 4.27-4.21 (m; 4H), 2.67 – 2.61 (m; 4H), 2.44 – 2.33 (m; 10H), 1.80-1.75 (m; 2H), and 1.75 – 1.64 (m; 4H); ^{13}C NMR (101 MHz, $CDCl_3$) δ 174.70, 154.07, 143.94, 136.35, 136.16, 129.69, 128.61, 128.12, 126.41, 64.98, 32.55, 26.12, 25.42, 21.77, and 21.16.

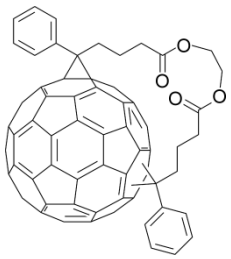

C2 Tethered C_{60} bisadduct. C2 bis(tosylhydrazone) (0.5g, 0.69 mmol) was dissolved in 50 mL pyridine in a flame dried 2 L flask under inert atmosphere. 0.22 mL 1,8-diazabicyclo[5.4.0]undec-7-ene (DBU) was added (1.47 mmol, 2.1 equiv.) and the resulting mixture was stirred for 30 minutes. A solution of 0.5 g C_{60} (0.69 mmol) in 1 L ODCB was added. The resulting solution was heated with aid of a heat-gun in 15 minutes to 82 ^{o}C and then overnight illumination with a 150 W sodium lamp was started. The mixture was concentrated *in vacuo* and purified by column chromatography (SiO_2, toluene). After removal of the eluent *in vacuo* a dark solid remained. The solid was precipitated from ODCB in pentane and subsequently centrifuged. The remaining red pellet was washed twice with pentane and dried in a vacuum oven at 40 ^{o}C overnight. This yielded 183 mg red brown solid (0.17 mmol, 25%). ^{1}H NMR (500 MHz, CS_2 with D_2O insert) 8.00-7.15 (broad, 10H), 4.72-3.87 (broad, 4H), and 3.47-0.95 (broad, 12H); ^{13}C NMR (126 MHz, CS_2 with D_2O insert) δ 169.15, 169.07, 168.90, 168.81, 168.75, 168.72, 168.66, 168.42, 168.33, 149.32, 148.30, 148.23, 147.86, 147.67, 147.05, 146.84, 146.62, 146.01, 145.49, 145.15, 145.06, 145.02, 144.97, 144.91, 144.74, 144.62, 144.59, 144.30, 144.26, 144.15, 144.02, 143.98, 143.80, 143.77, 143.74, 143.70, 143.66, 143.60, 143.52, 143.48, 143.41, 143.34, 143.27, 143.16, 143.12, 143.05, 143.01, 142.96, 142.90, 142.82, 142.79, 142.63, 142.56, 142.49, 142.42, 142.39, 142.31, 142.25, 142.22, 142.15, 142.07, 142.01, 141.96, 141.93, 141.85, 141.77, 141.61, 141.57, 141.53, 141.45, 141.36, 141.34, 141.30, 141.22, 141.16, 141.08, 141.02, 140.96, 140.87, 140.84, 140.77, 140.65, 140.40, 140.36, 140.27, 140.07, 139.99, 139.83, 139.76, 139.66, 139.59, 139.56, 139.41, 139.34, 139.29, 139.23, 139.21, 139.00, 138.90, 138.79, 138.75, 138.65, 138.62, 138.54, 138.42, 138.21, 138.13, 137.90, 137.20, 137.14, 136.56, 136.44, 136.30, 135.44, 135.36, 135.24, 135.15, 135.07, 134.96, 134.85, 134.56, 134.48, 134.35, 134.26, 133.94, 133.85, 133.76, 133.72, 133.40, 133.30, 133.16, 132.94, 132.75, 132.12, 131.21, 130.84, 130.75, 130.29, 129.86, 129.77, 129.65, 129.31, 129.14, 128.86, 128.43, 128.23, 128.10, 126.77,

126.71, 126.30, 126.20, 126.05, 125.94, 125.92, 125.87, 125.83, 125.44, 125.28, 124.58, 123.19, 78.57, 77.86, 77.65, 77.02, 76.71, 75.48, 75.28, 75.12, 75.02, 74.86, 74.80, 74.11, 73.96, 73.42, 72.66, 71.97, 60.87, 60.64, 60.47, 60.10, 60.03, 59.80, 59.54, 59.33, 59.27, 51.12, 47.54, 47.04, 46.94, 46.62, 45.45, 45.36, 44.98, 42.98, 32.60, 32.22, 32.08, 31.81, 31.61, 31.15, 30.95, 30.83, 30.77, 30.60, 30.43, 30.30, 30.19, 30.03, 29.86, 28.81, 28.68, 28.38, 27.99, 27.69, 23.24, 21.28, 21.21, 20.72, 20.23, 19.81, 19.76, 19.60, 19.50, 18.96, 18.61, and 12.54

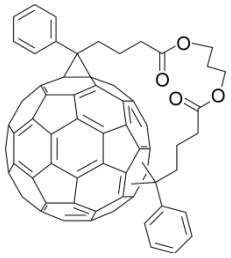

C3 tethered bisadduct. 1.1 g C3 bis(tosylhydrazone) was dissolved in 30 mL dry pyridine in a flame dried 2 L three-necked flask under N_2 atmosphere. 0.45 mL DBU was added and the solution was stirred for 20 min at room temperature. A solution of 1.0 g C_{60} (1.4 mmol) in 1 L ODCB was prepared. The C_{60} solution was degassed three times and added to the pyridine solution. The resulting mixture was degassed a second time (three vacuum/N_2 purges) and the solution was heated to 85 ^{o}C, after which illumination with a 150 W Sodium lamp was started. The reaction mixture was stirred overnight at 85 ^{o}C under illumination. The solvent was removed *in vacuo* and the residue was extracted with toluene. The soluble fraction was further purified by column chromatography (SiO_2, toluene/ethyl acetate 95:5). The C3 tethered bisadduct fraction was collected, precipitated with methanol, washed twice with methanol, once with pentane, and dried overnight in a vacuum oven at 40 ^{o}C. The pure product was obtained as 236 mg red powder (0.3 mmol, 22%).^{1}H NMR (500 MHz, CS_2 with D_2O insert) 8.25-7.07 (broad, 10H), 4.53-3.83 (broad, 4H), and 3.59-0.91 (broad, 14H); ^{13}C NMR (126 MHz, CS_2 with D_2O insert) δ 172.08, 172.08, 172.00, 172.00, 171.92, 171.74, 171.47, 171.47, 171.31, 171.31, 171.22, 171.22, 171.16, 171.05, 171.05, 170.94, 170.94, 170.86, 170.73, 170.73, 170.68, 170.43, 170.25, 170.25, 151.79, 151.35, 150.62, 150.20, 149.62, 149.54, 149.15, 148.41, 147.97, 147.52, 147.48, 147.43, 147.39, 147.18, 147.15, 147.13, 147.09, 146.79, 146.63, 146.56, 146.40, 146.36, 146.27, 146.20, 146.12,

146.08, 146.02, 145.98, 145.94, 145.88, 145.79, 145.71, 145.50, 145.43, 145.41, 145.34, 145.26, 145.24, 145.19, 145.04, 145.00, 144.97, 144.93, 144.85, 144.75, 144.71, 144.64, 144.57, 144.52, 144.42, 144.36, 144.27, 144.21, 144.11, 144.00, 143.97, 143.93, 143.89, 143.80, 143.75, 143.63, 143.58, 143.56, 143.50, 143.46, 143.40, 143.34, 143.30, 143.09, 143.05, 142.88, 142.78, 142.68, 142.60, 142.46, 142.40, 141.97, 141.86, 141.72, 141.63, 141.40, 141.27, 141.22, 141.18, 141.02, 140.96, 140.92, 140.78, 140.43, 140.36, 140.08, 139.88, 139.66, 138.99, 138.83, 138.46, 138.34, 138.17, 137.96, 137.86, 137.79, 137.70, 137.61, 137.54, 137.40, 137.29, 137.27, 137.02, 136.78, 136.57, 136.49, 136.26, 135.96, 135.62, 135.53, 135.13, 134.70, 133.73, 133.17, 132.81, 132.28, 132.18, 132.14, 131.78, 131.57, 131.42, 131.28, 130.86, 130.63, 130.26, 129.16, 128.60, 128.46, 128.35, 128.26, 128.22, 128.17, 128.09, 127.76, 127.67, 127.56, 125.59, 81.72, 80.73, 80.73, 80.11, 80.11, 80.06, 80.06, 79.85, 79.85, 79.34, 79.34, 79.32, 78.79, 78.03, 78.03, 77.74, 77.74, 77.55, 77.46, 76.29, 76.29, 75.99, 75.36, 75.36, 74.97, 63.68, 63.56, 62.96, 61.90, 61.84, 61.47, 61.17, 60.97, 60.91, 60.73, 60.37, 60.27, 60.19, 60.11, 59.74, 59.54, 59.32, 59.09, 53.38, 52.39, 52.05, 50.93, 50.70, 49.75, 49.45, 49.15, 48.12, 47.83, 47.76, 47.10, 46.50, 35.82, 35.34, 35.26, 35.00, 34.87, 34.72, 34.44, 34.20, 34.11, 33.82, 33.71, 33.53, 33.38, 33.26, 33.06, 32.94, 32.86, 32.75, 32.26, 31.58, 31.22, 30.37, 29.44, 29.27, 29.20, 29.04, 28.87, 28.80, 28.53, 27.51, 25.03, 24.17, 23.65, 23.49, 23.01, 22.55, 22.38, 22.27, 22.14, 21.98, 21.76, 21.25, 21.12, 21.04, 20.84, 20.80, 20.34, and 19.35.

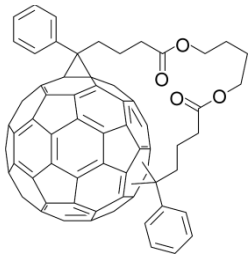

C4 tethered bis adduct. 1.1 g C4 bis(tosylhydrazone) was dissolved in 30 mL dry pyridine in a flame dried 2 L three neck flask under N_2 atmosphere. 0.45 mL DBU was added and the solution was stirred for 20 min at room temperature. A solution of 1.0 g C_{60} (1.4 mmol) in 1L ODCB was prepared. The C_{60} solution was degassed three times and added to the pyridine solution. The resulting mixture was degassed a second time (three vacuum/N_2

purges) and the solution was heated to 85 ^{o}C, after which illumination with a 150 W Sodium lamp was started. The reaction mixture was stirred overnight at 85 ^{o}C under illumination. The solvent was removed *in vacuo* and the residue was extracted with toluene. The soluble fraction was further purified by column chromatography (SiO_2, toluene/ethyl acetate 95:5). The C4 tethered bisadduct fraction was collected, precipitated with methanol, washed twice with methanol, once with pentane, and dried overnight in a vacuum oven at 40 ^{o}C. The pure products was obtained as 345 mg red powder (0.3 mmol, 22%). ^{1}H NMR (500 MHz, CS_2 with D_2O insert) 8.20-7.07 (broad, 10H), 4.49-3.92 (broad, 4H), and 3.37-0.90 (broad, 16H); ^{13}C NMR (126 MHz, CS_2 with D_2O insert) δ 171.88, 171.83, 171.59, 171.56, 171.40, 171.36, 171.34, 171.31, 171.28, 171.08, 170.94, 170.74, 170.69, 170.61, 151.77, 151.47, 150.70, 150.23, 150.02, 149.73, 149.66, 149.59, 149.14, 149.00, 148.25, 148.15, 148.05, 147.89, 147.59, 147.53, 147.50, 147.43, 147.39, 147.37, 147.31, 147.22, 147.15, 147.13, 147.10, 147.04, 146.97, 146.92, 146.81, 146.76, 146.71, 146.61, 146.57, 146.54, 146.52, 146.39, 146.33, 146.28, 146.26, 146.20, 146.18, 146.13, 146.09, 146.07, 146.05, 146.00, 145.98, 145.94, 145.91, 145.89, 145.82, 145.76, 145.69, 145.62, 145.59, 145.54, 145.52, 145.43, 145.39, 145.36, 145.33, 145.26, 145.23, 145.19, 145.14, 145.05, 145.01, 144.97, 144.95, 144.93, 144.92, 144.86, 144.83, 144.75, 144.73, 144.72, 144.63, 144.58, 144.55, 144.53, 144.51, 144.46, 144.43, 144.39, 144.38, 144.36, 144.33, 144.29, 144.24, 144.21, 144.02, 143.96, 143.94, 143.84, 143.82, 143.80, 143.74, 143.72, 143.65, 143.62, 143.55, 143.48, 143.46, 143.41, 143.40, 143.37, 143.30, 143.29, 143.21, 143.14, 143.13, 143.04, 142.97, 142.90, 142.86, 142.81, 142.75, 142.73, 142.70, 142.67, 142.63, 142.57, 142.44, 142.41, 142.30, 142.22, 142.13, 142.11, 141.96, 141.95, 141.87, 141.80, 141.76, 141.73, 141.68, 141.62, 141.60, 141.55, 141.40, 141.34, 141.28, 141.26, 141.22, 141.15, 141.08, 141.03, 140.98, 140.96, 140.92, 140.86, 140.84, 140.58, 140.48, 140.37, 140.31, 140.15, 140.05, 140.00, 139.92, 139.69, 139.63, 139.56, 139.53, 139.39, 139.17, 139.02, 139.01, 138.84, 138.77, 138.71, 138.67, 138.60, 138.53, 138.45, 138.35, 138.26, 138.15, 138.08, 137.92, 137.84, 137.75, 137.66, 137.64, 137.62, 137.45,

137.41, 137.36, 137.35, 137.30, 137.23, 137.19, 137.14, 137.11, 137.00, 136.86, 136.81, 136.77, 136.71, 136.59, 136.57, 136.48, 136.39, 136.27, 135.97, 135.89, 135.75, 135.57, 135.49, 135.10, 134.75, 134.45, 134.12, 133.78, 133.63, 133.46, 133.28, 132.86, 132.24, 132.20, 131.97, 131.83, 131.72, 131.55, 131.25, 131.20, 130.89, 130.63, 130.40, 129.66, 129.17, 129.02, 128.70, 128.59, 128.47, 128.46, 128.34, 128.29, 128.27, 128.22, 128.21, 128.18, 128.10, 128.08, 127.79, 127.68, 127.63, 127.58, 125.59, 81.92, 80.83, 80.60, 80.46, 80.30, 79.66, 79.36, 79.05, 78.97, 78.26, 78.16, 78.03, 77.81, 77.31, 76.14, 75.95, 74.92, 74.55, 64.75, 64.72, 64.63, 64.41, 64.36, 64.22, 64.20, 64.15, 63.99, 63.90, 63.81, 63.76, 63.71, 63.61, 63.57, 63.52, 63.41, 61.15, 60.65, 60.48, 60.36, 60.03, 53.64, 52.12, 51.92, 51.20, 50.44, 49.55, 49.29, 49.23, 48.14, 47.94, 47.75, 47.58, 46.36, 35.40, 35.37, 35.15, 34.97, 34.88, 34.82, 34.67, 34.60, 34.38, 34.23, 34.20, 34.14, 34.00, 33.92, 33.87, 33.73, 33.67, 33.60, 33.56, 33.48, 33.40, 33.37, 33.32, 33.27, 33.23, 33.16, 33.05, 31.89, 31.65, 31.21, 27.60, 27.32, 27.27, 27.11, 26.91, 26.83, 26.75, 26.73, 26.54, 26.36, 26.20, 26.13, 25.83, 25.77, 25.68, 25.58, 25.52, 25.35, 24.70, 23.44, 23.21, 23.02, 22.95, 22.84, 22.79, 22.58, 22.51, 22.47, 22.24, 22.09, 21.98, 21.14, 20.86, 20.49, 20.32, and 19.31.

General procedure for the transesterification. The tethered bis-adduct was dissolved in 100 mL ODCB and 10 mL methanol and a catalytic amount of concentrated sulfuric acid and the mixture was stirred for 5 days. The reaction mixture was stripped of solvent *in vacuo,* the residue was dissolved in toluene and purified by column chromatography (SiO_2, toluene). Precipitation from ODCB in methanol and subsequent washing with methanol yielded the pure bis methyl esters as a red-brown solids.

t_2Bis-PCBM. ^{1}H NMR (500 MHz, CS_2 with D_2O insert) 8.99-7.10 (broad, 10H), 3.80-3.63 (broad singlets, 6H), and 2.90-0.89 (broad, 12H); ^{13}C NMR (126 MHz, CS_2 with D_2O insert) δ 171.84, 171.68, 171.60, 171.47, 171.42, 170.82, 151.92, 151.67, 150.66, 150.57, 150.36, 149.80, 149.74, 149.43, 149.15, 148.71, 148.22, 147.57, 147.53,

147.45, 147.41, 147.30, 147.26, 147.14, 147.09, 146.85, 146.79, 146.72, 146.68, 146.66, 146.59, 146.39, 146.25, 146.21, 146.15, 146.13, 146.10, 146.07, 146.05, 146.04, 146.00, 145.94, 145.91, 145.87, 145.84, 145.82, 145.76, 145.71, 145.68, 145.55, 145.53, 145.41, 145.37, 145.35, 145.33, 145.28, 145.22, 145.21, 145.17, 145.15, 145.04, 145.01, 144.97, 144.95, 144.86, 144.84, 144.77, 144.72, 144.68, 144.66, 144.65, 144.63, 144.60, 144.58, 144.55, 144.48, 144.45, 144.43, 144.39, 144.35, 144.31, 144.26, 144.23, 144.16, 144.08, 144.03, 144.00, 143.98, 143.91, 143.89, 143.86, 143.83, 143.76, 143.74, 143.71, 143.64, 143.55, 143.52, 143.44, 143.40, 143.39, 143.31, 143.18, 143.08, 142.81, 142.76, 142.71, 142.66, 142.61, 142.55, 142.39, 142.22, 142.17, 142.05, 142.01, 141.93, 141.79, 141.68, 141.66, 141.59, 141.42, 141.38, 141.31, 141.20, 141.10, 141.01, 140.98, 140.94, 140.86, 140.82, 140.41, 139.76, 139.64, 139.49, 139.18, 139.12, 138.95, 137.65, 137.63, 137.24, 137.18, 137.07, 136.94, 136.85, 136.80, 136.70, 136.64, 136.44, 136.17, 136.11, 135.93, 135.91, 135.81, 135.79, 135.58, 135.51, 135.12, 133.57, 133.16, 133.08, 132.16, 132.13, 132.09, 132.03, 131.83, 131.60, 131.35, 131.24, 130.63, 129.79, 128.64, 128.59, 128.55, 128.52, 128.46, 128.35, 128.31, 128.30, 128.29, 128.23, 128.20, 128.16, 128.14, 127.68, 80.60, 80.54, 80.24, 80.03, 79.07, 78.77, 78.46, 78.24, 78.12, 78.00, 77.86, 76.42, 75.25, 75.19, 74.49, 74.40, 61.95, 53.74, 51.20, 51.17, 51.15, 51.14, 51.12, 50.81, 49.46, 49.43, 49.33, 48.96, 48.86, 47.69, 47.46, 47.34, 34.63, 34.30, 34.16, 33.98, 33.78, 33.77, 33.71, 33.58, 33.49, 33.46, 33.44, 33.28, 32.77, 32.54, 30.35, 23.12, 23.02, 22.80, 22.68, 22.58, 22.43, 22.40, 22.36, 21.79, and 20.19.

t_3BisPCBM. ^{1}H NMR (500 MHz, CS_2 with D_2O insert) 8.14 0-7.11 (broad, 10H), 3.88-3.59 (broad singlets, 6H), and 3.09-1.20-0.90 (broad, 12H); ^{13}C NMR (126 MHz, CS_2 with D_2O insert) δ 171.82, 171.71, 171.67, 171.58, 171.49, 171.45, 171.40, 171.34, 151.66, 150.65, 150.56, 150.36, 149.80, 149.73, 149.42, 149.14, 148.70, 148.35, 148.21, 148.16, 147.73, 147.57, 147.53, 147.50, 147.46, 147.41, 147.35, 147.30, 147.26, 147.14, 147.10, 147.07, 146.84, 146.79, 146.71, 146.66, 146.59, 146.50, 146.42,

146.39, 146.29, 146.21, 146.15, 146.13, 146.10, 146.08, 146.04, 146.00, 145.95, 145.91, 145.82, 145.75, 145.71, 145.69, 145.56, 145.41, 145.37, 145.33, 145.28, 145.22, 145.20, 145.17, 145.15, 145.04, 145.00, 144.97, 144.90, 144.86, 144.83, 144.80, 144.77, 144.72, 144.70, 144.69, 144.66, 144.65, 144.63, 144.60, 144.55, 144.47, 144.45, 144.39, 144.35, 144.31, 144.27, 144.23, 144.16, 144.03, 143.98, 143.91, 143.86, 143.80, 143.76, 143.71, 143.64, 143.55, 143.53, 143.49, 143.45, 143.40, 143.30, 143.23, 143.18, 143.08, 142.99, 142.96, 142.81, 142.75, 142.71, 142.66, 142.63, 142.58, 142.55, 142.48, 142.44, 142.39, 142.31, 142.26, 142.21, 142.17, 142.11, 142.04, 142.01, 141.97, 141.93, 141.79, 141.69, 141.66, 141.59, 141.42, 141.38, 141.31, 141.26, 141.20, 141.10, 141.01, 140.98, 140.94, 140.86, 140.82, 140.67, 140.54, 140.41, 140.25, 140.05, 139.90, 139.76, 139.66, 139.64, 139.49, 139.31, 139.18, 139.12, 138.95, 138.88, 138.73, 138.58, 138.54, 138.44, 138.34, 138.27, 138.21, 138.14, 138.04, 137.91, 137.81, 137.72, 137.69, 137.65, 137.62, 137.39, 137.25, 137.19, 137.16, 137.08, 137.04, 136.95, 136.91, 136.85, 136.80, 136.70, 136.65, 136.44, 136.18, 136.12, 135.94, 135.81, 135.79, 135.58, 135.51, 135.38, 135.12, 135.09, 134.43, 133.57, 133.28, 133.08, 132.85, 132.54, 132.30, 132.27, 132.16, 132.12, 132.09, 132.05, 132.03, 131.83, 131.61, 131.34, 131.24, 130.78, 130.63, 130.58, 130.46, 128.87, 128.64, 128.58, 128.54, 128.51, 128.45, 128.35, 128.29, 128.28, 128.22, 128.20, 128.13, 128.09, 127.79, 127.77, 127.66, 127.58, 82.49, 80.60, 80.54, 80.24, 80.02, 79.84, 79.78, 79.07, 78.77, 78.46, 78.24, 77.86, 76.89, 76.43, 76.32, 75.25, 74.41, 61.09, 60.75, 60.54, 60.14, 53.73, 52.26, 51.26, 51.19, 51.16, 51.14, 51.13, 51.10, 51.04, 50.80, 49.45, 49.43, 49.32, 48.96, 48.85, 47.69, 47.46, 47.34, 35.53, 35.39, 35.04, 34.97, 34.30, 34.15, 33.98, 33.93, 33.89, 33.84, 33.78, 33.76, 33.71, 33.58, 33.46, 33.44, 33.40, 33.34, 33.30, 33.23, 32.77, 32.54, 30.36, 23.01, 22.93, 22.81, 22.80, 22.73, 22.68, 22.58, 22.44, 22.40, 22.36, 21.79, 20.29, 20.23, 20.16, 20.09, and 19.87.

t_4Bis-PCBM. ^{1}H NMR (500 MHz, CS_2 with D_2O insert) 8.16-7.05 (broad, 10H), 3.80-3.59 (broad singlets, 6H), and 3.11-0.83 (broad, 12H); ^{13}C NMR (126 MHz, CS_2 with D_2O

insert) δ 192.72, 192.70, 192.69, 192.69, 192.68, 192.67, 192.67, 192.66, 192.65, 192.65, 192.64, 192.64, 192.58, 192.53, 192.52, 192.51, 192.51, 192.50, 192.49, 192.49, 192.48, 192.47, 192.47, 192.46, 192.46, 192.45, 192.44, 192.43, 192.41, 171.83, 171.72, 171.68, 171.58, 171.50, 171.46, 171.41, 171.35, 151.91, 151.66, 150.65, 150.56, 150.36, 149.80, 149.73, 149.42, 149.14, 148.70, 148.34, 148.21, 148.16, 147.88, 147.57, 147.53, 147.50, 147.46, 147.41, 147.35, 147.30, 147.26, 147.17, 147.14, 147.10, 147.07, 146.84, 146.79, 146.71, 146.66, 146.59, 146.50, 146.48, 146.43, 146.39, 146.29, 146.25, 146.21, 146.16, 146.13, 146.10, 146.08, 146.03, 146.00, 145.95, 145.91, 145.84, 145.82, 145.75, 145.71, 145.68, 145.63, 145.61, 145.57, 145.41, 145.37, 145.33, 145.31, 145.29, 145.22, 145.20, 145.17, 145.15, 145.05, 145.00, 144.97, 144.96, 144.90, 144.86, 144.83, 144.80, 144.77, 144.72, 144.70, 144.69, 144.66, 144.65, 144.63, 144.60, 144.55, 144.47, 144.45, 144.41, 144.39, 144.35, 144.31, 144.27, 144.23, 144.16, 144.03, 144.00, 143.98, 143.91, 143.86, 143.80, 143.76, 143.71, 143.64, 143.59, 143.55, 143.53, 143.49, 143.45, 143.40, 143.30, 143.18, 143.15, 143.08, 142.99, 142.96, 142.81, 142.75, 142.71, 142.66, 142.64, 142.58, 142.55, 142.48, 142.39, 142.26, 142.21, 142.17, 142.11, 142.05, 142.01, 141.97, 141.93, 141.79, 141.71, 141.69, 141.66, 141.59, 141.42, 141.38, 141.31, 141.26, 141.22, 141.20, 141.10, 141.01, 140.98, 140.95, 140.86, 140.82, 140.67, 140.65, 140.54, 140.41, 140.25, 140.05, 139.90, 139.76, 139.66, 139.64, 139.49, 139.31, 139.18, 139.12, 138.95, 138.88, 138.73, 138.58, 138.53, 138.44, 138.28, 138.14, 138.03, 137.91, 137.81, 137.69, 137.65, 137.62, 137.39, 137.25, 137.22, 137.19, 137.16, 137.08, 137.04, 136.95, 136.91, 136.85, 136.80, 136.77, 136.72, 136.70, 136.65, 136.44, 136.18, 136.12, 135.93, 135.81, 135.79, 135.58, 135.51, 135.38, 135.12, 135.09, 134.43, 134.21, 133.81, 133.62, 133.57, 133.28, 132.54, 132.27, 132.16, 132.13, 132.09, 132.05, 132.03, 131.83, 131.62, 131.35, 131.24, 130.78, 130.63, 130.57, 129.16, 128.87, 128.64, 128.58, 128.54, 128.51, 128.45, 128.35, 128.29, 128.28, 128.23, 128.20, 128.13, 128.09, 127.79, 127.67, 127.58, 127.37, 82.49, 80.60, 80.54, 80.24, 80.05, 80.02, 79.83, 79.78, 79.07, 78.77, 78.45, 78.23, 78.11, 77.99, 77.86, 76.88, 76.43, 76.31, 75.25, 74.40,

61.09, 60.74, 60.54, 60.51, 60.14, 53.73, 52.26, 51.27, 51.19, 51.16, 51.15, 51.13, 51.11, 50.80, 49.45, 49.43, 49.32, 48.95, 48.85, 47.69, 47.46, 47.34, 35.53, 35.39, 35.04, 34.97, 34.30, 34.15, 33.98, 33.92, 33.89, 33.84, 33.78, 33.76, 33.71, 33.58, 33.49, 33.46, 33.44, 33.40, 33.34, 33.28, 33.23, 32.76, 32.54, 23.01, 22.93, 22.81, 22.80, 22.73, 22.68, 22.58, 22.44, 22.40, 22.36, 21.79, 20.28, 20.23, 20.16, 20.09, and 19.87.

3.7.4 Molecular Modeling

Molecular Modeling was done using the Hyperchem 7.5 professional software package. A first geometry optimalization was done using the Molecular Mechanics MM+ force field method. These geometries were taken as the starting points for the PM3 semi-empirical geometry optimalization. A single-point energy was then calculated for each of the geometry-optimized lowest-energy stereoisomers.

Table A1: Calculated energies for lowest energy isomers of the PM3 optimized geometries of the tethered bisadducts.

Isomer	Orientation*	relative energy (Kcal/mol)		
		C2	C3	C4
Cis 1	endo-endo	28,927	32,359	33,855
Cis 1	endo-exo	24,429	27,460	28,502
Cis 1	exo-exo	18,301	23,077	19,486
Cis 1	exo-exo 2	19,456	21,306	18,450
Cis 2	endo-endo	0,886	1,924	3,434
Cis 2	endo-exo	0,374	0,005	0,592
Cis 2	exo-exo	1,224	4,702	5,302
Cis 2	exo-exo 2	11,838	11,062	11,512
Cis 3	endo-endo	37,954	25,146	25,291
Cis 3	endo-exo	4,214	3,560	0,633
Cis 3	exo-exo	8,852	7,938	4,497
E	ph endo	16,626	6,525	1,934
E	ph exo	0,000	0,000	1,385
Trans 4	endo-endo	38,332	23,233	11,725
Trans 4	endo-exo	14,909	9,252	6,786
Trans 4	exo-exo	1,328	4,357	0,000
Trans 3	endo-endo	10,064	5,194	3,439
Trans 3	endo-exo	9,192	5,255	3,937
Trans 3	exo-endo	38,312	23,819	11,764
Trans 3	exo-exo	16,620	12,851	7,990
Trans 2	endo-endo	Not possible	Not possible	110,667
Trans 2	endo-exo	83,069	55,075	46,942
Trans 2	exo-exo	29,967	15,644	12,195
Trans 2	Not possible	Not possible	52,346	33,040
Trans 1	endo-endo	Not possible	Not possible	Not possible
Trans 1	endo-exo	Not possible	76,502	121,993
Trans 1	exo-exo	147,985	112,956	55,377

* “Exo/exo” meaning both phenyl groups are pointing away from each other and both the esters groups towards each other. “Endo/exo” meaning one of the phenyl rings is pointing toward an ester group. “Endo/Endo” meaning both the phenyl groups are pointing towards each other and the ester groups away from each other. “Endo” meaning the phenyl group is pointing towards the second addend. “Exo” meaning the phenyl rings is pointing away from the second addend.

3.8 References

1 Dojo, A. Herzog, I. Lamparth, F. Hampel and A. Hirsch, *Chem. Eur. J*. 1996, **2**, 1537

2 G. Schick, A. Hirsch, H. Mauser and T. Clark, *Chem. Eur. J.,*. 1996, **2**, 935

3 M. Prato, *J. Mater. Chem*., 1997, **7**, 1097

4 F. Diederich and M. Gómez-López, *Chem. Soc. Rev*., 1999, **28**, 263

5 A. Hirsch, *Chem., Rec.,* 2005, **5**, 196

6 M. Lenes, G. A. H. Wetzelaer, F. B. Kooistra, S. C. Veenstra, J. C. Hummelen and P. W. M. Blom, *Adv.Mater*, 2008, **20**, 2116

7 M. Lenes, S. W. Shelton, A. B. Sieval, D. F. Kronholm, J. C. Hummelen and P. W. M. Blom, *Adv.Funct.Mater*., 2009, **19**, 3002

8 M. Lenes, Ph.D. Thesis, University of Groningen, 2009

9 A. Sánchez-Díaz, M. Izquierdo, S. Filippone, N. Martin and E. Palomares, *Adv.Funct.Mater*., 2010, **20**, 2695

10 J. M. Frost, M. A. Faist and J. Nelson, Adv .Mater., 2010, *Adv. Mater*., 2010, **22**, 4881

11 F. Diederich and R. Kessinger, *Acc. Chem. Res*., 1999, **32**, 537

12 J. Bourgeois, C. R. Woods, F. Cardullo, T. Habicher, J. Nierengarten, R. Gehrig and F. Diederich, *Helv. Chim. Acta*, 2001, **84**, 1207

13 M. A. Yurovskaya and I. V. Trushkov, *Russ. Chem. Bull. Int Ed*., 2002, **51**, 367

14 Z. Zhou and S. R. Wilson, *Curr. Org. Chem*., 2005, **9**, 789

15 A. Hirsch and M. Brettreich, in Fullerenes, Chemistry and Reactions, Wiley-VCH Verlag GmbH & Co. KGaA, Weinheim, 2005, ch. 10, pp. 289

16 C. Thilgen and F. Diederich, *C. R. Chimie*, 2006, **9**, 868

17 I. Lamparth, C. Maichle-Mössmer and A. Hirsch, *Angew. Chem. Int. Ed. Engl.,* 1995, **34**, 1607

18 X. Camps and A. Hirsch, *J. Chem. Soc., Perkin Tran., 1,* 1997, 1595

19 M. Diekers, C. Luo, D. M. Guldi and A. Hirsch, *Chem. Eur. J*. 2002, **8**, 979

20 P. J. Fagan, J. C. Calabrese and B. Malone, *J. Am. Chem. Soc.,* 1991, **113**, 9408

21 A. Hirsch and O. Vostrowsky, *Eur. J. Chem*., 2001, 829

22 S. R. Wilson and Q. Lu, *Tet. Lett*., 1995, **36**, 5707

23 F. Cardullo, I. Isaacs, F. Diederich, J. Gisselbrecht, C. Boudon and M. Gross, *Chem. Commun*., 1996, 797

24 R. Schwenninger, T. Müller and B. Kräutler, *J. Am. Chem. Soc*., 1997, **119**, 9317

25 J. Nierengarten, U. Hahn, T. M. Figueira Duarte, F. Cardinali, N. Solladié, M. E. Walther, A. Van Dorsselaer, H. HerschBach, E. Leize, A. Albrecht-Gary, A. Trabolsi and M. Elhabiri, *C.R.Chimie*, **9**, 2006, 1022

26 T. Haino, M. Yanase and Y. Fukazawa, *Angew. Chem. Int. Ed.*, 1998, **37**, 997

27 J.C. Hummelen, B.W. Knight, F. Lepeq, F. Wudl, J. Yao and C. L. Wilkins, *J.Org.Chem*., 1995, **60**, 532

28 L. Isaacs, F. Diederich and R. F. Haldimann, *Helv. Chim. Acta*, 1997, **80**, 317

29 L. Isaacs, R. F. Haldimann and F. Diederich, *Angew. Chem. Int. Ed. Engl*., 1994, **33**, 2339

30 S. H. Friedman and G. L. Kenyon, *J. Am. Chem. Soc*., 1997, **119**, 447

31 S. Sergeyev and F. Diederich, *Angew. Chem. Int. Ed*., 2004, **43**, 1738

32 S. Sergeyev, M. Schär, P. Seiler, O. Lukoyanova, L. Echegoyen and F. Diederich, *Chem. Eur. J*., 2005, **11**, 2284

33 G. A. Burley, P. A. Keller, S. G. Pyne and G. E. Ball, *Chem. Commun*., 2000, 1717

34 T. Hino and K. Saigo, *Chem. Commun*., 2003, 402

35 L. Chaker, G. E. Ball, J. R. Williams, G. A. Burley, B. C. Hawkins, P. A. Keller and S. G. Pyne, *Eur. J. Org. Chem.*, 2005, 5158

36 Z. Zhou, D. I. Schuster and S. R. Wilson, *J. Org. Chem.*, 2006, **71**, 1545

37 Z. Zhou, D. I. Schuster and S. R. Wilson, *J. Org. Chem.*, 2003, **68**, 7612

38 N. Chronakis and A. Hirsch, *Chem. Commun*., 2005, 3709

39 M. Taki, S. Sugita, Y. Nakmura, E. Kasahima, E. Yashima, Y. Okamoto and J. Nishimura, *J. Am. Chem. Soc.*, 1997, **119**, 926

40 T. Ishi-I, K. Nakashima and S. Shinkai, *Chem. Commun*., 1998, 1047

41 T. Ishi-I, R. Iguchi and S. Shinkai, *Tetrahedron*, 1999, **55**, 3883

42 W. Qian and Y. Rubin, *J. Org. Chem*., 2002, **67**, 7683

43 G. Rotas and N. Tagmatarchis, *Tett. Lett*., 2009, **50**, 398

44 A. Hirsch, I. Lamparth and H. R. Karfunkel, *Angew. Chem., Int Ed. Engl*., 1994, **33**, 437

45 J. Otera, *Chem. Rev*., 1993, **93**, 1449

46 M. Nahmany and A. Melman, *Org. Biomol. Chem*., 2004, **2**, 1563

47 V. D. Mihailetchi, H. Xie, B. de Boer, L. J. A. Koster, and P. W. M. Blom, *Adv. Funct. Mater*., 2006, **16**, 699–708

48 V.D. Mihailetchi, L.J.A. Koster, J. C. Hummelen and P. W. M . Blom, *Phys. Rev. Lett.,* 2004, **93**, 216601

49 M. Lenes, M. Morana, C. J. Brabec and P. W. M. Blom, *Adv. Funct. Mater*. 2009, **19**, 110621

50 M. Lenes, F. B. Kooistra, J. C. Hummelen, I. Van Severen, L. Lutsen, D. Vanderzande, T. J. Cleij and P. W. M. Blom, *J. Appl. Phys*., 2008, **104**, 114517

51 D. Jarzab, F. Cordella, M. Lenes, F.B. Kooistra, P.W. Blom, J.C. Hummelen and M.A. Loi, *J. Phys. Chem. B*., 2009, **113**, 16513

Chapter 4

PCXMs: PCBM-like analogues with varying alkanoic acid moieties

Abstract. This chapter describes the synthesis, characterization, and use in organic bulk heterojunction solar cells of PCBM-like analogs with different length alkyl chains between the cyclopropane ring and the ester moiety. Monoadducts and bisadducts were synthesized, characterized, and tested in bulk heterojunction solar cell devices.

The work in this chapter is part of a cooperation with G. A. H. Wetzelaer and P.W.M. Blom of the University of Groningen. Devices fabrication and testing was performed by G. A. H. Wetzelaer.

4.1 Introduction

In the previous chapter it was shown that increasing the alkyl spacer length of the tether reduces the performance of tethered bisadducts in organic bulk heterojunction solar cells. This was partly caused be the increase in the number of isomers that were formed during synthesis. However the negative influence of the extra carbon atoms in the tethers became apparent when the tethers were removed through transesterification. The resulting tbis-PCBM isomeric mixtures all performed better than their tethered precursors. It may therefore prove worthwhile to further investigate the influence of the number of carbon atoms in the substituent of PCBM on the performance of (bis-)PCBM analogs as acceptor material in organic solar cells.

4.1.1 PCBM

PCBM **(4.1)** was originally synthesized as a soluble fullerene derivative intermediate in the search for an HIV inhibitor.[1] Although the use of fullerene derivatives as a medicine for HIV never fully materialized,[2] PCBM is now the most widely used acceptor material in organic photovoltaic applications.

A weak point of PCBM (that is the C_{60} derivative or [60]PCBM), as photovoltaic material is its weak absorption in the visible region, due to the high degree of symmetry which makes the lowest-energy transition formally dipole forbidden. To improve the absorption properties of PCBM, Hummelen *et al.* synthesized the corresponding C_{70} derivative, [70]PCBM **(4.2)**.[3] The absorbance of [70]PCBM is much stronger than that of PCBM. For that reason [70]PCBM has been widely used in organic solar cells based on small band gap polymers in order to enhance light absorption. Many organic solar cells comprising [70]PCBM as acceptor show more than 10% (relative) higher PCEs than the corresponding devices with PCBM as acceptor.[3-5]

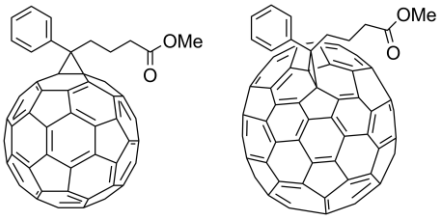

(4.1) **(4.2)**

Figure 4.1: *[60]PCBM* ***(4.1)*** *and one of the isomers comprising the isomeric mixture called [70]PCBM* ***(4.2)****.*

Next to light absorption the electrochemical properties of the fullerene derivatives are important for the application as acceptor material in organic solar cells. As already mentioned in Chapter 1, the open circuit voltage is determined by the difference in energy between the LUMO level of the fullerene acceptor and the HOMO level of the polymer donor.[6-9] Therefore, it is important to bear in mind the consequences of structural modification of the fullerene derivative on the LUMO energy level. For PCBM and [70]PCBM these levels are similar, therefore the increase in efficiency is caused mainly by the extra light absorption.[3-5]

To further improve the photovoltaic properties of PCBM various PCBM-like C_{60} derivatives were designed and synthesized by numerous groups by introducing structural modifications on the substituent of PCBM. For discussing these modifications the substituent can be divided into four parts: a phenyl ring, a butyl middle chain, the bridgehead and an ester group (**Figure 4.2**).

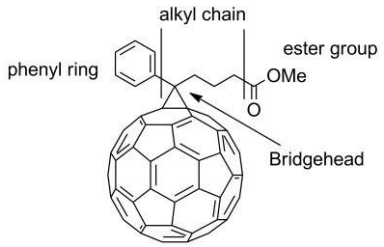

Figure 4.2: *Division of the substituent into four parts: a phenyl ring, an alkyl middle chain, the bridgehead and an ester group.*

4.2 Modifying the PCBM substituent

4.2.1 The ester moiety

Because of the relative ease of changing the ester moiety this has been done on various occasions by different groups. It was already shown in our group that increasing the lengths of the ester lowers the Tg of the PCBM monoadduct analogues.[10]

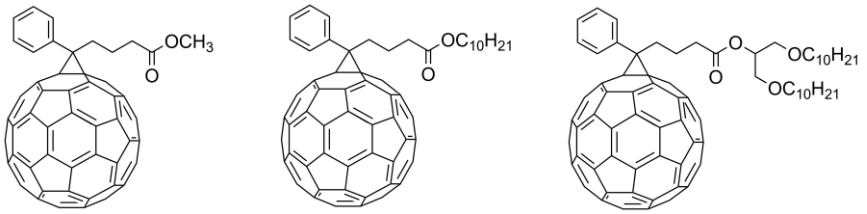

(4.1) **(4.3)** **(4.4)**

Figure 4.3: *PCBM-like derivatives with increasing length of the ester moiety.*

Increasing the ester length from a methyl ester in PCBM **(4.1)**, to a decyl ester in PCBD **(4.3)**, the Tg changed dramatically from 256 ^{o}C to 38 ^{o}C. PCB-didecyl, containing two decyl chains **(4.4)** even has a Tg as low as -2.3 ^{o}C. In another example from our group the methyl ester was replaced with different branched ester groups **(4.5-4.7)** to investigate the influence of the ester on the performance of MDMO-PPV solar cells. It was shown that an increase in the size of the ester

moiety causes a reduced mobility likely due to the higher degree of "insulating greasy chains".[11]

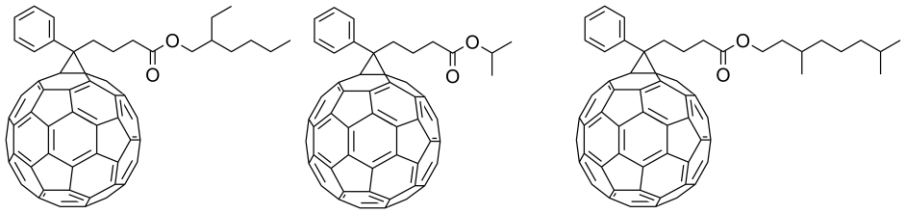

(4.5) **(4.6)** **(4.7)**

Figure 4.4*: Branched ester fullerene derivatives developed in our group.*

The group of Nguyen also investigated the effect of modifying the ester tail of PCBM-like analogs, this time in small molecule bulk heterojunctions based on diketopyrrolopyrrole-thiophene oligomers.[12] They synthesized PCBM analogs containing alkyl esters of various length; methyl, n-hexyl, and n-dodecyl. Upon mixing with the donor material the degree of phase separation could be controlled depending on the length of the ester. The as-cast films showed the highest efficiency for the n-dodecyl ester (2.63% compared to 2.21% for PCBM). However after thermal annealing the efficiencies of the longer esters dropped again to 1.49%. The shorter n-hexyl ester slightly improved from 2.41% to 2.79% with PCBM at 2.93%These effects were explained by changes in morphology through increased hydrophobicity.

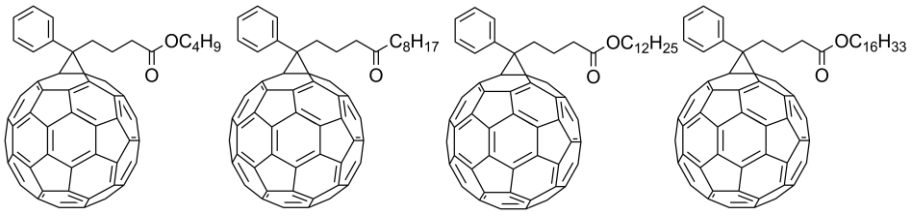

(4.8) **(4.9)** **(4.10)** **(4.11)**

Figure 4.5: *The PCBM-like derivatives developed by Zheng et al. with increasing length of the ester moieties.*

Zheng *et al.* [13] also investigated the influence of the alkyl ester on the performance of bulk heterojunction solar cells by synthesizing a series of PCBM analogs with increasing ester chain lengths; n-butyl, n-octyl, n-dodecyl, and n-hexadecyl (**4.8-4.11)**. Bulk heterojunctions were made in combination with MEH-PPV. The V_{oc} remained almost the same within these series (0.80-0.85 V). The short circuit current however varied largely with an optimum for the n-butyl ester, after which it decreased again with increasing ester chain length.

In a larger study by *Yang et al.* PCBM analogs were combined with P3HT in slow-growth active layers. In this study they not only used the linear methyl, ethyl, n-propyl, and n-butyl esters, but also the branched iso-propyl, sec-butyl, and iso-butyl esters **(4.6)**, **(4.12)** and **(4.13)**.[14] Compared to PCBM they found slight increases in light absorption between 450 and 500 nm, but no shift in the absorption. The reduction potentials did not change within these series. Even though the V_{oc} of OPV cells with these new acceptors was slightly improved compared to PCBM, all other cell characteristics were inferior to the PCBM-based cells.

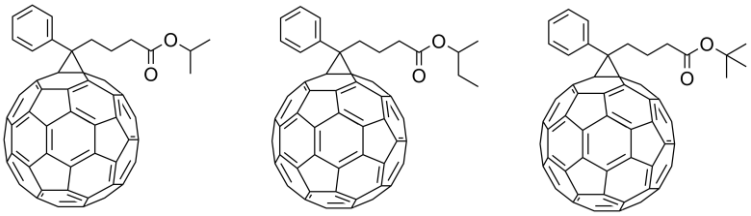

(4.6) **(4.12)** **(4.13)**

Figure 4.6: *The PCBM-like derivatives developed by Yang et al. with branched ester moieties.*

Similar work was done with [70]PCBM incorporating the linear methyl, n-propyl, n-pentyl, n-heptyl, and n-nonyl esters in combination with P3HT.[15] Also here little influence is seen on the electrochemical properties of the fullerene acceptors. An improvement in device efficiency was found for the PCBM-like derivatives with

increasing ester length with the maximum for the n-heptyl ester at 3.95% compared to 3.50% for PCBM. These results were explained through a better morphology of the active layer. The longer n-nonyl ester showed a drop in efficiency to 3.51%, probably due to poorer charge transport across the excessively long intermolecular distance.

In all studies, a single solvent was used in making the active layer. Therefore the results merely reflect the optimum chain length in the acceptor only for *that* specific polymer:acceptor/solvent combination. It is to be expected that upon changing the solvent, a different PCBM-analog is the better one.

4.2.2 The phenyl group

A different approach was taken by the groups of Heeger and Wudl in which a branched alkoxy side chain was added to the phenyl ring **(4.14)** and **(4.15)** instead of elongating or branching the ester moiety.[16]

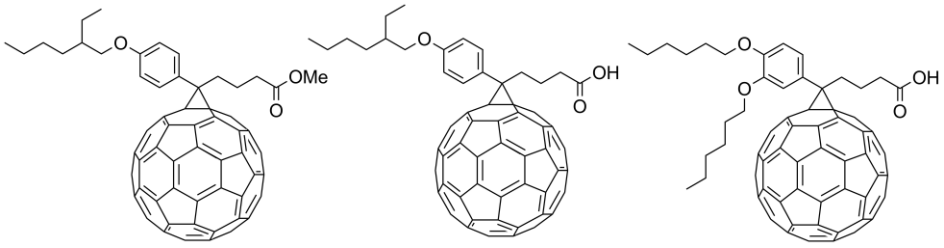

(4.14) **(4.15)** **(4.16)**

Figure 4.7: *The branched alkoxy side chain PCBM-like derivatives developed by the groups of Heeger and Wudl.*

Due to the improved solubility of the fullerene derivative it also became possible to synthesize the carboxylic acid analog, which in the case of PCBM (PCBA) is an insoluble material. The move to the substituted phenyl ring resulted in a negative shift in reduction potential, due to the electron donating properties of the alkoxy group, which was even larger for the carboxylic acid analog. Solar cells comprising

these materials showed an increase in V_{oc}, due to more negative reduction potential. However for the methyl ester analog, J_{sc} en FF dropped to 4.43 A/m^2 and 0.35, respectively. These increased again with the carboxylic acid analog to 5.83 A/m^2 and 0.46, resulting in an efficiency of 1.73% compared to 1.81% for PCBM due to more effective interface interaction. Addition of a TiO_x optical spacer improved this even further to 2.64% for the carboxylic acid analog.

Similar work was performed earlier in our group in the search for ways to obtain desired bulk heterojunction architectures through supramolecular assembly of the constituents. For this reason PCBA analogs were synthesized containing hexyloxybenzene groups **(4.16)**.[17] Later these derivatives were used as pendant fullerenes in conjugated polymers in order to study photoinduced electron transfer[18] and in the surface modification of semiconductor nanocrystals.[19]

Our group,[20,21] the groups of Sariciftci and Razumov[22] as well as the group of Jen[23] and the group of Li[24] synthesized various fullerene derivatives in which the phenyl group was replaced by other aromatic groups such as triphenylamine- **(4.17)**, thiophene- **(4.18)**, and furan- **(4.19)** moieties in order to suppress the crystallization of the fullerene derivative to improve the long term (thermal) stability of the photovoltaic devices.

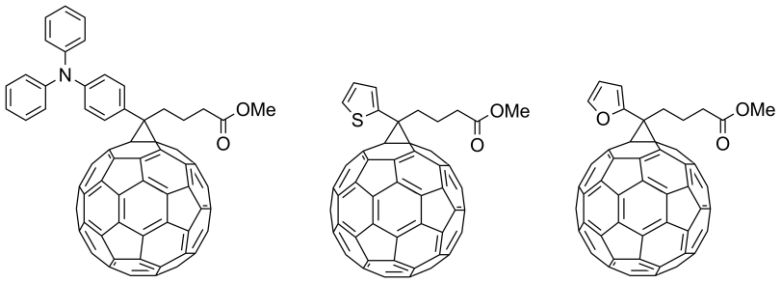

(4.17) **(4.18)** **(4.19)**

Figure 4.8: *Some examples of modified PCBM-like derivatives in which the phenyl group is replaced by other aromatic moieties.*

Similar work from our hand is presented in Chapter 5 where mono- as well as bisadducts of PCBM-like fullerenes are presented in which the phenyl group is replaced with a dialkylfluorene group to improve compatibility with fluorene containing small bandgap polymers.[20]

4.2.3 The bridgehead

The group of Wudl synthesized a new PCBM-like molecule, APCBM **(4.20)**, by inserting a nitrogen bridge between the side chain and the fullerene moiety.[25,26] The electrochemical properties are close to those of PCBM. Devices based on this PCBM-like analog in combination with P3HT gave efficiencies of 2.3%.

The group of Morvillo designed a novel Si-containing PCBM like derivative, Si-PCBM **(4.21)**.[27] They performed theoretical calculations on the LUMO energy level which resulted in a 0.25 eV increase compared to PCBM. Therefore, it is expected that Si-PCBM will result in a higher V_{oc} for devices based on this material compared to conventional PCBM.

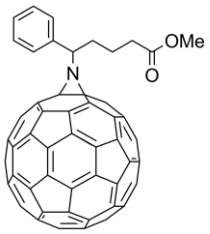

(4.20)

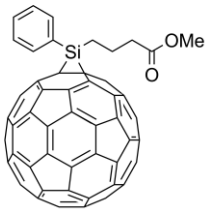

(4.21)

Figure 4.9: *APCBM **(4.20)** and Si-PCBM **(4.21)**.*

4.2.4 The carbon chain length

As already mentioned above, PCBM was initially designed as an intermediate for HIV protease inhibitors.[1,2] Hence the specific length of the butyl chain between the phenyl group and the ester moiety. The length of the spacer and the presence or absence of side groups therein are expected to influence properties as solubility

and crystallinity of the fullerene derivative and thus forms an easily accessible handle for tuning the morphology of the active layer.

The group of Yang and Li synthesized a series of PCBM-like C_{60} derivatives by varying the alkyl chain between the cyclopropane ring and the ester moiety to investigate its effect on the physical properties and photovoltaic performance.[28] The length was varied from two **(4.22)**, one carbon atom shorter than PCBM, to six carbon atoms **(4.26)**, three carbon atoms longer than PCBM.

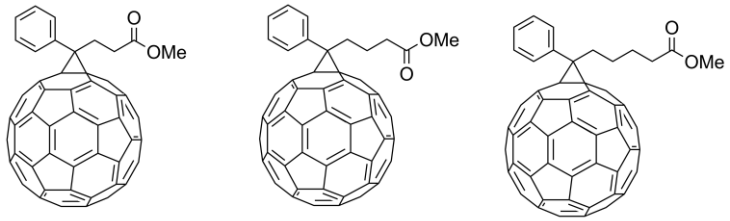

(4.22) **(4.1)** **(4.23)**

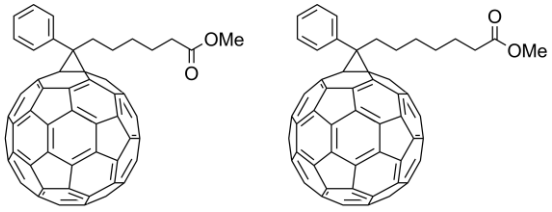

(4.24) **(4.25)**

Figure 4.10: *The PCBM-like derivatives developed by Zhao et al. with increasing length of the alkyl spacer.*

They found that these PCBM-like analogs possess almost the same first reduction potential and absorption characteristics. But interestingly the devices based on P3HT as donor and these PCBM-like analogs as acceptors showed different photovoltaic performance depending on the spacer length. The devices based on **(4.22)**, **(4.1**, PCBM) and **(4.24)** as the acceptor displayed higher photovoltaic performance with efficiencies above 3.5% while those with **(4.23)** and **(4.25)** as acceptor showed relatively lower efficiencies below 3.0%. In comparison with

PCBM **(4.1)**, propanioc ester **(4.22)** and hexanoic ester **(4.24)** display similar or a slightly better photovoltaic performance than PCBM, while pentanoic ester **(4.23)** and heptanoic ester **(4.25)** show a poorer photovoltaic performance. No correlation between increasing spacer length and efficiency was found.

To further extent this research towards higher adducts and compare our results with those obtained by Zhao *et al*., bisadduct analogs of PCBM-like derivatives as well as their parent monoadducts were designed with different alkanoic acid moieties. Four different lengths were chosen: formic **(4.27)** and (**4.28)**, containing no carbon atoms between the ester moiety and cyclopropane ring, propanoic **(4.22)** synthesized in our group already in 2004, and **(4.29)**, containing two carbon atoms, butanoic **(4.1)** and **(4.30)**, i.e. PCBM, and pentanoic **(4.23)** and **(4.31)**, containing one carbon atom more than PCBM.

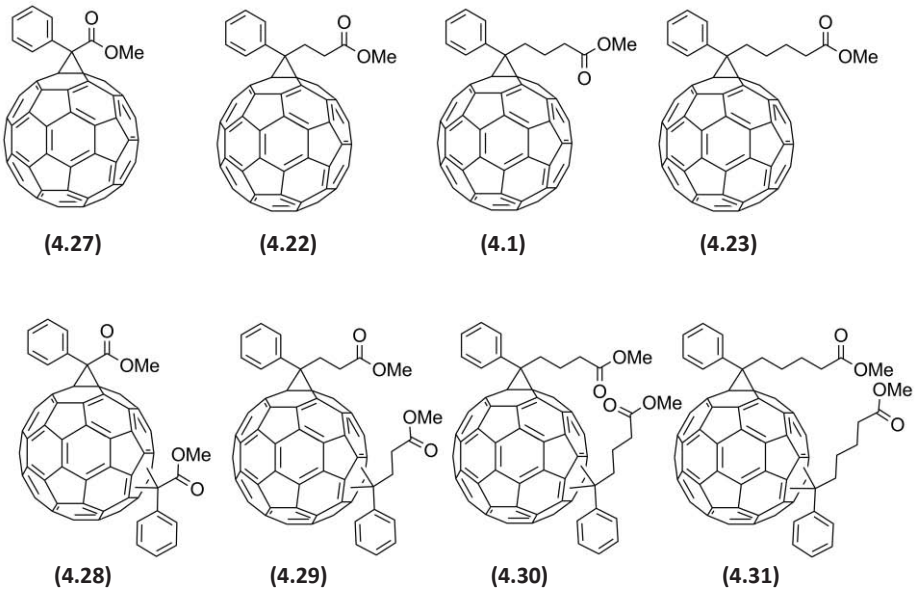

Figure 4.11: *The mono- and bisadduct PCBM analogs (PCXMs) with increasing alkyl chain length used in this chapter.*

The (bis-)PCBM-like analogs were synthesized, characterized and their optical and

electrochemical properties were determined. Their performance in organic bulk heterojunction devices was tested in combination with P3HT.

4.3 Experimental results

4.3.1 Synthesis

PCXM monoadducts **(4.22)**, **(4.1)** and **(4.23)** as well as their bisadduct analogs **(4.28-4.31)** were synthesized through the standard synthetic route used for PCBM (**Scheme 4.1**).[1] The respective acid chlorides were reacted via a Friedel-Crafts acylation with toluene-free benzene. Purification by column chromatography (SiO_2,toluene) yielded the pure keto esters. These keto esters were reacted with tosylhydrazide in toluene in a Dean-Stark setup. Subsequent recrystallization from hot methanol yielded the tosylhydrazones as white crystals. Deprotonation of the tosylhydrazones with sodium methoxide in pyridine generated the diazo compounds which were used *in situ* in the 1,3-dipolar diazo addition to C_{60} in *ortho*-dichlorobenzene. The pure products were obtained by column chromatography (SiO_2,CS_2 to remove unreacted C_{60}, then 1:1 toluene/cyclohexane to obtain the monoadducts, followed by toluene to obtain the respective bisadduct analogs as an isomeric mixture).

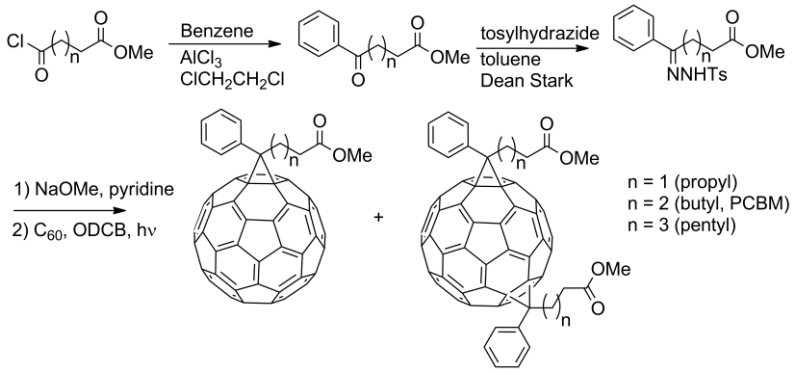

Scheme 4.1: *Synthesis of PCXM mono- and bisadducts and their respective keto esters and tosylhydrazone precursors.*

PCXM monoadduct **(4.27)** and its bisadduct analog **(4.28)** were synthesized directly through a Bingel addition[29] of methyl bromo(phenyl)acetate to C_{60}; C_{60} and methyl bromo(phenyl)acetate were dissolved along with 1,8-diazabicycloundec-7-ene (DBU) in ODCB and stirred overnight at room temperature. The pure products were obtained by column chromatography (SiO_2,CS_2 to remove unreacted C_{60}, then 1:1 toluene/cyclohexane to obtain the monoadducts, followed by toluene to obtain the bisadduct analog as an isomeric mixture).

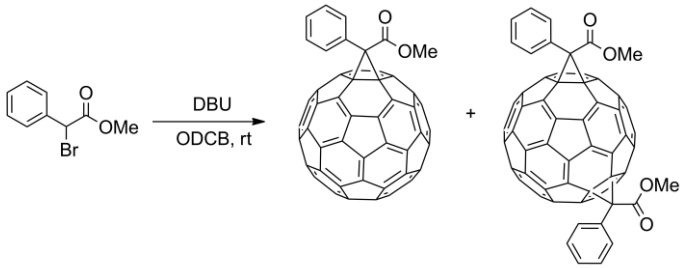

Scheme 4.2: *Synthesis of PCXM mono- (4.27) and bisadduct (4.28) by Bingel addition of methyl bromo(phenyl)acetate.*

4.3.2 PCXM monoadducts

4.3.2.1 UV-Vis

Zhao *et al.* explained the difference in efficiency with varying alkyl chain lengths between the cyclopropane ring and ester moiety in terms of difference in absorption between the different PCBM-like derivatives when combined with P3HT.[28] The absorption properties of these fullerene adducts are almost the same regardless of the length of the alkyl chain. Therefore the difference in absorption has to find its origin in differences in morphology of the active layer. This effect on crystallinity of the active layer is also seen with DPM12 resulting in increased absorption and a shift in the light absorption of the donor material is a possible reason.[30-33]

In agreement with the work of Zhao *et al.*, the PCBM-like monoadducts synthesized in our lab show almost no difference in absorption (**Figure 4.11**).

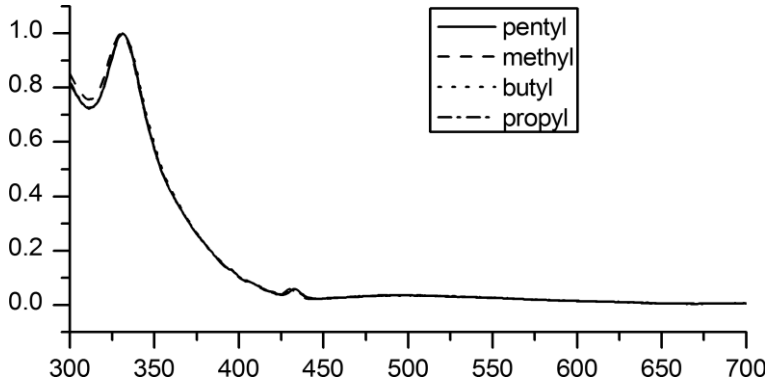

Figure 4.11: *Absorption spectra of the PCXM monoadducts.*

4.3.2.2 HPLC analysis

With increasing length of the alkanoic acid moieties the retention times of the PCXM monoadducts on a silica column increases (1.8 min for the formic-, 2.8 for the propionic-, 3.25 for the butanoic-, and 3.75 minutes for the pentanoic monoadduct).

4.3.2.3 Cyclic voltammetry

Cyclic voltammetry was performed on the PCXM monoadducts to investigate the influence of the alkyl chain on the electrochemical properties of these PCBM variations. The results are given in **Table 4.1**. It was found that for increasing alkyl length the first reduction potential is shifted to more negative values. It is therefore expected that the V_{oc} will also increase slightly with increasing alkyl chain length. The group of Yang and Li found almost no difference in reduction potential (difference of 10 mV), however their published voltammograms are not very convincing due to the low intensity of the peaks.

PCXM	$E1_{1/2red}$ (V)	$E2_{1/2red}$ (V)	$\Delta E1_{1/2red}^{*}$ (V)	$\Delta E2_{1/2red}^{*}$ (V)
4.27	1.051	1.445	0.042	0.048
4.22	1.070	1.465	0.023	0.028
4.1	1.093	1.493	--	--
4.23	1.083	1.481	0.010	0.012

Table 4.1: *The first and second reduction potential of the PCXM monoadducts. Reduction potentials were measured in 4:1 ODCB/acetonitrile and are relative to ferrocene (that is, $E_{1/2\,ox}$ of ferrocene was placed at 0V). $^{*}\Delta E$ is the energy difference compared to the most negative $E_{1/2\,red}$ within the series.*

4.3.2.4 Molecular modeling

To investigate the origin of this shift towards more negative reduction potential with increasing alkyl chain length found with CV measurements and to see if this is caused by an interaction between the ester moiety and the fullerene core, the molecular orbitals were calculated for the monoadducts. The structures were geometry optimized using PM3 semi-empirical calculations after which the orbitals were calculated. It was found that in all cases the LUMO is fully located on the fullerene sphere. No apparent interaction between the alkyl chain or ester moiety is seen. Therefore the origin of this negative shift in reduction potential must lie somewhere else. Decreasing the local polarity at the electrode surface in the CV measurements with increasing alkyl chain length can cause this trend as well.

4.3.3 PCXM bisadducts

4.3.3.1 HPLC analysis

The HPLC chromatograms of the bisadduct analogs are similar to those of the monoadducts: longer alkyl chains result in longer retention times on a silica column. The most striking difference between the Bingel adduct and the adducts synthesized through conventional diazoalkane addition. However, because Bingel additions are performed at room temperature it is possible that the distribution of isomers is distinctly different from those of the isomeric bisadduct mixtures

formed at higher temperature through diazoalkane additions.

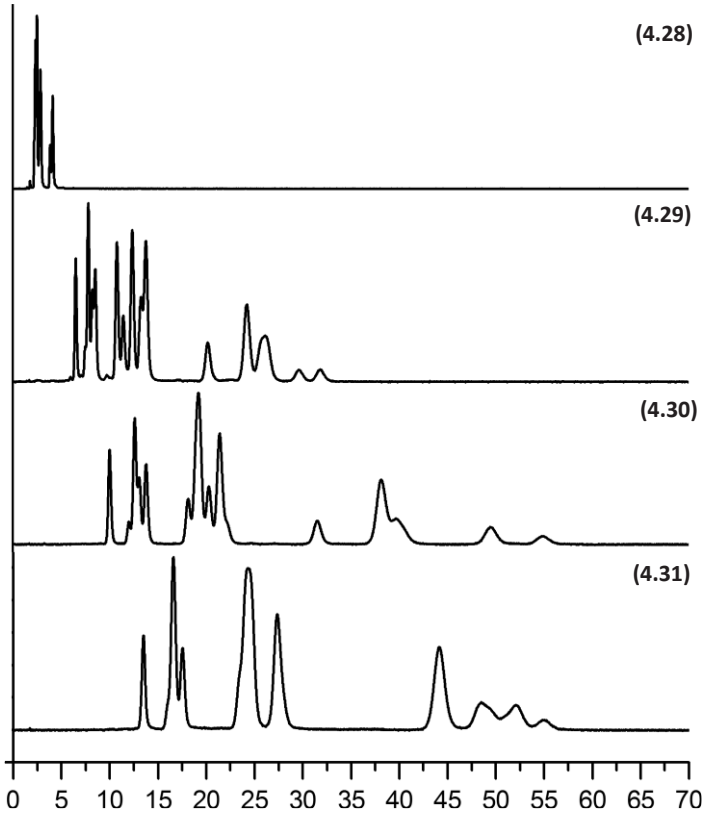

Figure 4.13: *HPLC chromatograms of the PCXM bisadduct analogs (**(4.28)** top, **(4.29)** second chromatogram, **(4.30)** third and **(4.31)** bottom chromatogram).*

4.3.3.2 Cyclic voltammetry

Cyclic voltammetry was performed on the bisadduct analogs to investigate their electrical properties. The results are given in **Table 4.2**.

Bis-PCXM	$E1_{1/2red}$ (V)	$E2_{1/2red}$ (V)	$\Delta E1_{1/2red}^{*}$ (V)	$\Delta E2_{1/2red}^{*}$ (V)
4.28	1.130	1.518	0.071	0.080
4.29	1.177	1.568	0.024	0.030
4.30	1.201	1.598	--	--
4.31	1.198	1.596	0.003	0.002

Table 4.2: *First and second reduction potentials of the PCXM bisadduct analogs. Reduction potentials were measured in 4:1 ODCB/acetonitrile and are relative to ferrocene (that is, $E_{1/2\,ox}$ of ferrocene was placed at 0V).* $^{*}\Delta E$ *is the energy difference compared to the most negative $E_{1/2\,red}$ within the series.*

The PCXM bisadducts show behavior similar to that of the monoadducts. Increasing the alkyl chain length leads to more negative reduction potentials up to bis-PCBM after which a further increase in alkyl chain length seems to results in a positive shift in first reduction potential compared to bis-PCBM. However the difference in reduction potential (3 mV) is too small to draw any solid conclusions on the behavior of the reduction potential with longer alkyl chains.

4.4 Device testing

To investigate the influence of the length of the alkyl chain devices were made comprising these new acceptor materials in combination with P3HT. Devices were made with both the mono- as well as the PCXM bisadducts.

4.4.1 PXCM monoadducts

Table 4.3 lists the device characteristics of the best cells obtained with the PCXM monoadducts in combination with P3HT. Due to the lower solubility of especially the shorter alkyl chain monoadducts, difficulties in acquiring solutions for spin-coating were met. Solutions were made in ODCB (15 mg/ml P3HT, 1:1 with PCXM monoadduct). The low solubility in chloroform prevented deposition of the active layer from this solvent. Even in ODCB monoadduct **(4.27)** could not be dissolved in the desired concentration and therefore no devices could be obtained. Devices were annealed for 15 min at 135^{o}C.

PCXM	V_{oc} (V)	J_{sc} (A/m^2)	FF	Efficiency (%)
4.22	0.61	76.2	0.62	2.89
4.1	0.61	75.6	0.44	2.01
4.23	0.61	45.05	0.59	1.62

Table 4.3: *The device characteristics of P3HT devices in combination with the PCXM monoadducts.*

Contrary to the cyclic voltammetry measurements the V_{oc} of the devices comprising the different length alkyl chains are all similar. However within a series of cells containing the same acceptor material deviations existed most likely caused by the lower solubility of these derivatives. Monoadduct **(4.22)** performs slightly better than PCBM, **(4.1)**, however the fill factor obtained for these PCBM cells is lower than usual. Monoadduct **(4.23)**, having the longest alkyl chain, performs less well, mainly due to a lower current which is likely caused by an increase in intermolecular distance decreasing the electronic interaction between the fullerene spheres.

4.4.2 PCXM bisadducts

Table 4.4 lists the device characteristics of the best cells obtained with the PCXM bisadduct in combination with P3HT. Due to the better solubility also devices containing the bisadduct analog of **(4.27)** could be obtained (that is **(4.28)**).

Bis-PCXM	V_{oc} (V)	J_{sc} (A/m^2)	FF	Efficiency (%)	Mobility (m^2/Vs)
4.28	0.68	68.2	0.49	2.26	$1.7 * 10^{-7}$
4.29	0.70	70.9	0.59	2.95	$6.0 * 10^{-7}$
4.30	0.73	77.4	0.62	3.46	$9.0 * 10^{-7}$
4.31	0.71	70.4	0.63	3.16	$1.4 * 10^{-6}$

Table 4.4: *The device characteristics of P3HT devices in combination with the PCXM bisadducts.*

As expected from cyclic voltammetry the V_{oc} increases with increasing alkyl chain length up to bis-PCBM, **(4.1)**, after which it decreases again. Also the current is highest for bis-PCBM. Electron mobilities were extracted from the dark current of the devices, showing only small difference in electron mobility of the blend. However it appears that in the case of the bisadduct analogs the mobility increases with increasing alkyl chain length, which is somewhat counterintuitive. Insulating alkyl chains and increasing intermolecular distance are expected to lower the mobility of the active layer. It was expected that especially bisadduct **(4.28)** would have high mobility due to absence of the alkyl chain and thus have better π–π overlap between the fullerene cores combined with a higher tendency to crystallize. However this seems not to be the case. An explanation could be a difference in isomers distribution compared to those adducts synthesized through diazoalkane addition. Further research to investigate the poor performance of the methyl analog is underway.

4.5 Conclusions

Monoadducts as well as bisadducts of PCBM-like analogs with different length alkyl chains between the cyclopropane ring and the ester moiety were synthesized and characterized. No difference in absorption within the series of monoadducts was found. However there was a clear effect of the alkyl chain length of the first reduction potentials of these PCBM-like analogs in both the mono- as well as the bisadducts. A distinct difference in polarity was found when comparing the HPLC chromatograms. Increasing alkyl chain length leads to an increase in polarity for both mono- as well as bisadducts. Their performance as acceptor material in organic bulk heterojunction solar cells as a function of the length of the alkyl spacers was investigated. As expected from cyclic voltammetry measurements an increase in V_{oc} was found for increasing alkyl chain length up to bis-PCBM. The bis-PCXM analog **(4.28)** did not outperform bis-PCBM: Higher mobility was expected due to the absence of the alkyl chain, which potentially would have leaded to better π–π overlap between the fullerene cores combined with a higher tendency to crystallize. An explanation could be a difference in isomer distribution compared to those adducts synthesized through diazoalkane additions. Further research to investigate the poor performance of bisadduct **(4.28)** is underway.

4.6 Outlook

Even though bis-PCBM performed best in the series of bisadducts presented in this chapter it may be worthwhile to expand this research towards other polymers. Especially the (bis-)PCXM analogs **(4.27)** and **(4.28)** lacking the alkyl spacer between the cyclopropyl ring and the ester moiety can be an interesting candidate to test with other less crystalline polymers than P3HT. Efforts to understand why this particular adduct performs less well than expected are under way. Incorporating side groups in the alkyl chain is also an area that is still unexplored. The introduction of electron donating groups on this position can prove to be an elegant method to further fine tune the energy levels of the fullerene acceptor.

4.7 Experimental

4.7.1 Device fabrication

Photovoltaic devices were made by spin-coating EL grade PEDOT:PSS onto pre-cleaned, patterned indium tin oxide (ITO) substrates. The photoactive layer was deposited by spin-coating from dichlorobenzene solutions. The spin-coating conditions were varied from 500 rpm up to 2500 rpm. Devices were annealed for 15 minutes at 135^{o}C. The top electrode of LiF (1 nm) and aluminum (80 nm) was deposited by vacuum evaporation at 1 x 10^{-6} mbar. Electrical device characterization was performed under a N_2 atmosphere. Current density-voltage measurements were carried out using a tungsten/halogen lamp (12 V/50 W) and a Keithley SMU 2400 source meter. From the overlap of the spectral response (SR) of the sample with the standard AM 1.5 (1000 W/m^2) spectrum we calculated the short circuit current density under AM 1.5 conditions (J_{SC},SR) assuming a linear relation between the illumination intensity and the short circuit current density. The J_{SC}, SR is in this way largely insensitive to aging of the tungsten/halogen lamp, (long term) intensity variations and spectral mismatch errors.

4.7.2 Materials

All reagents and solvents were purchased from Aldrich or Acros and used as received or purified using standard procedures. [60]Fullerene (99.5%) was purchased from Solenne BV or BuckyUSA and was used without further purification. Column chromatography was performed using silica gel (Aldrich 60, 230-240 mesh). ^{1}H NMR and ^{13}C NMR were recorded on a Varian Unity Plus (500 MHz), on a Varian AMX400 (400 MHz) or a Varian VXR-200 (200 MHz) instrument as indicated in the specifications, at 298 K. Chemical shifts are reported in δ values (ppm). HPLC-MS analyses were performed on a Hewlett Packard Chemstation Agilent 1100 Series using an analytical Cosmosil Buckyprep Type column (4.6 x 250 mm) or an analytical Alltima HP Silica column (3 x 100 mm). Cyclic voltammetry was performed using an Autolab PGStat 100. All reactions were carried out in flame-dried glassware under an N_2-atmosphere.

4.7.3 Synthesis

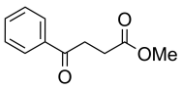

Benzoylpropionic acid methyl ester. A suspension of $AlCl_3$ (20 g, 150 mmol, 3 eq.) and toluene-free benzene (25 mL in 1,2-dichloroethane (200 mL) was cooled with an ice bath to 0 °C and methyl 4-chloro-4-oxobutanoate (6.7 mL, 50 mmol) was slowly added with a syringe. The resulting dark red solution was allowed to warm up to room temperature and stirred overnight. The mixture was poured onto crushed ice and the organic phase was collected. The aqueous layer was extracted with CH_2Cl_2 (2 x 50 mL). The combined organic layers were washed with 2% aq. NaOH solution (50 mL), brine (50 mL), and dried over Na_2SO_4. Evaporation of the solvent *in vacuo* yielded a pale yellow oil which was purified by column chromatography (SiO_2,toluene) giving the pure keto ester as 8.3 g white solid (43 mmol, 85%).

^{1}H NMR (400 MHz, $CDCl_3$) δ ppm 8.12 (m, 2H), 7.68 (m, 3H), 3.81 (s, 3H), 3.38 (m, 2H), and 2.89 (m, 2H); ^{13}C NMR (100 MHz, $CDCl_3$) δ ppm 170.34, 142.51, 141.32, 138.43, 133.42, 131.74, 129.68, 51.32, 51.09, 33.45, and 31.03.

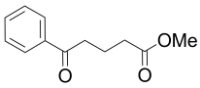

Benzoylbutanoic acid methyl ester. A suspension of $AlCl_3$ (20 g, 150 mmol, 3 eq.) and toluene-free benzene (25 mL in 1,2-dichloroethane (200 mL) was cooled with an ice bath to 0 °C and methyl 5-chloro-5-oxopentanoate (6.9 mL, 50 mmol) was slowly added with a syringe. The resulting dark red solution was allowed to warm up to room temperature and stirred overnight. The mixture was poured onto crushed ice and the organic phase was collected. The aqueous layer was extracted with CH_2Cl_2 (2 x 50 mL). The combined organic layers were washed with 2% aq. NaOH solution (50 mL), brine (50 mL), and dried over Na_2SO_4. Evaporation of the solvent *in vacuo* yielded a pale yellow oil which was purified by column chromatography (SiO_2,toluene) giving the pure keto ester as 7.2 g white solid (35 mmol, 70%).

^{1}H NMR (400 MHz, $CDCl_3$) δ ppm 7.98 (m, 2H), 7.42 (m, 3H), 3.71 (s, 3H), 2.78 (m, 2H), 2.43 (m, 2H), and 2.12 (m, 2H); ^{13}C NMR (100 MHz, $CDCl_3$) δ ppm 171.23,

142.31, 139.67, 138.01, 133.65, 129.58, 128.21, 53.12, 52.23, 35.67, 33.26, and 27.56.

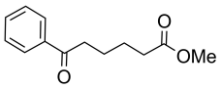

Benzoylpentanoic acid metyl ester. A suspension of $AlCl_3$ (20 g, 150 mmol, 3 eq.) and toluene-free benzene (25 mL in 1,2-dichloroethane (200 mL) was cooled with an ice bath to 0 °C and methyl 6-chloro-6-oxohexanoate (7.8 mL, 50 mmol) was slowly added with a syringe. The resulting dark red solution was allowed to warm up to room temperature and stirred overnight. The mixture was poured onto crushed ice and the organic phase was collected. The aqueous layer was extracted with CH_2Cl_2 (2 x 50 mL). The combined organic layers were washed with 2% aq. NaOH solution (50 mL), brine (50 mL), and dried over Na_2SO_4. Evaporation of the solvent *in vacuo* yielded a pale yellow oil which was purified by column chromatography (SiO_2/toluene) giving the pure keto ester as 9.0 g white solid (41 mmol, 82%). ^{1}H NMR (400 MHz, $CDCl_3$) δ ppm 8.01 (m, 2H), 7.78 (m, 2H), 7.65 (m, 1H), 3.94 (s, 3H), 2.67 (m, 2H), 2.48 (m, 2H), 1.95 (m, 2H), and 1.88 (m, 2H); ^{13}C NMR (100MHz, $CDCl_3$) δ ppm 172, 03, 142.88, 140.32, 138.21, 133.97, 129.87, 128.22, 52.18, 51.31, 34.98, 33.43, 26.44, and 25.89.

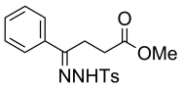

Benzoylpropionic acid methyl ester tosylhydrazone. Benzoylpropionic acid methyl ester (5.0 g, 26 mmol) and p-tosylhydrazide (5.3 g, 28 mmol, 1.1 eq.) were dissolved in toluene (100 mL). The resulting solution was refluxed in a Dean-Stark setup for 4 hours. The reaction mixture was cooled to room temperature and the white precipitate was filtered off. The filtrate was stripped of solvent *in vacuo* and recrystalized from hot methanol to yield 7.2 g of the product as white crystals (20 mmol, 80%).

^{1}H NMR (400 MHz, $CDCl_3$) δ ppm 9.74 (s, 1H), 7.92 (m, 2H), 7.54 (m, 2H), 7.31 (m, 5H), 3.58 (s, 3H), 2.92 (m, 2H), 2.61 (m, 2H), and 2.40 (s, 3H); ^{13}C NMR (100 MHz, $CDCl_3$) δ ppm 174.77, 154.54, 143.72, 135.14, 129.79, 129.27, 128.50, 128.30, 126.34, 52.43, 44.42, 30.93, 21.58, and 21.03

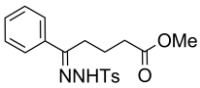

Benzoylbutanoic acid methyl ester tosylhydrazone. Benzoylbutanoic acid methyl ester (5.0 g, 24 mmol) and p-tosylhydrazide (5.3 g, 28 mmol, 1.1 eq.) were dissolved in toluene (100 mL). The resulting solution was refluxed in a Dean-Stark setup for 4 hours. The reaction mixture was cooled to room temperature and the white precipitate was filtered off. The filtrate was stripped of solvent *in vacuo* and recrystallized from hot methanol to yield 6.7 g of the product as white crystals (18 mmol, 78%).

^{1}H NMR (400 MHz, $CDCl_3$) δ ppm 8.77 (s, 1H), 7.89 (m, 2H), 7.63 (m, 2H), 7.28 (m, 5H), 3.63 (s, 3H), 2.59 (m, 2H), 2.38 (s, 3H), 2.12 (m, 2H), and 1.56 (m, 2H); ^{13}C NMR (100 MHz, $CDCl_3$) δ ppm 173.21, 142.19, 134.32, 138.01, 134.78, 129.64, 128.67, 128.13, 126.74, 53.23, 52.12, 36.71, 34.09, 27.65 and 22.06

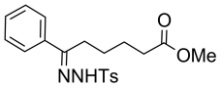

Benzoylpentanoic acid methyl ester tosylhydrazone. Benzoylpentanoic acid metyl ester (5.0 g, 23 mmol) and p-tosylhydrazide (5.0 g, 26 mmol, 1.1 eq.) were dissolved in toluene (100 mL). The resulting solution was refluxed in a Dean-Stark setup for 3 hours. The reaction mixture was cooled to room temperature and the white precipitate was filtered off. The filtrate was stripped of solvent *in vacuo* and recrystallized from hot methanol to yield 7.0 g of the product as white crystals (18 mmol, 70%).

^{1}H NMR (400 MHz, $CDCl_3$) δ ppm 8.94 (s, 1H), 7.91 (m, 2H), 7.61 (m, 2H), 7.33 (m, 5H), 3.66 (s, 3H), 2.60 (m, 2H), 2.41 (s, 3H), 2.31 (m, 2H), 1.63 (m, 2H), and 1.48 (m, 2H); ^{13}C NMR (100MHz, $CDCl_3$) δ ppm 172, 13, 143.55, 141.76, 138.67, 134.54, 123.69, 128.30, 128.14, 126.09, 53.81, 51.32, 35.09, 33.45, 27.89, 25.05, and 22.08.

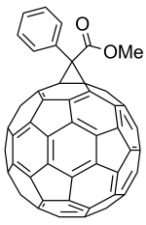

PXCM monoadduct 4.27. A solution of 1.5 g C_{60} (2.1 mmol), 0.65 mL methyl bromo(phenyl)acetate (4.2 mmol) and 0.62 mL 1,8-diazabicyclo-undec-7-ene (DBU, 4.2 mmol) in 100 mL ODCB was stirred for 4 hours at room temperature. The reaction mixture was concentrated and purified by column chromatography (SiO_2,toluene).

The monoadduct fraction was concentrated and precipitated with methanol. The obtained solids were washed with methanol (2 x 100 mL), pentane (50 mL) and dried overnight at 40°C in a vacuum oven yielding 638 mg red solid (0.75 mmol, 36%).[1]H NMR (500 MHz, CS_2 with D_2O insert) δ ppm 8.15 (m, 2H), 7.62 (m, 3H), and 4.03 (s, 3H); [13]C NMR (126 MHz, CS_2 with D_2O insert) δ ppm 165.76, 147.60, 146.24, 145.56, 145.37, 145.32, 144.88, 144.84, 144.67, 144.63, 144.08, 143.87, 143.29, 143.25, 143.16, 143.10, 142.48, 142.39, 142.32, 142.13, 141.19, 141.17, 138.56, 138.04, 132.54, 132.50, 129.55, 128.96, 75.66, and 53.32.

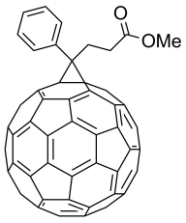

PCXM monoadduct 4.22. A mixture of benzoylpropionic acid methyl ester tosylhydrazone (2.5 g, 7 mmol, 2.2 eq.) and sodium methoxide (416 mg, 7.7 mmol) was dissolved in dry pyridine (10 mL) and stirred at room temperature for 30 minutes. Then a degassed solution of C_{60} (2.3 g, 3.2 mmol) in ODCB chlorobenzene (100 mL) was added. The mixture was heated to 90 °C and irradiated with a 150 W Na-lamp. The solution was concentrated *in vacuo* after reacting overnight. The product was purified by column chromatography (SiO_2,toluene). The monoadduct fraction was concentrated and precipitated with methanol. The obtained solids were washed with methanol (2 x 100 mL), pentane (50 mL) and dried overnight at 40°C in a vacuum oven yielding 986 mg red solids (1.1 mmol, 35%).

[1]H NMR (500 MHz, CS_2 with D_2O insert) δ 8.03 (m, 2H), 7.63 (m, 3H), 3.77 (s, 3H), 3.28 (m, 2H), and 2.93 (m, 2H); [13]C NMR (126 MHz, CS_2 with D_2O insert) δ 171.14, 148.57, 147.51, 145.95, 145.40, 145.38, 145.28, 145.19, 145.01, 144.98, 144.88, 144.70, 144.36, 143.96, 143.27, 143.22, 143.19, 143.16, 142.44, 142.36, 142.22, 141.28, 141.02, 138.43, 137.94, 136.28, 132.32, 130.74, 128.85, 128.71, 127.77, 79.62, 51.58, 51.06, 31.67, and 30.13.

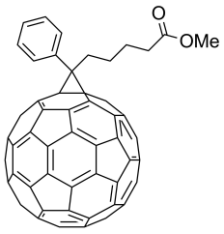

PCXM monoadduct 4.23. A mixture of benzoylpentanoic acid methyl ester tosylhydrazone (2.5 g, 6.4 mmol, 2.2 eq.) and sodium methoxide (380 mg, 7.0 mmol) was dissolved in dry pyridine (10 mL) and stirred at room temperature for 30 minutes. Then a degassed solution of C_{60} (2.1 g, 2.9 mmol) in ODCB (100 mL) was added. The mixture was heated to 90 °C and irradiated with a 150 W Na-lamp. The solution was concentrated *in vacuo* after reacting overnight. The product was purified by column chromatography (SiO_2,toluene). The monoadduct fraction was concentrated and precipitated with methanol. The obtained solids were washed with methanol (2 x 100 mL), pentane (50 mL) and dried overnight at 40^{o}C in a vacuum oven yielding 1.2 g red solids (1.1 mmol, 38%).

^{1}H NMR (500 MHz, CS_2 with D_2O insert) δ ppm 7.97 (m, 2H), 7.61 (m, 2H), 7.53 (m, 1H), 3.67 (s, 3H), 2.94 (m, 2H), 2.41 (m, 2H), 1.97 (m, 2H), and 1.90 (m, 2H); ^{13}C NMR (126 MHz, CS_2 with D_2O insert) δ 171.77, 148.75, 147.92, 145.94, 145.33, 145.21, 144.94, 144.85, 144.80, 144.61, 144.57, 144.26, 144.21, 143.91, 143.28, 143.21, 143.15, 143.10, 143.06, 142.39, 142.29, 142.21, 141.21, 141.17, 140.94, 140.88, 138.22, 137.83, 136.95, 132.24, 132.19, 128.66, 128.53, 128.42, 128.37, 79.98, 52.31, 51.18, 34.33, 33.98, 26.97, and 25.44.

PCXM bisadducts were obtained from the same reaction as the monoadducts. Further elution of the reaction mixture after obtaining the monoadducts by column chromatography (SiO_2,toluene) afforded the respective bis-PCXM fractions as isomeric mixtures. After removal of the eluens *in vacuo* a dark solid remained. The solid was precipitated from ODCB in methanol and subsequently centrifuged. The remaining brown pellet was washed twice with methanol and dried *in vacuo* at 40 ^{o}C overnight.

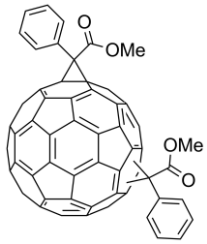

PCXM bisadduct 4.28. The pure product was obtained as 886 mg red solid (0.87 mmol, 42%). ^{1}H NMR (500 MHz, CS_2 with D_2O insert) δ ppm 8.40-8.27 (m, broad, 2H), 8.20-7.83 (m, broad, 4H), 7.79-7.07 (m, broad, 4H) 4.23-3.43 and (broad singlets, 6H); ^{13}C NMR (126 MHz, CS_2 with D_2O insert) δ ppm 168.89, 168.73, 168.71, 168.53, 168.49, 168.45, 168.40, 168.35, 168.29, 168.25, 168.09, 153.07, 152.94, 152.48, 152.34, 151.73, 151.60, 151.45, 151.29, 151.13, 151.06, 151.01, 150.92, 150.84, 150.55, 150.33, 150.28, 150.16, 150.08, 150.04, 149.99, 149.91, 149.86, 149.81, 149.76, 149.69, 149.63, 149.59, 149.54, 149.48, 149.34, 149.30, 149.26, 149.23, 149.19, 149.14, 149.09, 149.07, 149.03, 149.00, 148.97, 148.93, 148.86, 148.80, 148.74, 148.66, 148.63, 148.53, 148.48, 148.44, 148.40, 148.35, 148.27, 148.22, 148.20, 148.17, 148.14, 148.10, 148.04, 148.01, 147.90, 147.88, 147.84, 147.79, 147.76, 147.72, 147.61, 147.57, 147.54, 147.46, 147.44, 147.37, 147.34, 147.16, 147.13, 147.05, 147.01, 146.98, 146.96, 146.90, 146.85, 146.82, 146.76, 146.71, 146.61, 146.53, 146.49, 146.45, 146.41, 146.37, 146.32, 146.29, 146.19, 146.17, 146.12, 146.09, 145.95, 145.90, 145.82, 145.79, 145.76, 145.71, 145.64, 145.57, 145.54, 145.46, 145.43, 145.41, 145.38, 145.20, 145.16, 145.13, 145.07, 145.01, 144.97, 144.90, 144.80, 144.76, 144.75, 144.68, 144.65, 144.61, 144.57, 144.55, 144.47, 144.43, 144.33, 144.29, 144.24, 144.19, 144.15, 143.98, 143.92, 143.86, 143.84, 143.78, 143.67, 143.60, 143.27, 143.22, 143.09, 143.05, 142.99, 142.81, 142.77, 142.68, 142.43, 142.21, 142.17, 141.99, 141.56, 141.54, 141.38, 141.28, 141.18, 141.13, 141.05, 141.02, 140.84, 140.81, 140.70, 140.66, 140.48, 140.20, 140.14, 140.11, 139.87, 139.72, 139.61, 139.30, 139.18, 139.15, 139.08, 138.22, 138.04, 137.70, 137.62, 137.26, 135.82, 135.64, 135.51, 135.43, 135.40, 135.36, 135.27, 135.21, 135.16, 135.13, 135.11, 135.07, 135.02, 135.00, 134.95, 134.88, 134.81, 134.69, 134.56, 134.41, 133.36, 132.24, 132.14, 132.11, 132.08, 132.01, 131.93, 131.90, 131.73, 131.69, 131.61, 131.57, 131.52, 131.49, 131.44, 131.35, 131.19, 130.42, 128.32, 78.74, 78.68, 78.54, 78.45, 78.38, 78.33, 77.95, 77.89, 77.59, 77.50, 77.42, 77.36, 77.15, 77.03, 75.96, 74.23,

60.13, 59.70, 57.88, 57.83, 57.81, 57.61, 57.39, 56.27, 56.23, 56.18, 56.15, 56.05, 56.02, 55.93, 55.91, 55.86, 55.84, 55.81, 55.73, 55.69, 55.46, and 49.14.

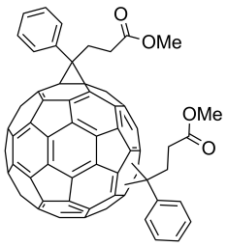

PCXM bisadduct 4.29. The pure product was obtained as 1.18 g red solid (1.1 mmol, 33%). ^{1}H NMR (500 MHz, CS_2 with D_2O insert) δ ppm 8.31-7.69 (m, broad, 4H), 7.67-7.14 (m, broad, 6H), 3.87-3.52 (broad singlets, 6H), 3.36-2.99 (m, broad, 4H), and 2.96-2.48 (m, broad, 4H); ^{13}C NMR (126 MHz, CS_2 with D_2O insert) δ ppm 171.33, 171.31, 171.20, 171.18, 171.16, 171.15, 171.11, 171.08, 171.04, 151.45, 151.43, 150.64, 150.59, 150.43, 149.72, 149.66, 149.59, 149.38, 149.08, 148.76, 148.70, 148.62, 148.32, 148.24, 148.15, 148.12, 148.06, 148.05, 147.96, 147.74, 147.71, 147.64, 147.58, 147.36, 147.33, 147.29, 147.22, 147.16, 147.07, 147.03, 146.93, 146.88, 146.82, 146.78, 146.74, 146.68, 146.66, 146.61, 146.58, 146.50, 146.45, 146.37, 146.33, 146.30, 146.27, 146.24, 146.20, 146.18, 146.15, 146.13, 146.11, 146.05, 146.02, 145.98, 145.94, 145.89, 145.83, 145.80, 145.78, 145.74, 145.68, 145.66, 145.60, 145.56, 145.54, 145.49, 145.47, 145.43, 145.40, 145.39, 145.36, 145.34, 145.25, 145.20, 145.15, 145.11, 145.06, 144.99, 144.94, 144.89, 144.81, 144.80, 144.75, 144.68, 144.67, 144.61, 144.54, 144.49, 144.47, 144.46, 144.43, 144.35, 144.32, 144.30, 144.27, 144.24, 144.15, 144.10, 144.07, 144.05, 144.03, 144.01, 143.98, 143.89, 143.85, 143.74, 143.66, 143.61, 143.57, 143.55, 143.50, 143.41, 143.37, 143.32, 143.27, 143.18, 143.11, 143.07, 143.02, 142.90, 142.83, 142.75, 142.71, 142.65, 142.60, 142.51, 142.47, 142.44, 142.36, 142.25, 142.17, 142.13, 142.07, 142.03, 141.97, 141.91, 141.89, 141.84, 141.78, 141.74, 141.70, 141.68, 141.66, 141.54, 141.51, 141.42, 141.30, 141.26, 141.20, 141.15, 141.10, 141.03, 140.95, 140.93, 140.84, 140.70, 140.52, 140.48, 140.23, 140.18, 139.97, 139.82, 139.37, 139.08, 138.78, 138.59, 138.40, 138.31, 138.18, 137.99, 137.94, 137.90, 137.87, 137.78, 137.46, 137.39, 137.31, 137.08, 136.98, 136.91, 136.86, 136.81, 136.75, 136.67, 136.64, 136.61, 136.58, 136.54, 136.44, 136.40, 136.35, 136.32, 136.16, 135.99, 135.69, 135.34,

135.04, 134.35, 133.27, 132.60, 132.53, 132.51, 132.47, 132.29, 132.27, 132.24, 132.21, 132.20, 132.17, 132.15, 132.10, 132.04, 132.00, 131.98, 131.85, 130.73, 128.94, 128.82, 128.80, 128.77, 128.73, 128.71, 128.68, 128.65, 128.59, 128.53, 128.50, 128.48, 128.38, 128.35, 128.25, 127.93, 127.77, 80.43, 80.38, 80.27, 80.15, 79.89, 79.62, 79.09, 79.06, 78.89, 78.77, 78.63, 78.49, 78.21, 78.16, 78.03, 76.56, 52.81, 52.55, 51.62, 51.57, 51.54, 51.52, 51.50, 51.48, 51.45, 51.40, 50.16, 50.14, 50.10, 50.09, 49.97, 49.80, 48.68, 48.63, 48.58, 48.51, 48.48, 48.40, 48.32, 48.22, 46.73, 43.91, 31.80, 31.79, 31.74, 31.65, 31.63, 31.60, 31.58, 31.55, 31.50, 31.42, 31.29, 30.74, 30.62, 30.49, 30.39, 30.22, 30.18, 30.10, 29.97, 29.67, 29.59, 29.54, 29.46, 29.35, and 29.18.

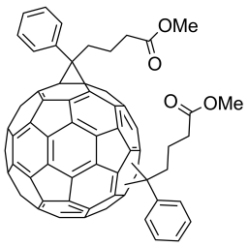

PXBM bisadduct 4.30. The pure product was obtained as 1.5 g red solid (1.4 mmol, 45%). ^{1}H NMR (500 MHz, CS_2 with D_2O insert) δ ppm 8.25-7.25 (broad signals 10H), 3.81-3.56 (broad singlets, 6H), and 3.25-1.30 (broad signals, 12H); ^{13}C NMR (126 MHz, CS_2 with D_2O insert) δ ppm 171.93, 171.79, 171.75, 171.74, 171.72, 171.67, 171.64, 171.62, 171.58, 171.57, 171.50, 151.95, 151.70, 151.59, 151.55, 150.77, 150.75, 150.72, 150.61, 150.39, 149.89, 149.86, 149.80, 149.78, 149.51, 149.47, 149.19, 149.16, 149.14, 149.02, 148.93, 148.87, 148.80, 148.75, 148.60, 148.57, 148.39, 148.32, 148.30, 148.27, 148.06, 148.00, 147.96, 147.91, 147.85, 147.84, 147.81, 147.71, 147.65, 147.54, 147.49, 147.48, 147.41, 147.38, 147.35, 147.31, 147.27, 147.22, 147.18, 147.14, 147.11, 147.09, 147.06, 147.04, 147.00, 146.96, 146.95, 146.90, 146.88, 146.85, 146.82, 146.77, 146.75, 146.70, 146.66, 146.65, 146.61, 146.57, 146.54, 146.51, 146.49, 146.48, 146.46, 146.44, 146.42, 146.38, 146.33, 146.28, 146.26, 146.23, 146.17, 146.14, 146.07, 146.05, 146.04, 146.01, 145.97, 145.93, 145.88, 145.85, 145.82, 145.78, 145.73, 145.70, 145.66, 145.65, 145.60, 145.57, 145.52, 145.49, 145.45, 145.40, 145.37, 145.33, 145.31, 145.30, 145.27, 145.25, 145.21, 145.18, 145.16, 145.14, 145.08, 145.05, 145.01, 144.99, 144.96, 144.92, 144.88, 144.83,

144.82, 144.78, 144.75, 144.73, 144.70, 144.67, 144.64, 144.61, 144.57, 144.54, 144.52, 144.42, 144.36, 144.33, 144.30, 144.28, 144.26, 144.24, 144.20, 144.15, 144.09, 144.05, 144.03, 143.99, 143.96, 143.93, 143.89, 143.84, 143.82, 143.78, 143.74, 143.70, 143.67, 143.63, 143.60, 143.57, 143.50, 143.48, 143.45, 143.43, 143.40, 143.38, 143.31, 143.28, 143.26, 143.19, 143.15, 143.11, 143.10, 143.08, 143.04, 142.97, 142.93, 142.91, 142.88, 142.85, 142.81, 142.75, 142.74, 142.72, 142.66, 142.64, 142.61, 142.60, 142.57, 142.54, 142.51, 142.47, 142.39, 142.38, 142.35, 142.30, 142.28, 142.22, 142.20, 142.17, 142.10, 142.08, 142.05, 142.01, 141.99, 141.98, 141.93, 141.90, 141.80, 141.75, 141.72, 141.68, 141.64, 141.59, 141.54, 141.47, 141.45, 141.40, 141.32, 141.28, 141.27, 141.22, 141.20, 141.17, 141.12, 141.07, 141.02, 140.98, 140.94, 140.85, 140.78, 140.74, 140.71, 140.62, 140.56, 140.48, 140.42, 140.39, 140.34, 140.32, 140.30, 140.06, 140.04, 139.74, 139.63, 139.49, 139.25, 139.18, 139.15, 139.12, 138.93, 138.89, 138.68, 138.43, 138.33, 138.17, 138.13, 138.09, 137.97, 137.94, 137.86, 137.77, 137.69, 137.64, 137.61, 137.59, 137.57, 137.43, 137.38, 137.36, 137.30, 137.23, 137.22, 137.21, 137.14, 137.11, 137.08, 137.04, 137.02, 136.99, 136.93, 136.86, 136.85, 136.82, 136.77, 136.75, 136.72, 136.67, 136.65, 136.63, 136.44, 136.42, 136.38, 136.26, 136.21, 136.19, 136.15, 136.09, 135.92, 135.89, 135.80, 135.77, 135.56, 135.54, 135.47, 135.45, 135.10, 135.08, 134.81, 134.48, 134.22, 133.54, 133.07, 133.04, 132.48, 132.34, 132.32, 132.28, 132.20, 132.14, 132.10, 132.06, 132.03, 131.99, 131.93, 131.82, 131.80, 131.62, 131.49, 131.34, 131.25, 130.65, 130.58, 129.19, 129.01, 128.77, 128.62, 128.60, 128.55, 128.53, 128.46, 128.41, 128.36, 128.33, 128.29, 128.24, 128.21, 128.15, 128.12, 127.77, 127.68, 127.38, 125.59, 125.10, 80.66, 80.62, 80.56, 80.52, 80.33, 80.28, 80.16, 80.15, 79.91, 79.90, 79.85, 79.81, 79.32, 79.25, 79.14, 78.94, 78.91, 78.84, 78.81, 78.78, 78.74, 78.70, 78.55, 78.43, 78.38, 78.31, 78.22, 78.18, 78.07, 77.94, 77.82, 76.96, 76.79, 76.69, 76.48, 76.34, 75.31, 75.28, 74.57, 74.47, 53.80, 53.57, 51.30, 51.26, 51.24, 51.20, 51.18, 51.13, 51.10, 51.09, 51.04, 50.98, 50.86, 50.83, 50.79, 49.52, 49.49, 49.41, 49.31, 49.24, 49.23, 49.15, 49.12, 49.02, 48.93, 48.86, 47.75, 47.52, 47.41, 47.38, 47.16, 47.10, 44.77,

34.43, 34.34, 34.29, 34.15, 34.06, 34.01, 33.98, 33.95, 33.87, 33.84, 33.80, 33.76, 33.73, 33.59, 33.49, 33.42, 33.37, 33.29, 33.25, 33.21, 33.10, 32.76, 32.67, 32.50, 32.23, 29.73, 22.99, 22.88, 22.87, 22.79, 22.73, 22.70, 22.65, 22.61, 22.57, 22.53, 22.41, 22.36, 22.28, 21.98, 21.86, 21.76, and 21.69.

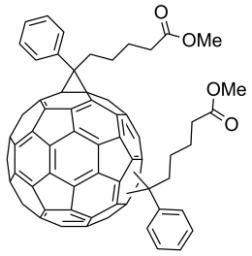

PCXM bisadduct 4.31. The pure product was obtained as 1.0 g red solid (0.9 mmol, 31%). ^{1}H NMR (500 MHz, d_2o) δ ppm 8.31-6.98 (m, broad, 10H) 3.80-3.43 (broad singlets, 6H), 3.19-2.53 (m, broad, 4H), 2.51-2.24 (m, broad, 4H), and 2.09-1.59 (m, broad, 8H); ^{13}C NMR (126 MHz, CS_2 with D_2O insert) δ ppm 171.95, 171.88, 171.83, 171.80, 171.78, 171.75, 171.71, 151.79, 151.67, 151.62, 150.93, 150.88, 150.80, 150.72, 150.01, 149.95, 149.86, 149.59, 149.55, 149.42, 149.24, 149.17, 149.10, 148.97, 148.86, 148.77, 148.73, 148.45, 148.33, 148.08, 148.04, 147.96, 147.94, 147.89, 147.74, 147.68, 147.62, 147.56, 147.43, 147.39, 147.31, 147.28, 147.23, 147.21, 147.18, 147.12, 147.10, 147.02, 146.97, 146.95, 146.84, 146.83, 146.74, 146.72, 146.69, 146.64, 146.61, 146.58, 146.55, 146.51, 146.49, 146.46, 146.43, 146.39, 146.33, 146.31, 146.28, 146.25, 146.23, 146.17, 146.15, 146.14, 146.04, 145.98, 145.88, 145.84, 145.78, 145.72, 145.67, 145.64, 145.58, 145.48, 145.43, 145.39, 145.36, 145.33, 145.30, 145.27, 145.24, 145.21, 145.12, 145.10, 145.06, 145.03, 145.00, 144.91, 144.87, 144.79, 144.72, 144.65, 144.58, 144.53, 144.49, 144.42, 144.39, 144.33, 144.32, 144.30, 144.25, 144.23, 144.20, 144.13, 144.09, 144.03, 144.00, 143.97, 143.91, 143.85, 143.81, 143.75, 143.71, 143.68, 143.62, 143.59, 143.54, 143.49, 143.46, 143.41, 143.39, 143.33, 143.26, 143.20, 143.17, 143.14, 143.04, 143.00, 142.97, 142.95, 142.79, 142.77, 142.74, 142.68, 142.61, 142.55, 142.46, 142.44, 142.39, 142.37, 142.35, 142.30, 142.23, 142.20, 142.14, 142.05, 142.01, 141.97, 141.86, 141.81, 141.75, 141.71, 141.60, 141.56, 141.54, 141.45, 141.38, 141.34, 141.33, 141.27, 141.19, 141.16, 141.11, 141.06, 141.01, 140.92, 140.88, 140.85, 140.82, 140.73, 140.70, 140.64, 140.46, 140.41, 140.13, 140.11, 139.74, 139.64,

139.32, 139.26, 139.22, 139.17, 139.01, 138.98, 138.74, 138.43, 138.35, 138.17, 138.14, 138.09, 138.04, 138.00, 137.96, 137.93, 137.82, 137.71, 137.65, 137.62, 137.56, 137.51, 137.46, 137.41, 137.37, 137.34, 137.31, 137.19, 137.16, 137.11, 137.08, 137.03, 136.99, 136.86, 136.75, 136.71, 136.67, 136.64, 136.43, 136.33, 136.26, 136.23, 136.19, 135.76, 135.50, 135.09, 134.83, 134.57, 134.25, 132.45, 132.43, 132.40, 132.31, 132.21, 132.19, 132.17, 132.14, 132.09, 132.04, 131.92, 131.72, 131.59, 131.49, 130.68, 129.22, 128.74, 128.59, 128.57, 128.51, 128.44, 128.38, 128.33, 128.29, 128.24, 128.17, 128.07, 127.98, 127.73, 127.61, 125.64, 80.79, 80.70, 80.68, 80.55, 80.41, 80.01, 79.96, 79.46, 79.42, 79.26, 79.08, 79.01, 78.97, 78.92, 78.87, 78.83, 78.70, 78.57, 78.52, 78.46, 78.38, 78.02, 77.24, 76.81, 75.25, 74.95, 74.62, 54.09, 53.80, 51.34, 51.27, 51.19, 51.18, 51.15, 51.13, 51.11, 51.10, 51.06, 51.04, 49.73, 49.70, 49.68, 49.65, 49.55, 49.48, 49.46, 49.39, 49.25, 49.08, 47.86, 47.71, 47.61, 47.36, 44.99, 34.87, 34.77, 34.58, 34.47, 34.45, 34.42, 34.38, 34.34, 34.28, 34.14, 34.08, 34.02, 33.97, 33.94, 33.92, 33.88, 33.85, 33.79, 33.70, 33.57, 33.00, 32.86, 27.16, 27.07, 27.05, 26.95, 26.91, 26.89, 26.84, 26.78, 26.73, 26.55, 26.53, 26.13, 25.59, 25.47, 25.44, 25.42, 25.38, 25.35, 25.29, 25.15, 25.11, and 22.03.

4.8 References

1 J. C. Hummelen, B. W. Knight, F. Lepeq, F. Wudl, J. Yao and C. L. Wilkins, *J. Org. Chem*., 1995, **60**, 532

2 Schinazi, A. McMillan, A. S. Juodawlkis, J. Pharr, R. Sijbesma, G. Srdanov, J. C. Hummelen, F. D. Boudinot, C. L. Hill and F. Wudl, *Proc. Electrochem. Soc.*, 1994, **94-24**, 689

3 M. M. Wienk, M. J. Kroon, W. J. H. Verhees, J. Knol, J. C. Hummelen, P. A. V. Hal and R. A. J. Janssen*, Angew. Chem. Int. Ed*., 2003, **42**, 3371

4 S. Yoo, W. J. Potscavage, B. Domercq, J. Kim, J. Holt and B. Kippelen, *Appl. Phys. Lett.*, 2006, **89**, 233516

5 Y. Yao, C. J. Shi, G. Li, V. Shrotriya, Q. B. Pei and Y. Yang, *Appl. Phys. Lett.*, 2006, **89**,153507

6 L. J. A. Koster, V. D. Mihailetchi, R. Ramaker and P. W. M. Blom, *Appl. Phys. Lett.*, 2005, **86**, 123509

7 V. D. Mihailetchi, L. J. A. Koster, J. C. Hummelen and P. W. M. Blom, *Phys. Rev. Lett.*, 2004, **93**, 216601

8 L. J. A. Koster, E. C. P. Smits, V. D. Mihailetchi and P. W. M. Blom, *Phys. Rev. B*, 2005, **72**, 085205

9 D. Veldman, O. Ipek, S. C. J. Meskers, J. Sweelssen, M. M. Koetse, S. C. Veenstra, J. M. Kroon, S. S. van Bavel, J. Loos and R. A. J. Janssen, *J. Am. Chem. Soc.*, 2008, **130**, 7721

10 F. B. Kooistra, PhD thesis, University of Groningen, Chapter 5.3, pp131-135, 2007

11 J. Knol, M. T. Rispens, L. Sánchez and J. C. Hummelen, *Quantsol, Abstr*., **13**, 2001

12 A. Tamayo, T. Kent, M. Tantitiwat, M. A. Dante, J. Rogers and T. Nguyen, *Energy Environ, Sci*., 2009, **2**, 1180

13 L. Zheng, Q. Zhou, X. Deng, M. Yuan and G. Yu, Y. Cao, *J. Phys. Chem. B*, 2004, **108**, 11921

14 C. Yang, J. Chang, P. Yeh and T. Guo, *Carbon*, 2007, **45**, 2951
W. S. Shin, J. Lee, J. Kim, H. Y. Lee, S. K. Lee, S. C. Yoon and S. Moon, *J. Mater. Chem.*, 2011, **21**, 960

15 W. S. Shin, J. Lee, J. Kim, H. Y. Lee, S. K. Lee, S. C. Yoon and S. Moon, *J. Mater. Chem*., 2011, **21**, 960

16 C. Yang, J. y. Kim, S. Cho, J. K. Lee, A. J. Heeger and F. Wudl, *J. Am. Chem. Soc.*, 2008, **130**, 6444

17 M. T. Rispens, L. Sánchez, J. Knol and J. C. Hummelen, *Chem, Commun*, 2001, **2**, 161

18 A. M. Ramos, M. T. Rispens, J. K. J. van Duren, J. C. Hummelen and R. A. J. Jansen, *J. Am. Chem. Soc*., 2001, **123**, 6714

19 K. Szendrei, D. Jarzab, M. Yarema, M. Sytnyk, S. Pichler, J. C. Hummelen, W. Heiss and M. A. Loi, *J. Mater. Chem*., 2010, **20**, 8470

20 Jan-Carlos Kuhlmann, Paul de Bruyn, Ricardo K. M. Bouwer, Auke Meetsma, Paul W. M. Blom, and Jan C. Hummelen, *Chem. Commun*., 2010, **46**, 7232

21 L. M. Popescu, P. van't Hof, A. B. Sieval, H. T. Jonkman and J. C. Hummelen, *Appl. Phys. Lett.*, 2006, **89**, 213507

22 P. A. Troshin, H. Hoppe, J. Renz, M. Egginger, J. Y. Mayorova, A. E. Goryachev, A. S. Peregudov, R. N. Lyubovskaya, G. gobsch, N. S. Sariciftci and V. F. Razumov, *Adv. Funct. Mater*., 2009, **19**, 779

23 Y. Zhang, H. L. Yip, O. Acton, S. K. Hau, F. Huang and Y. K. Y. Jen, *Chem. Mater.*, 2009, **21**, 2598

24 G. J. Zhao, Y. J. He, Z. Xu, J. H. Hou, M. J. Zhang, J. Min, H. Y. Chen, M. F. Ye, Z. R. Hong, Y. Yang and Y. F. Li, *Adv. Funct. Mater*., 2009, **19**, 779

25 S. H. Park, C. Yang, S. Cowan, J. K. Lee, F. Wudl, K. Lee and A. J. Heeger, *J. Mater. Chem.*, 2009, **19**, 5624

26 C. Yang, S. Cho, A. J. Heeger and F. Wudl, *Angew. Chem. Int. Ed.*, 2009, **48**, 1592

27 P. Morvillo and E. Bobeico, *Phys. Status. Solidi RRL*, 2008, **2**, 260

28 G. J. Zhao, Y. He, Z. Xu, J. Hou, M. Zhang, J. Min, H. Chen, M. Ye, Z. Hong, Y. Yang and Y. Li, *Adv. Funct. Mater*, 2010, **20**, 1480

29 C. Bingel, *Chemische Berichte*, 1993, **126**, 1957

30 N. Martin, J. L. Delgado and S. Filippone, *Meet. Abstr. - Electrochem. Soc.*, 2009, **901**, 1119

31 I. Riedel, N. Martin, F. Giacalone, J. L. Segura, D. Chirvase, J. Parisi and V. Dyakonov, *Thin Solid Films*, 2004, 43, 451

32 I. Riedel, E. von Hauff, J. Parisi, N. Martin, F. Giacalone and V. Dyakonov, *Adv. Funct. Mater.*, 2005, **15**, 1979

33 A. Sánchez-Díaz, M. Izquierdo, S. Filippone, N. Martin and E. Palomares, *Adv. Funct. Mater.*, 2010, **20**, 2695

Chapter 5

PCBM analogues for blends with fluorene-based small bandgap polymers

Abstract. This chapter describes the synthesis and characterization of fluorene-containing PCBM analogues as compatibilizing agents for fluorene-bearing small bandgap polymers. Their performance as acceptor material in bulk heterojunction solar cells is tested both as a substitute for PCBM and as an additive in cells comprising PCBM as the acceptor in order to improve the morphology of the active layer. Substitution of PCBM for these fluorene-bearing analogs resulted in a higher V_{oc} compared to PCBM. Strikingly, cyclic voltammetry measurements indicated a reduction potential similar to PCBM. This unexpected extra increase in V_{oc} ($\Delta\Delta V_{oc}$) was already observed in some other fullerene derivatives but never to this extent.

This chapter is part of a cooperation with J. C. Kuhlmann, P. de Bruyn and P. W. M. Blom. Part of this chapter has been published: *Chem. Commun*., 2010, **46**, 7232, "Improving the compatibility of fullerene acceptors with fluorene-containing donor-polymers in organic photovoltaic devices" Device fabrication and testing was performed by P. de Bruyn.

5.1 Introduction

5.1.1 Small bandgap polymers

The work horse combination used in organic photovoltaic devices nowadays consists of regioregular poly(3-hexylthiophene) (P3HT) as the donor material and [6,6]-phenyl-C_{61}-butyric acid methyl ester (PCBM) as the acceptor resulting in efficiencies typically between 3-5%. A disadvantage of this combination is its capability of absorbing only a small part of the solar spectrum. With its relatively large bandgap of 1.9 eV , P3HT is only capable of absorbing light with wavelengths lower than ~650 nm thereby losing in efficiency. To increase the part of the solar spectrum that is absorbed it is necessary to reduce the optical bandgap of the light absorbing material. It is calculated, that the optimal bandgap for a donor material in organic photovoltaics is about 1.4-1.5 eV.[1]

Two different strategies are followed in designing polymers with reduced bandgaps.[2-5] The first approach is based on polymers build from a single monomer unit with aromatic and quinoid resonance structures close in energy thus decreasing bond length alternation in the polymer chain. The classical example of this class is poly(isothionaphthene), which features a bandgap of about 1 eV due to a large contribution of the quinoid resonance form in the ground state.[6.7]

The second approach is based on pending alternating electron-rich and electron-deficient monomer units along the polymer chain.[8-10] As a result the high-lying HOMO of the donor unit is combined with the low-lying LUMO of the acceptor unit and an overall small bandgap for the polymer chain is obtained. Presently, the majority of small bandgap polymers developed for solar cell applications is based on this donor-acceptor approach. This method has the advantage that not only the bandgap of the polymer can be tuned to further optimize it for light absorption by the choice of the monomers but also other properties like mobility and stacking can be influenced.

5.2 Optimizing the morphology of the active layer

5.2.1 Morphology

Varieties of conjugated alternating copolymers consisting of different electron-rich and electron-poor aromatic units have been synthesized and tested as donor material in bulk heterojunction organic solar cells over the years in combination with either [60]- or [70]PCBM.[11] Efficiencies of over 7% were reached with V_{oc} around 0.75 V and J_{sc} ranging from 11.5 to 14.5 mA/cm^2.[12] However there are still many polymers known which result in lower than expected efficiencies based on their bandgap alone. It was concluded that the morphology of the active layer within these bulk heterojunctions often limits the function of these materials.[13,14]

Besides the optical and electronic properties of the materials, the morphology of the active layer is crucial for efficient bulk heterojunction organic solar cells.[15] The nanophase segregated morphology initially formed in polymer fullerene blends is a kinetically trapped, non-equilibrium state that is formed during spin-casting and subsequent evaporation of the solvent at temperatures below that of the glass transition (Tg) of the polymers. However the immiscibility of both donor and acceptor and their tendency to crystallize can drive larger scale phase segregation and can cause discontinuity of the bicontinuous network. For improving the morphology of the active layer, there are two major factors that must be considered. One is the mobility of the charge carriers, which depends on the crystalline ordering within the active layer.[16] The other is the exciton dissociation, which mainly takes place at the interface between donor and acceptor.[17] Several possibilities to tune the extent of phase separation have been demonstrated: depositing from various solvents having different boiling temperatures and/or polarities; chancing the regio regulartity of the polymer; and varying the subsequent annealing conditions of the cast films.[18-24]

5.2.2 Additives

Recently, small amounts of volatile additives such as α,ω-alkanedithiols or 1,8-diiodooctane were introduced as "processing additives", which allow for additional structural rearrangement to take place prior to finalization of the active layer morphology resulting in fine phase separation of the polymer and fullerene domains with improved mobilities.[25] Efficiencies of 5-7% have been reported for PSCs fabricated using processing additives. Increased performance was also achieved by introducing poly(oxyethylenetridecyl ether) (PTE) as a "surfactant additive" in P3HT/PCBM cells either as extra layer between the active layer and the electrode[26] or as third component mixed in the active layer.[27] Due to the difference in hydrophobicity between the donor and the acceptor, the PTE surfactant molecules form interfacial layers between the phase-separated domains. Addition of this "surfactant additive" (1.20:0.88 P3HT/PCBM ratio with 0.1 w% of PTE) led to an increase in both short circuit current density and fill factor resulting in efficiencies of 4.5% compared to 3.9% for the reference device without the surfactant. This improvement was attributed to the increased dissociation efficiency of the bound electron-hole pairs, due to the oriented PTE surfactant molecules at the donor-acceptor interfaces. However due to the low HOMO (-8.1 eV) and the high LUMO (-2.1 eV) associated with the dipolar characteristics of PTE, it is expected that the PTE surfactant also changes the electrical properties of the donor acceptor interfaces by forming an electronic barrier between both material. Other non-volatile hydrophobic additives that were found to selectively partition into P3HT enhancing phase separation between donor and acceptor include organometallic species. The extent of phase separation is directly influenced by the hydrophobicity of the additives and can be tuned by the choose of the ligands.[28]

5.2.3 Compatibilizers

Borrowed from established methods of blending chemically incompatible polymers, compatibilizers have been introduced in an attempt to improve the morphology of the active layer. These materials, also known as interfacial agents, generally reside at the interfaces of the mixed materials to minimize unfavorable enthalpic contacts. Recent examples of this method are the solution-processable small molecule thiophene-C_{60} dyads employed as compatibilizers in inverted P3HT:PCBM devices. These donor-acceptor dyads were synthesized directly from the corresponding thiophene-carbaldehyde and N-methylglycine via a Prato reaction.[29] The similarities in the chemical structures of the dyads to both P3HT and PCBM should encourage their placement at the donor-acceptor interface**.** Organic solar cells comprising P3HT:PCBM that are compatibilized with 5 w% of the thiophene-C_{60} dyads exhibit device characteristics that are stable even with prolonged thermal annealing. An increase in short circuit current density of up to 1.1 mA/cm^2 was found without significant change in the open circuit voltage.[30]

An improvement in thermal stability was also found for P3HT:PCBM devices compatibilized with 2.5 w% C_{60}-endcapped P3HT.[31] Even though initial efficiencies were lower than that of reference devices, an extended thermal stability, attributed to suppression of the phase segregation by reduction of interfacial tension between donor and acceptor phases, was found.

Diblock copolymers containing parts of both donor and acceptor have been used as surfactants[32] or compatibilizers.[33] with similar results. Improved performances were found either by creating more suitable domains thus increasing the short circuit current[32] or by improving long term thermal stability through a lowering of the interfacial energy preventing phase segregation.[33]

5.2.4 Compatible fullerenes

A different method to improve the morphology of the active layer was already shown some years ago in our group by taking sub-structures of the donor and incorporating them into the acceptor thus improving the miscibility of donor and acceptor.[34] By incorperating a thiophene unit in the fullerene acceptor **(5.1)** compatibility with polythiophene donors, particularly regioregular poly(3-hexylthiophene) (rr-P3HT) was enlarged leading to improved morphologies of the active layer after thermal annealing by increasing the ability of the P3HT to crystallize. This method eliminates the need for a third component in the donor-acceptor blend avoiding potential problems with differences in energy levels as these structural modifications normally do not change the LUMO level of the acceptor significantly compared to that of PCBM **(5.2)**.

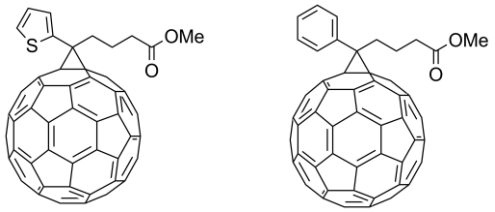

(5.1) **(5.2)**

Figure 5.1: *The compatibilized fullerene ThCBM* ***(5.1)*** *and PCBM* ***(5.2)****.*

5.2.5 Locking the morphology

Attempt to accomplish and maintain a stable morphology of the active layer over extended periods of time has led to the development of materials that are capable of locking the morphology in a certain state. Instead of preventing segregation of donor and acceptor phases by lowering the interfacial energy, materials have been applied which are solution processable but become insoluble after a thermal treatment, thus providing better operational stability for the devices. Examples of these systems that lock their morphology upon thermal annealing include cleavable polymers based on thermally labile esters which become insoluble after cleaving[35,36], polymers containing crosslinkable side chains[37,38], fullerene derivates containing similar crosslinkable

groups[39-41] and fullerenes that are covalently bound to the polymer backbone upon thermal annealing.[42] However these latter form fullerene multiadducts through the addition of the azide functional group upon locking the morphology. This results in a fraction of the fullerene residues having a higher LUMO level than the parent PCBM.

5.3 Fluorene-bearing small bandgap polymers

Among the building blocks for p-type conjugated copolymers for organic solar cells, the fluorene group is widely used for its high charge carrier mobility, good processability, stability, and high absorption coefficients.[43,44] Particularly the group of Andersson synthesized a variety of alternating polyfluorene copolymers (APFOs) (**Figure 5.2**).[45-47] In these polymers the fluorene unit is combined with donor-acceptor-donor units, like for example thiophene-benzothiadiazole-thiophene oligomers. By varying the building blocks, the optical absorption properties and the energy levels of the polymer can be controlled.[48] To prevent oxidation and to increase the solubility of the polymer, the fluorene moiety is generally dialkylated on the 9-position, most common are n-hexyl, n-octyl, and n-decyl alkyl chains.[11]

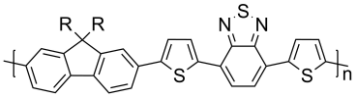

Figure 5.2: *General structure of a fluorene containing copolymer, R = C_8H_{17}: APFO-3, R = $C_{10}H_{21}$: PF10TBT.*

The performance of various polyfluorene copolymers in organic solar cells was extensively investigated by different research groups, resulting in moderate to excellent PCEs.[14,49-53] The highest efficiency of fluorene-based copolymers was reported with poly[2,7-(9,9-didecylfluorene)-*alt*-5,5-(4',7'-di-2-thienyl-2',1',3'-benzothiadiazole)] (PF10TBT) (**Figure 5.2**).[54] In blends with [60]PCBM an efficiency of 4.2% was reported. A similar polymer (APFO-3), in which the fluorene moiety was dialkylated with octyl side chains, reached efficiencies of 3.5%.[55]

To test both the compatibility and compatibilizer method with fluorene-containing small bandgap polymers, PCBM analogs were synthesized containing dialkylated fluorene moieties instead of a phenyl ring. These new acceptor materials differ from each other by the substituents at the 9-position of the fluorene unit. Three alkyl chains lenghts that are most commonly used in fluorene-based copolymers were chosen; n-hexyl, n-octyl and n-decyl. The resulting 9,9-dialkyl-9H-fluoren-2-yl-C_{61}-butyric-acid methyl esters are abbreviated F*n*CBM where *n* is the number of carbon atoms of the alkyl chain. As shown in previous chapters the open circuit voltage can be improved through the use of bisadducts. Therefore the bisadduct analogs of these fluorene-bearing fullerenes were also synthesized and tested. Compatibilization through the incorporation of these fluorene moieties should not negatively influence the electronic properties of the fullerene acceptors with respect to PCBM, therefore the electronic properties of these new acceptors were characterized with cyclic voltammetry.

5.4 Experimental results

The syntheses described in this paragraph were mainly performed by J. C. Kuhlman.

5.4.1 Synthesis of F_nCBMs

The synthesis of the F_nCBM series is given in **Scheme 5.1**.

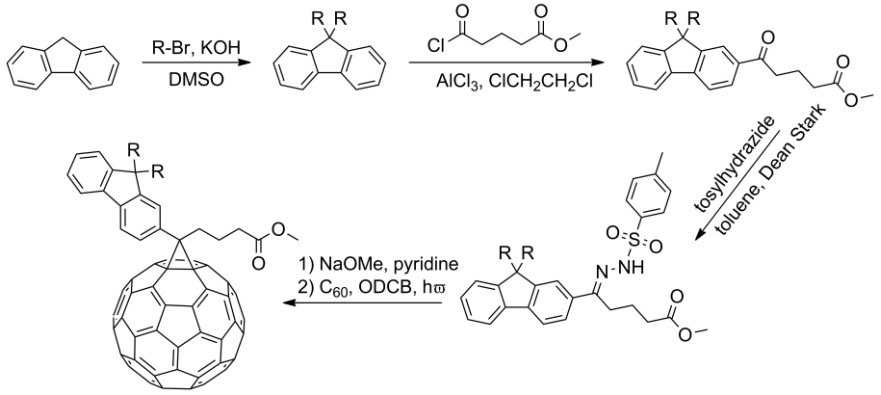

Scheme 5.1: *Synthesis of dialkylated fluorene tosylhydrazones and their addition to C_{60} to obtain the fluorene-bearing PCBM analogs.*

Fluorene was dialkylated with the appropriate alkylbromide in dimethylsulfoxide in the presence of potassium hydroxide. Purification by column chromatography (SiO_2,heptane) yielded the products as colorless oils. The dialkylated fluorenes were further functionalized by Friedel-Crafts acylation with methyl 5-chloro-5-oxopentanoate. Column chromatography (SiO_2,toluene) yielded the pure keto-esters. These keto-esters were reacted with tosylhydrazide in toluene in a Dean-Stark setup. Subsequent recrystallization from hot methanol yielded the tosylhydrazones as pale yellow crystals. From all tosylhydrazones only one isomer was detected by ^{1}H-NMR spectroscopy, which was determined by crystal structure to be the *anti*-isomer for the hexyl-substituted tosylhydrazone. Deprotonation of the tosylhydrazones with sodium methoxide in pyridine generated the diazo compounds which were used *in situ* in the 1,3-dipolar diazo addition to C_{60} in *ortho*-dichlorobenzene. The pure products were obtained by column chromatography (SiO_2,CS_2 to remove unreacted C_{60}, then 1:1 toluene/cyclohexane to obtain the monoadducts followed by toluene to obtain the respective bisadduct analogs as an isomeric mixture). The fluorene bearing PCBM analogs were characterized by NMR, HPLC, and mass spectroscopy.

5.4.2 Friedel Crafts acylation of fluorene

The Friedel-Crafts acylation of fluorene using acetylchloride as reagent and aluminum chloride as Lewis acid catalyst is known from literature.[56] Depending on reaction parameters, such as the solvent polarity, the reaction temperature, and the molar ratio of the reactants, different product ratios can be formed. Besides the diacylated 2,7-diacetyl-9H-fluorene, two different mono-acylated species can be observed, 2-acetyl-9H-fluorene and 4-diacetyl-9H-fluorene. However, 2-acetyl-9H-fluorene was found to be the predominant isomer under all conditions.[57]

To identify which isomer has been formed, the crystal structure of the hexyl-substituted tosylhydrazone was obtained (**Figure 5.2**). The crystal structure shows that the fluorene core was acylated at the 2-position. Earlier attempts to elucidate the

structure of the keto-esters by 2D-NMR experiments, HSQC (^{1}H – ^{13}C –correlation), and INADEQUATE (^{13}C – ^{13}C –correlation) could not verify which isomer was formed, due to overlapping peaks of the aromatic protons combined with the low solubility of the compounds for a well resolved ^{13}C – ^{13}C –correlation. Because the keto-esters were liquids at room temperature, it was not possible to obtain crystal structures for those compounds.

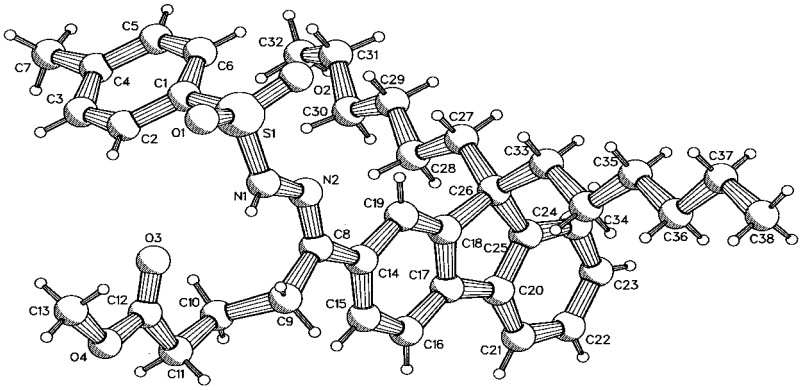

Figure 5.3: *X-ray crystal structure of 9,9-dihexyl-9H-fluoren-2-yl-methylbutyrate-p-tosylhydrazone.*

5.4.3 Cyclic voltammetry

In order to determine whether the alkylated fluorene moieties affect the electron accepting properties of the new acceptors compared to PCBM, the first reduction potentials ($E_{1/2\ red}$) were measured by cyclic voltammetry. The data are shown in **Table 5.1**. All reductions were reversible.

The measurements showed that the first reduction potentials of the three new compounds are slightly more negative compared to PCBM. This correlates with a small raise in energy of the LUMO levels. The largest difference of 16 mV was measured in the case of the methanofullerene including the decyl-substituted fluorene, whereas the methanofullerenes with the hexyl- and octyl-substituted fluorenes only showed marginal differences of 7 and 6 mV, respectively. These differences can be partly

related to the electron donating properties of the alkyl chains on the fluorene, but remain within the error margin of the measurement.

Compound	$E1_{1/2red}$ (V)	$\Delta E1_{1/2red}^{*}$ (mV)
PCBM	-1,080	-
F_6CBM	-1,087	7
F_8CBM	-1,086	6
F_{10}CBM	-1,096	16

Table 5.1: *Cyclic voltammetry data of the fluorene bearing PCBM analogs, FnCBM. Reduction potentials were measured in 4:1 ODCB/acetonitrile and are relative to ferrocene (that is, $E_{1/2\,ox}$ of ferrocene was placed at 0V). $^{*}\Delta E$ is the energy difference compared to the most negative $E_{1/2\,red}$ within the series.*

5.5 Device testing

To evaluate the effect of the fluorene moieties on the performance of OPVs, a series of photovoltaic devices was fabricated with the F*n*CBMs as acceptors and PF10TBT as the donor. One reference device with PCBM as the acceptor was made. The devices were fabricated by spin-coating PF10TBT and the appropriate fullerene acceptor from a chlorobenzene solution on a PEDOT:PSS-coated ITO glass substrate, followed by evaporating LiF and aluminum on top of the active layer.

5.5.1 Monoadducts

In an initial series the devices were fabricated with a 1:4 polymer:fullerene ratio (by weight); the optimal conditions to obtain high efficient solar cells with PCBM as acceptor material. The results obtained from the best of these devices with a similar active layer thickness (120 nm) are summarized in **Table 5.2**.

Acceptor	ratio D:A	J_{SC} [A/m²]	V_{OC} [V]	FF	PCE
PCBM	1:4	60,63	0,95	0,60	3,46
F_6CBM	1:4	42,45	1,07	0,44	2,02
	1:5.1*	46,30	1,07	0,45	2,24
F_8CBM	1:4	34,43	1,08	0,39	1,46
	1:5.4*	40,20	1,08	0,43	1,88
F_{10}CBM	1:4	31,43	1,08	0,39	1,33
	1:5.6*	33,70	1,08	0,40	1,44

Table 5.2: *Parameters from best working solar cell devices with PF10TBT as donor material;* * *adjusted for the volume fraction of PCBM.*

Compared to PCBM, the devices with F*n*CBM as acceptor showed lower J_{sc} and FF values but increased V_{oc} values by up to 130 mV (for F_8CBM and F_{10}CBM). It is known that in devices comprising PF10TBT:PCBM the V_{oc} increases with decreasing concentrations of fullerene.[54] Due to their increased molecular weight compared to PCBM, the volume fraction of fullerene is lower in the devices containing F*n*CBM than in the PCBM-containing reference device. A second series of devices was therefore prepared with an adjusted volume fraction of F*n*CBM compared to PCBM (**Table 5.2**). Contrary to expectations the V_{oc} remained unaffected from the higher fullerene concentration but J_{sc} and FF values were slightly improved raising the overall efficiency of the organic solar cell.

5.5.2 Bisadducts

As shown in previous chapters the open circuit voltage can be improved through the use of bisadducts due to an increase of ~100 mV of their LUMO level compared to the parent monoadduct. To see if this also holds for the F_nCBM bisadducts cyclic voltammetry of these fluorene bearing analogs was measured (**Table 5.3**).

Compound	$E1_{1/2red}$ (V)	$\Delta E1_{1/2red}$* (mV)
Bis- F_6CBM	-1.198	118
Bis- F_8CBM	-1.208	128
Bis- F_{10}CBM	-1.194	114

Table 5.3: *Cyclic voltammetry data of the bisadduct analogs of FnCBM. Reduction potentials were measured in 4:1 ODCB/acetonitrile and are relative to ferrocene (that is, $E_{1/2\,ox}$ of ferrocene was placed at 0V).* *ΔE *is the energy difference compared to the most negative $E_{1/2\,red}$ within the series.*

A similar increase in reduction potential compared to PCBM was found for the F*n*CBM bisadduct analogs as for bis-PCBM. It is known for bis-PCBM that even though its use in organic solar cells results in a significant increase in V_{oc} the overall efficiency is often not raised due to a decrease in J_{sc}. For polymers other than P3HT, bisadduct analogs (and even more the higher adducts) typically perform less well than their parent monoadduct. This drop in J_{sc} could be solely of a morphological nature, therefore the more compatible F_nCBM bisadducts could improve the performance of these cells. The devices were made with a 1:4 polymer:fullerene ratio (by weight) as normally is the case for bisadducts. The results are given in **Table 5.4**.

Acceptor	J_{SC} [A/m²]	V_{OC} [V]	FF	PCE
Bis-PCBM	25.2	1.13	0.45	1.27
Bis-F_6CBM (thickness)	2.0	1.14	0.33	0.07
	2.2	1.14	0.33	0.08

Table 5.4: *Preliminary solar cell results of cells comprising PF10TBT and the bisadduct analog of F_6CBM (bis-F_6CBM).*

Even though the expected increase in V_{oc} compared to the monoadduct was found, albeit somewhat lower than anticipated (70 mV), the lowering of the J_{sc} (from 46.3 to 2,2 A/m^2) was so strong that overall efficiency dropped to 0.08%. There are several possible explanations for this drop in short circuit current. The low fill factor of 0.33 is

a indication to either unbalanced charge transport or difficulties in charge separation leading to increased recombination.[58,59] Both possibilities can be the result of a bad morphology, which would be expected to decrease the J_{sc} but to a lesser extent, or due to a broad distribution of LUMO levels among the different isomers of the bisadduct. As shown in Chapter 2 bisadducts exist as a mixture of isomers with different energy levels. When these levels become too high, the fullerene instead of an acceptor becomes an insulator decreasing the amount of possible pathways in the acceptor phase resulting in more recombination and a lower J_{sc}.

5.5.3 F_6CBM as compatibilizer in PF10TBT:PCBM devices

A series of PCBM:PF10TBT devices was made containing increasing volume fractions of F_6CBM to investigate the effect of this fluorene-bearing PCBM analogue as additive to improve donor-acceptor interfaces in the active layer. The results are shown in **Table 5.5**.

% F6CBM	J_{sc} (A/m^{-2})	V_{0c} (V)	FF	MPP
0	60.9	0.953	0.66	3.86
5	51.5	0.938	0.48	2.30
10	53.1	0.949	0.63	3.16
10 (annealed)	31.8	0.945	0.55	1.65

Table 5.5: Compatibilizing the active layer of PCBM:PF10TBT devices by the addition of F6CBM

No direct positive effect was observed from the addition of F_6CBM to the PCBM:PF10TBT mixture; both J_{sc} and V_{oc} remained almost the same as without the compatibilizer. The fill factor and the maximum power point however were negatively affected by the amount of F_6CBM that is added to the active layer. Annealing of the device after fabrication leads to a drop in J_{sc}, however this is a known effect in devices comprising this polymer. Effects on thermal stability and lifetime compared to normal device composition as well as a comparison between the different morphologies are still to be investigated.

5.5.4 $\Delta\Delta V_{oc}$

The increase in V_{oc} ($\Delta\Delta V_{oc}$) found for the FnCBM analogs, compared to that of devices comprising PF10TBT:PCBM, is unexpected and cannot be reasoned in the energy levels of the polymer and that of the fullerene measured with cyclic voltammetry or the volume fraction of fullerene alone. Literature shows this phenomenon also to occur with certain other fullerene acceptors, but never to this extent (one exception being DPM12 with $\Delta\Delta V_{oc}$ ~ 100 mV) (**Table 5.5**).[60,61]

	polymer	$\Delta E1_{Red}$ (PCBM)	V_{oc}	V_{oc} PCBM	V_{oc} - V_{oc} PCBM	$\Delta\Delta V_{oc}$
bisPCBM[62]	P3HT	-100	730	580	150	50
F6CBM	PF10TBT	-7	1070	950	120	113
F8CBM	PF10TBT	-6	1080	950	130	124
F10CBM	PF10TBT	-16	1080	950	130	114
Bis-F6CBM	PF10TBT	-118	1140	950	190	72
Fullerene benzoate 3[63]	P3HT	0	654	610	44	44
p-EHO-PCBM[64]	P3HT	-8	650	600	50	42
p-EHO-PCBA[64]	P3HT	-18	640	600	40	22
Lu 3 N@C_{80} – PCBH[65]	P3HT	-280	890	630	260	-20
ICMA[66]	P3HT	-50	630	580	50	0
ICBA[66]	P3HT	-190	840	580	260	70
DPM12[60,61]	P3HT	similar	629	524	105	~100

Table 5.5: *$\Delta\Delta V_{oc}$ observed in other fullerene acceptors.*

A possible reason for this unexpected increase in open circuit voltage is given by the groups of Martin and Palomares who explain this phenomenon in differences in crystallization properties of the different fullerenes affecting charge recombination dynamics and shifting the HOMO energy level of the donor material.[67] However the

origin of this increased V_{oc} needs to be further investigated to fully understand and exploit its beneficial effect on the performance of organic solar cells.

5.6 Conclusions

Three fluorene-containing analogs of PCBM and their bisadduct analogs were synthesized, characterized, and tested in organic solar cells both as substitute for PCBM and as compatibilizer in combination with PCBM. Cyclic voltammetry measurements of these fluorene-bearing acceptors revealed only slight differences compared to their PCBM analogs. Preliminary testing of these new acceptors in combination with PF10TBT as donor material resulted in lower J_{sc} and FF values compared to the reference devices, however an unexpected increase in V_{oc} was observed. The origin of this increased V_{oc} needs to be investigated in more detail.

No direct positive effect was observed from the addition of F_6CBM to the PCBM:PF10TBT mixture; both J_{sc} and V_{oc} remain almost the same as without the compatibilizer. The fill factor and the maximum power point however are negatively affected by the amount of F_6CBM that is added to the active layer. Effects on thermal stability and lifetime compared to normal device composition as well as a comparison between the different morphologies are still to be investigated.

5.7 Outlook

Even though no direct proof for an improved morphology was found the concept of compatibilizing the fullerene should still be tested in combination with other promising polymers. Also the long term thermal stability of device comprising these fluorene-containing fullerenes either as substitute or as compatibilizer should be further investigated. A closer look at the morphologies of the active layer could lead to a better insight in their compatibilizing properties and possibly explain the unexpected high V_{oc} in terms of differences in morphology and crystallinity. Further optimization of the processing conditions, investigation of the device morphology, and transport measurements are needed to evaluate if these new acceptors are superior to PCBM in

blends with fluorene-containing polymers. These measurements are currently performed in cooperation with the group of Prof. Dr. Sean Shaheen at the University of Denver, USA.

5.8 Experimental

5.8.1 Device Fabrication

Photovoltaic devices were made by spin-coating EL grade PEDOT:PSS onto pre-cleaned, patterned indium tin oxide (ITO) substrates. The photoactive layer was deposited by spin-coating from chlorobenzene solutions. The spin-coating conditions were varied from 500 rpm up to 2500 rpm. The top electrode of LiF (1 nm) and aluminum (80 nm) was deposited by vacuum evaporation at 1 x 10^{-6} mbar. Electrical device characterization was performed under a N_2 atmosphere. Current density-voltage measurements were carried out using a tungsten/halogen lamp (12 V/50 W) and a Keithley SMU 2400 source meter. From the overlap of the spectral response (SR) of the sample with the standard AM 1.5 (1000 W/m^2) spectrum we calculated the short circuit current density under AM 1.5 conditions (J_{SC},SR) assuming a linear relation between the illumination intensity and the short circuit current density. The J_{SC}, SR is in this way largely insensitive to aging of the tungsten/halogen lamp, (long term) intensity variations and spectral mismatch errors.

5.8.2 Materials

All reagents and solvents were purchased from Aldrich or Acros and used as received or purified using standard procedures. [60]Fullerene (99.5%) was purchased from Solenne BV and BuckyUSA and was used without further purification. Column chromatography was performed using silica gel (Aldrich 60, 230-240 mesh). Melting points were determined with a Mettler FP1 melting point apparatus equipped with a Mettler FP2 microscope. ^{1}H NMR and ^{13}C NMR were recorded on a Varian Unity Plus (500 MHz), on a Varian AMX400 (400 MHz) or a Varian VXR-200 (200 MHz) instrument as indicated in the specifications, at 298 K. Chemical shifts are reported in δ values

(ppm) relative to TMS. FT-IR measurements were performed on a Nicolette Nexus FT-IR instrument. High Resolution Mass Spectroscopy (HRMS) was performed on a JEOL JMS 600 spectrometer. HPLC-MS analyses were performed on a Hewlett Packard Chemstation Agilent 1100 Series using an analytical Cosmosil Buckyprep Waters Type column (4.6 x 250 mm). Preparative HPLC was performed on a Hewlett Packard Chemstation Agilent 1100 Series equipped with a Cosmosil Buckprep Waters type column (10 x 250 mm). Cyclic voltammetry was performed using an Autolab PGStat 100. All reactions were carried out in flame-dried glassware under an N_2-atmosphere.

5.8.3 Synthesis

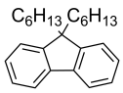

9,9-dihexyl-9H-fluorene. A suspension of fluorene (4.0 g, 24 mmol) and potassium hydroxide (13.0 g, 240 mmol, 10 eq.) in dimethyl sulfoxide (40 mL) was stirred at room temperature for 10 minutes and 1-bromooctane (9.9 g, 60 mmol, 2.5 eq.) was added using a syringe. The mixture was heated to 60 °C and stirred for 5 days. The mixture was poured into water (100 mL) and extracted with ethyl acetate (3 x 100 ml). The organic layers were combined and washed with brine (100 mL) and dried over sodium sulfate. The solvent was removed *in vacuo* and the crude product was purified by column chromatography (SiO_2,heptane) to give the pure product as colorless oil (5.1 g, 15 mmol, 63%). FT-IR (cm^{-1}): 3066 (m), 3039 (m), 3014 (m), 2954 (s), 2925 (s), 2852 (s), 1475 (w), 1465 (m), 1448 (s), 1376 (w), 773 (m), 736 (s). ^{1}H NMR (500 MHz, $CDCl_3$): δ (ppm) 7.72 (d, *J* = 7.2, 2H), 7.50 – 7.28 (m, 6H), 2.19 – 1.83 (m, 4H), 1.32 – 0.96 (m, 12H), 0.78 (t, *J* = 7.2, 6H), and 0.72 – 0.54 (m, 4H). ^{13}C NMR (125 MHz, $CDCl_3$): δ (ppm) 150.80, 141.22, 127.09, 126.79, 122.95, 119.75, 55.13, 40.55, 31.64, 29.87, 23.85, 22.73, and 14.15. APCI-MS (m/z) = 335.27321, calculated [$M+H^+$]: 335.27333.

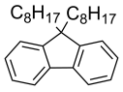

9,9-dioctyl-9H-fluorene. The dialkylated fluorene was prepared following the procedure as described above giving 7.4 g (19 mmol, 63%) of the pure product as colorless oil. FT-IR (cm^{-1}): 3066 (m), 3039 (m), 3014 (m), 2954 (s), 2925 (s), 2852 (s), 1475 (w), 1465 (m), 1448 (s), 1376 (w), 773 (m), 736 (s). ^{1}H

NMR (500 MHz, $CDCl_3$): δ (ppm) 7.71 (d, *J* = 6.6, 2H), 7.60 – 7.10 (m, 6H), 2.16 – 1.77 (m, 4H), 1.39 – 0.95 (m, 20H), 0.83 (t, *J* = 7.2, 6H), and 0.74 – 0.52 (m, 4H). ^{13}C NMR (125 MHz, $CDCl_3$): δ (ppm) 150.81, 141.22, 127.09, 126.79, 122.96, 119.75, 55.13, 40.51, 31.93, 30.19, 29.36, 23.88, 22.74, and 14.23. APCI-MS (m/z) = 391.33585, calculated [$M+H^+$]: 391.33593.

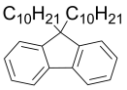

9,9-didodecyl-9H-fluorene. The dialkylated fluorene was prepared following the procedure as described above giving 8.5 g (19 mmol, 64%) of the pure product as colorless oil. FT-IR (cm^{-1}): 3066 (m), 3039 (m), 3014 (m), 2954 (s), 2925 (s), 2852 (s), 1475 (w), 1465 (m), 1448 (s), 1376 (w), 773 (m), 736 (s). ^1H NMR (500 MHz, $CDCl_3$): δ (ppm) 7.71 (d, 2H), 7.42 – 7.18 (m, 6H), 2.04 – 1.86 (m, 4H), 1.36 – 0.94 (m, 28H), 0.86 (t, *J* = 7.1, 6H), and 0.71 – 0.52 (m, 4H). ^{13}C NMR (125 MHz, $CDCl_3$): δ (ppm) 150.81, 141.22, 127.09, 126.79, 122.96, 119.75, 55.13, 40.51, 32.02, 30.19, 29.70, 29.66, 29.41, 29.41, 23.88, 22.81, and 14.26. APCI-MS (m/z) = 447.39809, calculated [$M+H^+$]: 447.39853.

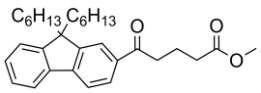

methyl 5-(9,9-dihexyl-9H-fluoren-2-yl)-5-oxopentanoate. A suspension of $AlCl_3$ (5.97 g, 44.83 mmol, 3 eq.) in 1,2-dichloroethane (100 mL) was cooled with an ice bath to 0 °C and the dialkylated fluorene (5.0 g, 14.95 mmol,) was added. After stirring the mixture for 10 minutes methyl 5-chloro-5-oxopentanoate (2.53 g, 15.69 mmol, 1.05 eq.) was slowly added with a syringe. The resulting dark green solution was allowed to warm up and was stirred at room temperature overnight. The mixture was poured onto crushed ice and the organic phase was separated. The aqueous layer was extracted with CH_2Cl_2 (2 x 50 ml). The combined organic layers were washed with 2% aq. NaOH solution (50 mL), brine (50 mL), and dried over Na_2SO_4. Evaporation of the solvent *in vacuo* yielded a pale yellow oil which was purified by column chromatography (SiO_2,toluene) giving the pure keto-ester as colorless oil (3.61 g, 7.8 mmol, 52%). FT-IR (cm^{-1}): 3066 (w), 2954 (s), 2929 (s), 2854 (s), 1739 (s), 1679 (s), 1606 (m), 1571 (w), 1465 (m), 1419 (m), 1367

(m), 1205 (m), 1006 (w), 740 (s). ^{1}H NMR (500 MHz, $CDCl_3$): δ (ppm) 8.07 – 7.87 (m, 2H), 7.80 – 7.66 (m, 2H), 7.46 – 7.29 (m, 3H), 3.69 (s, 3H), 3.12 (t, *J* = 7.1, 2H), 2.49 (t, *J* = 7.2, 2H), 2.12 (p, *J* = 7.1, 2H), 2.07 – 1.89 (m, 4H), 1.16 – 0.92 (m, 12H), 0.74 (t, *J* = 7.2, 6H), and 0.66 – 0.47 (m, 4H). ^{13}C NMR (125 MHz, $CDCl_3$): δ (ppm) 199.38, 173.90, 152.05, 151.15, 146.14, 139.86, 135.55, 128.48, 127.79, 127.09, 123.15, 122.31, 120.78, 119.55, 55.40, 51.68, 40.30, 37.70, 33.33, 31.56, 29.71, 23.81, 22.64, 19.63, and 14.08. ESI-MS (m/z) = 485.30151, calculated [M+Na$^+$]: 485.30262.

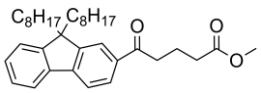

methyl 5-(9,9-dioctyl-9H-fluoren-2-yl)-5-oxopentanoate. The keto-ester was prepared following the procedure as described above except that the reaction mixture was refluxed overnight, giving 6.54 g (12.6 mmol, 82%) of the pure product as colorless oil. FT-IR (cm^{-1}): 3066 (w), 2954 (s), 2929 (s), 2854 (s), 1739 (s), 1679 (s), 1606 (m), 1571 (w), 1465 (m) 1419 (m), 1367 (m), 1205 (m), 1006 (w), 740 (s). ^{1}H NMR ($CDCl_3$, 400 MHz): ä (ppm) δ 8.02 – 7.90 (m, 2H), 7.82 – 7.68 (m, 2H), 7.42 – 7.31 (m, 3H), 3.70 (s, 3H), 3.12 (t, *J* = 7.2, 2H), 2.49 (t, *J* = 7.2, 2H), 2.12 (p, *J* = 7.2, 2H), 1.99 (dd, *J* = 14.2, 7.2, 4H), 1.28 – 0.93 (m, 20H), 0.80 (t, *J* = 7.1, 6H), and 0.67 – 0.46 (m, 4H). ^{13}C NMR (75 MHz, $CDCl_3$): δ (ppm) 199.35, 173.90, 152.07, 151.16, 146.15, 139.88, 135.57, 128.49, 127.80, 127.10, 123.17, 122.32, 120.78, 119.55, 55.41, 51.68, 40.29, 37.70, 33.34, 31.85, 30.04, 29.30, 23.85, 22.68, 19.63, and 14.17. ESI-MS (m/z) = 541.36365, calculated [M+Na$^+$]: 541.36522.

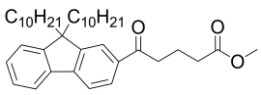

methyl 5-(9,9-didodecyl-9H-fluoren-2-yl)-5-oxopentanoate. The keto-ester was prepared following the procedure as described above except that the reaction mixture was refluxed overnight, yielding 8.14 g (14.2 mmol, 84%) of the pure product as colorless oil. FT-IR (cm^{-1}): 3066 (w), 2954 (s) 2929 (s), 2854 (s), 1739 (s), 1679 (s), 1606 (m), 1571 (w), 1465 (m), 1419 (m), 1367(m), 1205 (m), 1006 (w), 740 (s). ^{1}H NMR (500 MHz, $CDCl_3$): δ (ppm) 7.99 (s, 1H), 7.95 (d, *J* = 7.9, 1H), 7.76 – 7.67 (m, 2H), 7.38 – 7.27 (m, 3H), 3.71 (s, 3H), 3.10 (t, *J* = 7.0, 2H), 2.47 (t, *J* = 7.0, 2H), 2.11 (p, *J* = 7.0, 2H), 2.07 – 1.90 (m, 4H), 1.32 – 0.91 (m, 28H), 0.91 (t, *J* = 7.0, 6H), and 0.69 – 0.46 (m, 4H). ^{13}C NMR (125 MHz,

$CDCl_3$): δ (ppm) 198.97, 173.62, 151.90, 151.01, 146.00, 139.76, 135.49, 128.35, 127.68, 126.98, 122.99, 122.21, 120.66, 119.42, 55.27, 51.43, 40.19, 37.55, 33.16, 31.85, 29.95, 29.52, 29.49, 29.25, 29.24, 23.75, 22.64, 19.52, and 14.08. ESI-MS (m/z) = 597.42596, calculated [$M+Na^+$]: 597.42782.

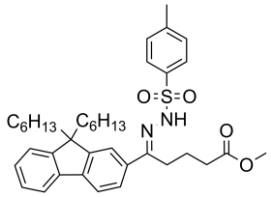

9,9-dihexyl-9H-fluoren-2-yl-methylbutyrate-p-tosylhydrazone. Methyl 5-(9,9-dihexyl-9H-fluoren-2-yl)-5-oxopentanoate (2.86 g, 6.18 mmol) and p-tosylhydrazide (1.38 g, 7.42 mmol, 1.2 eq.) were dissolved in toluene (80 mL). The resulting solution was refluxed overnight using a Dean-Stark setup. After cooling to room temperature the white precipitate was filtered off. The solution was concentrated *in vacuo*. The remaining yellow oil was recrystallized from methanol to yield 2.35 g (3.7 mmol, 60%) of the product as pale yellow crystals. FT-IR (cm^{-1}): 3182 (s) 2954 (s), 2921 (s), 2854 (s), 1716 (s), 1600 (m), 1467 (m), 1438 (m), 1367 (m), 1322 (m), 1268 (m), 1224 (m), 1172 (s), 1078 (m), 1022 (m), 995 (m), 937 (m), 873 (m), 815 (m), 746 (m), 667 (m), 553 (s). ^{1}H NMR (400 MHz, $CDCl_3$): δ (ppm) 9.10 (s, 1H), 7.96 (d, *J* = 8.3, 2H), 7.74 – 7.50 (m, 4H), 7.40 – 7.21 (m, 5H), 3.81 (s, 3H), 2.68 (t, 2H), 2.47 – 2.28 (m, 5H), 1.96 (dd, *J* = 11.3, 5.4, 4H), 1.81 – 1.64 (m, 2H), 1.19 – 0.90 (m, 12H), 0.75 (t, *J* = 7.1, 6H), and 0.66 – 0.49 (m, 4H). ^{13}C NMR (50 MHz, $CDCl_3$): δ (ppm) 174.90, 154.39, 151.37, 151.00, 143.85, 142.77, 140.39, 136.12, 134.98, 129.52, 128.28, 127.67, 126.97, 125.38, 123.06, 120.58, 120.15, 119.55, 55.19, 52.55, 40.45, 32.25, 31.61, 29.84, 26.22, 23.83, 22.70, 21.72, 21.22, and 14.13. APCI-MS (m/z) = 631.35686, calculated [$M+H^+$]: 631.35641. Melting Point: 94.0 – 96.0°C.

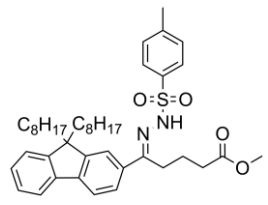

9,9-dioctyl-9H-fluoren-2-yl-methylbutyrate-p-tosylhydrazo-ne. The tosylhydrazone was prepared following the procedure described above except that the reaction was stopped after 5 hours instead of reacting overnight, yielding 6.68 g (9.7 mmol, 92%) of the pure

product as pale yellow crystals. FT-IR (neat) = í (cm^{-1}): 3118 (s), 2952 (s), 2925 (s), 2854 (s), 1710 (s), 1596 (m), 1465 (m), 1438 (m), 1369 (m), 1321 (m), 1265 (m), 1230 (m), 1170 (s), 1022 (m), 995 (m), 937 (m), 873 (m), 815 (m), 746 (m), 667 (m), 553 (s). ^{1}H NMR (200 MHz, $CDCl_3$): ä (ppm) 9.13 (s, 1H), 7.97 (d, *J* = 8.3, 2H), 7.73 – 7.51 (m, 4H), 7.37 – 7.27 (m, 5H), 3.81 (s, 3H), 2.68 (t, 2H), 2.45 – 2.26 (m, 5H), 2.05 – 1.85 (m, 4H), 1.84 (t, 2H), 1.32 – 0.90 (m, 20H), 0.80 (t, *J* = 6.6, 6H), 0.69 – 0.40 (m, 4H). ^{13}C NMR (50 MHz, $CDCl_3$): ä (ppm) 174.91, 154.31, 151.38, 151.01, 143.84, 142.77, 140.40, 136.15, 134.99, 129.52, 128.29, 127.68, 126.97, 125.38, 123.08, 120.58, 120.16, 119.56, 55.20, 52.56, 40.45, 32.25, 31.90, 30.21, 29.39, 26.21, 23.91, 22.73, 21.73, 21.22, 14.21. APCI-MS (m/z) = 687.41944, calculated [M+H$^+$]: 687.41901. Melting Point: 99.5 – 101.0°C.

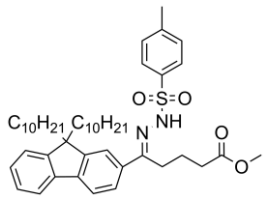

9,9-didodecyl-9H-fluoren-2-yl-methylbutyrate-p-tosylhydrazone. The tosylhydrazone was prepared following the same procedure as described above except that the reaction was stopped after 4 hours instead of reacting overnight, giving 7.14 g (9.6 mmol, 84%) of the pure product as pale yellow crystals. FT-IR (cm^{-1}): 3108 (s), 2952 (s), 2919 (s), 2854 (s), 1708 (s), 1596 (m), 1469 (m), 1438 (m), 1369 (m), 1322 (m), 1265 (m), 1230 (m), 1170 (s), 1022 (m), 995 (m), 937 (m), 873 (m), 815 (m), 746 (m), 667 (m), 553 (s). ^{1}H NMR (200 MHz, $CDCl_3$): δ (ppm) 9.13 (s, 1H), 7.97 (d, *J* = 8.2, 2H), 7.74 – 7.50 (m, 4H), 7.42 – 7.27 (m, 5H), 3.81 (s, 3H), 2.79 (t, 2H), 2.44 – 2.28 (m, 5H), 2.03 – 1.84 (m, 4H), 1.84 – 1.61 (m, 2H), 1.37 – 0.92 (m, 28H), 0.84 (t, *J* = 6.5, 6H), and 0.73 – 0.43 (m, 4H). ^{13}C NMR (50 MHz, $CDCl_3$): δ (ppm) 174.90, 154.37, 151.38, 151.02, 143.83, 142.78, 140.39, 136.14, 134.97, 129.52, 128.29, 127.68, 126.97, 125.39, 123.08, 120.59, 120.15, 119.56, 55.20, 52.55, 40.46, 32.25, 32.00, 30.23, 29.74, 29.65, 29.45, 29.40, 26.22, 23.93, 22.78, 21.73, 21.23, and 14.24. APCI-MS (m/z) = 743.48216, calculated [M+H$^+$]: 743.48161. Melting Point: 74.5 – 76.0°C.

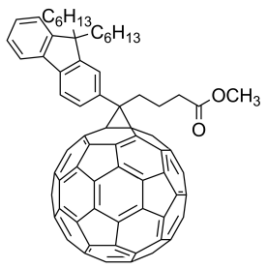

9,9-dihexyl-9H-fluoren-2-yl-C_{61}-butyric-acid methylester. A mixture of 9,9-dihexyl-9H-fluoren-2-yl-methylbutyrate-p-tosylhydrazone (400 mg, 0.64 mmol, 1.1 eq.) and sodium methoxide (36 mg, 0.66 mmol, 1.1 eq.) was dissolved in dry pyridine (10 mL) and stirred at room temperature for 30 minutes. Then a degassed solution of C_{60} (427 mg, 0.59 mmol) in *ortho*-dichlorobenzene (50 mL) was added. The mixture was heated to 90 °C and irradiated with a 150 W Na-lamp. The solution was concentrated *in vacuo* after reacting overnight. The product was purified on a SiO_2 column. The unreacted C_{60} was eluted with CS_2 and then the product with a 1:1 mixture of toluene and cyclohexane. After removal of the eluens *in vacuo* a dark solid remained. The solid was precipitated from *ortho*-dichlorobenzene in methanol and subsequently centrifuged. The remaining brown pellet was washed twice with methanol and dried *in vacuo* at 40 ^{o}C overnight. Yielding 361 mg (0.3 mmol, 52%) of the product as a brown solid. FT-IR (cm^{-1}): 2921 (s), 2850 (s), 1743 (s), 1463 (m), 1432 (m), 1241 (w), 1186 (m), 742 (m), 586 (w), 574 (w), 553 (w), 526 (s), 441 (w). ^{1}H NMR (500 MHz, CS_2 with D_2O insert): δ (ppm) 8.16 – 8.07 (m, 3H), 8.00 – 7.95 (m, 1H), 7.62 – 7.55 (m, 3H), 3.89 (s, 3H), 3.32 – 3.18 (m, 2H), 2.78 (t, *J* = 7.3 Hz, 2H), 2.55 – 2.42 (m, 2H), 2.40 – 2.19 (m, 4H), and 1.56 – 0.69 (m, 22H). ^{13}C NMR (125 MHz, CS_2 with D_2O insert): δ (ppm) 171.46, 150.89, 150.42, 148.92, 147.80, 145.94, 145.27, 145.25, 145.13, 145.04, 144.87, 144.72, 144.68, 144.58, 144.55, 144.06, 143.87, 143.80, 143.22, 143.10, 143.04, 143.02, 142.35, 142.22, 142.03, 141.33, 141.16, 140.80, 140.49, 138.24, 137.56, 135.12, 130.75, 127.78, 127.24, 127.16, 122.81, 120.27, 119.94, 80.19, 55.06, 52.44, 51.14, 40.98, 33.78, 33.70, 32.25, 30.46, 24.54, 23.46, 22.90, and 14.73. APCI-MS (m/z) = 1167.32692, calculated [$M+H^{+}$]: 1167.32576.

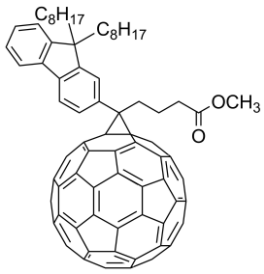

9,9-dioctyl-9H-fluoren-2-yl-C_{61}-butyric-acid methylester. The methanofullerene was prepared following the procedure described above, yielding 2.99 g (2.45 mmol, 64%) of the pure product as a brown solid. FT-IR (cm^{-1}): 2921 (s), 2850 (s), 1741 (s), 1463 (m), 1432 (m), 1259 (w), 1187 (m), 740 (m), 584 (w), 574 (w), 553 (w), 526 (s), 480 (w), 447 (w). ^{1}H NMR (500 MHz, CS_2 with D_2O insert): δ (ppm) 8.10 – 7.99 (m, 3H), 7.93 – 7.88 (m, 1H), 7.56 – 7.48 (m, 3H), 3.82 (s, 3H), 3.27 – 3.10 (m, 2H), 2.71 (t, *J* = 7.1 Hz, 2H), 2.50 – 2.38 (m, 2H), 2.34 – 2.10 (m, 4H), and 1.60 – 0.60 (m, 30H). ^{13}C NMR (125 MHz, CS_2 with D_2O insert): δ (ppm) 171.49, 150.89, 150.42, 148.94, 147.81, 145.96, 145.28, 145.25, 145.12, 145.05, 144.87, 144.72, 144.71, 144.58, 144.55, 144.06, 143.87, 143.81, 143.23, 143.11, 143.09, 143.04, 143.03, 142.35, 142.22, 142.03, 141.32, 141.16, 140.80, 140.49, 138.25, 137.56, 135.11, 130.75, 127.79, 127.24, 127.20, 122.82, 120.29, 119.97, 80.12, 55.05, 52.46, 51.17, 41.00, 33.75, 33.70, 32.45, 30.86, 30.01, 24.66, 23.47, 22.90, and 14.89. APCI-MS (m/z) = 1223.38857, calculated [$M+H^+$]: 1223.38836.

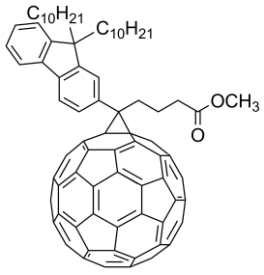

9,9-didecyl-9H-fluoren-2-yl-C_{61}-butyric-acid methylester. The methanofullerene was prepared following the procedure described above, yielding 4.30 g (3.36 mmol, 56%) of the pure product as a brown solid. FT-IR (cm^{-1}): 2921 (s), 2850 (s), 1741 (s) 1463 (m), 1432 (m), 1249 (w), 1187 (m), 742 (m), 584 (w), 574 (w), 553 (w), 526 (s), 480(w), 435 (w). ^{1}H NMR (500 MHz, CS_2 with D_2O insert): δ (ppm) 8.13 – 8.00 (m, 3H), 7.94 – 7.88 (m, 1H), 7.59 – 7.49 (m, 3H), 3.83 (s, 3H), 3.30 – 3.10 (m, 2H), 2.72 (t, *J* = 7.1 Hz, 2H), 2.51 – 2.38 (m, 2H), 2.35 – 2.11 (m, 4H), and 1.63 – 0.57 (m, *J* = 168.1 Hz, 38H). ^{13}C NMR (125 MHz, CS_2 with D_2O insert): δ (ppm) 171.48, 150.88, 150.41, 148.93, 147.80, 145.94, 145.28, 145.25, 145.10, 145.05, 144.87, 144.86, 144.72, 144.69, 144.58, 144.55, 144.06, 143.87, 143.80, 143.22, 143.10, 143.04, 143.02, 142.35, 142.22,

142.02, 141.31, 141.16, 140.79, 140.49, 138.25, 137.55, 135.11, 130.74, 127.78, 127.24, 127.20, 122.82, 120.28, 119.95, 80.18, 55.04, 52.44, 51.16, 40.99, 33.74, 33.69, 32.53, 30.86, 30.35, 30.24, 29.97, 24.65, 23.52, 22.89, and 14.87. APCI-MS (m/z) = 1279.45150, calculated [$M+H^+$]: 1279.45096.

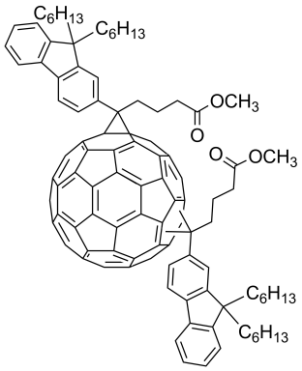

Bis-F_6CBM. ^{1}H NMR (500 MHz, CS_2 with D_2O insert): δ 8.17 – 7.58 (m, Ar-H), 7.46 – 7.25 (m, Ar-H), 3.75-3.38 (m, -OMe), 3.24 – 1.86 (m, -CH_2), and 1.43 – 0.39 (m, alkyl). ^{13}C NMR (126 MHz, CS_2 with D_2O insert) δ 171.70, 171.63, 171.60, 171.58, 171.55, 171.52, 171.51, 171.50, 171.49, 171.45, 171.29, 151.14, 151.00, 150.93, 150.89, 150.85, 150.82, 150.61, 150.49, 150.33, 150.28, 150.23, 150.19, 149.99, 149.85, 149.75, 149.43, 149.07, 148.64, 148.38, 148.31, 148.10, 148.06, 147.98, 147.90, 147.84, 147.76, 147.72, 147.64, 147.60, 147.54, 147.45, 147.41, 147.38, 147.25, 147.20, 147.18, 147.15, 147.12, 147.07, 146.98, 146.94, 146.89, 146.83, 146.79, 146.73, 146.72, 146.68, 146.64, 146.61, 146.58, 146.55, 146.52, 146.46, 146.44, 146.34, 146.31, 146.29, 146.21, 146.19, 146.16, 146.11, 146.05, 146.00, 145.92, 145.86, 145.82, 145.77, 145.70, 145.66, 145.64, 145.59, 145.56, 145.50, 145.45, 145.43, 145.40, 145.32, 145.28, 145.26, 145.19, 145.16, 145.11, 145.02, 144.95, 144.93, 144.89, 144.79, 144.71, 144.68, 144.65, 144.61, 144.54, 144.50, 144.47, 144.43, 144.42, 144.39, 144.34, 144.32, 144.25, 144.22, 144.20, 144.16, 144.13, 144.03, 144.00, 143.96, 143.91, 143.89, 143.86, 143.81, 143.80, 143.77, 143.63, 143.61, 143.54, 143.49, 143.46, 143.43, 143.39, 143.38, 143.32, 143.23, 143.21, 143.15, 143.11, 143.09, 143.00, 142.97, 142.95, 142.93, 142.88, 142.76, 142.67, 142.61, 142.42, 142.40, 142.28, 142.25, 142.20, 142.14, 142.08, 142.02, 141.98, 141.95, 141.84, 141.81, 141.77, 141.76, 141.66, 141.64, 141.60, 141.48, 141.47, 141.37, 141.34, 141.32, 141.24, 141.21, 141.17, 141.11, 141.09, 140.96, 140.95, 140.90, 140.83, 140.78, 140.69, 140.65, 140.62, 140.60, 140.56, 140.50, 140.38, 140.35, 139.79, 139.53, 139.24, 138.88, 138.70, 138.49, 138.35, 138.14, 138.10, 137.96, 137.68, 137.56, 136.92,

136.72, 136.67, 135.74, 135.63, 135.56, 135.54, 135.36, 135.32, 135.17, 135.13, 134.77, 134.42, 134.27, 130.99, 130.72, 130.67, 130.63, 130.44, 130.01, 127.72, 127.67, 127.49, 127.38, 127.18, 127.07, 127.01, 126.89, 126.60, 122.90, 122.85, 122.78, 122.75, 122.70, 120.33, 120.27, 120.23, 120.22, 120.12, 120.09, 120.07, 120.05, 120.01, 119.96, 119.93, 119.87, 119.84, 119.81, 119.75, 81.04, 80.91, 80.75, 80.72, 80.60, 80.33, 80.31, 80.28, 80.07, 79.99, 79.97, 79.81, 79.80, 79.74, 79.70, 79.58, 79.56, 79.51, 79.49, 79.20, 79.04, 79.01, 78.93, 78.73, 78.68, 78.58, 77.06, 76.98, 76.89, 76.83, 76.82, 75.44, 75.33, 75.27, 55.16, 55.15, 55.10, 55.08, 55.05, 55.02, 55.00, 54.98, 54.92, 54.88, 54.77, 54.29, 53.96, 51.50, 51.47, 51.43, 51.39, 51.25, 51.21, 51.19, 51.17, 51.15, 51.13, 51.11, 51.08, 51.05, 50.99, 50.94, 49.86, 49.79, 49.71, 49.63, 49.61, 49.56, 49.49, 45.08, 40.98, 34.43, 34.25, 33.90, 33.79, 33.75, 33.71, 33.67, 33.59, 33.31, 33.11, 32.31, 32.25, 32.23, 32.21, 32.19, 32.18, 32.14, 30.49, 30.47, 30.43, 30.39, 30.27, 30.24, 24.62, 24.59, 24.56, 24.51, 24.49, 24.48, 24.43, 24.37, 23.48, 23.43, 23.39, 23.36, 23.33, 23.04, 23.01, 22.96, 22.88, 22.83, 22.76, 22.71, 22.67, 22.61, 22.55, 14.76, 14.75, 14.73, 14.72, 14.69, and 14.59.

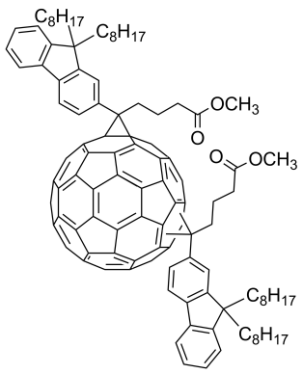

Bis-F_8CBM. ^{1}H NMR (500 MHz, CS_2 with D_2O insert): δ 8.20 – 7.55 (m, Ar-H), 7.48 – 7.22 (m, Ar-H), 3.72-3.48 (m, -OMe), 3.30 – 1.80 (m, -CH_2), and 1.40 – 0.30 (m, alkyl). ^{13}C NMR (126 MHz, CS_2 with D_2O insert) δ 174.52, 174.40, 174.34, 174.31, 174.28, 174.26, 174.23, 174.21, 174.19, 174.15, 174.00, 167.16, 154.57, 153.90, 153.82, 153.69, 153.61, 153.58, 153.23, 153.19, 152.98, 152.89, 152.68, 152.55, 152.45, 152.13, 151.77, 151.49, 151.45, 151.36, 151.10, 151.03, 150.76, 150.68, 150.65, 150.60, 150.47, 150.42, 150.33, 150.27, 150.22, 150.16, 150.09, 150.05, 149.93, 149.88, 149.86, 149.84, 149.79, 149.75, 149.69, 149.66, 149.63, 149.58, 149.46, 149.42, 149.34, 149.31, 149.22, 149.17, 149.14, 149.11, 149.00, 148.90, 148.87, 148.80, 148.74, 148.72, 148.66, 148.57, 148.49, 148.39, 148.34, 148.30, 148.25, 148.18, 148.12, 148.10, 148.00,

147.95, 147.87, 147.84, 147.80, 147.70, 147.60, 147.57, 147.47, 147.40, 147.36, 147.30, 147.21, 147.14, 147.10, 147.07, 147.03, 147.01, 146.93, 146.91, 146.89, 146.86, 146.80, 146.71, 146.65, 146.59, 146.55, 146.47, 146.30, 146.22, 146.18, 146.12, 146.08, 146.02, 145.93, 145.89, 145.79, 145.69, 145.65, 145.62, 145.57, 145.45, 145.36, 145.31, 145.11, 145.08, 144.96, 144.92, 144.89, 144.84, 144.77, 144.69, 144.66, 144.62, 144.53, 144.48, 144.45, 144.42, 144.32, 144.28, 144.18, 144.15, 144.06, 144.02, 144.00, 143.93, 143.88, 143.85, 143.78, 143.64, 143.60, 143.57, 143.52, 143.37, 143.29, 143.26, 143.20, 143.07, 143.03, 142.66, 142.48, 142.45, 142.25, 142.21, 141.92, 141.57, 141.39, 141.18, 141.04, 140.83, 140.78, 140.65, 140.38, 140.26, 140.07, 139.92, 139.61, 139.41, 139.35, 138.72, 138.59, 138.50, 138.42, 138.31, 138.26, 138.22, 138.03, 137.86, 137.82, 137.62, 137.46, 137.11, 136.93, 135.82, 133.62, 133.36, 133.31, 132.70, 130.36, 130.16, 129.86, 129.32, 125.47, 123.02, 122.89, 122.77, 122.55, 122.46, 83.71, 83.68, 83.66, 83.63, 83.55, 83.51, 83.45, 83.42, 83.08, 83.04, 83.03, 82.92, 82.91, 82.59, 82.55, 82.53, 82.06, 82.04, 81.99, 81.97, 81.91, 81.73, 81.54, 81.51, 81.49, 81.18, 81.14, 81.09, 80.18, 79.84, 79.78, 79.71, 79.60, 79.52, 78.14, 78.10, 77.57, 57.84, 57.82, 57.76, 57.74, 57.69, 57.66, 57.60, 57.57, 57.44, 57.00, 56.66, 54.18, 54.16, 54.12, 54.09, 53.95, 53.90, 53.86, 53.83, 53.79, 53.73, 53.67, 53.63, 52.56, 52.49, 52.41, 52.32, 52.23, 52.17, 50.77, 47.77, 43.65, 37.09, 36.93, 36.70, 36.58, 36.55, 36.47, 36.43, 36.39, 36.36, 36.29, 35.97, 35.76, 35.10, 33.48, 33.32, 33.03, 32.89, 32.71, 32.67, 32.43, 27.39, 27.29, 27.23, 26.11, 25.72, 25.64, 25.56, 25.50, 25.40, 25.34, and 17.52.

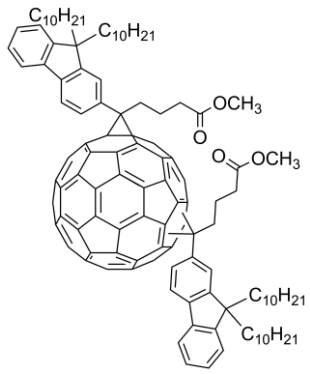

Bis-F_{10}CBM. ^{1}H NMR (500 MHz, CS_2 with D_2O insert): δ 8.13 – 7.23 (m, Ar-H), 7.49 – 7.23 (m, Ar-H), 3.74-3.50 (m, -OMe), 3.30 – 1.85 (m, -CH_2), and 1.42 – 0.45 (m, alkyl). ^{13}C NMR (126 MHz, CS_2 with D_2O insert) δ 171.71, 171.65, 171.61, 171.59, 171.57, 171.54, 171.53, 171.52, 171.49, 171.46, 171.45, 171.31, 151.15, 151.01, 150.99, 150.93, 150.89, 150.88, 150.84, 150.54, 150.50, 150.48, 150.46, 150.32, 150.29, 150.26, 150.21, 150.00, 149.87, 149.42, 149.38, 149.09, 148.67, 148.40, 148.37, 148.13, 148.08, 148.00, 147.96, 147.81, 147.73, 147.60, 147.56, 147.50, 147.47, 147.40, 147.36, 147.26, 147.21, 147.19, 147.16, 147.14, 147.11, 147.06, 147.01, 146.98, 146.95, 146.89, 146.77, 146.73, 146.70, 146.66, 146.63, 146.59, 146.57, 146.53, 146.50, 146.48, 146.42, 146.36, 146.32, 146.22, 146.19, 146.17, 146.11, 146.01, 145.98, 145.88, 145.83, 145.81, 145.78, 145.71, 145.66, 145.64, 145.57, 145.52, 145.50, 145.47, 145.44, 145.42, 145.33, 145.31, 145.26, 145.20, 145.15, 145.11, 145.02, 144.92, 144.90, 144.79, 144.72, 144.68, 144.62, 144.55, 144.53, 144.46, 144.42, 144.40, 144.36, 144.32, 144.24, 144.22, 144.15, 144.04, 143.97, 143.92, 143.87, 143.80, 143.76, 143.68, 143.62, 143.50, 143.47, 143.44, 143.40, 143.34, 143.16, 143.10, 143.02, 142.97, 142.94, 142.89, 142.77, 142.68, 142.63, 142.43, 142.41, 142.28, 142.24, 142.20, 142.16, 142.09, 142.02, 141.98, 141.95, 141.85, 141.82, 141.77, 141.64, 141.61, 141.58, 141.50, 141.38, 141.33, 141.28, 141.25, 141.21, 141.18, 141.12, 141.10, 141.09, 140.95, 140.92, 140.84, 140.70, 140.64, 140.61, 140.58, 140.53, 140.39, 140.34, 139.80, 139.57, 139.53, 139.25, 138.90, 138.71, 138.49, 138.45, 138.37, 138.34, 138.16, 138.13, 138.11, 137.98, 137.70, 137.59, 137.39, 137.24, 136.93, 136.73, 136.67, 135.91, 135.86, 135.75, 135.64, 135.59, 135.57, 135.55, 135.53, 135.46, 135.35, 135.18, 135.14, 135.05, 134.77, 134.57, 134.43, 134.25, 133.15, 131.31, 130.94, 130.71, 130.64, 130.54, 130.46, 130.01, 127.74, 127.68, 127.61, 127.58, 127.24, 127.18, 127.06, 127.01, 126.91, 122.86, 122.82, 122.80, 122.72, 120.34, 120.28, 120.24, 120.21, 120.09, 119.90, 119.87, 119.79, 80.96, 80.76,

79.98, 79.90, 79.84, 79.52, 79.49, 79.39, 79.35, 79.29, 79.18, 79.04, 79.01, 78.96, 78.75, 78.44, 77.79, 77.63, 77.55, 77.41, 77.17, 77.05, 76.97, 76.89, 75.09, 55.17, 55.15, 55.12, 55.09, 55.06, 55.02, 54.99, 54.95, 54.92, 54.89, 54.76, 54.31, 53.98, 51.50, 51.47, 51.43, 51.26, 51.22, 51.17, 51.16, 51.12, 51.05, 50.99, 50.95, 49.88, 49.80, 49.72, 49.64, 49.56, 49.49, 49.10, 48.08, 45.09, 41.00, 40.85, 40.64, 40.55, 40.37, 40.07, 34.24, 34.02, 33.91, 33.87, 33.79, 33.75, 33.71, 33.68, 33.59, 33.49, 33.29, 33.08, 32.52, 32.42, 32.39, 30.84, 30.81, 30.30, 30.21, 30.10, 29.94, 29.25, 24.62, 24.55, 23.49, 23.04, 22.96, 22.88, 22.82, 22.72, 22.66, 22.61, 14.86, 14.85, 14.82, 14.70, and 12.01.

5.9 References

1 M. C. Scharber, D. Mühlbacher, M. Koppe, P. Denk, C. Waldauf, A. J. Heeger and C. L. Brabec, *Adv. Mater*., 2006, **18**, 789

2 J. Roncali, *Chem. Rev*., 1997, **97**, 173

3 H. A. M. Van Mullekom, J. A. J. M. Vekemans, E. E. Havinga and E. W. Meijer, *Mat. Sci. Eng. R.*, 2001, **32**, 1

4 M. Kertesz, C. H. Choi and S. J. Yang, *Chem. Rev*., 2005, **105**, 3448

5 S. C. Rasmussen and M. Pomerantz, *Handbook of Conducting Polymers*, 3rd ed, CRC Press: Boca Raton, FL, 2007

6 F. Wudl, M. Kobayashi and A. J. Heeger, *J. Org. Chem*., 1984, **49**, 3382

7 M. Kobayashi, N. Colaneri, M. Boysel, F. Wudl and A. J. Heeger, *J. Chem. Phys*., 1985, **82**, 5717

8 E. E. Havinga, W. Ten Hoeve and H. Wynberg, *Polym. Bull.*, 1992, **29**, 199

9 E. E. Havinga, W. Ten Hoeve and H. Wynberg, *Synth. Met.*, 1993, **55**, 299

10 C. Kitamura, S. Tanaka and Y. Yamashita, *Chem. Mater*., 1996, **8**, 570

11 R. Kroon, M. Lenes, J. C. Hummelen, P. W. M. Blom and B. De Boer, *Polym. Rev*. 2008, **48**, 531

12 Y. Liang, Z. Xu, J. Xia, s. Tsai, Y. Wu, G. Li, C. Ray and L. Yu, *Adv. Mater*., 2010, **22**, E135

13 D. Veldman, O. Ipek, S. C. J. Meskers, J. Sweelssen, M. M. Koetse, S. C. Veenstra, J. M. Kroon, S. S. van Bavel, J. Loos and R. A. J. Janssen, *J. Am. Chem. Soc.* 2008, **130**, 7721

14 L. J. Lindgren, F. L. Zhang, M. Andersson, S. Barrau, S. Hellstrom, W. Mammo, E. Perzon, O. Inganäs and M. R. Andersson, *Chem. Mater.* 2009, **21**, 3491

15 A. J. Moule and K. Meerholz, *Adv. Funct. Mater.* 2009, **19**, 3028

16 C. Deibel, A. Wagenpfahl and V. Dyakonov, *Phys. Stat. Sol*., 2008, **2**, 175

17 G. Garcia-Belmonte and J. Bisquert, *Appl. Phys. Lett*., 2010, **96**, 113301

18 J. Liu, Y. Shi and Y. Yang, *Adv. Funct. Mater*., 2001, **11**, 420

19 H. Hoppe, M. Niggemann, C. Winder, J. Kraut, R. Hiesgen, A. Hinsch, D. Meissner and N. S. Sariciftci, *Adv. Funct. Mater*, 2004, **14**, 1005

20 G. Li, V. Shrotriya, Y. Yao and Y. Yang, *J. Appl. Phys*., 2005, **98**, 043704

21 H. Zhong, X. Yang, B. de With and J. Loos, *Macromolecules*, 2006, **39**, 218

22 K. Sivula, C. K. Luscombe, B. C. Thompson and J. M. J. Fréchet, *J. Am. Chem. Soc.*, 2006, **128**, 13988

23 Y. Yao, J. Hou, Z. Xu, G. Li and Y. Yang, *Adv. Funct. Mater*., 2008, **18**, 1783

24 C. H. Woo, B. C. Thompson, B. J. Kim, M. F. Toney and J. M. J. Fréchet, *J. Am. Chem. Soc*., 2008, **130**, 16324

25 J. K. Lee, W. L. Ma, C. J. Brabec, J. Yuen, J. S. Moon, J. Y. Kim, K. Lee, G. C. Bazan and A. J. Heeger, *J. Am. Chem. Soc*., 2008, **130**, 3619

26 B. Park, Y. H. Huh and M. Kim, *J. Mater. Chem*., 2010, **20**, 10862

27 Y. I. Lee, M. Kim, Y. H. Huh, J. S. Lim, S. C. Yoon and B. Park*, Sol. Energy. Mater. Sol. Cells.*, 2010, **94**, 1152

28 C. S. Kim, L. L. Tinker, B. F. DiSalle, E. D. Gomez, S. Lee, S. Bernhard and Y. Loo, *Adv. Mater*., 2009, **21**, 3110

29 M. Maggini, G. Scorrano and M. Prato, *J. Am. Chem. Soc*., 1993, **11**, 9798

30 J. B. Kim, K. Allen, S. J. Oh, S. Lee, M. F. Toney, Y. S. kim, C. R. Kagan, C. Nuckolls and Y. Loo, *Chem. Mater*., 2010, **22**, 5762

31 J. U. Lee, J. W. Jung, T. Emrick, T. P. Russel and W. H. Jo, *J. Mater. Chem*. 2010, **20**, 3287

32 C. Yang, J. K. Lee, A. J. Heeger and F. Wudl, *J. Mater. Chem*., 2009, **19**, 5416

33 K. Sivula, Z. T. Ball, N. Watanabe and J. M. J. Fréchet, *Adv. Mater*., 2006, **18**. 206

34 L. M. Popescu, P. van't Hof, A. B. Sieval, H. T. Jonkman and J. C. Hummelen, *Appl. Phys. Lett.* 2006, **89,** 213507

35 M. Helgesen, S. A. Gevorgyan, F. C. Krebs and R. A. J. Janssen, *Chem. Mater*., 2009, **21**, 4669

36 M. Helgesen and F. C. Krebs, *Macromolecules*, 2010, **43**, 1253

37 B. J. Kim, Y. Miyamoto, B. Ma and J. M. J. Fréchet, *Adv. Func. Mater*., 2009, **19**, 2273

38 S. Miyanishi, K. Tajima and K. Hashimoto, *Macromolecules*, 2009, **42**, 1610

39 D. E. Markov, E. Amsterdam, P. W. M. Blom, A. Sieval and J. C. Hummelen, *J. Phys. Chem. A*, 2005, **109**, 5266

40 Y. Cheng, C. Hsieh, Y. He, C. Hsu and Y. Li, *J. Am. Chem. Soc*., 2010, **132**, 17381

41 V. A. Kostyanovsky, D. K. Susarova, A. S. Peregudov and P. A. Troshin, *Thin Solid Films*, 2010, **519**, 4119

42 B. Gholamkhass and S. Holdcroft, *Chem. Mater*., 2010, **22**, 5371

43 M. T. Bernius, M. Inbasekaran, J. O'Brien and W. S. Wu, *Adv. Mater.* 2000, **12**, 1737

44 U. Scherf and E. J. W. List, *Adv. Mater.* 2002, **14**, 477

45 O. Inganäs, M. Svensson, F. Zhang, A. Gadisa, N. K. Persson, X. Wang and M. R. Andersson*, Appl*. *Phys. A: Mater*. Sci. Process. 2004, **79**, 31

46 M. Svensson, F. L. Zhang, S. C. Veenstra, W. J. H. Verhees, J. C. Hummelen, J. M. Kroon, O. Inganäs and M. R. Andersson, *Adv. Mater.* 2003**, 15**, 988

47 F. L. Zhang, E. Perzon, X. J. Wang, W. Mammo, M. R. Andersson and O. Inganäs, *Adv. Funct. Mater.* 2005, **15**, 745

48 O. Inganäs, F. L. Zhang and M. R. Andersson, *Acc. Chem. Res.* 2009, **42**, 1731

49 S. Admassie, O. Inganäs, W. Mammo, E. Perzon and M. R. Andersson, *Synth. Met.* 2006, **156**, 614

50 A. Gadisa, W. Mammo, L. M. Andersson, S. Admassie, F. Zhang, M. R. Andersson and O. Inganäs, *Adv. Funct. Mater.* 2007, **17**, 3836

51 S. L. C. Hsu, Y. C. Lin, R. F. Lee, C. Sivakumar, J. S. Chen and W. Y. Chou, *J. Polymer Sci. Polymer Chem.* 2009, **47**, 5336

51 E. G. Wang, M. Wang, L. Wang, C. H. Duan, J. Zhang, W. Z. Cai, C. He, H. B. Wu and Y. Cao, *Macromolecules* 2009, **42**, 4410

52 F. L. Zhang, W. Mammo, L. M. Andersson, S. Admassie, M. R. Andersson, L. Inganäs and O. Ingands, *Adv. Mater.* 2006, **18**, 2169

53 Q. M. Zhou, Q. Hou, L. P. Zheng, X. Y. Deng, G. Yu and Y. Cao, *Appl. Phys. Lett.* 2004, **84**, 1653

54 L. H. Slooff, S. C. Veenstra, J. M. Kroon, D. J. D. Moet, J. Sweelssen and M. M. Koetse, *Appl. Phys. Lett.* 2007, **90**

55 K. Vandewal, K. Tvingstedt, A. Gadisa, O. Inganäs and J. V. Manca, *Nat. Mater.* 2009, **8**, 904

56 A. I. Bokova and N. G. Sidorova, *Zh. Org. Khim.* 1970, **6**, 1711

57 S. J. J. Titinchi, F. S. Kamounah, H. S. Abbo and O. Hammerich, *ARKIVOC* 2008, 91

58 V. D. Mihailetchi, J. Wildeman and P. W. M. Blom, *Phys. Rev. Lett*, 2005, **94**, 126602

59 M. Lenes, M. Morana, C. J. Brabec and P. W. M. Blom, *Adv. Funct. Mater*., 2009, **19**, 1106

60 I. Riedel, N. Martin, F. Giacalone, J. L. Segura, D. Chirvase, J. Parisi and V. Dyakonov, *Thin Solid Films*, 2004, **451-452**, 43

61 I. Riedel, E. von Hauff, J. Parisi, N. Martin, F. Giacalone and V. Dyakonov, *Adv. Funct. Mater.*, 2005, **15**, 1979

62 M. Lenes, G. J. A. H. Wetzelaer, F. B. Kooistra, S. C. Veenstra, J. C. Hummelen and P. W. M. Blom, *Adv. Mater.*, 2008, **20**, 2116.

63 S. A. Backer, K. Sivula, D. F. Kavulak and J. M. J. Frechet, *Chem. Mater.*, 2007, **19**, 2927.

64 C. Yang, J. Y. Kim, S. Cho, J. K. Lee, A. J. Heeger and F. Wudl, *J. Am. Chem. Soc.*, 2008, **130**, 6444.

65 R. B. Ross, C. M. Cardona, D. M. Guldi, S. G. Sankaranarayanan, M. O. Reese, N. Kopidakis, J. Peet, B. Walker, G. C. Bazan, E. Van Keuren, B. C. Holloway and M. Drees, *Nat. Mater.*, 2009, **8**, 208.

66 Y. He, H.-Y. Chen, J. Hou and Y. Li, *J. Am. Chem. Soc.*, 2010, **132**, 1377

67 A. Sanchéz-Díaz, M. Izquierdo, S. Filippone, N. Martin and E. Palomares, *Adv. Funct. Mater.*, 2010, **20**, 2695

Chapter 6

Charge separation and recombination in small bandgap oligomer-fullerene triads

Abstract. This chapter describes the synthesis and characterization of two series of small band gap oligomers, consisting of thienopyrazine-thiophene and DPP-thiophene, end-capped at both ends with C_{60}. In these triads photoinduced electron transfer takes place between the oligomer as donor and the fullerene as acceptor. Femtosecond photoinduced absorption has been used to determine the rates for charge separation and recombination.

This chapter is part of a cooperation with B. P. Karsten, R. A. J. Janssen and R. M. Williams. Part of this chapter has been published: *J. Phys. Chem. B*, 2010, **114**, 14149, "Charge Separation and Recombination in Small Band Gap Oligomer-Fullerene Triads" and *Photochem. Photobiol. Sci*., 2010, **9**, 1055 "Charge Separation and (Triplet) Recombination in Diketopyrrolopyrrole-Fullerene Triads" The oligomer synthesis was performed by B. P. Karsten and photoinduced absorption measurements were performed by B. P. Karsten and R. M. Williams.

6.1 Introduction

6.1.1 Small bandgap polymers

As described in Chapter 5, polymers with reduced bandgaps are of growing interest to the field of organic photovoltaics. Polymers like poly(3-hexylthiophene), most commonly used in organic photovoltaic devices, have a bandgap that is too large for harvesting the low energy part of the solar spectrum resulting in a limited photocurrent. By reducing the bandgap more light can be absorbed and efficiencies of over 8% have been reached. Small bandgap polymers nowadays mostly consist of alternating electron rich and electron poor units in the polymer backbone. The electron rich units mostly being thiophene or derivatives thereof, the electron poor units vary. In this chapter we take a closer look at the thienopyrazine-thiophene[1,2,3] **(6.1)** and diketopyrrolopyrrole (DPP, **(6.2)**) -thiophene combinations.[4-11]

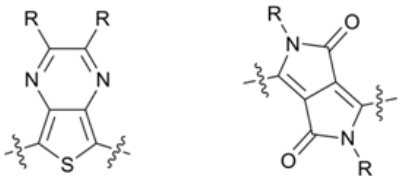

(6.1) **(6.2)**

Figure 6.1: *The thienopyrazine* ***(6.1)*** *and diketopyrrolopyrrole* ***(6.2)*** *unit.*

Besides having an optimized bandgap the kinetics of electron transfer from polymer to fullerene are of crucial importance for solar cells. As described in Chapter 1 an exciton is formed upon absorption of a photon. This exciton has to diffuse to a donor-acceptor interface where charge transfer takes place. Even though the hole and electron are now on different materials they are still strongly bound by Coulomb forces and need to be dissociated into free carriers. This so-called charge transfer state has a finite lifetime in which it can undergo multiple dissociations and recombinations before either dissociating into free charges which are transported through the two respective phases and collected at the electrodes or decaying to the ground state, in which case it is lost. As triplet energy levels in small bandgap polymers are generally low, even

below the energy of the charge separated state, recombination to such a triplet state is likely to be an additional loss mechanism in organic solar cell based on these polymers.[11-13]

6.1.2 Electronic transitions

As transitions between states of different spin-multiplicity are forbidden, these transitions are usually weak and therefore not observed. Hence, excitation usually yields the singlet excited state (corresponding to a S0→ S1 transition in **Figure 6.2**). The triplet excited state (T1) can be reached through intersystem crossing (ISC) from the singlet excited state, facilitated by spin-orbit coupling. This triplet state is long lived, because decay to the ground state (T1 → S0) is a spin forbidden transition. When a mixture of a fullerene and a conjugated oligomer or polymer is photo-excited, the excited singlet state of that oligomer or polymer that is initially formed can decay to the ground state, either radiatively (fluorescence) or non-radiatively, form a long lived triplet state through intersystem crossing, or by energy or electron transfer from the oligomer to the fullerene (which is a good electron acceptor). It depends on the relative energy of the charge separated state (CSS) if the last process can take place. This energy depends, among others, on solvent polarity and polarizability.[14-18] The charge separated state will be stabilized by polar solvents. Therefore, while charge transfer may take place in o-dichlorobenzene, intersystem crossing and/or energy transfer may be observed in toluene for the same donor-acceptor pair.

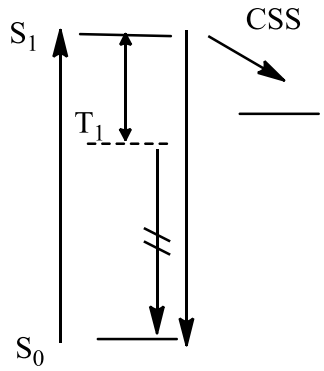

Figure 6.2: *Possible primary processes after absorption of a photon by the donor in a donor-acceptor system.*

As explained above, several processes can occur after a molecule is excited by a photon. Many detailed studies on electron transfer processes in linked donor-fullerene systems have emerged in literature during the past decades.[19-26] Electron transfer in this type of donor–acceptor systems usually occurs rapidly, in the Marcus normal region. The electron transfer is often followed by slower back electron transfer to the ground state in the Marcus inverted region. Also, intersystem crossing in the charge separated state followed by charge recombination into a low-lying triplet state has been observed frequently.[21,27-33] To further investigate the thienopyrazine-thiophene and diketopyrrolopyrrole-based small bandgap polymers, triads consisting of oligomers based on these units and two C_{60} end-caps were synthesized and the nature of their excited states was analyzed with photoinduced absorption.

6.1.4 Photoinduced absorption

The absorption of the different excited states can be investigated by photoinduced absorption (PIA). In a PIA experiment, a solution of the compound under study is excited by a chopped laser and the transmission of white light is measured. By means of a lock-in amplifier, the difference between light transmission in the excited state (laser “on”) and the ground state (laser “off”) is recorded. In this way an absorption

spectrum of the excited state can be reconstructed. The lifetimes of the species that can be detected by this setup are in the micro to milisecond range and consequently only long-living species, like triplet excited states, can be detected. For detecting short-living species and kinetic studies shortly after excitation, also femtosecond PIA has been performed. The basic difference between femtosecond PIA and steady state setup described here is that both excitation and detection are performed by short light pulses (instead of using a continuous wave laser and a halogen lamp) in the femtosecond setup. By varying the delay of the probe pulse with respect to the excitation pulse, a series of PIA spectra can be obtained at various times after excitation.

6.2 Experimental results

6.2.1 Synthesis

6.2.1.1 Thienopyrazine-thiophene-fullerene triads

The synthesis of the monomers, subsequent monobromination with NBS, coupling through nickel catalyzed Yamamoto coupling[34] into oligomers and formylation on both ends of the oligomers via Vilsmeier-Haack formylation[35] was performed by our collaborators at the Technical University Eindhoven. The four bis-formylated oligomers **(6.3-6.6)** were then end-capped with fullerene units through a Prato reaction[36] with tenfold excess of C_{60} and N-methylglycine to prevent bisfunctionalisation of the fullerene moiety (**Figure 6.3**). The fullerene adducts were purified through column chromatography (SiO_2, first CS_2 to remove unreacted C_{60}, followed by toluene) to obtain the triads T_{11} (based on **(6.3)**), T_{12} (based on **(6.4)**), T_{21} (based on **(6.5)**), and-T_{22} (based on **(6.6)**) in moderate to good yields. Preparative HPLC was used to obtain the triads in the appropriate purity needed for further analysis. The triads, a mixture of diastereomers as is the case for all bis-Prato adducts, were fully characterized by NMR and MALDI-TOF.

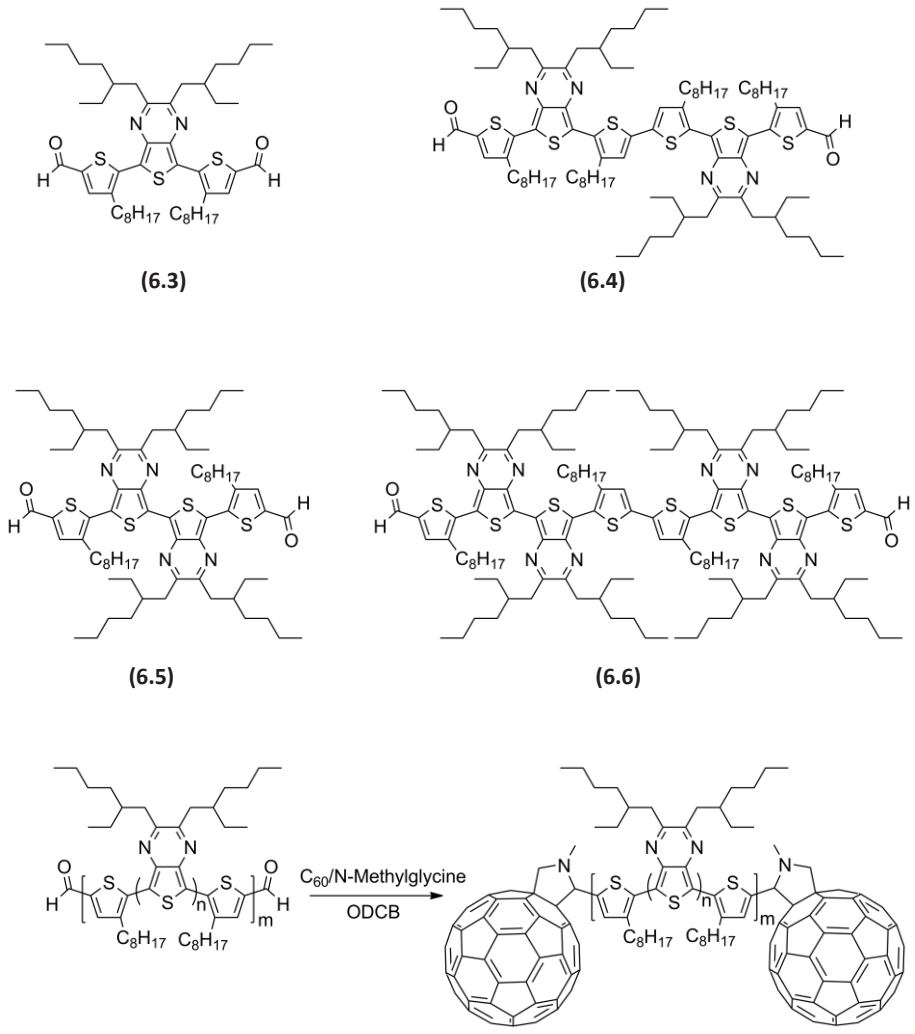

Figure 6.3: *Top: the four thienopyrazine-thiophene oligomers. Bottom: the end-capping of the oligomers with* C_{60}.

6.2.1.2 Diketopyrrolopyrrole-thiophene-fullerene triads

Oligomer synthesis according to modified literature procedures,[6,37] subsequent lithiation with lithium diisopropylamide (LDA), followed by quenching of the anion with N,N-dimethylformamide (DMF) to give the corresponding aldehydes was performed elsewhere. The obtained aldehyde-functionalized oligomers **(6.7-6.8)** were reacted

with a tenfold excess of C_{60} and N-methylglycine in a Prato reaction,[36] yielding the fullerene end-capped triads DPP-T1 (obtained from **(6.7)**) and DPP-T2 (obtained from **(6.8)**) as a mixture of diastereomers (**Figure 6.4**). Purification through column chromatography (SiO_2, first CS_2 to remove unreacted C_{60}, followed by toluene) gave the pure triads in moderate to good yields. Due to low solubility of the diketopyrrolopyrrole triads only small amounts were further purified by preparative HPLC for further analysis. The triads were characterized by NMR and MALDI-TOF.

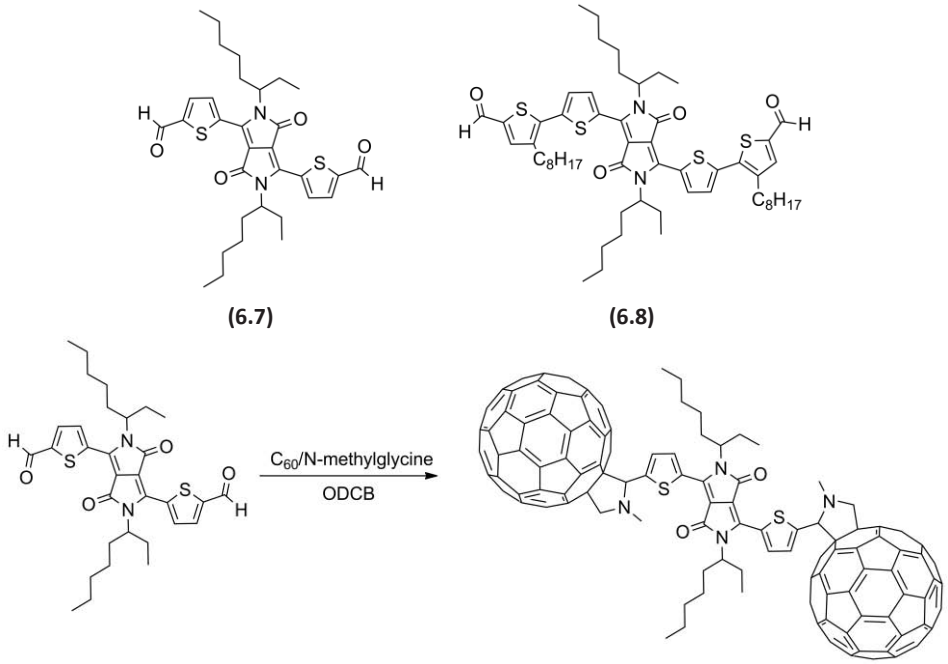

Figure 6.4: *Top: the two diketopyrrolopyrrole-thiophene oligomers. Bottom: the end-capping of the oligomers with C_{60}.*

6.2.2 Photoinduced absorption

The optical absorption of both groups of triads were found to be close to a superposition of the absorption spectra of the bare oligomers and N-methylfulleropyrrolidine (as a mixture of diastereomers), the 'bare' Prato adduct. Fluorescence of both the oligomers and C_{60} were quenched in all oligomer-fullerene triads, indicating efficient charge transfer in these systems. To investigate in detail the

charge separation and recombination in the small bandgap oligomer-fullerene systems photoinduced absorption measurements in the femtosecond to picosecond time range were performed by our collaborators at the Technical University Eindhoven and at the University of Amsterdam. We will briefly summarize these results in the following paragraph.

6.2.2.1 Thienopyrazine-thiophene-fullerene triads

Photoinduced absorption studies on the thienopyrazine-thiophene-fullerene triads (**Table 6.1**) indicate very fast charge transfer close to the Marcus optimal region on time scales < 10 ps after excitation indicating small activation barriers for electron transfer in these triads. Charge recombination in these triads is also fast; recombination occurs in the Marcus inverted region in toluene and again close to the optimal region in *ortho*-dichlorobenzene (within 90-730 ps in toluene and within 15-50 ps in *ortho*-dichlorobenzene). No signs of charge recombination into a triplet state have been found for these thienopyrazine-thiophene-fullerene triads, probably because the lifetime of the charge separated state is too short for intersystem crossing in the charge separated state.

	Charge separation (ps)		Charge recombination (ps)	
	toluene	ODCB	toluene	ODCB
T_{11}	21.5	10.1	727	44.9
T_{12}	6.3	7.1	275	13.5
T_{21}	4.3	6.2	201	15.8
T_{22}	2.7	7.2	91.4	15.1

Table 6.2*: The lifetimes of the excited states of the thienopyrazine-thiophene-fullerene triads.*

6.2.2.2 Diketopyrrolopyrrole-thiophene-fullerene triads

After excitation of the diketopyrrolopyrrole-oligomer-fullerene triads, charge transfer takes place via two simultaneously occurring routes. The first route is direct electron transfer in the Marcus optimal regime from the excited diketopyrrolopyrrole (DPP) oligomer to the fullerene. The second route is a two step process consisting of ultrafast energy transfer from the DPP-oligomer to the fullerene, followed by charge separation

from the formed excited state (hole transfer). In the latter case, the charge transfer process occurs in the Marcus normal regime, with time constants in the range of 18-47 ps (**Table 6.2**). The formed charge separated state subsequently recombines via two distinct pathways. The first pathway is direct recombination to the ground state, which occurs in the Marcus inverted region, with time constants in the range of 37 ps to 1.5 ns. Because the charge separated state has a lower energy in the more polar ODCB, this process is much faster in ODCB than in toluene. The other pathway consists of intersystem crossing in the charge separated state, with time constants of 0.8 to 15 ns, and subsequent recombination into the triplet state of the DPP oligomer. Intersystem crossing into the charge separated state is the rate limiting step in this process. Clear signals for the triplet absorption of the oligomer could be observed by near steady-state PIA and femtosecond PIA. As the ISC process is slow compared to direct recombination to the ground state, triplet recombination was found to be of more importance in toluene than in ODCB, because of the slower direct recombination process in toluene. Approximately 14% of the charge transfer state was found to recombine into the low lying triplet state of the oligomer for the smaller system in ODCB.

	Charge separation (ps)		Charge recombination (ps)	
	toluene	ODCB	toluene	ODCB
DPP T1	-	47	-	110
DPP T2	41	18	1500	37

Table 6.1: *The lifetimes of the excited states of the diketopyrrolopyrrole-thiophene-fullerene triads.*

6.3 Conclusions

Two series of small band gap oligomer-fullerene triads based on thienopyrazine-thiophene and DPP were synthesized and purified through preparative HPLC for photoinduced absorption studies. It was found, that in the series based on thienopyrazine-thiophene very fast charge separation took place close to the Marcus

optimal region. Charge recombination occurred in the Marcus inverted region. In these systems no recombination into low-lying triplet state could be observed, most probably due to the short lifetime of the charge separated state, preventing intersystem crossing into the triplet state. It is therefore not likely that for bulk heterojunction solar cells comprising small bandgap polymers based on the thienopyrazine-thiophene recombination into the triplet state will be a loss mechanism. However for the oligomer-fullerene triads based on the DPP-core as the electron deficient unit in the oligomers charge transfer takes place in a two-step fashion. In the first step, energy transfer to the fullerene moiety takes place, followed by electron transfer in the Marcus normal region. Charge recombination takes place in the Marcus inverted regime resulting in lifetimes long enough to allow relatively slow intersystem crossing followed by much faster charge recombination into the triplet excited state of the oligomer confirming triplet formation as a likely loss mechanism for solar cells comprising small bandgap polymers based on the DPP moiety.

6.4 Outlook

Photoinduced absorption of oligomer-fullerene triads offers a valuable insight into the electronic processes that occur after excitation and helps to identify recombination into low lying triplet states as possible loss mechanisms in small bandgap polymers. It is therefore worthwhile to further explore this method with other polymer systems that show lower efficiencies than expected for their physical properties alone. However dyads and triads containing fullerenes as the acceptor moiety have the donor part linked to a fulleropyrrolidine moiety. The electronic properties of this fullerene moiety can be distinctly different form for example a cyclopropyl addends as in the case of PCBM. This being the most widely used acceptor material in organic photovoltaics today a comparison between triads with different attachment groups on the fullerene core could perhaps give a better insight in the electronic processes occurring under working conditions in actual solar cells.

6.5 Experimental

6.5.1 General Procedures

^{1}H-NMR and ^{13}C-NMR spectra were recorded on a 500 MHz NMR (Varian Unity Plus, 500 Hz for ^{1}H-NMR and 125 MHz for ^{13}C-NMR) in CS_2, using a D_2O insert for locking and shimming. Chemical shifts are reported in ppm downfield from tetramethylsilane (TMS). IR spectra were recorded on a Perkin Elmer 1600 FT-IR. Matrix-assisted laser desorption ionization time-of-flight (MALDI-TOF) mass spectrometry has been performed on a PerSeptive Biosystems Voyager-DE PRO spectrometer. Preparative HPLC was performed using a Cosmosil Buckyprep Waters packed column (10 x 250 mm), using toluene as the eluent at a flow rate of 5 mL min-1. Analytical HPLC analysis was performed on a Hewlett Packard HP LC-Chemstation 3D (Agilent/HP1100 Series) using an analytical Cosmosil Buckyprep column (4.6 x 250 mm). Cyclic voltammograms were recorded in an inert atmosphere with 0.1M tetrabutyl ammonium hexafluorophosphate ($TBAPF_6$) in ODCB as supporting electrolyte. The working electrode was a platinum disc (0.2 cm2) and the counter electrode was a silver electrode.The sampleswere measured using an Ag/AgCl reference electrode with Fc/Fc+ as an internal standard using a mAutolab II with a PGSTAT30 potentiostat. UV/vis/nearIR absorption spectra were recorded using a PerkinElmer Lambda 900 spectrophotometer. Fluorescence spectra were recorded on an Edinburgh Instruments FS920 double monochromator spectrophotometer with a Peltier-cooled red sensitive photomultiplier. The emission spectra were corrected for the wavelength dependence of the sensitivity of the detection system. Time-correlated single photon counting fluorescence studies were performed on an Edinburgh Instruments LifeSpec-PS spectrometer by photoexcitation with a 400 nm picosecond laser (PicoQuant PDL800B) operated at 2.5MHz and by detectionwith a Peltier-cooled Hamamatsu microchannel plate photomultiplier (R3809U-50). The data were deconvoluted with the instrument response function of the instrument, recorded using dispersed light, and fitted to a monoexponential function using the Fluofit package (PicoQuant, Berlin). Near-steady state PIA spectra were recorded by exciting with a mechanically modulated cw Ar-ion

laser (*l* = 351 and 364 nm or 514 nm, 275 Hz) pump beam and monitoring the resulting change in transmission of a tungsten-halogen probe light through the sample (D*T*) with a phase-sensitive lock-in amplifier after dispersion by a grating monochromator and detection, using Si, InGaAs, and cooled InSb detectors. The pump power incident on the sample was typically 25 mW with a beam diameter of 2 mm.

The PIA (D*T*/*T*) was corrected for the photoluminescence, which was recorded in a separate experiment. Photoinduced absorption spectra and photoluminescence spectra were recorded with the pump beam in a direction almost parallel to the direction of the probe beam. The solutions were studied in a 1 mm near-IR grade quartz cell at room temperature. Femtosecond transient absorption experiments were performed with a Spectra-Physics Hurricane Titanium:Sapphire regenerative amplifier system. The full spectrum setup was based on an optical parametric amplifier (Spectra-Physics OPA 800C) as the pump. The residual fundamental light, from the pump OPA, was used for white/probe light generation, which was detected with a CCD spectrograph (Ocean Optics) for Vis detection. The polarization of the pump light was controlled by a Berek Polarization Compensator (New Focus). The Berek-Polarizer was always included in the setup to provide the Magic-Angle conditions. The probe light was double-passed over a delay line (Physik Instrumente, M-531DD) that provides an experimental time window of 3.6 ns with a maximal resolution of 0.6 fs per step. The OPA was used to generate excitation pulses at 530 nm. The laser outputwas typically 3.5–5 mJ pulse-1 (130 fs FWHM) with a repetition rate of 1 kHz. The samples were placed into cells of 2 mm path length (Hellma) and were stirred with a downward projected PTFE shaft, using a direct drive spectro-stir (SPECTRO-CELL). This stir system was also used for the white light generation in a 2 mm water cell. For the optical layout see supporting information of reference 67. All photophysical data reported here have a 5 to 10% error limit. All experiments were performed at room temperature.

6.5.2 Synthesis

Synthesis of compounds **DPP-TA1** and **DPP-TA2** has been reported previously.[38-40]

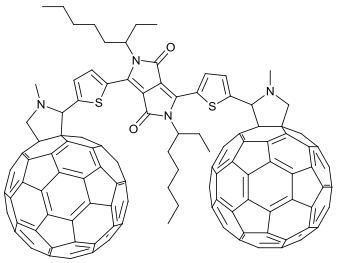

2',2"'-[[2,5-Bis(2-ethylhexyl)pyrrolo[3,4-*c*]pyrrole-1,4(2*H*,5*H*) dione-3,6-diyl]bis(4-octyl-5,2-thiophenediyl)]bis[1',5'-dihydro -1'-methyl-2'H-[5,6]fullereno-C_{60}-*I*h-[1,9-*c*]pyrrole] (DPP-T1-C_{60}).Compound **DPP-TA1** (50 mg, 0.086 mmol), C_{60} (0.63 g, 0.87 mmol) and *N*-methylglycine (77 mg, 0.87 mmol) were dissolved in ODCB (125 mL). The mixture was stirred at 120 ^{o}C for 5 h. The reaction mixture was concentrated *in vacuo* and purified by column chromatography on silica, using CS_2 as the eluent to remove unreacted C_{60}, the product was subsequently eluted with toluene. Yield: 42 mg (40%). 14 mg of the product was further purified by preparative HPLC. ^{1}H-NMR (500 MHz, CS_2) δ (ppm): 8.92 (s, 2H), 5.32 (s, 2H), 4.97 (d, *J* = 9.0 Hz, 2H), 4.28 (d, *J* = 10.0 Hz, 2H), 3.92 (m, 4H), and 2.95 (s, 6H,). IR (cm^{-1}): 2948, 2923, 2856, 2782, 1668, 1574, 1456, 1091, 746, 736, 706. MALDI-TOF-MS *m*/*z* : 2074.39 (50%), 2075.36 (100), 2076.40 (90), 2077.37 (70), 2078.4 (40), 2079.38 (25). HPLC: 1 peak at 13.7 min.

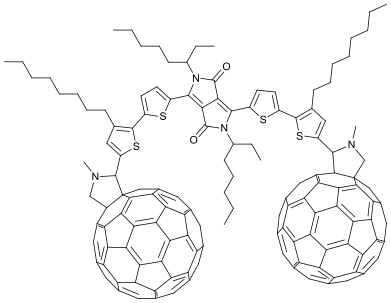

2',2'"-[[2,5-Bis(2-ethylhexyl)pyrrolo[3,4-*c*]pyrrole-1,4(2*H*,5*H*)-dione - 3,6 - diyl]bis(3' - octyl - 5,5' - [2,2' - bithiophene]diyl)]bis[1',5' - dihydro-1'-methyl-2'H-[5,6]fullereno-C_{60}-*I*h-[1,9-*c*]pyrrole] (DPPT2-C_{60}). Compound **DPP-TA2** (59 mg, 0.05 mmol), C_{60} (0.45 g, 0.62 mmol) and *N*-methylglycine (58 mg, 0.65 mmol) were dissolved in ODCB (125 mL). The mixture was stirred at 120 ^{o}C for 5 h. The reaction mixture was concentrated *in vacuo* and purified by column chromatography on silica, using CS_2 as the eluent to remove unreacted C_{60}, the product was subsequently eluted with toluene–ethyl acetate. Yield: 95 mg (77%). 20 mg of the product was further

purified by preparative HPLC. ^{1}H-NMR (500 MHz, CS_2) δ (ppm): 8.98 (d, *J* = 4.1 Hz, 2H), 7.20 (s, 2H), 7.18 (d, *J* = 4.1 Hz, 2H), 5.14 (s, 2H), 4.93 (d, *J* = 9.5 Hz, 2H), 4.23 (d, *J* = 9.5 Hz, 2H), 3.92 (d, *J* = 7.5 Hz, 4H), 2.93 (s, 6H,), 2.80 (t, *J* = 7.3 Hz, 4H), 1.84 (m, 2H,), 1.63 (m, 4H), 1.40–1.16 (m, 36H), and 0.92–0.82 (m, 18H). ^{13}C-NMR (125 MHz, CS_2) δ (ppm): 160.61, 155.82, 153.76, 153.01, 152.83, 147.49, 146.85, 146.55, 146.51, 146.41, 146.39, 146.34, 146.29, 146.15, 145.92, 145.88, 145.83, 145.62, 145.57, 145.47, 145.44, 145.38, 144.92, 144.85, 144.57, 144.54, 143.38, 143.24, 142.94, 142.84, 142.47, 142.38, 142.30, 142.28, 142.24, 142.16, 142.14, 142.07, 141.88, 141.82, 141.45, 141.44, 140.47, 140.45, 140.22, 140.20, 139.96, 138.87, 137.31, 136.88, 136.86, 136.11, 135.78, 131.45, 130.74, 129.55, 129.54, 127.76, 126.87, 126.85, 108.73, 104.99, 79.30, 77.17, 70.27, 68.80, 45.83, 40.69, 39.76, 32.62, 30.85, 30.63, 30.38, 30.29, 30.25, 30.07, 28.96, 24.14, 24.11, 23.65, 14.96, and 11.10. IR (cm^{-1}): 2951, 2922, 2851, 2781, 1663, 1543, 1456, 1429, 733. MALDI-TOF-MS *m*/*z*: 2462.50 (40%), 2463.50(80), 2464.49 (100), 2465.47 (80), 2466.46 (55), 2467.44 (30), 2468.43 (10). HPLC: 1 peak at 9.0 min.

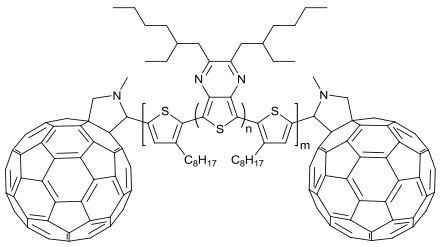

T11: Compound **2** (n=1, m=1) (226 mg, 0.28 mmol), C_{60} (2.0 g, 2.8 mmol), and N-methylglycine (0.26 g, 3.0 mmol) were dissolved in ODCB (250 mL) and stirred at 120°C for 5h. The solvent was evaporated. The excess of C_{60} was removed by column chromatography on silica, using CS_2 as the eluent. The product was subsequently eluted with toluene and the solvent was evaporated. The product was redissolved in ODCB, precipitated in methanol and dried in a vacuum oven. Yield: 453 mg (67 %). About 7 mg of the product was further purified by preparative HPLC. ^{1}H-NMR (500 MHz, CS_2) δ (ppm): 7.19 (s, 2H, Ar-*H*), 5.16 (s, 2H, MP*H*), 4.93 (d, *J* = 9.4 Hz, 2H, MP-*H*), 4.23 (d, *J* = 9.4 Hz, 2H, MP-*H*), 2.93 (s, 6H, N-C*H*3), 2.89 (t, *J* = 7.2 Hz, 4H, Ar-C*H*2-), 2.77 (d, *J* = 6.8 Hz, 4H, -C*H*2CH(C4H9)(C2H5)), 2.30-2.19 (m, 2H, - H2C*H*(C4H9)(C2H5)), 1.65 (m, 4H, -CH2C*H*2C6H13), 1.50-1.14 (m,

36H, -C*H*2-), and 0.97- 0.80 (m, 18H, -C*H*3). ^{13}C-NMR (125 MHz, CS2) δ (ppm): 155.71, 155.67, 154.90, 53.55, 153.07, 152.98, 147.06, 147.04, 146.73, 146.72, 146.16, 146.11, 146.02, 146.00, 145.95, 145.89, 145.84, 145.71, 145.51, 145.42, 145.25, 145.20, 145.12, 145.10, 145.02, 145.00, 144.92, 144.48, 144.45, 144.14, 142.93, 142.90, 142.80, 142.49, 142.40, 142.01, 141.95, 141.89, 141.84, 141.78, 141.71, 141.68, 141.66, 141.45, 141.39, 140.54, 140.03, 139.95, 139.72, 139.54, 138.75, 137.37, 136.77, 136.69, 136.60, 136.54, 135.62, 135.47, 130.35, 129.82, 129.79, 127.37, 123.75, 79.23, 79.15, 77.04, 77.02, 69.91, 69.89, 68.46, 40.24, 40.22, 39.34, 39.21, 37.19, 36.91, 33.31, 33.29, 33.25, 33.23, 32.24, 30.83, 30.81, 30.21, 30.19, 29.95, 29.85, 29.70, 29.37, 29.27, 26.46, 26.42, 26.30, 26.27, 23.77, 23.74, 23.24, 14.74, 14.57, 11.37, 11.36, 11.23, and 11.21. IR (cm^{-1}): 2953, 2920, 2850, 2777, 1461, 1260, 1088, 1016, 796, 768. MALDI-TOF-MS m/z (intensity, %): 2298.30 (50), 2299.30 (100), 2300.30 (95), 2301.31 (70), 2302.28 (50). HPLC: 1 peak at 5.3 min.

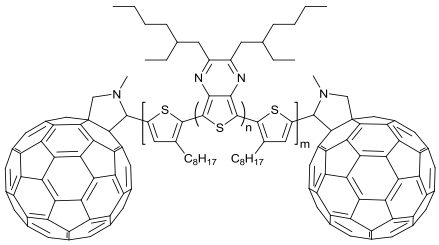

T12: Compound **2** (n=1, m=2) (281 mg, 0.18 mmol), C_{60} (1.3 g, 1.8 mmol), and N-methylglycine (0.18 g, 2.0 mmol) were dissolved in ODCB (225 mL) and stirred at 120°C for 5h. The solvent was evaporated. The excess of C_{60} was removed by column chromatography on silica, using CS_2 as the eluent. The product was subsequently eluted with toluene and the solvent was evaporated. The product was redissolved in ODCB, precipitated in methanol and dried in a vacuum oven. Yield: 161 mg (29 %). About 15 mg of the product was further purified by preparative HPLC. ^{1}H-NMR (400 MHz, CS_2) δ (ppm): 7.19 (s, 2H, Ar-*H*), 6.92 (s, 2H, Ar-*H*), 5.15 (s, 2H, MP-*H*), 4.91 (d, *J* = 9.4 Hz, 2H, MP-*H*), 4.22 (d, *J* = 9.4 Hz, 2H, MP-*H*), 2.92 (s, 6H, N-C*H*3), 2.92-2.70 (m, 16H, Ar-C*H*2-), 2.31-2.20 (m, 4H, -CH2C*H*(C4H9)(C2H5)), 1.76-1.61 (m, 8H, -CH2C*H*2C6H13), 1.52-1.10 (m, 72H, -C*H*2-), and 0.99-0.77 (m, 36H, -C*H*3). ^{13}CNMR (100 MHz, CS_2) δ (ppm): 155.74, 155.69, 154.90, 154.57, 153.58, 153.11, 153.02, 147.07, 147.05, 146.76, 146.75, 146.19, 146.13, 146.03, 146.01, 145.96, 145.91, 145.85, 145.72, 145.52, 145.43, 145.42, 145.26,

145.21, 145.13, 145.04, 145.01, 144.93, 144.49, 144.47, 144.16, 142.94, 142.91, 142.81, 142.50, 142.41, 142.03, 142.01, 141.96, 141.91, 141.85, 141.79, 141.73, 141.70, 141.68, 141.46, 141.41, 140.44, 140.04, 139.96, 139.73, 139.56, 138.62, 137.83, 137.50, 137.37, 136.78, 136.70, 136.62, 136.56, 135.62, 135.48, 129.97, 129.85, 129.83, 128.00, 125.59, 124.00, 123.36, 79.25, 79.19, 77.07, 69.92, 68.48, 40.25, 40.23, 39.36, 39.24, 39.14, 37.26, 37.21, 36.98, 36.93, 33.31, 33.26, 33.06, 33.03, 32.26, 31.03, 30.86, 30.21, 30.16, 30.10, 29.97, 29.86, 29.72, 29.39, 29.29, 29.20, 26.46, 26.44, 26.29, 26.25, 23.79, 23.76, 23.62, 23.25, 23.23, 14.73, 14.56, 11.38, 11.30, 11.28, and 11.24. IR (cm^{-1}): 2952, 2960, 2851, 2780, 1494, 1462, 1376, 1332, 1241, 1216, 1179, 1121, 1107, 1030, 825, 768, 725. MALDI-TOF-MS m/z (intensity, %): 3045.55 (30), 3046.53 (75), 3047.53 (100), 3048.53 (100), 3049.53 (80), 3050.53 (55), 3051.52 (30), 3052.55 (15). HPLC: 1 peak at 4.6 min.

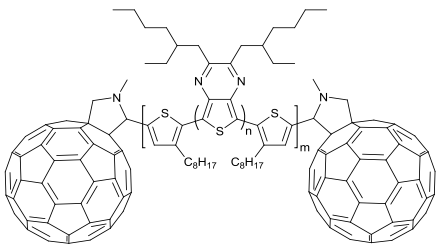

T21: Compound **2** (n=2, m=1) (135 mg, 0.12 mmol), C_{60} (0.86 g, 1.2 mmol), and N-methylglycine (0.12 g, 1.4 mmol) were dissolved in ODCB (150 mL) and stirred at 120°C for 5h. The solvent was evaporated. The excess of C_{60} was removed by column chromatography on silica, using CS_2 as the eluent. The product was subsequently eluted with toluene and the solvent was evaporated. The product was redissolved in ODCB, precipitated in methanol and dried in a vacuum oven. Yield: 238 mg (77 %). About 50 mg of the product was further purified by preparative HPLC. ^{1}H-NMR (400 MHz, CS_2) δ (ppm): 7.19 (s, 2H, Ar-*H*), 5.15 (s, 2H, MP-*H*), 4.91 (d, *J* = 9.4 Hz, 2H, MP-*H*), 4.22 (d, *J* = 9.4 Hz, 2H, MP-*H*), 2.98 (t, *J* = 7.0 Hz, 4H, Ar-C*H*2-), 2.92 (s, 6H, N-C*H*3), 2.84 (d, *J* = 6.8 Hz, 4H, -C*H*2CH(C4H9)(C2H5)), 2.79 (d, *J* = 6.6 Hz, 4H, -C*H*2CH(C4H9)(C2H5)), 2.31-2.18 (m, 4H, -CH2C*H*(C4H9)(C2H5)), 1.67 (qu, *J* = 7.0 Hz, 4H, -CH2C*H*2C6H13), 1.50-1.10 (m, 52H, -C*H*2-), and 0.97-0.75 (m, 30H, -C*H*3). ^{13}C-NMR (100 MHz, CS_2) δ (ppm): 155.75, 155.71, 154.95, 154.43, 153.57, 153.59, 153.15, 153.05, 147.06, 147.03, 146.79, 146.22, 146.11, 146.00, 145.95, 145.90, 145.84, 145.71, 145.51, 145.42,

145.40, 145.26, 145.18, 145.13, 145.11, 145.13, 145.02, 144.99, 144.92, 144.46, 144.14, 142.92, 142.89, 142.80, 142.48, 142.39, 142.02, 142.01, 141.95, 141.89, 141.83, 141.79, 141.73, 141.69, 141.67, 141.45, 141.39, 140.45, 140.03, 139.94,139.71, 139.57, 138.72, 137.73, 137.69, 136.74, 136.67, 136.63, 136.57, 135.60, 135.49, 130.69, 129.88, 126.13, 123.14, 79.18, 77.46, 77.07, 69.90, 68.47, 40.21, 40.18, 39.36, 39.25, 37.70, 37.34, 37.09, 33.24, 33.20, 32.21, 30.74, 30.07, 30.02, 29.64, 29.61, 29.36, 29.28, 29.14, 26.35, 26.31, 23.75, 23.71, 23.68, 23.19, 14.68, 14.53, 14.50, 11.33, 11.22, 11.19, 11.17, 11.14. IR(cm^{-1}): 2952, 2921, 2852, 2779, 1541, 1495, 1462, 1429, 1376, 1331, 1242, 1179, 1122, 1030, 900, 768, 726. MALDI-TOF-MS m/z (intensity, %): 2656.52 (40), 2657.51 (85), 2658.51 (100), 2659.51 (85), 2660.50 (60), 2661.51 (40), 2662.46 (20). HPLC: 1 peak at 4.7 min.

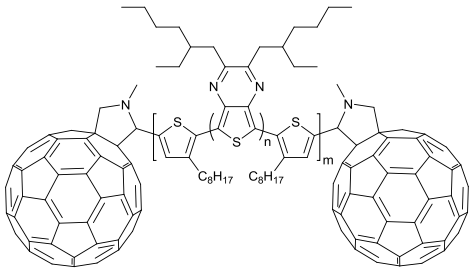

T22: Compound **2** (n=2, m=2) (243 mg, 0.11 mmol), C_{60} (0.98 g, 1.4 mmol), and N-methylglycine (0.12 g, 1.4 mmol) were dissolved in ODCB (225 mL) and stirred at 120°C for 5h. The solvent was evaporated. The excess of C_{60} was removed by column chromatography on silica, using CS_2 as the eluent. The product was subsequently eluted with toluene and the solvent was evaporated. The product was redissolved in ODCB, precipitated in methanol and dried in a vacuum oven. Yield: 260 mg (64 %). About 50 mg of the product was further purified by preparative HPLC. ^{1}H-NMR (400 MHz, CS_2) δ (ppm): 7.21 (s, 2H, Ar-*H*), 6.97 (s, 2H, Ar-*H*), 5.16 (s, 2H, MP-*H*), 4.92 (d, *J* = 9.5 Hz, 2H, MP-*H*), 4.22 (d, *J* = 9.4 Hz, 2H, MP-*H*), 3.04-2.95 (m, 8H, Ar-C*H*2-), 2.93 (s, 6H, N-C*H*3), 2.90-2.79 (m, 16H, -C*H*2CH(C4H9)(C2H5)), 2.35-2.18 (m, 8H, -CH2C*H*(C4H9)(C2H5)), 1.81-1.65 (m, 8H, -CH2C*H*2C6H13), 1.56-1.10 (m, 104H, -C*H*2-), and 1.02-0.75 (m, 60H, -C*H*3). ^{13}C-NMR (100 MHz, CS^{2}) δ (ppm): 155.77, 55.73, 154.95, 154.56, 154.48, 154.35, 153.60, 153.18, 153.08, 147.08, 147.05, 146.82, 46.80, 146.24, 146.13, 146.03, 146.01, 145.97, 145.91, 145.85, 145.72, 145.54, 145.44, 145.42, 145.27, 145.21, 145.15, 145.05, 145.02, 145.01, 144.93, 144.49, 144.17, 144.15,

142.93, 142.91, 142.81, 142.50, 142.40, 142.04, 142.02, 141.96, 141.91, 141.85, 141.80, 141.74, 141.71, 141.46, 141.41, 140.59, 140.38, 140.35, 140.04, 139.95, 139.73, 139.60, 138.64, 137.98, 137.81, 137.77, 136.77, 136.69, 136.65, 136.60, 135.61, 135.50, 130.77, 129.89, 129.03, 126.61, 125.86, 125.70, 123.34, 122.73, 79.26, 77.12, 77.10, 69.93, 68.50, 40.25, 40.22, 39.48, 39.40, 39.28, 37.87, 37.75, 37.40, 37.12, 33.32, 33.27, 33.24, 33.20, 33.10, 33.07, 32.26, 31.05, 30.80, 30.11, 30.08, 29.70, 29.66, 29.41, 29.32, 29.25, 29.23, 29.19, 26.36, 26.32, 26.28, 26.23, 23.80, 23.77, 23.74, 23.72, 23.64, 23.24, 23.21, 14.74, 14.58, 14.55, 14.52, 11.38, 11.31, 11.28, 11.26, 11.21, 11.19, 11.18, and 11.15. IR (cm^{-1}): 2953, 2921, 2852, 2780, 1541, 1490, 1456, 1376, 1332, 1242, 1179, 1121, 1030, 900, 829, 769, 726. MALDI-TOF-MS m/z (intensity, %): 3762.9 (50), 3063.9 (70), 3764.9 (90), 3765.87 (100), 3766.90 (70), 3767.82 (50). HPLC: 1 peak at 4.3 min.

6.6 References

1 M. Pomerantz, B. Chaloner-gill, L. O. Harding, J. J. Tseng and W. J. Pomerantz, *J. Chem. Soc. Chem. Commun*., 1992, 1672

2 J. P. Nietfeld, C. L. Heth and S. C. Rasmussen, *Chem. Commun*., 2008, 981

3 M. M. Wienk, M. G. R. Turbiez, M. P. Struijk, M. Fonrodona and R. A. J. Janssen, *Appl. Phys. Lett.*, 2006, **88**, 153511

4 M. M. Wienk, M. Turbiez, J. Gilot and R. A. J. Janssen, *Adv. Mater*., 2008, **20**, 2556

5 J. C. Bijleveld, A. P. Zoombelt, S. G. J. Mathijssen, M. M. Wienk, M. Turbiez, D. M. De Leeuw and R. A. J. Janssen, *J. Am. Chem. Soc*., 2009, **131**, 16616

6 Y. Zou, D. Gendron, R. Neagu-Plesu and M. Leclerc, *Macromolecules*, 2009, **42**, 6361

7 E. Zhou, Q Wei, S. Yamakawa, Y. Zhang, K. Tajima, C. Yang and K. Hashimoto, *Macromolecules*, 2010, **43**, 821

8 A. B. Tamayo, B. Walker and T. Q. J. Nguyen, *J. Phys. Chem. C*, 2008, **112**, 11545

9 A. B. Tamayo, X. D. Dang, B. Walker, J. Seo, T. Kent and T. Q. Nguyen, *Appl. Phys. Lett*., 2009, **94**, 103301

10 B. Walker, A. B. Tamayo, X. D. Dang, P. Zalar, J. H. Seo, A. Garcia, M. Tantiwiwat and T. Q. Nguyen, *Adv. Funct. Mater*., 2009, **19**, 3063

11 T. A. Ford, I. Avilov, D. Beljonne and N. C. Greenham, *Phys. Rev. B*, 2005, **71**, 125212

12 T. Offermans, P. A. Van Hal, S. C. J. Meskers, M. M. Koetse and R. A. J. Janssen, *Phys. Rev. B*, 2005, **72**, 045213

13 T. A. Ford, H. Ohkita, S. Cook, J. R. Durrant and N. C. Greenham, *Chem. Phys. Lett*., 2008, **454**, 237

14 R. A. J. Marcus, *J. Chem. Phys*., 1965, **43**, 679

15 R. A. Marcus, *Angew. Chem. Int. Ed*., 1993, **32**, 1111

16 N. R. Kestner, J. Logan and J. Jortner, *J. Phys. Chem*., 1974, **78**, 2148

17 J. Ulstrup and J. Jortner, *J. Chem. Phys*., 1975, **63**, 4358

18 E. H. A. Beckers, S. C. J. Meskers, A. P. H. J. Schenning, Z. J. Chen, F. Würthner and R. A. J. Janssen, *J. Phys. Chem. A*, 2004, **108**, 6933

19 H. Imahori, *Bull.Chem. Soc. Jpn*., 2007, **80**, 621

20 D. M. Guldi, B. M. Illescas, C. M. Atienza, M. Wielopolskia and N. Martin, *Chem. Soc. Rev*., 2009, **38**, 1587

21 R. M. Williams, J. M. Zwier and J. W. J. Verhoeven, *J. Am. Chem. Soc*., 1995, **117**, 4093

22 R. M. Williams, M. Koeberg, J. M. Lawson, Y. Z. An, Y. Rubin, M. N. PaddonRow and J. W. J. Verhoeven, *J. Org. Chem.*, 1996, **61**, 5055

23 D. I. Schuster, P. Cheng, S. R. Wilson, V. Prokhorenko, M. Katterle, A. R. Holzwarth, S. E. Braslavsky, R. M. Williams and C. P. J. Luo, *J. Am. Chem. Soc*., 1999, **121**, 11599

24 D. I. Schuster, P. Cheng, P. D. Jarowski, D. M. Guldi, C.P. Luo, L. Echegoyen, S. Pyo, A. R. Holzwarth, S. E. Braslavsky, R. M. Williams and G. J. Klihm, *J. Am. Chem. Soc*., 2004, **126**, 7257

25 N. D. McClenaghan, Z. Grote, K. Darriet, M, Zimine, R. M. Williams, L. De Cola and D. M. Bassani, *Org. Lett*., 2005, **7**, 807

26 P. Galloni, B. Floris, L. De Cola, E. Cecehetto and R. M. Williams, *J. Phys. Chem. C*, 2007, **111**, 1517

27 J. W. J Verhoeven, *Photochem. Photobiol. C. Photochem. Rev*., 2006, **7**, 40

28 Z. E. X. Dance, Q. Mi, D. W. McCamant, M. J. Ahrens, M. A. Ratner and M. R. Wasielewski, *J. Phys. Chem. B*, 2006, **110**, 25163

29 M. R. Wasielewski, D. G. Johnson, W. A. Svec, K. M. Kersey and D. W. J. Minsek, *J. Am. Chem. Soc*., 1988, **110**, 7219

30 G. P. Wiederrecht, W. A. Svec, M. R. Wasielewski,T. Galili and H. J. Levanon, *J. Am. Chem. Soc*., 2000, **122**, 9715

31 T. Okada, I. Karaki, E. Matsuzawa, N. Mataga, Y. Sakata and S. Misumi, *J. Phys. Chem*., 1981, **85**, 3957

32 A. C. Benniston, A. Harriman, P. Li, J. P. Rostron, H. J. Van Ramesdonk, M. M. Groeneveld, H. Zhang and J. W. J. Verhoeven, *J. Am.Chem. Soc*., 2005, **127**, 16054

33 A. Harriman, L. J. Mallon, G. Ulrich and R. Ziessel, *Chemphyschem*., 2007, **8**, 1207

34 T. Yamamoto, A. Morita, Y. Miyazaki, T. Maruyama, H. Wakayama, Z. Zhou, Y. Nakamura, T. Kanbara, S. Sasaki and K. Kubota, *Macromolecules*, 1992, **25**, 1214

35 A. Vilsmeier and A. Haack, *Ber. Dtsch. Chem. Ges*., 1927, **60B**, 119

36 M. Maggini, G. Scorrano and M. Prato, *J. Am. Chem. Soc*., 1993, **11**, 9798

37 A. B. Tamayo, M. Tantiwiwat, B. Walker and T. Q. J. Nguyen, *J. Phys. Chem. C*, 2008, **112**, 15543

38 J. Baffreau, S. Leroy-Lhez, N. Vân Anh, R. M. Williams and P Hudhomme, *Chem. Eur. J*., 2008, **14**, 4974

39 E. Zhou, S. Yamakawa, K. Tajima, C. Yang and K. Hashimoto, *Chem. Mater*., 2009, **21**, 4055

40 L. M. Campos, A. Tontcheva, S. Gunes, G. Sonmez, H. Neugebauer, N. S. Sariciftci and F. Wudl, *Chem. Mater*., 2005, **17**, 4031

Summary

In 1985 the discovery of a soluble form of carbon, the so-called fullerenes, started a new, still expanding field of research in chemistry. Carbon exist naturally in different forms, the so-called allotropes of carbon; graphite (the well know black carbon), diamond and fullerene. Fullerenes are spherical molecules existing entirely of carbon atoms. A fourth form are the so-called carbon nanotubes; tubular carbon molecules.

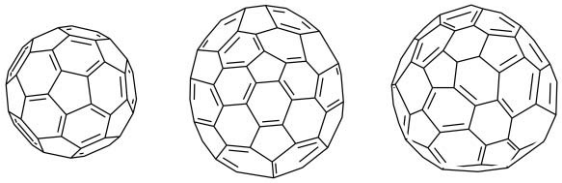

Figure 1: *Some examples of fullerenes; C_{60} (left), C_{70} (middle) en C_{84} (right).*

Fullerenes consist of five-membered and six-membered rings, where every five-membered ring is surrounded by six-membered rings only. The best known fullerene is C_{60}, also called buckminsterfullerene, named after the famous American architect Richard Buckminster Fuller. Fullerenes are a very suitable material for electronics, for they are exceptionally good in accepting and conducting electrons. Electrics based on organic molecules is called organic electronics. Examples of organic electronics include organic transistors, organic LEDs (OLEDs), and organic solar cells, which are the subject of this thesis.

Organic solar cells normally consist of two materials. One light absorbing material that is capable of conducting positive charges, often a conjugated polymer, and a light absorbing material that is capable of conducting negative charges, in our case a fullerene. The working principle of organic solar cells is as follows: light is absorbed by the polymer causing an electron to move to an excited (that is, higher energy) state. When there is a material close by that is capable of accepting electrons (for example a fullerene) this electron can “jump” to this molecule. The fullerene now has a negative

charge (one electron extra) and the polymer is left with a positive charge (one electron short, a so-called “hole”). When these materials are connected to electrodes, the positive charge can travel to one electrode and the negative charge to the other. At that moment a current is flowing. Advantages of organic solar cells over conventional silicon solar cells are their cheaper production, high flexibility of the solar cell and the light weight.

Because fullerenes do not have all the properties desired for use in organic solar cells, they need to be modified first. We can differentiate between three groups of modified fullerenes. Those with only one side group attached to the ball, so-called monoadducts, those with two side groups, so-called bisadducts, or even more side groups attached to the ball, so-called higher adducts (**Figure 2**).

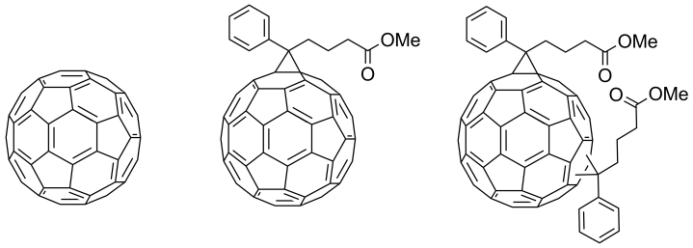

Figure 2: *Unmodified C_{60}, a C_{60} monoadduct (PCBM) and a C_{60} bisadduct (bis-PCBM).*

In this thesis the emphasis is on the development of fullerene bisadducts and their use as electron accepting material in organic solar cells. This form of modified fullerenes is only recently being used in solar cells. Therefore little is yet known about the properties and performance of such materials. With this thesis a contribution to the understanding and further development of this promising class of material is made.
It used to be unthinkable to use more than one type of molecule as electron accepting material in a solar cell. With the introduction of bis-PCBM (**Figure 2**, right) in 2006 this changed. For bis-PCBM is a mixture of different molecules that differ only in the position and relative orientation of the side groups on the fullerene sphere. These almost identical molecules are called isomers. Understanding which isomers are

formed and trying to separate these isomers of bis-PCBM are the subjects of Chapter 2.

Even though it proved possible to make efficient solar cells from mixtures of isomers, this does not apply to all cases. It is expected that a higher efficiency can be reached when there are less isomers present in the active layer. In **Chapter 3** we present a synthetic route to reduce the number of isomers. This is achieved by, instead of reacting both side groups one after the other, making first a connection between both groups using a small bridge. Now only particular isomers can be formed depending on the length of the bridge.

In Chapter 3 it was found that when the extra carbon atoms from the bridges were present a lower efficiency was obtained than when these bridges were removed. To further investigate the influence of the number of carbon atom present in the side group, new fullerenes containing different length alkyl chains are presented in Chapter 4 (**Figure 3**).

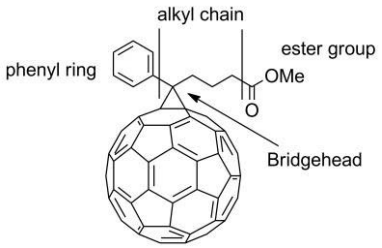

Figure 3: *Division of the side groups into four part: the phenyl ring, the alkyl chain that is varied, the bridgehead and the ester group.*

Organic solar cells often show a lower current than would be expected. This is mainly caused by a non-optimal formation of the active layer due to bad mixing of polymer and fullerene. Chapter 5 describes our efforts to compatibilize both materials by incorporating a small piece of the polymer in the fullerene molecule (**Figure 4**).

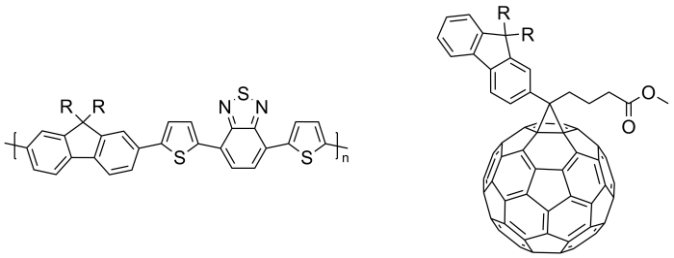

Figure 4: *Left a unit cell of a polymer, right a PCBM-like fullerene with a small part of the polymer incorporated.*

After absorption of light by a solar cell many processes play a role in the conversion of light to current. Some processes contribute in a positive way, while others affect the efficiency in a negative way. In Chapter 6 we investigate some of these processes. For this reason so-called triads were made. These are molecules consisting of a small part of the polymer, also called oligomer, sandwiched between two fullerenes (**Figure 5**). Ultrafast spectroscopy is used to study the processes occurring in the triads after absorption of light.

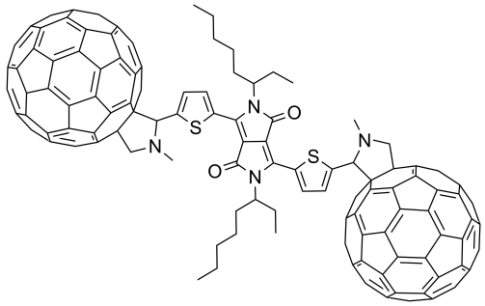

Figure 5: *A so-called triads; a small part of a polymer sandwiched between two fullerenes.*

Samenvatting

In 1985 ontstond met de ontdekking van een oplosbare vorm van koolstof, de zogenaamde fullerenen, een nieuw, zich nog steeds uitbreidend, veld in de scheikunde. Koolstof komt in verschillende vormen in de natuur voor, de zogenaamde allotropen van koolstof; als grafiet (het bekende zwarte koolstof), diamant of als fullereen (sferische moleculen die alleen uit koolstof atomen bestaan (**Figuur 1**)). Een vierde vorm zijn de zogenaamde carbon nanotubes; koolstof moleculen in de vorm van buis.

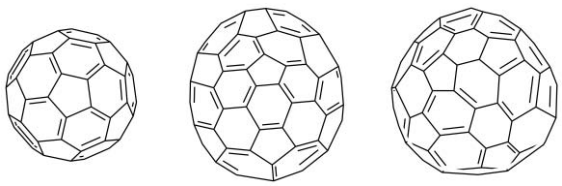

Figuur 1: Enkele voorbeelden van fullerenen: C_{60} (links), C_{70} (midden) en C_{84} (rechts).

Fullerenen zijn opgebouwd uit vijfringen en zesringen, waarbij elke vijfring omringd wordt door alleen zesringen. De meest bekende fullereen is C_{60}, ook wel buckminsterfullereen genaamd, vernoemd naar de bekende Amerikaanse architect Richard Buckminster Fuller. Fullerenen zijn uiterst geschikt voor toepassingen in de elektronica. Dit komt doordat fullerenen erg goed elektronen kunnen opnemen en geleiden. Omdat deze elektronica gebaseerd is op organische moleculen spreken we ook wel van organische elektronica. Voorbeelden van toepassing in organische elektronica zijn organische transistors, organische LEDs (OLEDs) en organische zonnecellen welke het onderwerp van dit proefschrift vormen.

Organische zonnecellen bestaan over het algemeen uit twee materialen. Een materiaal dat licht kan absorberen en tevens positieve ladingen kan geleiden, een zogenaamd geconjugeerd polymeer, en een materiaal, in ons geval een fullereen, dat negatieve ladingen kan geleiden. Organische zonnecellen werken als volgt: licht wordt door het

polymeer geabsorbeerd waardoor er een elektron in een aangeslagen (dat wil zeggen hoger energetische) toestand komt. Wanneer zich in de buurt van dit aangeslagen polymeer een materiaal bevindt dat goed elektronen kan accepteren (een fullereen bijvoorbeeld) dan kan dit elektron daarheen overspringen. Het fullereen krijgt nu dus een negatieve lading (een extra elektron), terwijl er op het polymeer een positieve lading (een elektron te weinig, een zogenaamd "gat") achterblijft. Wanneer deze materialen in verbinding staan met elektrodes, dan kan de positieve lading naar de ene elektrode reizen en de negatieve lading naar de andere. Op dat moment loopt er dus een stroom. Voordelen van organische zonnecellen boven conventionele silicium zonnecellen zijn een goedkopere productie, een hoge flexibiliteit van de zonnecel en het geringe gewicht.

Omdat fullerenen van zichzelf nog niet alle eigenschappen hebben die wenselijk zijn voor het gebruik in zonnecellen, moeten deze eerst gemodificeerd worden. We kunnen onderscheid maken tussen drie verschillende groepen gemodificeerde fullerenen; fullerenen met één extra groep bevestigd aan de bal, de zogenaamde monoadducten, fullerenen met twee groepen aan de bal, de zogenaamde bisadducten, en fullerenen met meer dan twee groepen aan de bal, de hogere adducten (**Figuur 2**).

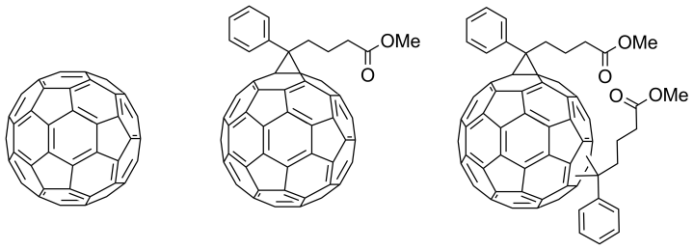

Figuur 2: *Ongemodificeerd C_{60}, een C_{60} monoadduct (PCBM) en een C_{60} bisadduct (bis-PCBM).*

In dit proefschrift ligt de nadruk op het ontwikkelen van bisadducten en het gebruik hiervan als elektronenaccepterend materiaal in organische zonnecellen. Deze vorm van gemodificeerde fullerenen wordt pas sinds kort in zonnecellen gebruikt. Hierdoor is er nog weinig bekend over de eigenschappen en de prestaties van dit materiaal. Met

dit proefschrift wordt een bijdrage geleverd aan het begrip en de verdere ontwikkeling van dit veel belovende materiaal voor organische zonnecellen.

Lang was het ondenkbaar om meerdere verbindingen tegelijk als elektronen accepterend materiaal in een zonnecel te gebruiken. Met de komst van bis-PCBM (**Figuur 2**, rechts) in 2006 veranderde dit. Bis-PCBM is namelijk een mengsel van verschillende moleculen die alleen verschillen in de positie en oriëntatie van de zijgroepen op de bal. Dit soort moleculen worden isomeren genoemd. Het onderzoeken welke isomeren gevormd worden en het isoleren van deze isomeren van bis-PCBM zijn de onderwerpen van Hoofdstuk 2.

Ook al is het nu aangetoond dat het mogelijk is efficiënte zonnecellen met mengsels van verschillende isomeren te maken, werkt dit niet in alle gevallen. De verwachting blijft ook nu nog dat het beter is zo min mogelijk verschillende moleculen in de actieve laag te hebben. In Hoofdstuk 3 wordt daarom een synthesemethode gepresenteerd om het aantal isomeren te verminderen. Dit wordt gedaan door de zijgroepen niet één voor één met het fullereen te laten reageren, maar deze eerst aan elkaar te bevestigen met een bruggetje. Hierdoor kunnen de zijgroepen niet meer op posities onafhankelijk van elkaar op de bal komen, maar is dit nu afhankelijk van de lengte van het bruggetje.

In Hoofdstuk 3 vonden we dat wanneer er extra koolstofatomen aan de zijgroep toegevoegd worden voor het maken van de bruggetjes er een vermindering in efficiëntie is. Om uit te zoeken wat de invloed van het aantal koolstofatomen in de zijgroep op de efficiëntie is, zijn er in Hoofdstuk 4 nieuwe fullerenen gesynthetiseerd met verschillende lengte van de alkylketens (**Figuur 3**).

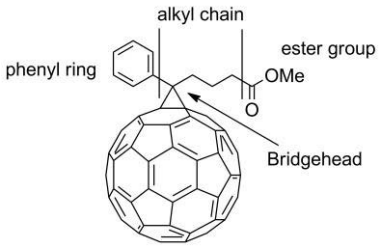

Figuur 3: *De verdeling van de zijgroep in vier delen; de phenylring, de alkylketen waarvan de lengte gevarieerd wordt, het bruggenhoofd en de ester groep.*

Zonnecellen gebaseerd op een bepaalde klasse polymeren, zogenaamde "low bandgap" polymeren, hebben vaak een lagere stroom dan theoretisch mogelijk is. Dit is voornamelijk te wijten aan een slechte structuur van de actieve laag in de zonnecel, door slechte menging van polymeer en fullereen. In Hoofdstuk 5 wordt hiervoor een oplossing gezocht door een klein stukje van het polymeer in te bouwen in het fullereenmolecuul (**Figuur 4**).

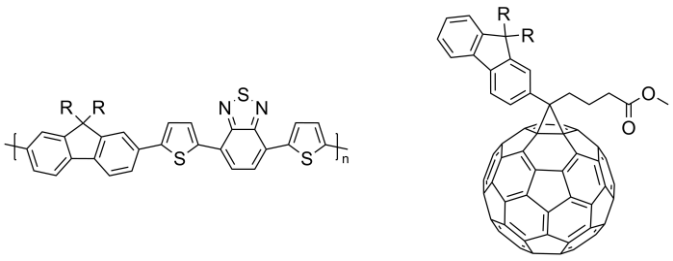

Figuur 4: *Links een éénheidscel van een polymeer, rechts een op PCBM gelijkend fullereen, maar nu met een stukje van het polymeer eraan vast.*

Na absorptie van licht door een zonnecel zijn er veel verschillende processen die een rol spelen bij de omzetting van licht naar stroom. Hierbij zijn er processen die een positieve bijdrage leveren, maar ook processen die de efficiëntie negatief beïnvloeden. In Hoofdstuk 6 wordt geprobeerd een inzicht te krijgen in deze processen. Hiervoor zijn zogenaamde triades gesynthetiseerd. Dit zijn moleculen die bestaan uit een klein stukje polymer, ook wel oligomeer genoemd, gesandwiched tussen twee fullerenen

(**Figuur 5**). Met ultrasnelle spectroscopie worden de processen in deze triades onderzocht.

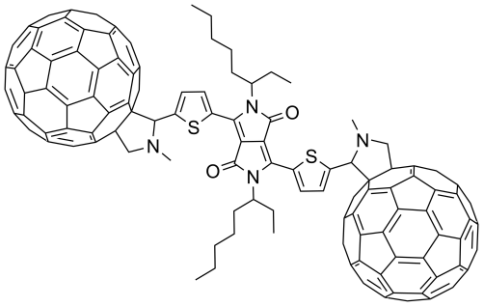

Figuur 5: *Een zogenaamde triade; een stukje polymeer gesandwiched tussen twee fullerenen.*

Dankwoord (Acknowledgements)

Het zit er nu, weliswaar meer dan een jaar te laat, toch eindelijk op. De laatste paar pagina's van dit proefschrift, maar misschien ook wel de belangrijkste. Zonder de mensen in dit dankwoord was het proefschrift er nooit gekomen of had het er in elk geval heel anders uitgezien.

In de eerste plaats wil ik Kees bedanken. Door jou heb ik de mogelijkheid gehad om kennis te maken met fullereen chemie en organische zonnecellen. Onderwerpen waar ik in de toekomst zeker nog verder in wil gaan.

Ook de leescommissie zou ik graag bedanken voor hun snelle correcties bij dit toch al erg vertraagde werk; Sjoerd Harder, Jean-Francois Nierengarten en Klaus Meerholz, mijn dank hiervoor.

Floris, van jou heb ik, zeker in het begin, veel geleerd over dit voor mij nieuwe onderzoeksveld, maar ook op het gebied van whiskey kon je mij nog veel leren. Ook Alex en Patrick wisten altijd wel antwoorden op allerlei fullereen en lab gerelateerde vragen. Natuurlijk had het nooit zover kunnen komen zonder de zorg van Reinder voor alle apperatuur. Zonder Theodora had ik nu waarschijnlijk nog steeds gewacht op een nieuwe kolom en had het onderzoek naar de samenstelling van bisadducten zonder HPLC analyses gemoeten. Frank, het was altijd gezellig met jou op het lab, maar ook daarbuiten bij de bbqs en de borrels.

In een proefschrift over fullerenen voor organische zonnecellen kunnen de daadwerkelijk cellen en de karakterisatie daarvan natuurlijk niet ontbreken. Hiervoor mijn dank aan Gert-Jan, Paul en Wenqiang. Zonder jullie was dit proefschrift niet compleet geweest.

Ook al kwam Ryan pas in mijn laatste jaar, ik heb veel van hem geleerd over het verwerken van resultaten en het schrijven van artikelen. Renate, voor al het andere papierwerk kon ik altijd bij jou terecht. Zonder jou had ik nog steeds niet geweten welke formulieren ik waarheen moest sturen. Alfred, als er iets gescand moest worden, kon ik altijd op je rekenen. Mijn presentaties hadden er een stuk minder interessant uitgezien zonder jouw plaatjes. Hiervoor mijn dank.

Bram, het was leuk om je op het lab te hebben. Bedankt voor de fijne samenwerking en de mooie artikelen die daaruit voortgekomen zijn. John Dennis, we made a nice start in separating the isomers of bis-PCBM. I hope you will continue this work and maybe in the future we can collaborate again.

Natuurlijk werk je niet alleen tijdens je promotie en ik heb dan ook een leuke tijd gehad met het begeleiden van studenten. Marc en Jelmer, het was een gezellige tijd en ook al werkte niet altijd alles mee, we hebben toch leuke resultaten behaald. Carlos, niet alleen op het lab hadden we het gezellig, maar ook tijdens het fitnessen en de borrels. Ik ben blij dat je straks samen met Reinder als paranimf bij mijn promotie bent.

Iedereen van de groep bedankt voor de goede werksfeer en de gezelligheid op het lab. Ook alle de mensen vanuit de DPI gemeenschap, bedankt voor de goede adviezen en de gezellige avonden op de DPI meetings. De Anorganische chemie groep bedankt voor de goede koffie en de gezellige filmavonden. Julia bedankt voor het meerijden en het duitse bier. En alle andere mensen die ik vergeten ben, het waren er ook zoveel in de deze vijf jaar, bedankt voor jullie hulp, adviezen en gezelligheid.

En dan zijn er natuurlijk nog mijn ouders. Jullie hebben mij de hele periode gesteund en stonden altijd voor me klaar met raad en daad. Hiervoor mijn dank.

Als laatste wil ik Tessa bedanken. Elke keer bedenk ik meer dingen waar ik je voor zou willen bedanken. Helaas is niet alles gelopen zoals we zouden willen, maar zonder jou was dit boekje er zeker niet gekomen. Hiervoor blijf ik je altijd dankbaar.